STUDY OF NEUTRON AND PHOTON INDUCED NUCLEAR REACTIONS

THESIS SUBMITTED TO THE

THE MAHARAJA SAYAJIRAO UNIVERSITY OF

BARODA

FOR THE DEGREE OF

DOCTOR OF PHILOSOPHY

IN

PHYSICS

BY
RAJNIKANT MAKWANA

UNDER THE GUIDANCE OF
PROF. S. MUKHERJEE
2017

"*Study of neutron and photon induced nuclear reactions*"

Thesis submitted to the
The Maharaja Sayajirao University of Baroda
for the degree of

Doctor of Philosophy
in
Physics

By
Rajnikant Makwana

Under the Guidance of
Prof. S. Mukherjee

Physics Department
Faculty of Science
The Maharaja Sayajirao University of Baroda,
Vadodara – 390 002,
Gujarat, India.

2017

Declaration by the candidate

I hereby declare that the work carried for the present thesis entitled *"Study of neutron and photon induced nuclear reactions"*, is done by me under the supervision of Prof. S. Mukherjee. This work has been carried out in Physics Department, Faculty of Science, The Maharaja Sayajirao University of Baroda, Vadodara in active collaboration with Bhabha Atomic Research Center BARC) and Tata Institute for Fundamental Research (TIFR), Mumbai, Defense Laboratory Jodhpur, Institute for Plasma Research (IPR), Gandhinagar, Institute of Modern Physics, Lanzhou, China.

I have taken more than twenty two months in completion of the work with full attendance at the university. I further declare that the work is original and the thesis or any part of the present work has been never submitted elsewhere for any degree whatsoever.

Date:

Rajnikant J. Makwana
Physics Department
Faculty of Science
The Maharaja Sayajirao University of Baroda,
Vadodara, India – 390 002

THE MAHARAJA SAYAJIRAO UNIVERSITY OF BARODA

Prof. S. Mukherjee

Tel. **0265-2795339 (O)**

Department of Physics
Faculty of Science
The M. S. University of Baroda
Vadodara – 390 002
Email: sk.mukherjee-phy@msubaroda.ac.in

Certificate from the Thesis Supervisor

This is to certify that that the thesis work entitled "Study of neutron and photon induced nuclear reactions" is a piece of work done by Mr. Rajnikant J. Makwana, under my guidance and supervision for the award the degree of the Doctor of Philosophy from the Maharaja Sayajirao University of Baroda, India and the candidate has taken more than twenty two months attendance in completion of the work.

To the best of my knowledge and belief the thesis

1. embodies the work of the candidate himself,
2. has been duly completed,
3. fulfill all the necessary ordinances related to the Ph. D. degree of the University, and
4. is up to the standard both content point of view and language for being referred to the examiner.

Prof. S. Mukherjee
Thesis Supervisor

Forwarded through:

Head,
Physics Department

Dean,
Faculty of Science

Lord Krishna, the mentor, the guide and the Omniscient!! Made the Arjun ready for Mahabharata!!

Preface

The development of the nuclear reactors with the safe use of nuclear operation and nuclear proliferation are the focus of the research from the several decades. After the discovery of tokamak, our vision to the production of power from nuclear fusion becomes important. The present research is focused not only in the direction of the conventional fission reactor but also for the development of the safe fusion reactor. In view of this, the International Thermonuclear Experimental Reactor (ITER) is under construction at Cadarache, France. The production of neutrons and photons in the fission and fusion reactor demands the nuclear data for the further development which is based on the reduction of the nuclear waste production, reduction of the transmutation of the structural materials and long life of the reactor. A complete data set is useful to fulfill these objectives, which enhance the nuclear data libraries. Further for the nuclear data is important for the nuclear transport calculations.

The present work is based on the theme of the nuclear data for the neutrons and photons to enhance the nuclear data libraries and the validation of the nuclear reaction models. The entire work can be divided into two parts, the study of photo induced nuclear reactions and study of neutron induced nuclear reactions. The mechanism of the giant dipole resonance was explained with the derivation of empirical formula using different terminology than the conventional. The validation of the formula for isotopes with $Z \geq 60$ has been done with the experimental data available in EXFOR data library and nuclear modular codes TALYS – 1.6 and EMPIRE – 3.2.2.

In addition to the above, neutron induced nuclear reaction experiments are performed at BARC – TIFR Pelletron facility, Defense Lab Jodhpur and at BHU in the energy range from 1 MeV to 20 MeV for some

structural isotopes. The offline gamma ray spectroscopy and neutron activation analysis technique were used for the data measurement and analysis. The measured cross section data were computed using different models available in TALYS – 1.6/1.8 and EMPIRE – 3.2.2 and compared.

Overall the present thesis has been made in view of providing nuclear data that can be compiled for the nuclear data libraries.

Acknowledgement

Acknowledgment is the place where I can express my gratitude towards all those persons who have helped me throughout or some stages during the entire Ph.D. work. I can begin with the name that was the pioneer and backbone and sole inspiration throughout – my Ph.D. guide ***Prof. S. Mukherjee****. I also convey my thanks with equal respect to Prof. N. L. Singh, Head of the Department for his cooperation and support. I have got a big support from the Defense Laboratory Jodhpur, who helped me in caring out the first experiment of my thesis work Mr. Surendrasingh Barala, Mr. Mahaveer Singh and Dr. Gopalani. I acknowledge them gracefully. I thank to my small unit at Institute for Plasma Research, Gandhinagar – Mayur Mehta, Mitul Abhangi, Shailja Tiwari, Sudhir Singh Vala, Shrichand Jakhar, C. V. S. Rao, T. K. Basu and Ajay Kumar Sir. Special thanks to Mayur Mehta for his support in the experiment and being a true friend. I sincerely thank Dr. Haladhar Naik of Radio Chemistry Division, BARC for his selflessness help and support throughout the experiment at TIFR, Mumbai. I am also thankful to Dr. S. V. Suryanarayana, Dr. S. C. Sharma, R. Acharya and other participants who had helped me in carrying out the experiment.*

My special thanks to Dr. Naveen Agrawal for his continuous moral support, helping in the arrangement of the experimental setup and many other things. I would like to thank Prof. P. K. Mehta and his student Mr. Nishant for their nice suggestions and help. I also acknowledge Dr. M. N. Srinivas and his students Nimesh and Vishwnath. I thank each and every staff of the Physics Department, The M. S. University of Baroda. My special thanks to Dr. D. G. Rathod for his help and moral support. I am thankful my university for providing a minor research project for this work. I am thankful to my team in the Department P. Mishra, V. Vansola, S. Parashari, J. Acharya, N. Shetty who had helped me in carrying out this work, and their help in the experiment. My special thanks to Mr. Ketan Chaudhari and Mr. Rakesh Chauhan for their moral support.

I gracefully acknowledge Dr. Bhawna Pandey for his continuous support during the Ph.D. I would like to acknowledge Dr. A. T. T. Mostako and Dr. Paresh Prajapati equally for the motivation in the beginning of the work. I must acknowledge Luka Snoj from Jožef Stefan Institute, Slovenia and Prof. K. Karel from the Brno

University of Technology, Czech who helped me in carrying out the MCNP calculations. I also acknowledge the ITER team Micheal Walsh, Robin Barnsley, Dr. J. Govindrajan, Santosh Pandya and Mrs. Kumudani A. I cannot miss the name of my friend late Mr. J. Alejandro from ITER for his support and direction.

My special thanks to my friend Ketan Prajapati for being an ideal friend at every instant. I equally acknowledge my friend Chintan Shah for his moral support and extensive discussions.

Whatever the amount of thank I give it is always less for the support provided by my family. I am thankful in all manner to my parents and brother-sister for the shelter provided by them. The special thanks to my beloved wife Jyotika for her sacrifice, support, and dedication throughout the Ph.D. work. I equally acknowledge her family for their necessary support.

My special gratitude goes to Basant, Gnansagar, Rameshwar Chavan, Chaitanya, Abhishek, Manish Jaishwal, Dr. D. Bagchi, Ashis, Sunil, Bhavesh, B. K. Naik and many others. I am thankful to all the teachers who have made me capable to enroll myself as a Ph.D. candidate and at the end, I am at the stage where I have completed it so far.

In the end, I dedicate my thesis work to the creature of this universe, with all respect I thank thou for everything.

Rajnikant Makwana

List of Publications from the Thesis

1. **Rajnikant Makwana,** S. Mukherjee, P. Mishra, H. Naik, N.L. Singh, M. Mehta, K. Karel, S. V. Suryanarayana, V. Vansola, Y. Shanthisheela, M. Karkera, R. Acharya, S. Khirwadkar, **"**Measurements of cross sections of ^{186}W(n, γ)^{187}W, ^{182}W(n, p)^{182}Ta, ^{154}Gd(n, 2n)^{153}Gd, ^{160}Gd(n, 2n)^{159}Gd reactions between 5 to 17 MeV neutron energies"
   Physical Review C (In Press)
   Impact Factor: 3.82

2. **Rajnikant Makwana**, S. Mukherjee, Jian-Song Wang, and Zhi-Qiang Chen, "New empirical formula for (γ, n) reaction cross section near GDR Peak for elements with $Z \geq 60$",

   Chinese Physics C Vol. 41, No. 4 (2017) 044105
   Impact Factor 5.084

3. **Rajnikant Makwana**, S. Mukherjee, L. Snoj, S. S. Barala, M. Mehta, P. Mishra, S. Tivari, M. Abhangi, S. Khirwadkar, H. Naik, "Spectrum average cross section measurement of ^{183}W(n, p)^{183}Ta and ^{184}W(n, p)^{184}Ta reaction cross section in ^{252}Cf(sf) neutron field"
   Applied Radiation Isotopes
   DOI: http://dx.doi.org/10.1016/j.apradiso.2017.06.002
   Impact Factor 1.136

4. N. L. Singh, **Rajnikant Makwana**, S. Mukherjee, A. Chatterjee "Measurement of (n, p) Cross Section for Some Structural Materials at 14.2 MeV"

   Published in: IEEE Conference Proceedings; 2016 17th International Scientific Conference on Electric Power Engineering (EPE)
   DOI: https://doi.org/10.1109/EPE.2016.7521819
   Impact Factor: 5.629

Contents

List of Figures

List of Tables

Chapter – 1

Introduction

1.1 Importance of the present work

The idea of the green and peaceful use of nuclear energy is in the heart of the nuclear reactor technology. The nuclear reactions are the base of the energy production in the nuclear reactors. Most of the reactor uses fission of U, Th and Pu isotopes mixture as fuel. On the other hand, fusion reactor uses the hydrogen isotopes deuterium and tritium as fuel, and fusion of these two nuclei at high temperature produces neutrons. In fission reactors, neutrons have energy from thermal to few MeV, and in a fusion reactor, the neutrons have energy 14.6 MeV, which is scattered from the different reactor materials and get a spectrum of energy from thermal to 14.6 MeV [1-7]. These neutrons induce different nuclear reaction channels, such as (n, γ), (n, p), (n, n'), (n, d), (n, t), (n, α), (n, 2n) etc. These reaction channels transmute the base reactor material, which may have different mechanical, thermal and chemical properties. The mechanical properties are the strength of the material, Young's modulus, limit of elasticity etc. Thermal properties are directly related to the physical state of the material at a different temperature, which is also necessary for the mechanical strength. A reactor contains fuel, controlling, structural, shielding, and many other types of materials with specific purposes. In the case of a fusion reactor, the materials are selected as per different components, such as divertor, limiter, blanket, superconductor magnet, structural etc. The selection of these materials should be done very carefully taking into account the transmutation criteria [8]. The different materials such as Na, Ti, V, Cr, Co, Fe, Cu, Zn, Mn, Ni, Zr, W, Pb, Bi etc., are used in the reactor at several places, mostly as structural materials [9, 10]. These materials should have experimentally measured nuclear data at different energies of incident neutrons. The neutron and photon data are more important as they are the major products of the reactor fission/fusion reactions. Most of the reactor materials have measured reaction data at thermal neutron energy, 2.5 MeV and 14 MeV [11]. Using several natural as well as accelerator based neutron sources, several authors have reported nuclear data up to 20 MeV, which can be found in the experimental data library EXFOR [11]. These data are not only important for the nuclear reactor development but they are the key tools to validate the nuclear models [12-14]. The data required for the reactor development has been discussed by R. Forrest [15, 16].

In the present thesis, the nuclear data obtained from the measurements on the various structural materials are described below.

Tungsten is selected as a diverter material in the International Thermonuclear Experimental Reactor (ITER) as well as it is also being used in Accelerator Driven Subcritical System (ADS) [16]. In ITER, the neutrons are ranging from thermal energy to 14.6 MeV, and in ADS they can have higher energies. Tungsten will be irradiated with neutrons produced by the DT fusion in ITER [11, 17]. Thus the isotopes of tungsten $^{180,182\text{-}184,186}$W will be transmuted into different isotopes though different reaction channels. Hence it is necessary to know all the reaction data for all the possible reactions of tungsten isotopes. Most of the data for tungsten isotopes are available at thermal neutron energy, 2.5 MeV (DD neutrons) and 14 MeV (DT neutrons) in EXFOR data library [11]. The energy region, 1 MeV to 13 MeV and 14 to 20 MeV contains very few experimental data points. Therefore, it is important to have more data in this energy range to complete the data set.

In fission and fusion reactors, there are several transition elements used as structural materials such as V, Cu, Zn, Mn, Ni, and irradiated during the operation condition of the reactors and transmute into other materials. The measured data for the nuclear reactions for these elements are scarce and have large errors [11]. The rareearth materials, which are always present along with these structural materials (As, Gd) interact with neutrons. This leads to transmutation that can change their electronic, mechanical and thermal properties. The nuclear data for the capture reaction on the isotopes of these elements are available in a good amount below 1 MeV, but few data points are available beyond this range of neutron energy [11]. At neutron energies higher than 1 MeV, other reaction channels become important, but the data for all isotopes are not available. There are several evaluated nuclear data libraries available which provide the data for nuclear reactions. Some of these libraries are ENDF-B/VII.1 [18], JENDL-4 [19], FENDL [20], ROSFOND [21], CENDL-3.1 [22], JEEF-3.2 [23] etc. There are several nuclear models that are used for the prediction of these evaluated nuclear data libraries. The measured data can help to verify the nuclear reaction models [12, 13]. In this thesis, measurement of the neutron induced nuclear reaction cross sections in MeV energy range has been presented to enhance the nuclear data libraries.

Further, during the plasma shot in a fusion reactor, the runaway electrons can be generated and they can reach the energy from few keV to several MeV [24]. The

higher energy electrons can form a beam. Such runaway electron beam can strike on the wall of the vacuum vessel. It can either damage the vessel or partially damage it [25]. During this interaction, these electrons can produce high energy photons of several MeV energy. At lower photon energies, the photoelectric, Compton's scattering and pair production reactions dominate. The photons can reach beyond 10 MeV energy and they can open photonuclear reaction channels with the target nuclei. The lowest threshold among all photonuclear reactions is (γ, n) reaction. This interaction is energy dependent. The interactions are (1) Giant Dipole Resonance (6 – 30 MeV) – GDR, (2) Quasi – deuteron (30 – 150 MeV) and (3) Intra-nuclear Cascade (above 150 MeV) [26]. In a fusion reactor, it is important to study the GDR mechanism, as the most of the photons lie in this energy range. It can produce a considerable amount of neutrons, which can affect the total neutron yield, ultimately to the fusion power. Further, the reaction itself is a neutron source, and in designing a neutron source based on this reaction, target design and photon energy optimization are the main objectives. There are several experimental and evaluated data available in the EXFOR and evaluated data libraries respectively [11]. Due to the unavailability of several targets and other complications in experiments, it is not possible to have complete experimental data set. Alternatively, with the help of nuclear modeling, it is possible to get the evaluated data, which can complete the data set. Further, the development of suitable empirical formula based on primary nuclei properties can explain the photonuclear reactions. There are number of empirical formula at specific neutron energies that can be found in the literature [27-34]. The work done in this field of photon induced reactions can be found elsewhere [35,36]. In the present thesis, a new empirical formula has been developed which can explain the (γ, n) reaction cross section near to GDR peak energies for the isotopes with $Z \geq 60$. Systematic development of the formula using the different terms, with their physical interpretation has been discussed. Further, the applications of this formula in the development of a nuclear database for future reactor technology have been discussed.

1.2 Nuclear reactions

1.2.1 Overview

When a particle (with sufficient energy) incidents on a target nucleus, its interactions with the nucleus is called nuclear reaction. This interaction may be either elastic or inelastic. If the kinetic energy before and after interaction remains same, it is called elastic, and if not, then it is inelastic. Both interactions give information about the nuclear structure. The different incident particles are used worldwide to learn different nuclear reactions. When a neutron is an incident on a target atom, it directly reaches to the nucleus, as it doesn't possess any charge and hence no Coulomb barrier. Once it enters within the nuclear radius, it is under the strong force field of the target nucleus. For a moment, a neutron inside the nucleus loses its initial information and behaves as a nucleon of the target nucleus. At this moment a momentarily stable state called the compound nucleus of the target and the entered neutron is produced. This compound nucleus doesn't contain any information of its formation, and ultimately the transient state of compound nucleus decays into different channels as per its excitation energy. If the ejected particle is a neutron and has the same energy as incident one, it is called an elastic scattering and if the ejected neutron has different kinetic energy then the reaction is called inelastic scattering denoted as (n, n'). If in place of neutron a gamma photon is ejected, and the incident neutron is absorbed, then the reaction is called neutron capture. The other neutron induced nuclear reactions are (n, p), (n, d), (n, t), (n, α), (n, 2n) etc. If neutron energies are below 2-3 MeV the compound nuclear reaction mechanism is important. Above this neutron energy, another mechanism called pre-equilibrium mechanism gradually becomes important. In this mechanism, the nucleus does not go completely into the compound nucleus stage, but before it, it ejects some particles. And above 20 MeV, the mechanism is called direct reaction dominates. In this mechanism, neutron interacts to a nucleon in place of the whole nucleus. The details of all these three-reaction mechanisms are discussed in Chapter – 2.

When a neutron is able to break the target nucleus into small fragments, the reaction is called fission reaction. Heavy nucleus once captures the incident neutron, they get such excitation energy, so that they break into small parts (as separate nuclei), which is known as fission fragments. These reactions can produce 2-3 neutrons, along with these fission fragments. These neutrons can further incident on new targets and can

continue the reaction in chain form called a chain reaction. During this process, energy is produced by conversion of some mass into energy according to Einstein's formula. The controlled chain reaction is the principal of the nuclear reactor. Along with the neutron, the photonuclear reactions are the part of this thesis work. The details of the photonuclear reactions have been discussed in Chapter – 3.

1.2.2 The reaction kinematics

The energy released or consumed in a nuclear reaction is called Q value of the reaction. Suppose a nuclear reaction X(x, y)Y, in which the x is an incident particle (projectile), X is a target, y is ejected particle (ejectile), and Y is a residue nucleus. The masses of the each particles are m_x, m_X, m_y and m_Y respectively. E_x, E_X, E_y and E_Y are the kinetic energies of the each respectively If we think about the masses, then there is a difference in the mass on the either sides of the reaction, i.e. the total mass of the projectile and target before the reaction may not equal to the total mass of the ejectile and residue nucleus. This indicated some mass to energy conversion or vice versa. This energy is called Q value. Its mathematical expression can be written for the above reaction as follows,

$$Q = \{(m_X + m_x) - (m_Y + m_y)\} \cdot c^2 \quad 1.1$$

$$Q = (E_Y + E_y) - (E_X + E_x) \quad 1.2$$

The Q value energy either positive or negative. The positive value indicates exothermic reaction, whereas the negative value represents endothermic reaction.

In case of reaction kinematics, two frames of references are taken in general: the laboratory system (LS) and the center of mass system (CM). In laboratory system, the target is considered to be at rest, and incident particle is moving with certain velocity towards the target, and after interaction the ejectile deflects with certain velocity at certain angle. In contrast to this, in the CM system, the center of the mass of the target and projectile is to be considered at rest. Hence before the reaction both projectile and the target are moving towards each other, and after collision, both are moving at different angle with different speeds. Suppose in LS that the velocity of projectile and ejectile are v_x and v_y, the velocity of residue is v_Y. The velocities projectile, ejectile, target and residue in CM system are v_x - Vcm, v_y', -Vcm and V_Y' respectively.

The visualization of kinematics for both systems is given in Fig 1(a-b).

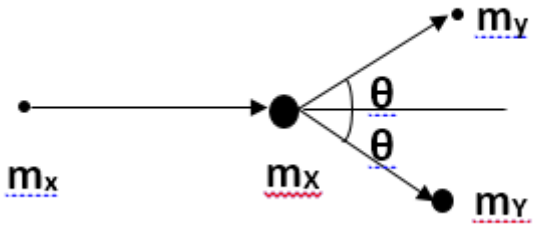

FIG 1.1 Laboratory System

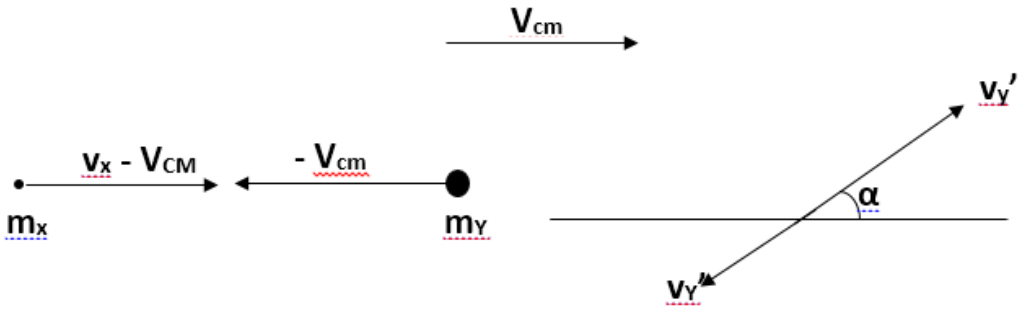

FIG 1.2 Center of Mass System

By applying the collision theory and energy conservation the Q value of the reaction can be given as,

$$Q = E_y\left(1+\frac{m_y}{m_Y}\right) - E_x\left(1-\frac{m_x}{m_b}\right) - \frac{2\sqrt{m_x m_y E_x E_y}}{m_Y}\cos\theta \qquad 1.3$$

From the present equation one can calculate the energy of the ejected particle as well as the energy distribution as per the angle.

There is one more term called threshold energy has been defined by following equation,

$$E_T = -Q\frac{m_x+m_X}{m_X} \qquad 1.4$$

This is the minimum energy required to initiate a nuclear reaction. For a charge particle reaction in addition with this, the Coulomb's barrier also need to be considered.

1.2.3 Neutron activation analysis

1.2.3.1 Introduction

Georg Hevesy and Hilde Levi were the first who reported a new method of activation analysis [37]. It was their observation that when materials are irradiated with neutrons they become radioactive. With the radioactive emission, one can identify the product isotopes. This method, which is based on neutron irradiation, activation and then analysis, is called the Neutron Activation Analysis (NAA). At that time, because of unavailability of high neutron flux sources, this method of NAA was not much explored. Later on with the development of the high neutron flux sources such as research reactors, this method becomes an important tool for research purpose. The most significant advantages are, the process is non-destructive and used on any material with any physical state [38]. NAA can simultaneously analyze multiple elements with high accuracy and sensitivity, while also only requiring a minimal amount of material for a sample, makes the NAA process very attractive for research purposes [39]. Its primary use is to determine the elemental concentrations within a sample of interest. Additionally, isotopes contained within a sample can be detected and separated from the base elements allowing the researcher to determine what percent of the sample is comprised of certain isotopes [40]. In this method after the irradiation, the parent isotope produces radioactive daughter isotopes, which emits the alpha, beta or gamma rays. After the development of the High Purity Germanium detector (HPGe), which has very high resolution, the method becomes very effective. The gamma photon emitted from the daughter can be measured using an HPGe detector, and the peak area of the interested peak energy contains the information of the reaction parameter – cross section. This method is very important for the cross section measurements and has been widely used by the researchers since its discovery.

In this method, a material is irradiated with the neutrons. The neutrons produce activation in the sample. The transmuted isotope must be radioactive and should have not too small and not too large half-life. Further, it must follow the radiation decay, which can be measured with the help of detector spectrometry. With these data, one can estimate the unknown parameters of the reaction. The mathematical formulism for this method is discussed in the next section.

1.2.3.2 Derivation of reaction rate

If we are dealing with a neutron induced reaction, which is a capture reaction, then it requires no threshold energy. But for the other reaction, the threshold energy is non-zero and this is in the MeV range as the binding energy of a nucleus is in MeV range. The derivation of the reaction rate can be found in the literature [41].

If a neutron induced reaction has threshold energy – E_{th} and we are using a mono energy neutron with E_n energy with $E_n > E_{th}$, then the reaction rate R can be given as

$$R = N \cdot \sigma \cdot \phi \quad 1.5$$

Where, N = number of target atoms,

σ = cross section of the reaction

ϕ = neutron flux with energy E_n

This equation contains a parameter cross section of the reaction, which is a probability of the reaction. Its dimension is per unit area, and measured in the barn (= 1 cm^2). This equation is only valid if neutrons are monoenergetic. If the neutrons are not mono energy but having energy spectrum, then the following expression should be considered [42].

$$R = \int_{E_{th}}^{E_{max}} N \cdot \sigma(E_i) \cdot \phi\,(E_i) dE \quad 1.6$$

Consider an isotope A is irradiated with neutrons, which transmute it into isotope B, which is also radioactive with decay constant λ_b, decays into isotope C. Hence, the process can be written as

$$A + n \rightarrow B(\lambda_b) \rightarrow C \quad 1.7$$

The irradiation of A produces B, but during the irradiation, some of the fraction of B also converts into another isotope (other reaction channels). Further, the isotope B decays into C, hence the overall reaction rate of production of isotope B can be written as,

$$R_b = N_a(t)\sigma_a\emptyset - N_b(t)\sigma_b\emptyset - \lambda_b N_b(t) \quad 1.8$$

$$\frac{dN_b}{dt} = N_a(t)\sigma_a\emptyset - N_b(t)\sigma_b\emptyset - \lambda_b N_b(t) \quad 1.9$$

Where, R_b is the reaction rate, $N_a(t)$ is the number of targets of isotope A at time t, N_b is the number of atoms of nuclei B at time t,

The solution of this reaction can be given as,

$$A_b = N_b(t_i)\lambda_b = \frac{N_a(0)\sigma_a\emptyset}{1+(\sigma_a-\sigma_b)\emptyset/\lambda_b}[e^{-\sigma_a\emptyset t_i} - e^{-(\lambda_b+\sigma_b\emptyset)t_i}] \quad 1.10$$

Practically, the target is selected such that very small fraction of destroyed in irradiation and hence it can be negligible ($\sigma_a\emptyset t_i \ll 1$). Also, it is necessary that the produced isotope must have followed the condition $\lambda_b \gg \sigma_b\emptyset$. With these conditions, the solution above can be simplified by,

$$A_b(t_i) = N_a(0)\sigma_a\emptyset[1 - e^{-\lambda_b t_i}] \quad 1.11$$

This formulism can be used to measure neutron flux or the cross section of the reaction. When a target is irradiated with the neutrons, the product isotope will be formed. The irradiation time is taken above as t_i. After irradiation, the activity produced in the target is measured using gamma ray spectrometer. The time duration from stopping the irradiation to the start counting is called cooling time (t_w). The counting time is t_c and the clock time (real time) is t_r. The cross section of the reaction can be given by the following expression. Suppose that an irradiated sample is counted between time t_1 and t_2.

$$\int_{t_1}^{t_2} A_b(t)dt = \frac{N_a(0)\sigma_a\emptyset}{\lambda_b}[1 - e^{-\lambda_b t_i}][e^{-\lambda_b t_1} - e^{-\lambda_b t_2}] \quad 1.12$$

The left side of the equation is the measured activity by some gamma spectroscopy,

$$A_\gamma = \frac{N_a(0)\sigma_a\emptyset}{\lambda_b}\left[1 - e^{-\lambda_b t_i}\right]\left[e^{-\lambda_b t_1} - e^{-\lambda_b t_2}\right]$$

$$\sigma_a = \frac{A_\gamma\lambda_b}{N_a(0)\emptyset[1 - e^{-\lambda_b t_i}][e^{-\lambda_b t_1} - e^{-\lambda_b t_2}]}$$

Suppose we considered start time as zero then,

$$\sigma_a = \frac{A_\gamma\lambda_b}{N_a(0)\emptyset[1 - e^{-\lambda_b t_i}][1 - e^{-\lambda_b t_c}]}$$

As during cooling, the isotope B will decay, hence with the correction of cooling time,

$$\sigma_a = \frac{A_\gamma\lambda_b}{N_a(0)\emptyset[1 - e^{-\lambda_b t_i}][1 - e^{-\lambda_b t_c}]e^{-\lambda\cdot t_w}}$$

Including the detector parameter gamma efficiency (ε), gamma abundance and time correction, the modified activation formula is now,

$$\sigma_a = \frac{A_\gamma\lambda_b(t_c/t_r)}{N_a(0)\emptyset I_\gamma\varepsilon[1-e^{-\lambda_b t_i}][1-e^{-\lambda_b t_c}]e^{-\lambda\cdot t_w}} \quad 1.13$$

This is the standard neutron activation equation. This equation can be used to measure the cross section of a neutron induced nuclear reaction. And for a monitor reaction, the neutron flux can also be measured. In the present thesis, the neutron induced nuclear reaction cross sections were analyzed using this above formalism.

1.2.3.3 Importance of neutron activation analysis

The neutron activation analysis – NAA is a spectroscopic method, used to measure several data of nuclear reactions. The major use of this method is in measurements of the neutron flux and reaction cross section. The method is used to calibrate the yield of the neutron sources by foil activation. The different standard foils, such as In, Au, Ni, Cu, Al, Th can be irradiated with the neutron sources. The activation produced in the foil carries the information of the source from which it got activated, which can be identified (gamma spectroscopy) and analyzed with NAA method. With this one can calibrate the source. In the Joint European Torus (JET), which is the world's largest tokamak, the neutron yield and ultimately the fusion power calibration has been done using this method [43,44]. The upcoming fusion devices will also use the same method for several diagnostics point of view.

Large cross section database, which is purely experimental, has been available in experimental data libraries such as EXFOR, is because of this method. The method is more important as it is nondestructive and any physical form of the sample can be used. Also, it does require a very small amount of the material. Further, as it is based on nuclear reaction, hence it is chemically independent.

The method is useful to know the material composition, which is up to the level of isotopes constitute in the material. It allows not only identifying the unknown isotope in the material, but also the amount of it present in the material. The primary requirement of this method is a neutron source, which is discussed in the next section.

In the present thesis, the NAA method was used to analyze the neutron induced nuclear reactions. The cross sections of (n, γ), (n, p), (n, 2n) etc. were measured and calculated for different selected materials.

1.3 Neutron sources

Chadwick discovered neutron in 1932. The natural neutron sources are based on (α, n) reaction. In such sources, an alpha emitter is used to incident alpha on a light element such as beryllium. These sources are potentially with large half-life and neutron yield. Some examples are polonium and beryllium, ^{241}Am+Be, Ra+Be. The disadvantages of these sources are they have a high gamma background as well as neutrons are not mono energy. There are some potential spontaneous neutron sources, such as ^{252}Cf. The detail of this source is given in Chapter – 5. The reactors are the good sources of the neutrons. Due to fission, they produce neutrons in each fission reactions. The neutron flux in reactors is very high.

The other way is the production of neutrons artificially. These sources are based on nuclear reactions. In these kinds of sources, a high energetic beam of the particle is made to incident on a target nucleus. The beam has sufficient high energy that the incident particle can cross the Coulomb's barrier of the target nucleus. Such energetic beam of particles can be produced by a particle accelerator, such as a cyclotron, tandem accelerator etc. The details of such accelerators can be found in any standard nuclear physics book. The major reactions used for neutron production using the accelerated beam are DD, DT, and Li(p, n) reactions.

$$^{2}_{1}\mathrm{H} + ^{2}_{1}\mathrm{H} \rightarrow ^{3}_{2}\mathrm{He} + ^{1}_{0}\mathrm{n} + 3.268\ \mathrm{MeV} \qquad 1.14$$

$$^{2}_{1}\mathrm{H} + ^{3}_{1}\mathrm{H} \rightarrow ^{4}_{2}\mathrm{He} + ^{1}_{0}\mathrm{n} + 17.589\ \mathrm{MeV} \qquad 1.15$$

$$^{1}_{1}\mathrm{H} + ^{7}_{3}\mathrm{Li} \rightarrow ^{7}_{4}\mathrm{Be} + ^{1}_{0}\mathrm{n} - 1.664\ \mathrm{MeV} \qquad 1.16$$

The first two reactions give mono-energetic neutrons. The DT reaction will be used for power generation in a fusion reactor. These reactions produce fixed energy neutrons. Compact DT neutron sources are available for the research purpose. The third reaction is used at various laboratories. This reaction is important because its threshold energy is 1.88 MeV, hence the accelerated proton beam kinetic energy can be transferred to neutrons. If E_p is the proton beam energy then the ejected neutrons will have E_p – 1.88 MeV neutron energy. The details of this reaction are discussed in Chapter – 4.

Apart from this, the (γ, n) neutron sources are also used. The high energy natural γ sources, as well as the bremsstrahlung γ source are made to fall high energy γ on target to do photo-fission. These sources are relatively lower yield and white spectrum.

In accelerator driven subcritical system (ADS), a very high energy proton will be targeted on heavy atomic number material, and through the spallation, reaction neutrons will be produced. Due to the impact of a high energy proton, the target nucleus breaks into fragments, this reaction is called spallation reaction. The neutrons produced in this reaction will have very high energy. The spallation reaction can be observed in earth's atmosphere by the cosmic rays.

1.4 Objective of the present thesis

In view of the above discussions, following are the main objectives of the present thesis:

1) The measurements of nuclear reactions cross-sections of $^{186}W(n, \gamma)^{187}W$, $^{182}W(n, p)^{182}Ta$, $^{154}Gd(n, 2n)^{153}Gd$, $^{160}Gd(n, 2n)^{159}Gd$ reactions between 5 to 17 MeV neutron energies using TIFR Pelletron facility, Mumbai, India. The neutrons were produced using $^{7}Li(p, n)$ reaction. And the analysis was done using neutron activation analysis method.
2) Development of the new empirical formula for the photoneutron production (γ, n) reaction cross-section near giant dipole resonance (GDR) for isotopes with $Z \geq 60$.
3) The measurements of nuclear reactions cross-sections of $^{183}W(n, p)^{183}Ta$ and $^{184}W(n, p)^{184}Ta$ in $^{252}Cf(sf)$ neutron field at Defense Laboratory, Jodhpur, and IPR, Gandhinagar.
4) The measurements of nuclear reactions cross-sections of $^{75}As(n, p)^{75}Ge$, $^{66}Zn(n, p)^{66}Cu$, $^{64}Zn(n, p)^{64}Cu$, $^{55}Mn(n, p)^{55}Cr$, $^{51}V\ (n, p)^{51}Ti$ and $^{58}Ni(n, p)^{58}Co$ at 14.2 ± 0.2 MeV using DT neutron source at BHU, Varanasi.
5) The calculations of reaction cross sections using various nuclear reaction codes (nuclear modular and transport) for nuclear data prediction.

1.5 Structure of present thesis

The present thesis contains seven chapters. Chapter – 1 introduces the topic of the present thesis. Chapters 2 – 7 contains a description of work carried out during this study. The Chapter – 2 is about the nuclear codes, which are the theoretical tools for development of nuclear data. It gives a description of different nuclear reaction models used in nuclear modular codes, which are TALYS and EMPIRE, and nuclear transport code, which is MCNP. These codes are described in this chapter.

In Chapter – 3, the development of the new empirical formula for the photonuclear reaction cross sections has been discussed. The Chapter – 4 describes the neutron induced reaction cross sections measurements performed at the Pelletron facility at Tata Institute for Fundamental Research, Mumbai, India. Chapter – 5 is about the nuclear reaction cross sections measurements using the ^{252}Cf spontaneous neutron source at Defense Laboratory, Jodhpur, India. The Chapter – 6 describes the cross section measurement at Banaras Hindu University, Varanasi, India, using 14 MeV neutrons. Finally, Chapter – 7 describes the summary of the work done so far in this study and the outcomes.

References

[1] J. Qing, Y. Wu, M. Regis, and J. W. Kwan, IEEE Trans. Nucl. Sci. 56 (2009) 1312.

[2] J. Reijonen, et al., Appl. Radiat. Isotopes 63 (2005) 757.

[3] Y. Wu, et al., IEEE Trans. Nucl. Sci. 56 (2009) 1306.

[4] V. Voitsenya et al., Rev. Sci. Instrum. 72 (2001) 475.

[5] G. De Temmerman, et al., J. Nucl. Mater. 363 (2007) 259.

[6] K. H. Behringer, J. Nucl. Mater. 145 (1987) 145.

[7] Yousry Gohar, et al., NEA/NSC/DOC(2015)7, 254.

[8] R. A. Forrest, Energy Procedia 7 (2011) 544.

[9] K. L. Murty and I. Charit, journal of Nuclear Materials 383 (2008) 189.

[10] M. Victoria, N. Baluc, and P. Spa˙tig, Nuclear Fusion 41 (2001) 8.

[11] EXFOR data library, https://www-nds.iaea.org/exfor/exfor.htm

[12] R. A. Pitts, et al., J. Nucl. Mater. 463 (2013) 39.

[13] Arjan Koning, et al., Validation of the JEFF-3.1 Nuclear Data Library, JEFF Report 23, https://www.oecd-nea.org/dbdata/nds_jefreports/jefreport-23/nea7079-jeff23.pdf

[14] A. J. Koning, et al., JRC Scientific and Technical report on Nuclear data for sustainable nuclear energy, https://cordis.europa.eu/pub/fp6-euratom/docs/candide-final report_en.pdf

[15] R. A. Forrest, Fusion Engineering and Design 81 (2006) 2143.

[16] R. A. Forrest, Energy Procedia 7 (2011) 540.

[17] R. A. Pitts, et al., J. Nucl. Mater. 463 (2013) 39.

[18] R. G. Abernethy, Material Science and Technology 33 (2017) 1.

[19] M.B. Chadwick, et al., "ENDF/B-VII.1: Nuclear Data for Science and Technology: Cross Sections, Covariances, Fission Product Yields and Decay Data", Nucl. Data Sheets 112(2011)2887.

[20] Keiichi Shibata, et al., Nucl. Sci. Technol. 48(1), 1-30 (2011).

[21] FENDL-3.1 data library, https://www-nds.iaea.org/fendl31/

[22] ROSFOND data library,

http://www.ippe.ru/podr/abbn/english/libr/rosfond.php

[23] Z. G. Ge, et al., Journal of the Korean Physical Society, Vol. 59, No. 2, August 2011, pp. 1052

[24] JEFF-3.2datalibrary, https://www.oecd nea.org/dbforms/data/eva/evatapes/jeff_32/]

[25] S. J. Zweben, H. Knoepfel, Phys. Rev. Lett. 35 (1975) 1340.

[26] R. D. Gill, et al., Nucl. Fusion 42 (2002) 1039.

[27] V. C. Petwal, et al., PRAMANA — journal of physics 68 (2007) 235.

[28] F. I. Habbani and Khalda T. Osman, Appl. Radiat. Isotopes 54 (2001) 283.

[29] S. Ait-Tahar, Nucl. Phys. 13 (1987) 121.

[30] V. N. Levkovski, Zh. Eksp. Teor. Fiz. 45 (1963) 305.

[31] Y. Lishan, Systematics of the (n, t) reaction cross-sections at 14 MeV. CNDP7 (1992) 85.

[32] Kasugai, Y., Ikeda, Y., Yamamoto, H., Kawade, K., 1995.

[33] K. T. Osman and F. I. Habbani, 1997. On the systematics for the (n, p) reaction cross-sections at 14.5 MeV neutrons. INDC (SUD)-002, NDS, IAEA.

[34] K. T. Osman and F. I. Habbani, 1998. On the systematics for the (n, a) reaction cross-sections at 14.5 MeV neutrons. INDC(SUD)-003, NDS, IAEA.

[35] K. T. Osman and F. I. Habbani, 1999. On the systematics for the (n, 2n) reaction cross-sections at 14.5 MeV neutrons. Submitted to INDC, NDS, IAEA. Systematics of activation cross-sections for 13.4±15.0 MeV neutrons. JAERI- Conf. 95-008. cross-section for 14±15 MeV neutrons. Zh. Eksp. Teor. Fiz. 45, 305.

[36] I. Raškinyte˙, et al., in Proc. Int. Conf. on Nuclear Reaction Mechanisms, (Varenna, Italy: Dapnia/SPhN, 2006), DAPNIA-06-147.

[37] Muna Ahmed Saeed, Journal of Al-Nahrain University 11 (2008) 66.

[38] G. Hevesy, H. Levi, Math Fys Medd 14 (1936) 34.

[39] Overview of Neutron Activation Analysis Hosted Online by The

University of Missouri Research Reactor,
< http://archaeometry.missouri.edu/naaoverview.html >

[40] Z. B. Alfassi, Activation Analysis, Volumes I and II. CRC Press: Boca Raton, FL. 1990.

[41] Cezar Ciprian Negoita, “Measurement of Neutron Flux Spectra in a Tungsten Benchmark by Neutron Foil Activation Method” (1973) 26. https://inis.iaea.org/search/search.aspx?orig_q=RN:36065997

[42] D. De Soete, R. Gijbels, and J. Hoste, Neutron Activation Analysis. John Wiley and Sons: New York, NY. 1972.

[43] C. C. Negoita, thesis on “Measurement of Neutron Flux Spectra in a Tungsten Benchmark by Neutron Foil Activation Method”, 1973.

[44] D. B. Syme, et al., Fusion Engineering and Design 89 (2014) 2766.

Chapter – 2

Nuclear Modular and Transport Codes

2.1 Introduction

The importance of the nuclear data in the frame of reactor development has been discussed in the previous chapter. In order to have a complete set of nuclear data, there should be complete measurements of all reaction channels on all targets and with all projectile energies. This cannot be possible to achieve with experiments only. It is not feasible to make all the isotopic targets, which may itself be radioactive and may not be available with proper physical states. In order to theoretically explain these experimental results, it is required to have a set of well-designed nuclear reaction models. There are several nuclear reaction models that have been provided by different authors. The worldwide nuclear community has taken them as a base and using the computer programming, they have made different nuclear codes, which can predict the nuclear data. The codes are of two types: (1) Nuclear modular codes, and (2) Nuclear transport codes. The nuclear modular codes can predict the nuclear data such as reaction cross section, the angular distribution of outgoing particles etc., i.e., they can generate the basic nuclear data, and by using nuclear data one can make nuclear data library. The nuclear transport codes use this data library to transport the particle of interest and predict answers of the certain problems/requirements such as particle flux, reaction rates etc. These codes are very important as they can predict the data interpolation, extrapolation for all kinds of targets, particles, and energies. It can delimit the experimental limitations. But it is also necessary to validate the codes by comparison of code predicted data with experimental data.

In the present thesis, the nuclear modular codes TALYS and EMPIRE, and nuclear transport code MCNP have been used. The different reaction models are discussed briefly in the following sections.

2.2 Nuclear Reaction Models

There are several nuclear reaction models that have been developed by several researchers in the past, in order to explain the experimental results. The agreement with the experimental data shows the reliability of the nuclear models as well as it also identifies the limits of the model. It is of great interest to make more and more accurate nuclear reaction models to achieve highly reliable data. Basically, there are three nuclear reaction mechanisms as per the energy range of the incident particles,

which have been incorporated in various reaction models: (1) compound nucleus, (2) direct reaction, and (3) pre-equilibrium reaction mechanisms. Overall nuclear reaction mechanisms are shown in FIG 2.1. The role of these reaction mechanisms in reaction products with respect to the energy of the projectile is shown in FIG 2.2.

2.2.1 Compound nucleus mechanism

This reaction mechanism was explained by Bohr (1936) [1]. When a low energy particle/nucleon is incident on a target nucleus and enters into it, it distributes all its kinetic energy among all the nucleons of the target nucleus. Hence, the nucleus, which was in the ground state, is now having some excess amount of energy, and it is now in the excited state. This state having an equilibrium with a very small mean lifetime of the order of ~10^{-16} s. It has no memory of its formation. It then decays and emits an ejectile and a residue. Suppose a nucleon 'a' incident on a target 'A', and the compound nucleus 'A*' has been formed before it gives the products, 'b' and 'B', can be written as,

$$a + A \rightarrow A^{*} \rightarrow b + B$$

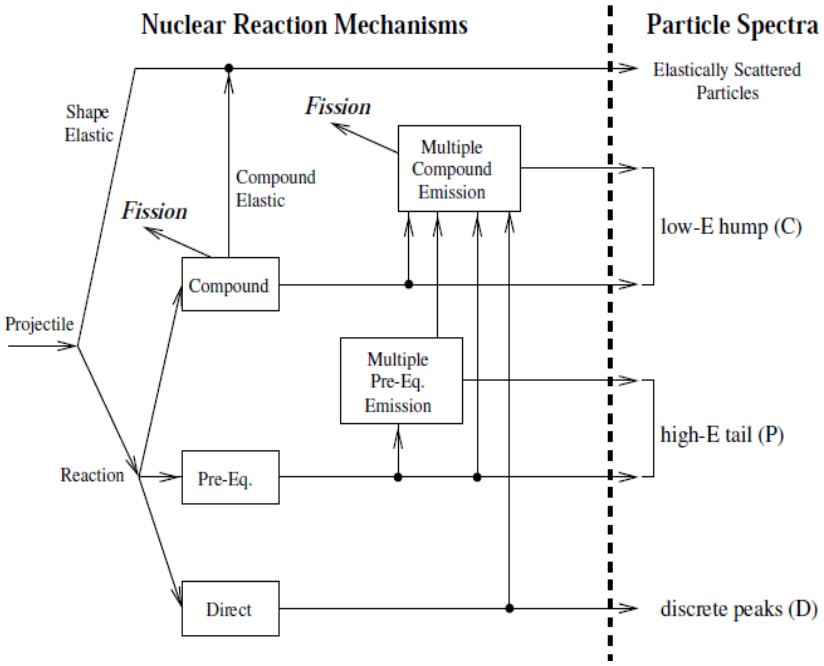

FIG 2.1 Nuclear reaction mechanisms

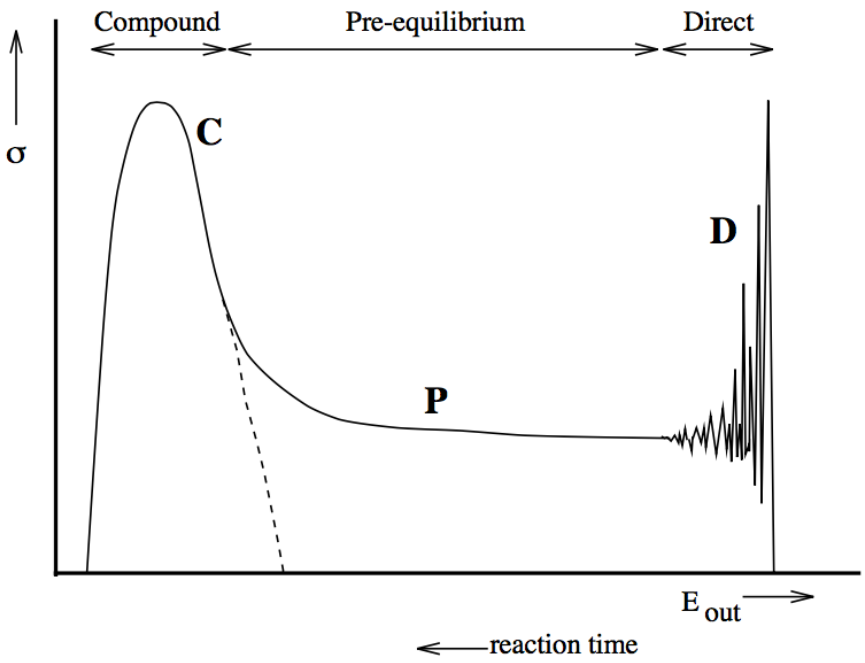

FIG 2.2 Outgoing particle spectra; the role of compound nucleus (C), pre-equilibrium (P) and direct reaction (D) mechanism with respect to incident particle energy

The compound nucleus mechanism has been incorporated in the Weisskopf – Ewing and Hauser-Feshbach models [2,3]. The reaction mechanism can be divided into two stages; in the first stage the formation and in the second stage the decay of compound nucleus takes place. The energy lost by the projectile in the target nucleus makes the compound nucleus, which is in the excited state. In the second stage, the excess amount of energy releases by the emission of electromagnetic radiation or an ejectile particle. The decay of the compound nucleus is shown in FIG 2.3.

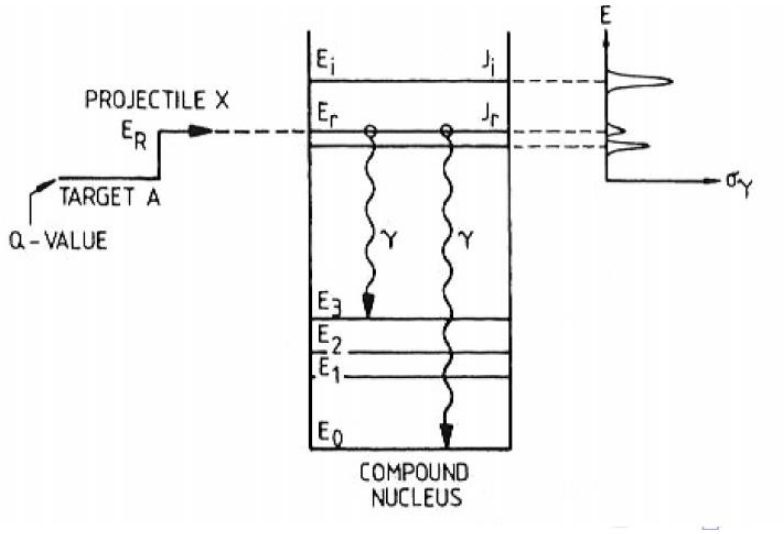

FIG 2.3 Decay of compound nucleus

2.2.2 Direct Reaction

The direct reaction takes place in the least time ~ 10^{-22} s, which is almost equal to a particle to pass through a nucleus. In this mechanism, an incident particle may pick a nucleon or nucleons from the target nucleus or it may lose its constituent particles in the target. The former reaction is called pick up while the later one is called stripping reaction. Another possibility is inelastic scattering in which, a particle just interact and loses or gains some amount of energy and ejects a particle. This reaction is probable for the particle with higher energy (>10MeV). In the direct reaction mechanism, the associated angular distributions are strongly peaked in the forward direction and have oscillatory behavior. It is possible to deduce the spin and parity of the residue from this oscillatory shape of the spectrum. The Distorted Wave Born Approximation (DWBA) or couple channeled approach can be helpful to understand the direct reaction mechanism. Here in this direct reaction mechanism, the target nucleus does not go into the compound nucleus stage, i.e., there is no transient equilibrium stage in the reaction.

The examples of direct reactions are as given below.

Stripping reaction: A(d, n)B, A(d, p)C, etc.

Pick up reaction: X(n, d)Y or X(n, t)Z, etc.

Inelastic scattering: A(n, n')A

2.2.3 Pre-equilibrium Reaction

In compound nucleus mechanism a nucleus goes in a transient equilibrium stage and then it decays, whereas, in the direct reaction mechanism, there is no equilibrium. In the process, before the nucleus goes to complete statistical equilibrium it decays to reaction products and such reactions are called the pre-equilibrium process. In the 1950s, the experimental data were found which cannot be completely explained by the compound nucleus or direct reaction mechanism. These data were in the moderated energy range. It suggests that there may be another kind of mechanism lies in between of these two mechanisms i.e., the pre-equilibrium. This mechanism is important from 10 MeV to ~200 MeV. The mechanism suggests that the nucleus goes to series of excited state and creates complex energy structure in the nucleus, but before it goes to a statistical stable stage with a particular angular momentum it

decays. This mechanism can be explained with two semi classical models from Griffin (1966) and Kalbach (1973), which are called exciton model and hybrid model respectively [4,5].

According to exciton model, once the projectile enters the target nucleus, the system gets excited with series of stages and different angular momenta. Before it goes to the final stage of equilibrium, it emits the ejectile (PE particles) and residue. The energy transferred by the projectile in the target nucleus decides the complexity of the stage, which can be estimated with the number of particles and holes excited. These excited particles and holes are called excitons. By solving the dynamical equations of these excitons one can calculate the resultant stage and products from the reaction. This mechanism can be explained by FIG 2.4. The E_F is the Fermi energy of the system.

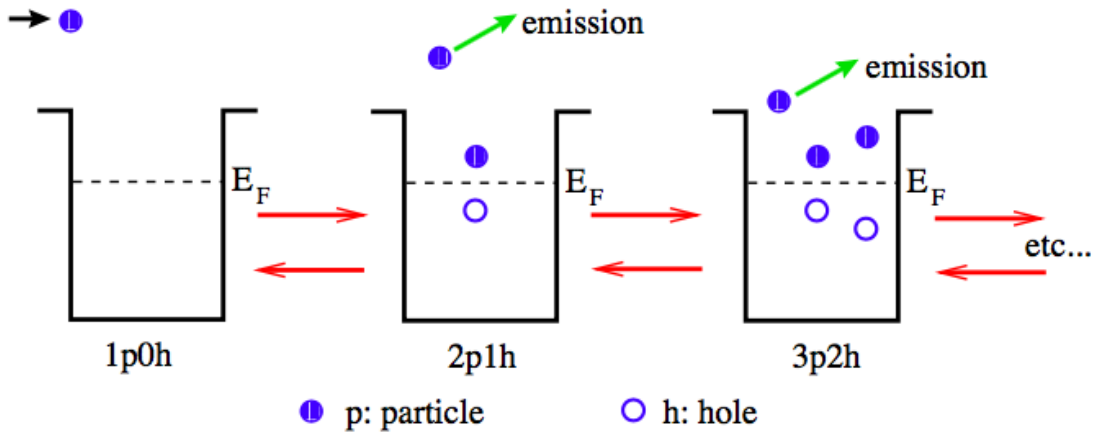

FIG 2.4 Pre-equilibrium mechanism as explained in the exciton model

From FIG 2.4, it can be understood that an incident particle p, interacts with another particle below the Fermi sea, and excites it to make 2p1h (h = hole) stage. In next stage, it reaches to stage 3p2h and so on. These stages are reversible. Before it goes to a stable stage any one stage can give the reaction products. In addition to this exciton model, there are many other pre-equilibrium models that have been proposed to explain this reaction mechanism. A quantum approach, which is used to overcome the deficiency of these models are the multi-step compound model (MSC) by Nishioka *et al*., (1986) [6] and multi-step direct model (MSD) by Nishioka *et al*., (1988) [7]. In MSC, all the particles are in the bound state, whereas in the MSD at least one particle is necessary to be in a continuum or above binding energy. Also, the MSC shows emission of particles is symmetric around 90º, whereas in MSD it is forward peaked.

The MSD uses the DWBA approach. For the data prediction, both the MSC and MSD should be applied together.

2.2.4 Optical Model

When a nuclear reaction takes place, the two nuclei combine together, and in this system, a single nucleon is in the field created by all the remaining nucleons. If we have N number of nucleons in a system then N number of Schrödinger's equations are required to represent the system. It is necessary to have the appropriate form of potential in order to solve the equations. In the optical model, this potential is considered complex, which has a real part as well as an imaginary part. The interaction between the incident particle and the nucleus is considered as an optical phenomenon. As an electromagnetic wave enters one media to another media, it may get refracted and when some obstacle is in the path it may get diffracted. In the same manner, the incident particle wave is diffracted by the nucleus. Hence the overall potential V(r) contains a real part representing the diffraction phenomenon and imaginary part representing the refraction part. The potential is represented by the following equation, with real part U(r), and imaginary part W(r).

$$V(r) = U(r) + jW(r)$$

The model was proposed by Bethe (1937) [8], which was explored by Feshbach *et al*. (1954) [3] in order to apply on neutron induced nuclear reactions. The Optical model is effective and reliable in explanation of most of the experimental data. This model has been modified as per the requirements from time to time.

2.2.5 Nuclear level density

The quantum mechanics says that the energy is quantized which generates the energy states. The energy states per unit energy interval are called nuclear level density. This parameter plays a crucial role in the nuclear reaction mechanism. In 1936, Bethe had done important work in the field of nuclear level density. If the density is more, then the spacing between the energy states is small. Ideally, if it is infinity, then the state will be a continuum. This parameter has given great importance to the development of nuclear modular codes. There are different level density models given in TALYS and EMPIRE codes [9, 10]. In present work, the effectiveness of these models has been tested and presented in Chapters – 4-5. The brief idea about each model used for level

density is given here. In the latest version of TALYS – 1.8, there are total six level density models are given, whereas in EMPIRE, in recent version there are five models are included.

The basic formula of the level density was given by Bethe as the expression below.

$$\Delta E^{ex} = \frac{1}{\rho(E^{ex})}$$

Where, ΔE^{ex} is the energy interval and $\rho(E^{ex})$ is the level density.

It suggests that a nucleus can be considered as a gas of nucleons, and a nucleon can occupy a particular energy level depending on the temperature of the nucleus. Hence, the nuclear level density can be written as,

$$\rho(E^{ex}) = ce^{2\sqrt{aE^{ex}}}$$

Where c is proportionality constant, a is the level density parameter and E^{ex} is the excitation energy of the compound nucleus. The parameter a is adjusted in such way that the evaluated data agrees with the experimental data. This model is also considered as constant temperature model. The other models of the level density are modification of this basic concept.

2.2.5.1 Composite Gilbert-Cameron model

The constant temperature level density formula was modified by Gilbert Cameron in 1965 as given below.

$$\rho_T(E) = \frac{1}{T} exp\left[\frac{E - \Delta - E_0}{T}\right]$$

Where T is the temperature, E is the excitation energy, Δ is the pairing energy, E_0 is the adjustable energy shift. And for the case where the excitation energy E > matching point energy Ux, the Fermi gas formula is used.

$$\rho_f(U) = \frac{\exp(2\sqrt{aU})}{12\sqrt{2}\sigma^2(U)a^{\frac{1}{4}}U^{\frac{5}{4}}}$$

Where, σ^2 is spin cut of parameter, a the level density parameter is given by,

$$a(U) = \tilde{a}\left(1 + \delta W \frac{1 - \exp(-\gamma U)}{U}\right)$$

Where, $\tilde{a}$ is the asymptotic level density parameter, δW is the shell correction energy and γ is the damping parameter. The asymptotic level density parameter is given by,

$$\tilde{a} = \alpha A + \beta A^{\frac{2}{3}}$$

Where A is the mass number, α and β are the global parameters.

2.2.5.2 The Back-shifted Fermi Gas Model

In this model, the pairing energy is treated as an adjustable parameter [11]. The Fermi gas expression is used to reach up to 0 MeV. The total density is given as,

$$\rho_F^{tot}(E_x) = \frac{1}{\sqrt{2\pi}\sigma}\frac{\sqrt{\pi}}{12}\frac{\exp(2\sqrt{aU})}{a^{1/4}U^{5/4}}$$

And the level density is,

$$\rho_F(E_x, J, \pi) = \frac{1}{2}\frac{2J+1}{2\sqrt{2\pi}\sigma^3}\exp\left[\frac{\left(J+\frac{1}{2}\right)^2}{2\sigma^2}\right]\frac{\sqrt{\pi}}{12}\frac{\exp(2\sqrt{aU})}{a^{1/4}U^{5/4}}$$

2.2.5.3 The Generalized Superfluid Model

The generalized superfluid model (GSM) is based on the theory of Bardeen-Cooper-Schrieffer on superconducting nature. The phenomenological model is characterized by a phase transition of superfluid behavior at low energy [12,13], where the level density is strongly influenced by pairing energy term. The GSM model distinguishes between a low and high energy region. An additional shift of the excitation energy δ_{shift} is introduced in the GSM was introduced to the enhancement of the level density parameter [13].

$$\mathrm{U} = E_x + \mathrm{n}\Delta_o + \delta_{shift}$$

Where $\Delta_o = 12/\sqrt{A}$ and n = 0, 1 and 2 for even-even, odd-A and odd-odd nuclei, respectively.

$$a(U,Z,A) = \begin{cases} \tilde{a}(A)\left(1 + \delta E_0 \frac{f(U^*)}{U^*}\right), U \geq U_{cr} \\ a_{cr}(U_{cr},Z,A), \quad U \leq U_{cr} \end{cases}$$

Where U_{cr} is the condensation energy is subtracted from the effective excitation energy. A further detail of the model is given in TALYS and EMPIRE manual [9,10].

2.2.5.4 The Enhanced Generalized Superfluid Model

The Enhanced Generalized Superfluid Model (EGSM) also uses the superfluid model below the excitation energy and above it the Fermi gas model as similar to GSM. It includes the enhancement of spin distribution contribution in Fermi gas model which is different from the GSM [14]. The enhancement of the level density for the evaluation is achieved from the non-adiabatic form of nuclear rotation. Hence it considers the shape of the nucleus in the dynamical situation. This deformation enters level densities formulas through moments of inertia and through the level density parameter that increases with increase in the surface of the nucleus. In the parameterization of ESGM, the role of the nuclear surface term and linear dependency on asymptotic $\tilde{a}$ vanished, and covers collective enhancement. EGSM global systematics does not account for discrete levels.

2.2.5.5 Microscopic level densities

There are different microscopic methods are available to calculate the level densities. The GSM approach has been used in the microscopic superfluid model to calculate the level density and other parameters of the excited nucleus. It considers realistic single particle level schemes [15]. The codes use this approach in the collective mode to generate the level density for the reaction data prediction. There is two main microscopic level density models are used in the development of the codes. For RIPL data library, S. Goriely has calculated the level densities using the Hartree-Fock calculations [15] for excitation energies up to 150 MeV and for spin values up to I = 30. Including this new energy, spin and parity dependent nuclear level densities based on the microscopic combinatorial model have been proposed by Hilaire and Goriely [16]. This model includes the intrinsic state density and collective enhancement. The calculations make coherent use of nuclear structure properties determined within the deformed Skyrme-Hartree-Fock-Bogolyubov framework [17]. The temperature-dependent Hartree-Fock-Bogolyubov calculations using the Gogny force is also included in the recent versions of the codes.

2.3 TALYS

The TALYS is a nuclear modular code, which was developed by A. J. Koning, S. Hilaire and M.C. Duijvestijn [9], which is a complex code using the different nuclear reaction models in a computer program. It is a Linux based program and can be installed on Linux and Mac OS with FORTRAN or c programming. The first version of TALYS – 1.0 was released in 2007. Time to time it was modified and next versions TALYS – 1.2, 1.4, 1.6, and latest TALYS – 1.8 (2016) were released. The code was developed to do a simulation on nuclear reactions induced by neutrons, photons, protons, deuterons, tritons, ^{3}He- and alpha-particles, in the energy range 1 keV – 200 MeV and for target nuclides of mass 12 and heavier [9].

In the evaluation of nuclear reaction data it uses different nuclear models which are written in the subroutines of the main code, and the parameters necessary for the evaluations are taken from the Reference Input Parameter data Library – 3 (RIPL) developed by IAEA [18]. The basic requirements of a TALYS input file are projectile, element, mass, and energy. One can run input with default parameters or with multiple options and parameters provided in the TALYS manual [9]. In the output, one can get all possible reaction channel nuclear data such as reaction cross sections, angular distribution, the cross section from different excitation levels, etc. It uses different level density models with ldmodel parameters. In TALYS – 1.8 there are six different combinations of nuclear level densities has been used [9].

ldmodel 1: Constant temperature + Fermi gas model

ldmodel 2: Back-shifted Fermi gas model

ldmodel 3: Generalised superfluid model

ldmodel 4: Microscopic level densities (Skyrme force) from Goriely's tables

ldmodel 5: Microscopic level densities (Skyrme force) from Hilaire's combinatorial tables

ldmodel 6: Microscopic level densities (temperature dependent HFB, Gogny force) from Hilaire's combinatorial tables

In present thesis work, the effect due to this parameter on selected nuclear reactions has been investigated. In the case of default input parameters, it uses ldmodel 1.

2.4 EMPIRE

EMPIRE (-3.2.2) Malta is a modular system for nuclear reaction calculations and nuclear data evaluation [10]. It can evaluate data for photons, nucleons, deuterons, tritons, helions (^{3}He), α's, and light or heavy ions. It takes range from few keV to several hundred MeV. It considers the major nuclear reaction models: Optical model, DWBA, Couple channels, MSD, MSC, exciton model (PCROSS) hybrid Monte Carlo simulation (DDHMS), and the full featured Hauser-Feshbach model including width fluctuations and the optical model for fission [10]. It uses CCFUS for heavy ion induced fusion. EMPIRE also uses the parameters from RIPL – 3 data library [18]. It is also Unix/Linux based code, but Windows version is also available. The first version of EMPIRE was released in 1980. The latest version of EMPIRE code is EMPIRE – 3.2.2 Malta. This version included combinatorial calculations of particle-hole level densities. In present thesis work, the following level density models were used for the investigation. It can be defined with LEVDEN mnemonic.

LEVDEN

= 0 EMPIRE-specific level densities, adjusted to RIPL-3 experimental Dobs and to discrete levels (default),

= 1 Generalized Superfluid Model (GSM, Ignatyuk et al), adjusted to RIPL experimental Dobs and to discrete levels,

= 2 Gilbert-Cameron level densities (parameterized by Ijinov et al), adjusted to RIPL experimental Dobs and to discrete levels,

= 3 RIPL-3 microscopic HFB level densities, parity dependent NLD,

= 4 Gilbert and Cameron NLD.

This parameter was changed to study the effect of on the magnitude and shape of nuclear reaction cross sections with respect to energy. Further detail of several parameters used for the data evaluation is discussed in EMPIRE manual.

2.5 Monte Carlo N-Particle Code (MCNP)

The Monte Carlo N-Particle – MCNP code was developed to transport the particles through the materials using Monte Carlo method. It was developed and maintained by Los Alamos National Laboratory [19-21]. It can transport neutron, proton, electron, photon and many other particles. It can transport in a single particle mode as well as in multiple particle transport mode. It is a worldwide recognized code for particle transport. It is useful in simulation for shielding design, radiation protection and dosimetry, medical physics, nuclear critical safety, detector design and analysis, accelerator and target design, reactor design parameters, detector signal generation etc. [20, 21].

The MCNP code gives facility to user to make a 3d model of the problem geometry. It has a particular input file consisting the description of the problem, which is described by different mnemonics known as CARDS. There are mainly three blocks: 1. Cell cards, 2. Surface cards and 3. Data cards. With these cards, the user has to define the problem geometry, materials to be used in the geometrical shapes, mode of transport, source description and the detectors. To perform these calculations, MCNP needs cross section data library. The inbuilt data library is ENDF-B/VI for neutron transport [20]. Further, there are different libraries such as IRDF-2002, FENDL-2.1, ENDF upgraded versions, and many other data libraries can be used to perform the calculations. For different particles different data libraries are available. While running the program it calls these libraries for the particle transport. A brief idea of an MCNP input file has been given here.

Input file:

The input file for MCNP is a text file containing geometry specification and data information using the above three parts in it. All the three parts are necessary to run a program.

1. Surface Cards;

   Surface cards are imaginary surfaces defined by these cards, e.g. plane, a spherical surface, cylindrical surfaces etc. These imaginary surfaces can be used to make the volume shapes by Boolean operations. The Boolean operations such as AND, OR, NOT are used to make shapes. AND operation is specified by space i.e., surface 1 and surface 2, the AND operation is specified by 1 2. The OR operation is specified by ‘:’ symbol in between

surfaces, e.g., 1:2. The NOT operation is specified by '#' symbol, e.g., #1. All surfaces are represented using the Cartesian coordinate system as an $f(x,y,z) = 0$. For example, a spherical surface with the origin as a center and R as a radius is given by $x^2 + y^2 + z^2 - R^2 = 0$. Its surface card is given as

1 S 0 0 0 10 $ center is origin, radius = 10cm

or 1 SO 10

With this card, the software will create an imaginary sphere with the center as origin and 10 cm radius. The number of this surface denoted is 1. Multiple surfaces with the Boolean operation can make shapes termed out as cells. More details of this card are available in Volume – 1 of manual of the code [14].

2. Cell Cards:

The cell cards are used to make three-dimensional geometrical shapes using the surface cards. One can make the experimental setup design in MCNP using this cards. These cells must be filled with the appropriate materials, which can be defined by using the material card.

For example, if a cube box is used to shield a radiation source, the box can be defined with six surfaces and Boolean logic. In a cell definition, the first number is a cell identity, secondly is for the material identification number. It may be zero (0) if no material (void) is selected, or a number followed by density. If density is in g/cc then negative sign (–) is used before it, and if it is an atom density then positive sign (+) is used. After that, the surface Boolean operations are used. At the end, the important card is used, which is defined by the particles, for neutron "n", photon "p", etc. and its weightage.

Surface cards:

1 px -10

2 px 10

3 py -10

4 py 10

5 pz -10

6 pz 10

Cell Cards:

Cell no	material	Boolean of surfaces	particle for transport
1	0	1 -2 3 -4 5 -6	imp:n=1

or

1	2	-1.0	1 -2 3 -4 5 -6	imp:n=1

3. Data Cards:

The data cards are in general contain a large number of information about source description, material description, detector description and run control cards.

The source is defined by SDEF (Source DEFination) card, which contains information about source position, particle type (n/p/e), particle energy, etc., which are necessary for complete source description. The position, energy, and dimension of the source can be written in terms of distribution if it is required. The details can be found in MCNP manual volume – II [22, 23].

Another card is a material card, which specifies the isotopic composition of the material used in the problem. It is specified by the "m" letter, followed by ZZZAAA.xx format, where ZZZ is for isotope number and AAA is for atomic mass number of the isotope. The .xx is for the data file extension that may be .60c, .21d, etc., likewise. The "c' stands for continuous and "d" for discrete data points in the data library. For e.g., water can be specified with two elements: H and O. Its atomic mass is 18 g, which is from 2 H atom and 1 O atom. The fraction of weight contribution from 18 g of H is 2 × H mass ÷ 18 g and from O is 1 × O mass ÷ 18 g. The values are 0.1112 and 0.8888 respectively. So m card for H_2O can be written as,

M1 1001.21c –0.1112

8016.21c –0.8888

Here we have taken only $^{1}_{1}H$ and $^{16}_{8}O$, one can use the remaining isotopes of both elements with consideration of their abundance.

The detector in MCNP is referred as Tally. Any volume, surface or point where the user is interested to calculate flux, current etc., needs to be written after the tally card. There are F1, F2, F4, F5, and F8 are the tallys used in MCNP. The descriptions of these tallys are as below in Table 2.1 [21-23].

Table 2.1 Details of tally description available in MCNP [21-23]

Mnemonic	Tally Type	Particle pl	Fn Unit	*Fn Unit
F1:pl	Surface current	N or P or N, P or E	-	MeV
F2:pl	Average flux on a surface	N or P or N, P or E	/cm^2	MeV/cm^2
F4:pl	Average flux in a cell	N or P or N, P or E	/cm^2	MeV/cm^2
FMESH4:pl	Mesh plot for volume average mesh flux in 3D	N or P or E	/cm^2	MeV/cm^2
F5a:pl	Flux at a point or ring	N or P	/cm^2	MeV/cm^2
FIP5:pl	Pin – hole flux image	N or P	/cm^2	MeV/cm^2
FIR5:pl	Planar radiograph flux image	N or P	/cm^2	MeV/cm^2
FIC5:pl	Cylindrical radiograph flux image	N or P	/cm^2	MeV/cm^2
F6:pl	energy deposition	N or P or N, P	MeV/g	jerks/g
F7:pl	fission energy deposition in a cell	N	MeV/g	jerks/g
F8:pl	pulse height distribution in a cell	P or E or P, E	pulses	MeV

These tallys can be modified with other data cards, e.g., if one is interested to calculate the dose rate in place of the flux, then one has to use DF card with flux to dose conversion factors in the definition of tally F4. There are plenty of

options are available in MCNP, which are discussed in details in MCNP manuals [22, 23].

In present thesis work, the F4 tally and F8 tallys were used with the MCNP – 6.1 version [19]. The tally F4 was used to calculate the average flux inside the target sample, and F8 tally to calculate the detector efficiency which is discussed in Chapter – 5.

2.6 Summary

The different nuclear reaction models were briefly introduced in the present chapter. The brief introduction of TALYS, EMPIRE and MCNP codes were given. The important level density models, which were used in the present thesis work, are listed. Brief idea about the MCNP input file and different blocks necessary for the problem description are discussed.

References

[1] N. Bohr, Nature, 137 (1936) 344.

[2] V. F. Weisskopf and D. H. Ewing, Phys. Rev. 57, 472, 935(1940).

[3] W. Hauser and H. Feshbach, Phys. Rev. 87, 366(1952).

[4] J. Griffin, Phys. Lett., 17, 478(1966).

[5] C. Kalbach-Cline, Nucl. Phys. A210, 590(1973).

[6] H. Nishioka, et al., Ann. Phys. (NY) 172, 67(1986).

[7] H. Nishioka, H. A. Weidenmuller and S. Yoshida, Ann. Phys. (NY) 183,166(1988).

[8] H. A. Bethe, Rev. Mod. Phys. 9, 69(1937).

[9] A. Koning, S. Hilaire, and S. Goriely, TALYS-1.6 - A Nuclear Reaction Program, User Manual, 1st edition (NRG, The Netherlands, 2013).

[10] M. Herman, et al., EMPIRE-3.2 Malta modular system for nuclear reaction calculations and nuclear data evaluation (2013).

[11] W. Dilg, W. Schantl, H. Vonach, and M. Uhl, Nucl. Phys. A217, 269 (1973).

[12] A. V. Ignatyuk, K.K. Istekov, and G. N. Smirenkin, Sov. J. Nucl. Phys. 29, no. 4, 450 (1979).

[13] A. V. Ignatyuk, J.L. Weil, S. Raman, and S. Kahane, Phys. Rev. C47, 1504 (1993).

[14] A. D'Arrigo et al., J. Phys. G20, 305 (1994).

[15] S. Goriely, F. Tondeur, J. M. Pearson, Atom. Data Nucl. Data Tables 77, 311 (2001).

[16] S. Goriely, S. Hilaire and A. J. Koning, Phys. Rev. C 78, 064307 (2008).

[17] S. Goriely, M. Samyn, and J. M. Pearson, Phys. Rev. C 75, 064312 (2007).

[18] R. Capote, et al., Nuclear Data Sheets 110, 3107 (2009).

[19] Retrieved from: https://laws.lanl.gov/vhosts/mcnp.lanl.gov/index.shtml, (24th May 24, 2017).

[20] J. K. Shultis and R. E. Faw, An MCNP Primer (2011).

[21] T. Goorley, et. al., "Features of MCNP6", Supercomputing in Nuclear Applications and Monte Carlo 2013, Paris, Oct 27-31, LA-UR-13-28114 (2013).

[22] X-5 Monte Carlo Team, MCNP — A General Monte Carlo N-Particle Transport Code, Version 5, Vol. I (2013).

[23] X-5 Monte Carlo Team, MCNP — A General Monte Carlo N-Particle Transport Code, Version 5, Vol. II (2013).

Chapter – 3

Development of New Empirical Formula for (γ, n) reaction cross section near to GDR Peak

---

Publication related to this chapter:

Rajnikant Makwana, S. Mukherjee, Jian-Song Wang, and Zhi-Qiang Chen, "New empirical formula for (γ, n) reaction cross section near GDR Peak for elements with Z >60",

Chinese Physics C Vol. 41, No. 4 (2017) 044105

Impact Factor 5.084

3.1. Introduction

Photonuclear reactions are becoming more important for the fusion reactors and accelerator driven sub-critical system (ADS), where high-energy photons will be generated and subsequently interact with the materials. The study of (γ, n) reactions is important for a variety of current and emerging fields, such as radiation shielding design, radiation transport, absorbed dose calculations for medical, physics, technology of fusion-fission reactors, nuclear transmutation and waste management applications [1,2]. In a fusion reactor, during the plasma shot, de-confined runaway electrons can interact with the first wall of the reactor and can produce high energy photons [3]. As a photon is a massless particle and its interaction is different than the neutron, and the mechanism is energy dependent. The high energetic photon can open reaction channels like (γ, n), (γ, p), (γ, 2n), (γ, 3n), etc. The most prominent reaction is (γ, n), as it has the lowest threshold than multi-neutron emission, whereas for charged particle emission the Coulomb barrier needs to be considered. Exact information about the cross section of such nuclear reaction is needed in order to perform accurate nuclear transport calculations. Tungsten (W) and beryllium (Be) are selected as first wall materials for the fusion reactor- International Thermonuclear Experimental Reactor (ITER) [4]. Among tungsten isotopes, only ^{182}W (26.5 %), ^{184}W (30.64%) and ^{186}W (28.43%) have experimental cross section data for (γ, n) reaction. It is necessary to have the cross section of (γ, n) reaction for ^{180}W (0.12%) and ^{183}W (14.31%) along with all the remaining long-lived unstable isotopes, as they will interact with high-energy photons during the confined runaways and disruption phase [5]. Gamma induced nuclear reaction are also important for the nuclear transmutation (e.g. ^{234}U(γ, n)^{233}U), which is useful for the nuclear safety and incineration. The importance of the gamma incineration technique has been studied in the case of many isotopes for nuclear waste management [6-8].

In ADSs, the high energy proton beam will interact with high Z elements such as W, Pb-Bi, Th, and U, which will produce neutrons through spallation reactions [9]. This spallation process will produce high energy photons, which will subsequently interact with the materials. It is necessary to have a complete nuclear dataset of photonuclear reactions for all isotopes of these elements. The experimental measurements of the nuclear reaction cross-section are one of the important methods to complete the nuclear dataset. However, there are always limitations in the experimental

measurements due to non-availability of all the energies of incident particles and preparation of target which may be unstable. For complete nuclear data for several isotopes, nuclear modular codes such as TALYS – 1.6 and EMPIRE – 3.2.2 are available. Using these codes one can predict the cross sections for different nuclear reaction channels. These codes basically use some nuclear models, and on the basis of the nuclear reaction theory, evaluation of the nuclear reaction data is done. The theory involved in photonuclear reaction cross section evaluation is discussed in the next section of this chapter. Apart from this, the nuclear systematics and empirical formula provide alternative method for such isotopes, as it can efficiently predict the nuclear properties. Many authors have used this theoretical approach. Several systematics and empirical studies have already been made for the photonuclear reactions [10]. These empirical formulae reduce experimental efforts, as they are basically dependent on well-known nuclear properties. In the present work, a new empirical formula has been developed and tested with nuclear modular codes and experimental data for $Z \geq 60$. With the help of the present empirical formula, one can predict the cross section datasets for those isotopes where there is a complete lack of the experimental data.

3.2. Theory of Photo Neutron Production

The known photon interactions are photoelectric effect, Compton scattering, and pair production. These interactions are the result of the interaction of a photon with atomic electrons. As the photon energy increases above 6 – 7 MeV, the interaction occurs with the nucleus. The interaction of high energy photon with the nucleus can cause ejection of nucleon/s. This reaction is referred as a photonuclear reaction. Photon should have sufficient energy above the binding energy of the nucleus for nucleon emission. As the nuclear binding energies are above 6 MeV for most of the isotopes, the photon should have such threshold energy [11]. Depending on the energy of the photon, three basic mechanisms are observed for the photonuclear reactions [12]:

(a) Giant dipole resonance (GDR)
(b) Quasi-deuteron (QD)
(c) Intra-nuclear cascade

If a gamma photon is having energy below 30 MeV, then it follows GDR mechanism. In this process, the photon energy is transferred to the nucleus by the oscillating electrical field of the photon, which induces oscillations inside nucleus

among nucleons. The photoneutron production is more probable since proton ejection needs to overcome a large Coulomb barrier. For different isotopes at a particular energy, there is a peak of photoneutron production for (γ, n) reaction. This energy is called GDR peak energy. For isotopes above Z = 60, the peak energies are between 10-18 MeV. Above 30 MeV, the photoneutron production is mainly due to the QD effect [12]. In this mechanism, a photon interacts with the dipole moment of a pair of proton-neutron in place of the nucleus as a whole [12]. Above 140 MeV, photoneutron production results from photo-pion production [12]. Further, the study of thermal fluctuation on GDR parameters is also of interest and studies are ongoing [13-16].

According to the semiclassical theory of the interaction of photons with nuclei, the shape of the fundamental resonance of the photoabsorption cross section follows a Lorentz curve [12, 17].

$$\sigma(E) = \frac{\sigma_i}{1 + [\frac{\left(E_\gamma^2 - E_m^2\right)^2}{E_\gamma^2 \gamma^2}]} \quad 3.1$$

Where, σ_i, E_γ and γ are the Lorentz parameters: peak cross section, resonance energy and full width at half maximum respectively [18].

In a more general way, in nuclear modular codes, such as TALYS – 1.6 and EMPIRE – 3.2.2, the photoabsorption cross section is calculated as the sum of two components [18-20],

$$\Sigma_{abs}(E_\gamma) = \sigma_{GDR}(E_\gamma) + \sigma_{QD}(E_\gamma) \quad 3.2$$

The component $\sigma_{GDR}(E_\gamma)$ represents the giant dipole resonance (GDR), in Lorentzian form. It is given by eq. 3.1 by as shown below,

$$\sigma(E) = \sum_i \frac{\sigma_i \cdot (E_\gamma \cdot \Gamma_i)^2}{\left(E_\gamma^2 - E_i^2\right)^2 + (E_\gamma \cdot \Gamma_i)^2} \quad 3.3$$

Where σ_i, E_i and Γ_i are: peak cross section, resonance energy and full width at half maximum respectively. The summation is limited to i=1 for spherical nuclei, while for deformed nuclei the resonance is split and one uses i = 1, 2. The component $\sigma_{QD}(E_\gamma)$, represents the Levinger form given by Chadwick et al. [19–22]. It is basically from the quasi-deuteron model. In the energy range from photonuclear threshold to 30 MeV, the GDR mechanism is dominant, while in the range 30 – 140

MeV QD mechanism is dominant. Above 140 MeV the threshold energy for pion production is achieved [21].

The above theory has been used in the TALYS – 1.6 and EMPIRE – 3.2.2 nuclear modular codes [23, 24]. Further details of these codes are given in literature [18–19]. Using these codes, (γ, n) nuclear reaction cross section for different isotopes ($Z \geq 60$) were calculated and are presented in the present thesis work. Until now, the photonuclear reaction cross sections have been evaluated using the Lorentz parameters. These parameters for several isotopes were calculated by fitting the experimental data or by systematics [25], but these parameters are not available for all the unstable isotopes.

3.3. Development of the Empirical Formula

3.3.1 Introduction

The present empirical formula has been developed using a few terms required to reproduce the cross section as a function of the incident photon energy. Initial derivation of the formula was done by using the earlier empirical formula used to explain neutron induced nuclear reaction cross section [26]. The present formula has three basic terms; 1. The fundamental term, 2. Isotopic resonance term and 3. Energy dependency term. These terms are discussed below.

3.3.2 Fundamental Term

In contrast to the Lorentzian parameters, the basic properties of nuclei A, N and Z were used to estimate the photonuclear cross section. Levovskii had given empirical formulae for (n, p) and (n, 2n) reaction cross section at 14.0 MeV [26],

$$\sigma(n, p) \propto \sigma_p \cdot e^{-\frac{33\cdot(N-Z)}{A}} \quad 3.4$$

$$\sigma(n, 2n) \propto \sigma_\alpha \cdot e^{-\frac{33\cdot(N-Z)}{A}} \quad 3.5$$

where $\sigma_p = \pi r_0^2 (A^{1/3} + 1)^2$ and $\sigma_\alpha = 0.4 \cdot \pi r_0^2 (A^{1/3} + 1)^2$

$r_0 = 1.2 \times 10^{-13}$ cm

These empirical formulae are based on A, N, and Z of a nucleus, and at fixed energy 14.0 MeV. These were modified to obtain an empirical formula for photo induced (γ,

n) nuclear reaction, which may be applied near to GDR peak energy. This modification is as given below.

$$\sigma(\gamma, n) \propto \sigma_m \cdot e^{-\frac{33.5\cdot(N-Z)}{A}} \quad 3.6$$

$$\sigma_m = \pi r_0^2 \cdot (A^{2/3} + 1)^2 \cdot (N - Z) \cdot A^{\frac{-4}{3}} \quad 3.7$$

where r_0 is the average nuclear radius. This is taken as the fundamental term of the present empirical formula.

3.3.3 Isotopic Resonance Term

The experimental data shows the resonance nature of the reaction cross section, which depends on the isotope, i.e., the GDR peak energy is different for the different isotopic number. Thus for a given GDR peak, the cross section decrement is distributed on the either sides of GDR peak energy. Hence a term representing such phenomena must be included.

The modified formula is given below,

$$\sigma(\gamma, n) \propto \sigma_m \cdot e^{-\frac{33.5\cdot(N-Z)}{A}} \cdot e^{\left(-\left(\frac{\left(Ei - S_j \cdot R_p\right)}{2}\right)^2\right)} \quad 3.8$$

Where E_i and R_p are the incident photon energy and resonance parameter respectively.

In this modification, two parameters are specifically used, R_p and S_j.

The parameter S_j can be calculated by,

$$S_j = \frac{A^2}{2(N-Z)^2} \quad 3.9$$

The parameter R_p is estimated for an isotope, by fitting the (γ, n) nuclear reaction cross section using the above formula for different isotopes of the same element. It was observed that this parameter R_p is following a linear relationship against the atomic mass of the different isotopes of the same element, which can be written in the form of the following equation,

$$R_p = m \cdot A + C \quad 3.10$$

Where A is the atomic mass of the isotope, and m and C are the slope and intercept respectively, More details of this parameter (R_p) for different elements is given in subsection 3.3.5.

This term $e^{-[\{\frac{(Ei-S_j \cdot Rp)}{2}\}^2]}$ depends on the energy of the incident photon and the isotopic nature of the target nucleus. When a photon is incident on the nucleus, the response depends on the photon energy. If the incident photon is below the threshold energy for photo fission, it cannot eject a nucleon from the nucleus. If energy of the photon is above the threshold energy of the (γ, n) reaction, the reaction cross section increases until the resonance peak energy is reached. After this energy, again the cross section decreases. This is incorporated using this exponential term. The subtraction of $S_j \cdot R_p$ from the incident photon energy shows the isotopic dependence of the resonance peak energy of the reaction. It was observed in the experimental data that as the isotopic number increases, the GDR peak shifts towards the lower energy side. This back shift effect can be calculated with the exponential term considered here. The value of $S_j \cdot R_p$ increases with addition of neutrons to the isotope nucleus. This means that when a photon is incident on the target isotope, it interacts with the last shell neutron in the nucleus. The binding energy of the last added neutron will be least. Hence the photon may require smaller energy to initiate the resonance isotope number.

This phenomenon can be observed in FIGS 3.1 and 3.2, showing the isotopic effect for the resonance peak energy back shifting in Nd and Pt isotopes using the above exponential term.

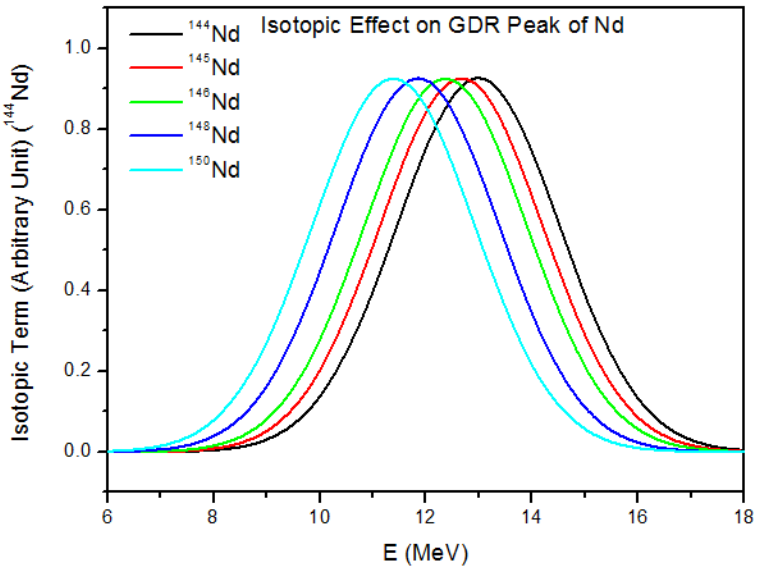

FIG 3.1 Backshift of Resonance Peak Energy in Nd isotopes which is result from the term $e^{\left(-(\frac{(Ei-Sj \cdot Rp)}{2})^2\right)}$

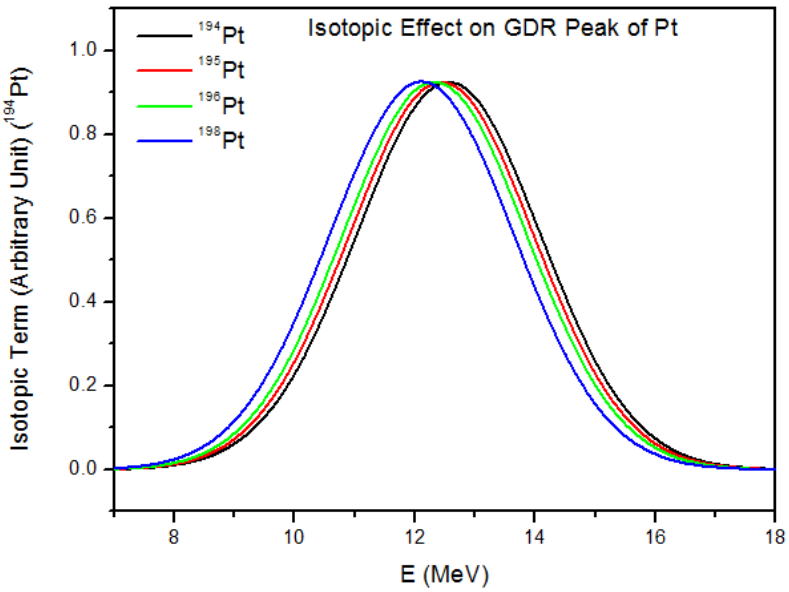

FIG 3.2 Backshift of Resonance Peak Energy in Pt isotopes which is result from the term $e^{\left(-(\frac{(Ei-Sj\cdot Rp)}{2})^2\right)}$

3.3.4 Energy Dependency Term

There is a need to introduce an energy related term to make the formula to predict the cross section more accurately. If the photon energy increases, then it can transfer more energy to the nucleus. In the mechanism of GDR, the oscillating electrical field transfers its energy to the nucleus by inducing an oscillation in the nucleus, which leads to the relative displacement of tightly bound neutrons and protons inside the nucleus [12]. When the energy of the photon is low (near to the threshold), the oscillating electric field of the photon interacts with the collective nuclear field produced by the sum effect of all the nucleons. However, as the energy of the photon increases, the oscillating electrical field interacts with a pair of neutron and proton rather than the whole nucleus. This can be accounted by the term $e^{\sqrt{1+E^{\frac{2}{3}}}}$, where E is the energy of the incident photon. This term shows that photon can have more energy to transfer to the nucleons as the incident photon energy increases. It also indicates that as the energy of the photon increases, it can have less interaction time with nucleons. In this way, the emission of neutrons by pre-equilibrium or direct reaction mechanism can also be explained.

Hence, by the addition of an energy dependent term, the modified formula becomes,

$$\sigma(\gamma, n) \propto \sigma_m \cdot e^{-\frac{33.5\cdot(N-Z)}{A}} \cdot e^{\left(-\left(\frac{\left(Ei-S_j\cdot Rp\right)}{2}\right)^2\right)} \cdot e^{\sqrt{1+E^{\frac{2}{3}}}} \qquad 3.11$$

An additional factor S_f which depends on isospin has been introduced to complete the formula. This factor was plotted and fitted for different isotopes of the same element. It was observed that factor follows some exponential relation, which is described in subsection 3.3.6. This empirical formula gives the cross section to the order of milli-barn.

The final modified formula is now given below,

$$\sigma(\gamma, n) = \sigma_m \cdot e^{-\frac{33.5\cdot(N-Z)}{A}} \cdot e^{\left(-\left(\frac{(Ei-Sj\cdot Rp)}{2}\right)^2\right)} \cdot e^{\sqrt{1+E^{\frac{2}{3}}}} \cdot S_f \qquad 3.12$$

3.3.5 R_p Parameter

As discussed in section 3.3.3, the parameter R_p is used to show the isotope dependency of the reaction cross section. In the empirical formula the term $e^{-[\{\frac{(E_i-S_j\cdot R_p)}{2}\}^2]}$, contains the S_j and R_p parameters. The parameter R_p is responsible for the change in the cross section due to atomic number, where the product of S_j and R_p accounts for the isotopic back shift effect, as shown in FIGS. 3.1 and 3.2. The parameter R_p for different isotopes can be calculated using a linear relation given by eq. 3.10 with the atomic mass number of isotopes for an element. Therefore, the plots of R_p against A for different elements should be parallel lines with different intercepts on R_p axis as shown in FIG 3.2. It is a property of parallel lines that they have same slope but different intercepts. Hence, the mean slope of the different element has been taken as the standard slope for all elements ($Z \geq 60$). This value of the slope (m) mentioned in eq. (10) is ~ 0.03164 ± 0.00409. The intercept C for different elements are plotted against the atomic number of an element, and fitted with mathematical software MATLAB, using 3rd degree polynomial as shown in FIG 3.3. The intercept C for a different element can be determined from the following equation.

$$C(Z) = p_1\cdot Z^3 + p_2\cdot Z^2 + p_3\cdot Z + p_4 \qquad 3.13$$

with $p_1 = -4.155 \times 10^{-5}$, $p_2 = 0.008971$, $p_3 = -0.7156$, and $p_4 = 15.78$, Z = Atomic number

(SSE: 0.00147; R-square: 0.9998: Adjusted R-square: 0.9996; RMSE: 0.01917)

Hence, the intercept for any element can be evaluated using the above eq. 3.13, which is fixed for different isotopes of the same element. Using this intercept and the slope 0.03164 ± 0.00409 one can calculate the parameter R_p from eq. 3.10. The model values of the parameter R_p for different elements are compared with the previous manually selected values as shown in FIG 3.2.

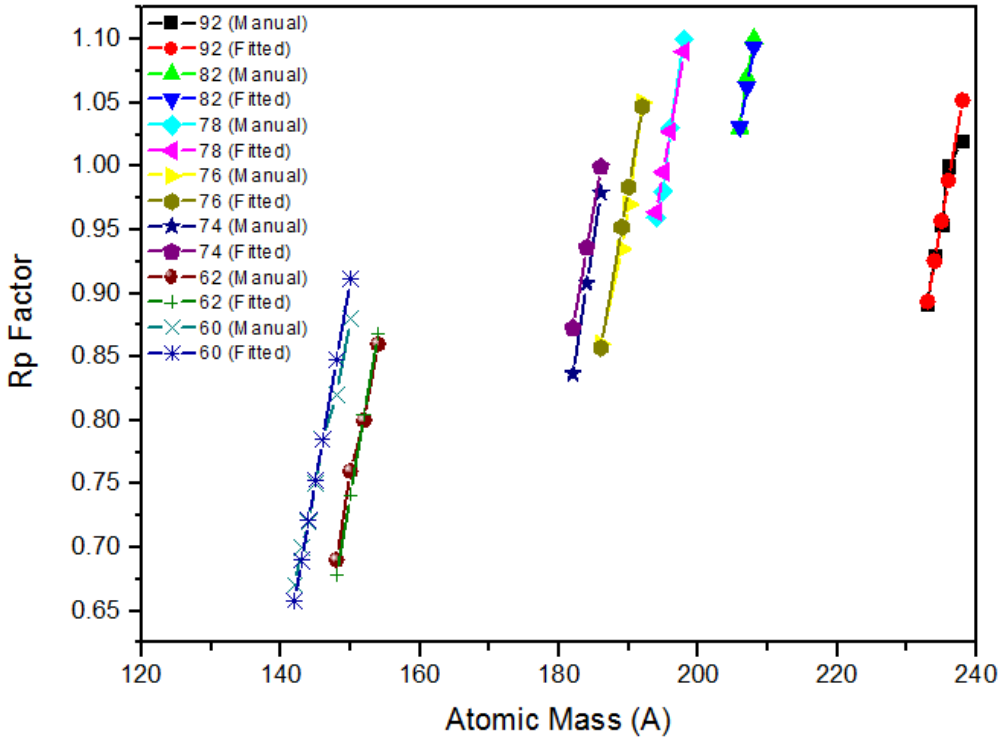

F IG 3.3 R_p parameter fitted for different elements using eq. 3.10

3.3.6 S_f Parameter

This parameter includes the isospin effect, as discussed by J. S. Wang *et al*., [27]. In order to include this effect in the empirical formula, an additional factor called S_f has been added. This factor was initially added and then, in order to generalize it is fitted with different combinations of N, Z and A. Thus it follows a complex exponential relation with exp((N – Z)/N) of an isotope. This parameter S_f is also considered as a result of the asymmetry of the nucleus. As there is a difference in neutron and proton number, the fraction (N – Z)/N is the available neutron fraction for a photon to eject. As this fraction value increases, the value of S_f also increases, which directly shows increment in the photoabsorption cross section of that isotope.

This isotopic factor S_f for different isotopes is plotted with respect to exp((N – Z)/N,) and fitted with MATLAB software as shown in FIG 3.4. The generalized expression to determine S_f parameter for an isotope is as given below.

$$S_f = ae^{bx} + ce^{dx} \qquad 3.14$$

where, x = (N – Z)/N, a = 1.21×10^{-22}, b = 34.21, c = 7.71×10^{-11}, d = 14.52

(SSE: 0.006977; R-square: 0.9781; Adjusted R-square: 0.9759; RMSE: 0.01551)

Looking at FIG 3.5 carefully, when $e^{\frac{(N-Z)}{N}}$ is between 1.40 to 1.42, then S_f factor has almost same values. These S_f values are for Z = 82 and N = 124, 125, 126, which is either a magic number or near to the magic number. S_f is purely dependent on (N – Z)/N, which is a shell dependent term. The anomalous behavior of the S_f factor values for these isotopes is due to the magic shell effect.

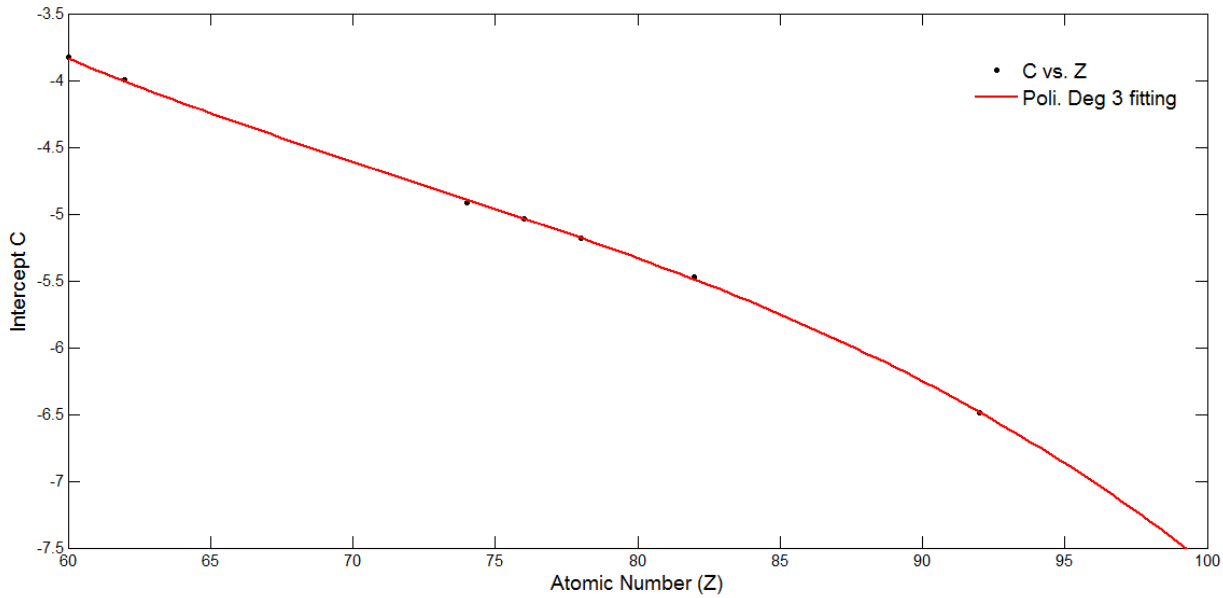

FIG 3.4 Intercept C for eq. 3.10 for different elements fitted with eq. 3.11

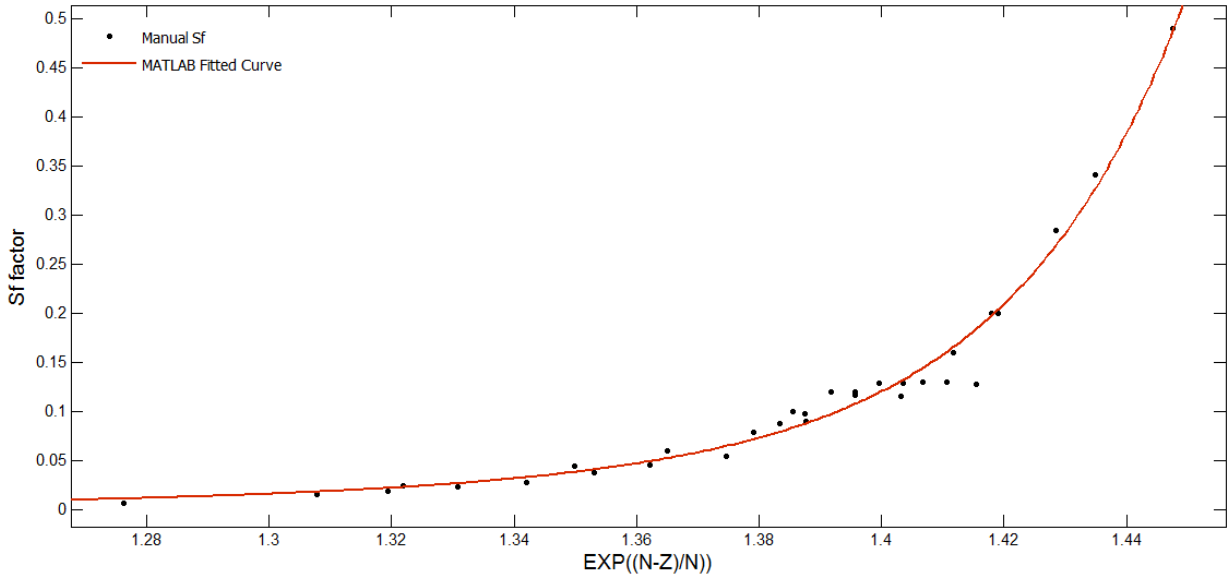

FIG 3.5 S_f parameter for different (N-Z)/N fitted with eq. 3.14

3.4. Results and discussion

The (γ, n) reaction cross section for different isotopes with Z ≥ 60 was calculated using the newly developed empirical formula. In addition, the nuclear modular codes TALYS – 1.6 and EMPIRE – 3.2.2 were also used to predict the same cross section in order to compare the predictability of present empirical formula and Lorentz curve based model. All the results are compared with the available EXFOR data [28] and are shown in FIGS. 3.6 – 3.10. The cross sections are calculated for the energy range near to GDR peak. The results obtained by modular codes and empirical formulae are in agreement with the experimental data as shown in FIGS. 3.6 – 3.10. However, the empirical formula is giving more appropriate cross section results and predicts the nuclei behavior near to the GDR peak energy region. This empirical formula is good for those isotopes which have a single GDR peak. In most of the cases studied here, that have a single GDR peak, the empirical formula gives good agreement near to the GDR peak energy as compared to the model based on Lorentz curve fitting.

In the case of the isotopes with Z from 63 to 75, it was found that collective model predicts large nuclear quadrupole moment. The quadrupole moment exists because of the asymmetry of the nucleus. The nuclei are found in the middle of the 1d, 2s shells in the range of 145 < A <185. The energy difference between the ground state and the first excited state is of the order of hundreds of keV. In the deformed nucleus, the incident photon can interact either with the ground state or with the excited state

nucleons and hence can produce a resonance at two different nearby energies. This is observed in the above isotopes. For such cases, the Lorentz curve based model, viz. TALYS – 1.6 and EMPIRE – 3.2.2, works reliably for these isotopes, as shown in FIG 3.11. For some cases, however, the TALYS – 1.6 and EMPIRE – 3.2.2 model does not work well, e.g. FIG 3.11(e – f). In order to apply the empirical formula for such isotopes, it is assumed that there may be two peaks due to unresolved resonances occurring near the energies of ground and excited nuclei, which are due to the quadrupole moment. This suggests parameters R_p and S_f can have two different values for these isotopes. It indicates that the energy dependence cross section curve is made of two curves with two different R_p (R_{p1} and R_{p2}) and S_f values (S_{f1} and S_{f2}) of parameters R_p and S_f respectively. These values can be estimated by multiplying the following factors to the R_p and S_f values calculated from Sections 3.3.5 and 3.3.6.

$$R_{p1} = 0.95 \text{ x } R_p \tag{3.15}$$

$$R_{p2} = 1.20 \text{ x } R_{p1} \tag{3.16}$$

$$S_{f1} = 1.39 \text{ x } S_f \tag{3.17}$$

$$S_{f2} = 0.28 \text{ x } S_{f1} \tag{3.18}$$

The two curves are intersecting at a deep point, where both curves should have the same value of cross section. This intersection point energy can be calculated by comparing the right side of the eq. 3.12 for above values.

$$\sigma_m \cdot e^{-\frac{33.5\cdot(N-Z)}{A}} \cdot e^{\left(-\left(\frac{(Ei-S_j\cdot R_{p1})}{2}\right)^2\right)} \cdot e^{\sqrt{1+E^{\frac{2}{3}}}} \cdot Sf1 = \sigma_m \cdot e^{-\frac{33.5\cdot(N-Z)}{A}} \cdot e^{\left(-\left(\frac{(Ei-S_j\cdot R_{p2})}{2}\right)^2\right)} \cdot e^{\sqrt{1+E^{\frac{2}{3}}}} \cdot Sf2 \tag{3.19}$$

Solving this eq. we get,

$$E_{deep} = \frac{1}{2} S_j \cdot (R_{p1} + R_{p2}) + \frac{2 \ln\left(\frac{S_{f2}}{S_{f1}}\right)}{S_j (R_{p1} - R_{p2})} \tag{3.20}$$

This energy E_{deep} is near to the threshold energy of the (γ, 2n) reaction. With this consideration, the results are plotted in FIG 3.11(a – f).

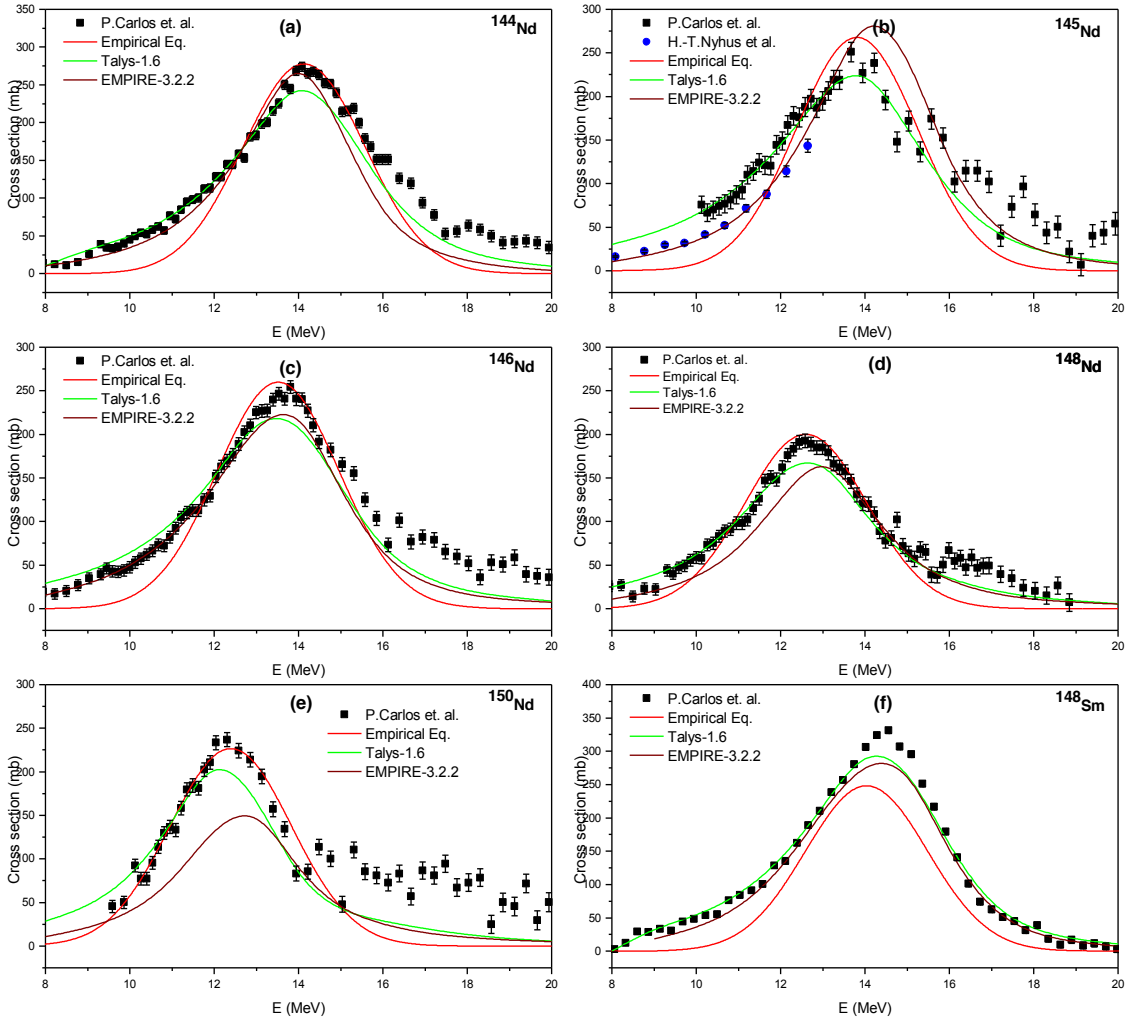

FIG 3.6 Comparison of Evaluated data using TALYS-1.6, EMPIRE-3.2.2, and Empirical Formula with Experimental data from EXFOR comparison for $^{144\text{-}146,148,150}$Nd, and ^{148}Sm

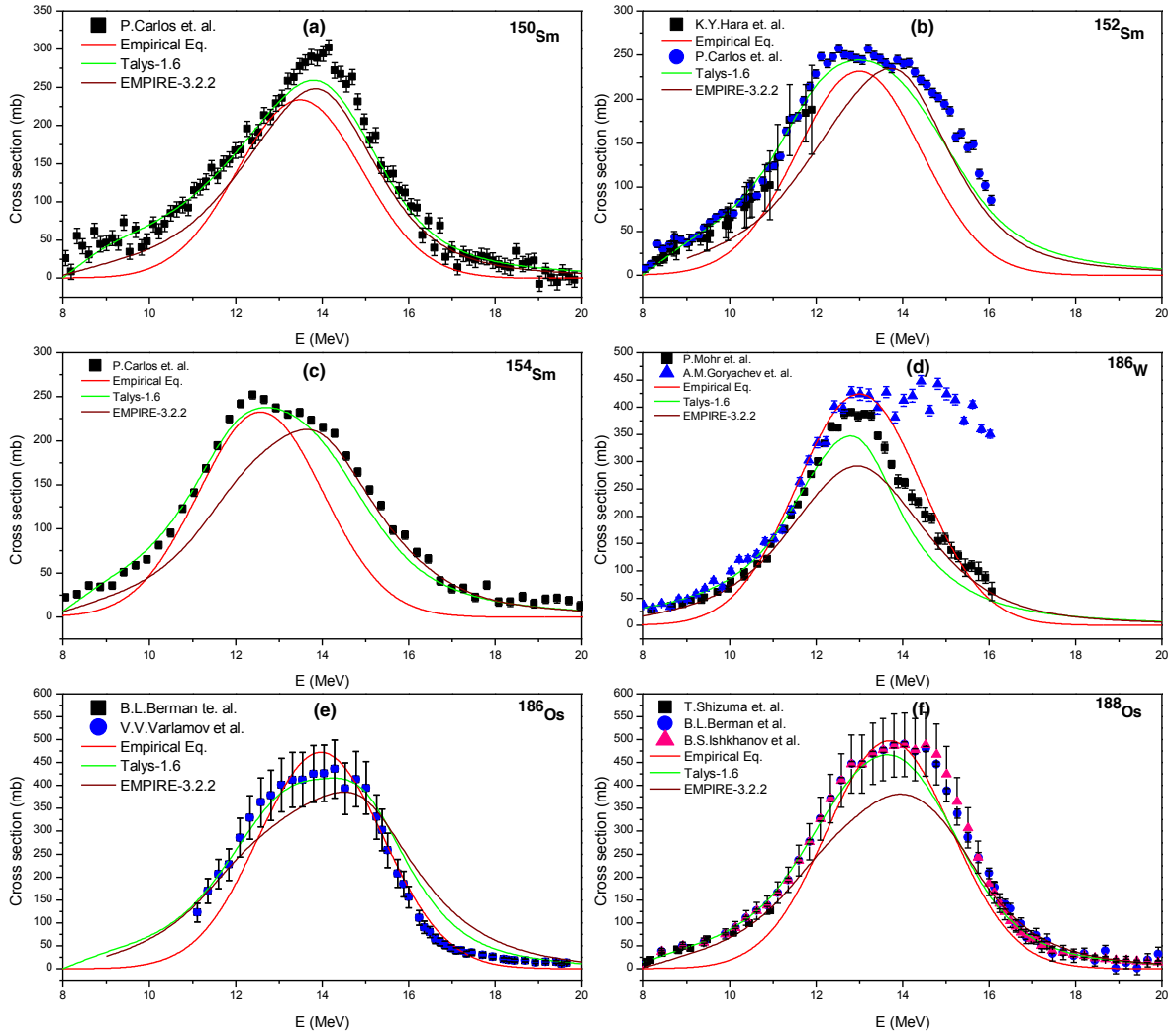

FIG 3.7 Comparison of Evaluated data using TALYS-1.6, EMPIRE-3.2.2, and Empirical Formula with Experimental data from EXFOR comparison for ^{150,152,154}Sm, ^{186}W, ^{186}Os, and ^{188}Os

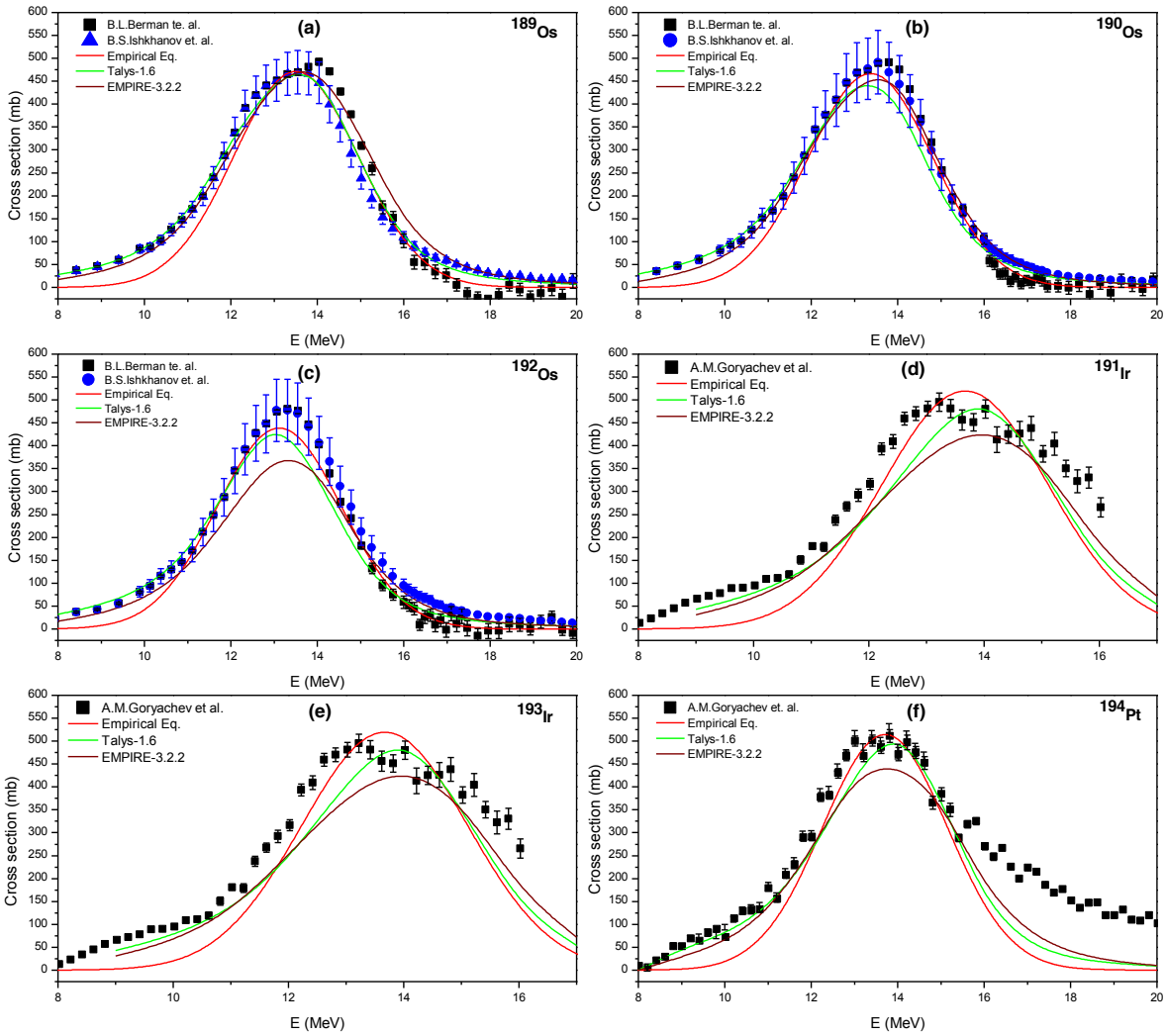

FIG 3.8 Comparison of Evaluated data using TALYS-1.6, EMPIRE-3.2.2, and Empirical Formula with Experimental data from EXFOR comparison for $^{189\text{-}190,192}$Os, ^{191,193}Ir, and ^{194}Pt

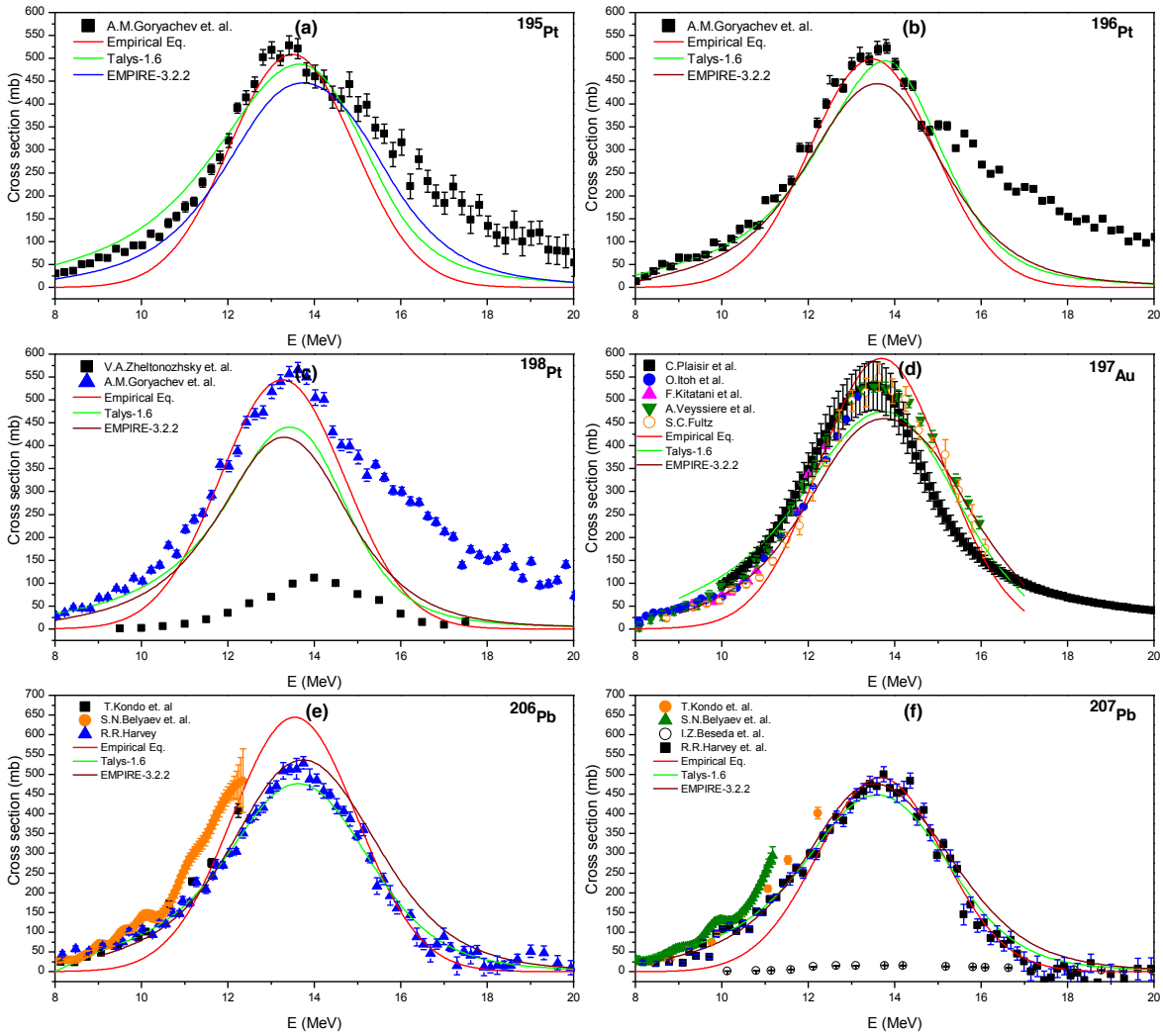

FIG 3.9 Comparison of Evaluated data using TALYS-1.6, EMPIRE-3.2.2, and Empirical Formula with Experimental data from EXFOR comparison for $^{195\text{-}196,198}$Pt, ^{197}Au, ^{206}Pb, and ^{207}Pb

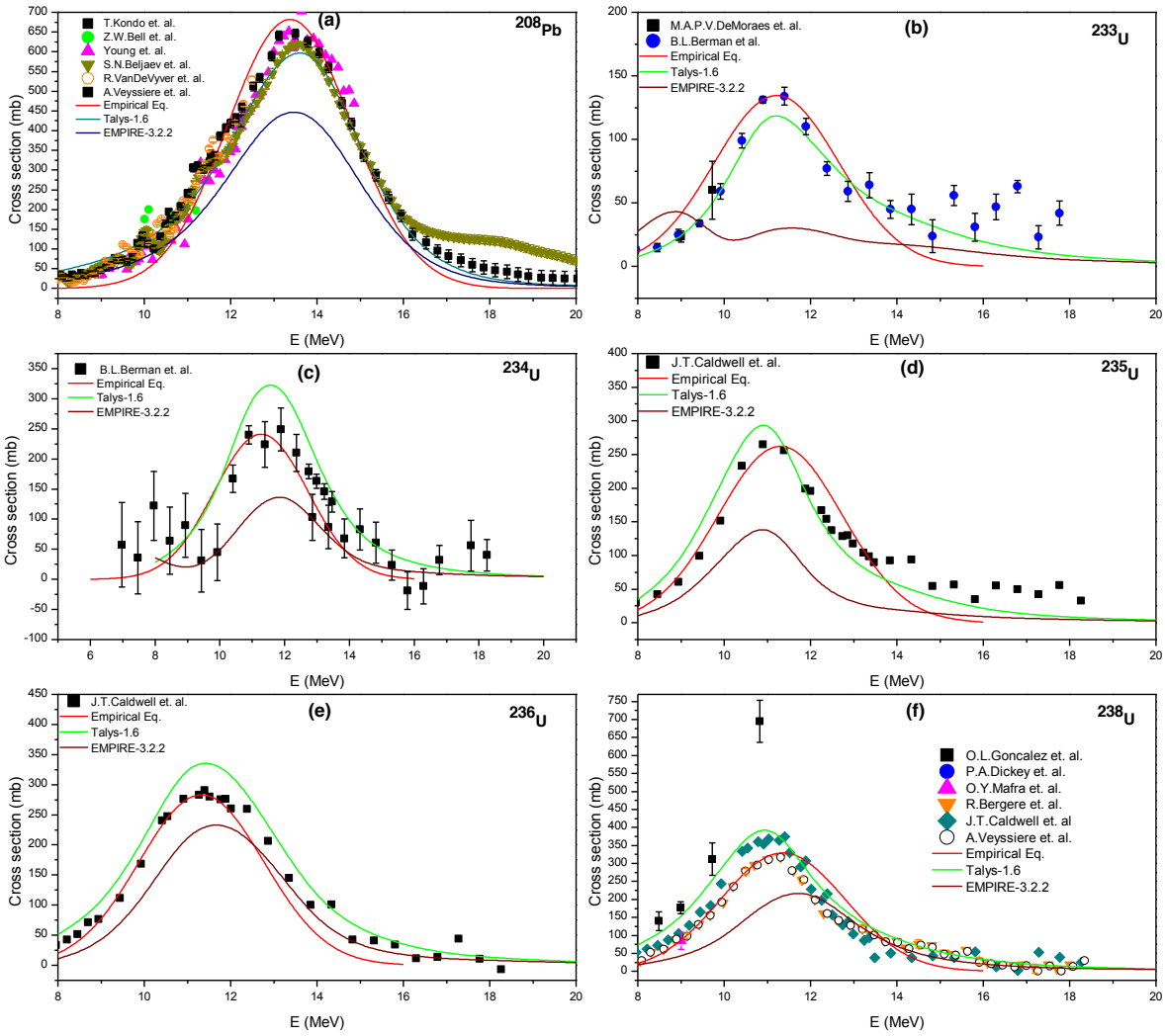

FIG 3.10 Comparison of Evaluated data using TALYS-1.6, EMPIRE-3.2.2, and Empirical Formula with Experimental data from EXFOR comparison for ^{208}Pb, $^{233-236}$U, and ^{238}U

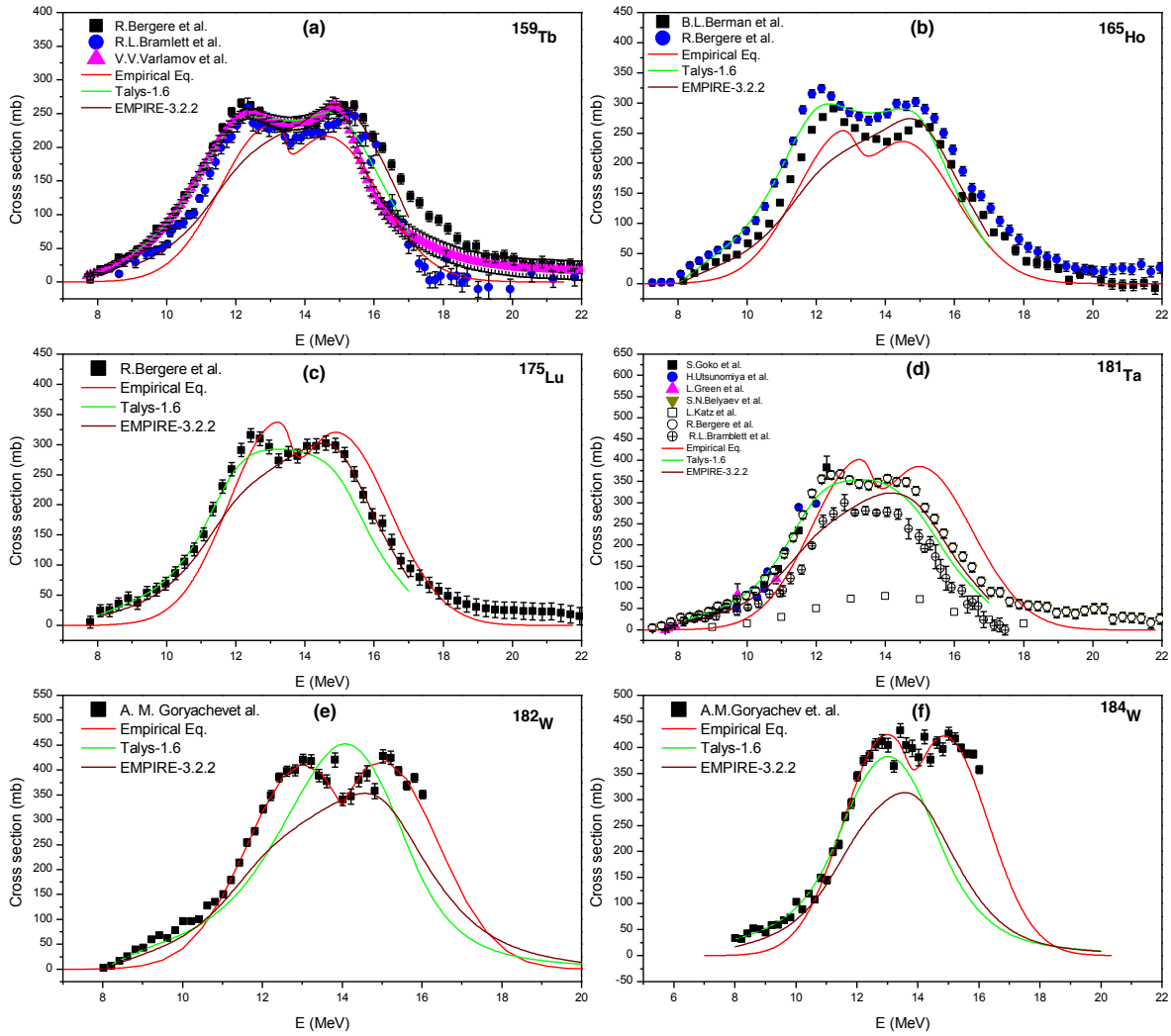

FIG 3.11 Effect of deformed nuclei in (γ, n) nuclear reaction, data comparisons for TALYS – 1.6, EMPIRE – 3.2.2 and Present Empirical formula

3.5. Applications of the Present Empirical Formula

The present empirical formula can be used to predict cross section for (γ, n) reaction for the isotopes with $Z \geq 60$. Here cross section of some selected (γ, n) reaction for some selected reactions was calculated and presented. The (γ, n) cross section for several isotopes of W, Pb, Pa, U and Pu, which have no available experimental data, were calculated using present empirical formula and compared with TALYS – 1.6, EMPIRE – 3.2.2 evaluated data.. Further, the predicted data of the isotopes were compared with different standard evaluated data libraries, wherever available.

Tungsten is a prime candidate for the plasma facing component in a fusion reactor. It is selected for the diverter material in the ITER fusion reactor [4]. Tungsten isotopes

^{182}W, ^{184}W and ^{186}W have experimental data for the (γ, n) reaction cross section [28]. The (γ, n) cross section for remaining isotopes ^{180}W(0.12%) and ^{183}W(14.31%) were calculated and compared with the evaluated data available in ENDF/B-VII.1. No other standard data library has photonuclear data for these tungsten isotopes [19]. There is an agreement between present evaluated data and ENDF/B-VII.1 as can be seen in FIG 3.12 (a – b), where there is not good agreement in FIG 3.13 (c – d). Lead is a prime element for the Pb-Li blanket module of the fusion reactors, as well as, it is also a candidate for the ADS target material [29]. Experimental data are available for lead isotopes ^{206}Pb, ^{207}Pb and ^{208}Pb. The (γ, n) cross section for remaining isotopes of lead ^{202}Pb (5.25×10^4 y, [30]), ^{203}Pb (51.92 h, [30]), ^{204}Pb (1.4×10^{17} y, [30]) and ^{205}Pb (1.73×10^7 y, [30]) were calculated and presented. These isotopes of lead have a large half-life and they are facing high energetic photons during the runaway electron generation and the disruption phase in plasma [5]. There are some isotopes of Pa and U: ^{231}Pa(3.27×10^4 y, [30]), ^{232}U(68.9 y, [30]) and ^{237}U(6.75 d, [30]) having no evaluated cross section data in various standard data libraries, such as ENDF/B-VII.1, JENDL-4.0, JEFF-3.1, ROSFOND and CENDL-3.1 [31,32]. The cross sections for these isotopes were also calculated and presented. The evaluated data for ^{239}Pu (2.41×10^4 y, [30]) and available data in ENDFB/VII.1 are presented in FIG 3.13 (d). Though in the present context, cross sections are evaluated for limited isotopes, it can be applied to calculate (γ, n) reaction cross section for actinides using the nuclear modular codes and present empirical formula. While the TALYS – 1.6 and EMPIRE – 3.2.2 codes can be used to calculate the (γ, n) reaction cross section for the isotopes, which have available GDR parameters, whereas the present empirical formula can be used to calculate cross section for any isotope with $Z \geq 60$.

Another important application is, to use the nuclear modular codes and the present formula to calculate the incident gamma energy for which, the cross section will have maximum value i.e. at the GDR peak energy. It can be used to calculate the incident charge particle (e.g. electron) beam energy for the bremsstrahlung production, which is required to design a photoneutron source. There are some theoretical transport codes available to transport the electrons and photons such as MCNP [12, 33-34], FLUKA [35, 36], GEANT [37] etc. Using these codes, one can estimate the bremsstrahlung spectra from the electron beam.

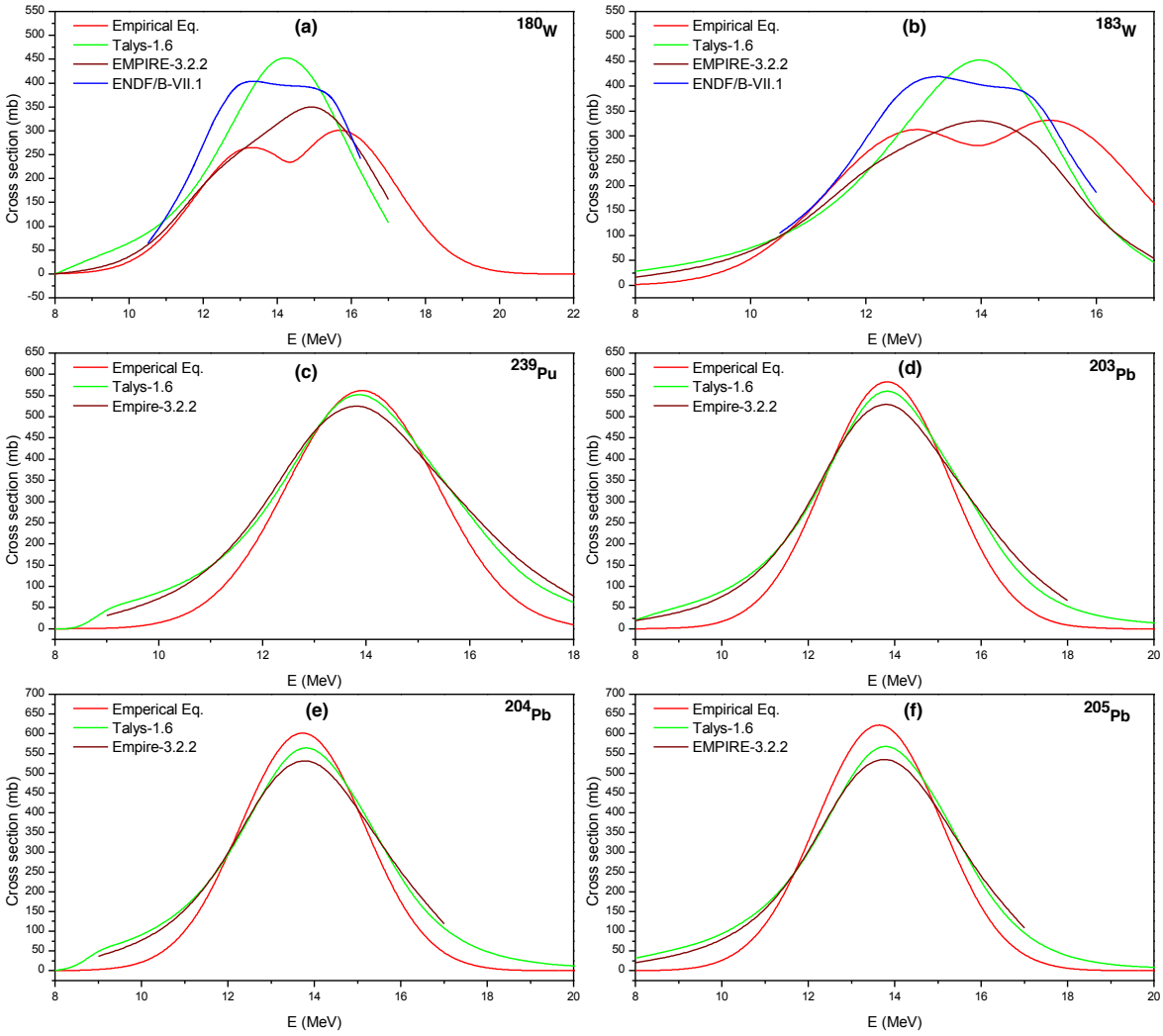

FIG 3.12 Comparison of Evaluated data for ^{180,183}W, $^{202\text{-}204}$Pb, and ^{205}Pb using TALYS -1.6, EMPIRE-3.2.2, and empirical formula

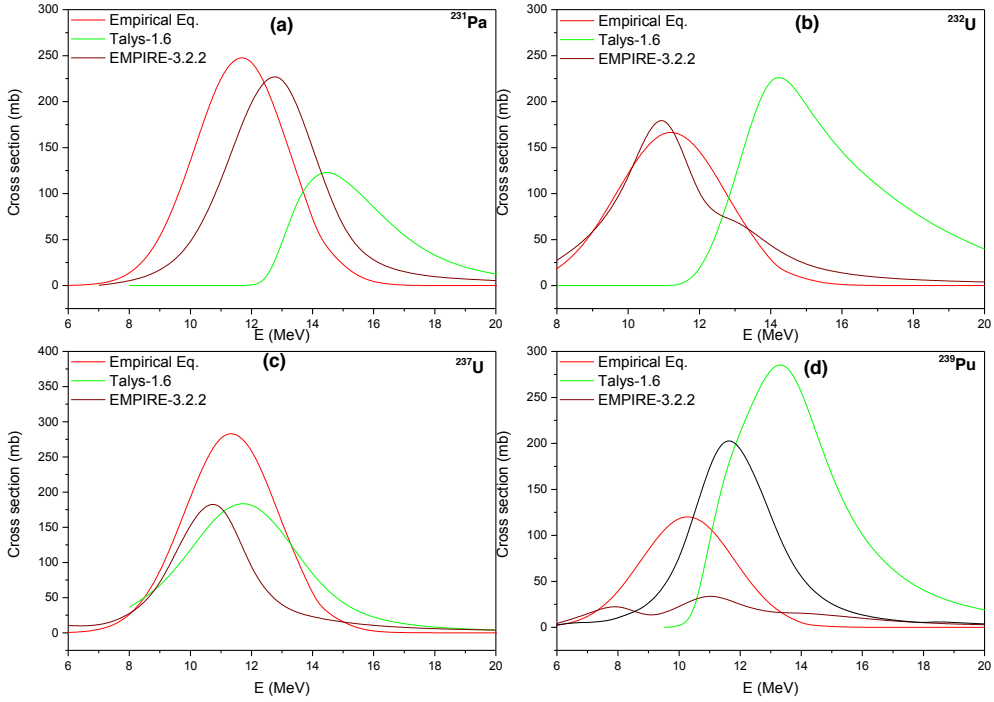

FIG 3.13 Comparison of Evaluated data for ^{231}Pa, ^{232,237}U, and ^{239}Pu using TALYS - 1.6, EMPIRE-3.2.2, and Empirical Formula

3.6. Summary and conclusions

A new empirical formula has been developed to investigate the (γ, n) reaction cross section for isotopes with Z ≥ 60 in the GDR energy region. The results for the (γ, n) reaction cross section obtained by using the above empirical formula has been reproduced by using the nuclear modular codes: TALYS – 1.6 and EMPIRE – 3.2.2. It has been shown that TALYS – 1.6, EMPIRE – 3.2.2 and the empirical formula is in agreement with the experimental data. Further, a conclusion may be drawn that there may be no deformation in the GDR peak of a pure (γ, n) reaction cross section for the spherical nucleus. As a result of the quadrupole moment, which is due to the asymmetric shape of the nucleus, the present deformation has been observed.

In addition to this, the evaluated data for $^{180\text{-}184}$W, $^{202\text{-}205}$Pb, ^{231}Pa, $^{232\text{-}237}$U, and ^{239}Pu using TALYS – 1.6, EMPIRE – 3.2.2 and our empirical formula have been presented. Among these only ^{180}W, ^{183}W and ^{239}Pu have evaluated data in ENDF/B-VII.1 [29], which are compared with the present evaluated data. For $^{180\text{-}184}$W, the present evaluated data are in good agreement, but in the case of ^{239}Pu, it is in disagreement. It is necessary to do experiments in the GDR energy range to validate the present

evaluated data for ^{239}Pu. Further, though here only limited isotopes have been used for the (γ, n) reaction cross section evaluation, the empirical formula can be applicable to other isotopes provided $Z \geq 60$.

References

[1] http://www-pub.iaea.org/MTCD/publications/PDF/te_1178_prn.pdf, retrieved 16th May 2016

[2] A.R. Junghans, et al., Phys. Lett. B, 670: 200 (2008)

[3] S. J. Zweben, H. Knoepfel, Phys. Rev. Lett., 35: 1340 (1975)

[4] R. A. Pitts, et al., Journal of Nuclear Materials, 463: 39-48 (2013)

[5] A. Shevelev, et al., doi: 10.1063/1.4894038, retrieved 17th May 2016

[6] B. L. Berman, et al., Phys. Rev., 162: 1098 (1967)

[7] C. H. M. Broeders, et al., Nucl. Eng. Des., 202: 157 (2000)

[8] F. R. Allum, et al., Nucl. Phys. A, 53 645 (1964)

[9] H. Naik, et al., Nucl. Phys. A, 916: 168-182 (2013)

[10] I. Raškinyte˙, et al., in Proc. Int. Conf. on Nuclear Reaction Mechanisms, (Varenna, Italy: Dapnia/SPhN, 2006), DAPNIA-06-147

[11] G. Kim, et al., Nucl. Instrum. Methods Phys. Res., Sect. A, 485: 458-467 (2002)

[12] V. C. Petwal, et al., PRAMANA — journal of physics, 68: 235 (2007)

[13] M. Gallardo, et al., Phys. Lett. B, 191: 222-226 (1987)

[14] M. Mattiuzzi, et al., Phys. Lett. B, 364: 13-18 (1995)

[15] P. Heckman, et al., Phys. Lett. B, 555: 43 (2003)

[16] Balaram Dey, et al., Phys. Lett. B, 731: 92-96 (2014)

[17] H. Steinwedel, et al., Z. Naturforsch., 5a: 413 (1950)

[18] B. L. Berman, At. Data Nucl. Data Tables, 15: 319-390 (1975)

[19] M. Danos, Nucl. Phys., 5: 23 (1958)

[20] G. Reffo, Phys. Rev. C, 44, 814 (1991)

[21] S. Levinger, Phys. Rev., 84: 43 (1951)

[22] J. S. Levinger, in Nuclear Photo Disintegration (Oxford University Press, Oxford, 1960) p.54

[23] A. Koning et al., TALYS – 1.6 A nuclear reaction program, (2013) p.62

[24] M. Herman et al., EMPIRE – 3.2 Malta modular system for nuclear reaction calculations and nuclear data evaluation, (2013) p.18-20

[25] T. Belgya, et al., Handbook For Calculations of Nuclear Reaction Data, (IAEA, Vienna, RIPL-2, IAEA-TECDOC-1506, 2006), http://www-nds.iaea.org/RIPL-2

[26] V. N. Levkovski, J. Phys., 18: 361 (1974)

[27] J. S. Wang et al., Eur. Phys. J. A, 7: 355-360 (2000)

[28] https://www-nds.iaea.org/exfor/exfor.htm, retrieved 4th December 2015

[29] Akito Takahashi, et al., Fusion Engineering and Design, 9: 323 (1989)

[30] http://www.nndc.bnl.gov/chart/chartNuc.jsp, retrieved 2nd November 2015

[31] https://www-nds.iaea.org/photonuclear/, retrieved 4th December 2015

[32] http://www.nndc.bnl.gov/sigma/index.jsp?dontshow=nn.6&as=9&lib=jendl3.3&nsub=20040, retrieved 4th December 2015

[33] Grady Hughes, Progress in Nuclear Science and Technology, 4: 454-458 (2014)

[34] X-5 Monte Carlo Team, MCNP-A General Monte Carlo N-Particle Transport Code, Version 5, (2000) 1

[35] A. Fassò, et al., Advanced Monte Carlo for Radiation Physics, Particle Transport Simulation and Applications, in Proceedings of the Monte Carlo 2000 Conference, edited by A. Kling, et. al., (Lisbon, 2000) 159-164

[36] P. K. Sahani et al., Indian J. Pure Appl. Phys, 50: 863-866 (2012)

[37] Boubaker Askri, Nucl. Instrum. Methods Phys. Res., Sect. B, 360: 1-8 (2015)

Chapter – 4

Measurement of (n, γ), (n, p) and (n, 2n) reaction cross sections of W and Gd isotopes

---

Publication related to this chapter:

Rajnikant Makwana, S. Mukherjee, P. Mishra, H. Naik, N.L. Singh, M. Mehta, K. Karel, S. V. Suryanarayana, V. Vansola, Y. Shanthisheela, M. Karkera, R. Acharya, S. Khirwadkar, "Measurements of cross sections of ^{186}W (n,γ) ^{187}W, ^{182}W (n, p) ^{182}Ta, ^{154}Gd (n, 2n) ^{153}Gd, ^{160}Gd (n, 2n) ^{159}Gd reactions between 5 to 17 MeV neutron energies"

Physical Review C (Accepted 8th July 2017; In press)

Impact Factor: 3.82

4.1. Introduction

Nuclear reaction cross section data is of prime importance for the reactor technology. When the reactor is in operation, it produces neutrons that penetrate through several materials, such as fuel, structural, controlling and shielding materials, etc. It is important to have nuclear reaction cross section data for all these materials, at all possible neutron energies [1] for the development of the reactor technology. There are numerous measured nuclear data available in the EXFOR data library [2]. However, it is important to have more experimental nuclear data, measured with high accuracy in the energy range between thermal to 20 MeV for a number of reactor materials [2]. Tungsten (W) and gadolinium (Gd) are two such materials. W is selected as a diverter material for the upcoming fusion device – International Thermonuclear Experimental Reactor (ITER) [3]. In ITER the DT reaction generates 14.6 MeV neutrons, which are scattered from the surrounding materials, thus neutrons will have energies from thermal to 14.6 MeV [4-9]. These neutrons interact with the diverter material of the reactor and can open different nuclear reaction channels. In Accelerator Driven Subcritical system (ADSs), W is used in different parts, hence it can face neutrons with higher energies [10]. Further, Gd is an important rareearth element, which is used in control rods. Its nitrate form is useful for reactor control through moderator as liquid poison, as well as a secondary shutdown device in PHWR reactors [11]. Gadolinium nitrate is more advantageous due to its properties, such as; high thermal neutron capture cross section, quick burnout, greater solubility and a more efficient removal by ion exchange systems compared with boron [12]. Hence it is important to have accurate cross section data for all the tungsten and gadolinium isotopes in the energy range from thermal to 20 MeV. Accurate experimental data is also needed to validate the various theoretical nuclear models [13]. In view of this, in the present work, cross sections for the $^{186}W(n, \gamma)^{187}W$, $^{183}W(n, p)^{183}Ta$, $^{154}Gd(n, 2n)^{153}Gd$ and $^{160}Gd(n, 2n)^{159}Gd$ reactions at the neutron energies of 5.08 ± 0.165, 8.96 ± 0.77, 12.47 ± 0.825 and 16.63 ± 0.95 MeV were measured by neutron activation analysis (NAA) and the off-line gamma ray spectrometry technique. The above mentioned reaction cross-sections were also calculated by using the computer codes TALYS – 1.8 and EMPIRE – 3.2.2. Different ldmodels available in TALYS – 1.8 and levden models in EMPIRE – 3.2.2 were used to validate the present experimental results.

4.2. Experimental details

4.2.1 Target Preparation

To conduct the experiment, four samples of W and two samples of GdO_2 were required for the irradiation. The W samples (99.9 % pure) were prepared at the Divertor Group, Institute for Plasma Research, Gandhinagar, India. The circular samples of W of the diameter of 10 mm and thicknesses of 1 mm to 3 mm were cut in four equal quadrants. The Gd samples were made from the GdO_2 powder (99.9 % pure). Pellets were made using pelletizer at the Physics Department, The M. S. University of Baroda, Vadodara. Gd samples were made in the pellet form with a radius of 0.65 cm and of thickness from 0.05 to 1.0 mm using Gd_2O_3 (99.9 %) powder. The weights of the samples were measured using digital weighing machine available at TIFR, Mumbai. The weights of W samples were 3.6689 g (Irradiation – 1), 0.7826 g (Irradiation – 2), 0.8344 g (Irradiation – 3) and 0.504 g (Irradiation – 4). The samples of Gd weighing 0.4071 g (irradiation – 1) and 0.9102 g (irradiation – 3) were used.

4.2.2 Neutron Irradiation at TIFR

The experiment was carried out using the 14UD BARC-TIFR Pelletron facility in Mumbai, India. A schematic layout of the Pelletron is given in FIG 4.1(a). The neutrons were produced using $^{7}Li(p, n)^{7}Be$ reaction. A proton beam was targeted on natural lithium foil of thickness 8.0 mg/cm^2 at 6.0 m from the analyzing magnet. The Li foil was wrapped with 3.7 mg/cm^2 tantalum in front and 4.12 mg/cm^2 in the back side like a sandwich structure. The samples were enclosed with aluminum foil to avoid contamination. The targets were irradiated with four different selected proton energies: 7.0, 11.0, 15.0 and 18.8 MeV. The spread of the proton energy at 6 m height was maximum 50 – 90 keV. The samples were kept at a distance of 2.1 cm from the Li - target in the forward direction. The targets were irradiated for different irradiation time. The irradiation details are given in Table 4.1. A schematic view of irradiation setup is shown in FIG 4.1(b). In each irradiation, the Indium (In) and thorium (Th) foils were used as flux monitor. After a suitable cooling time, the irradiated samples were mounted on different perspex plates and kept in front of the pre-calibrated High Purity Germanium (HPGe) detector. A Baltic company HPGe detector with 4k channels MCA and MAESTRO spectroscopic software were used to measure the

gamma ray spectra from the irradiated samples. The gamma spectrometer setup for activity counting is shown in FIG 4.1(c). The HPGe detector system was calibrated using standard ^{152}Eu multi-gamma source. The efficiency of the detector was also calculated at different energies using the same source. The gamma ray activities of the irradiated samples were measured for different counting time. The prominent gamma energies emitted from the irradiated samples and other spectroscopic data are given in Table 4.2. Isotopic abundances are taken from literature [14]. The threshold energies of the reactions are calculated using Q – value calculator provided online by NNDC [15]. The product half-life and details of the emitted prominent gamma rays are taken from ENDSF database [16]. Typical gamma ray spectra obtained from the irradiated W and Gd samples are shown in FIG 4.2 (a-b).

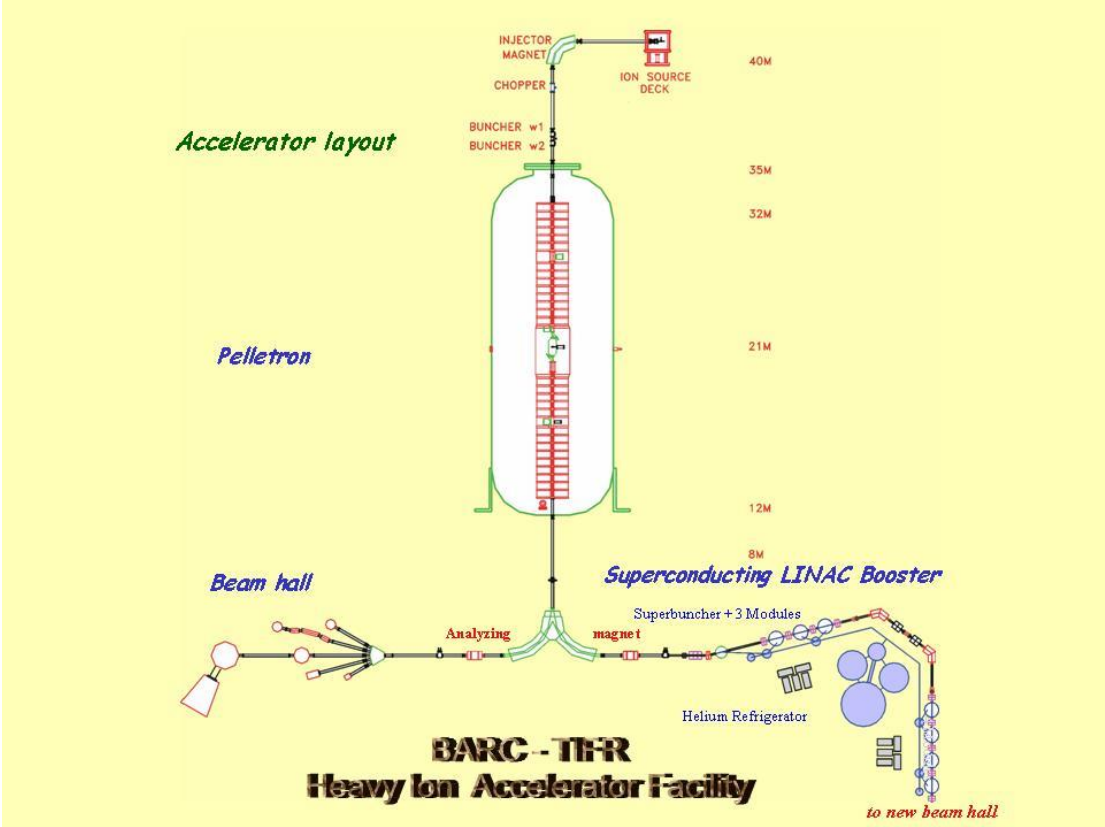

FIG 4.1(a) 14 UD TIFR-BARC Pelletron facillity

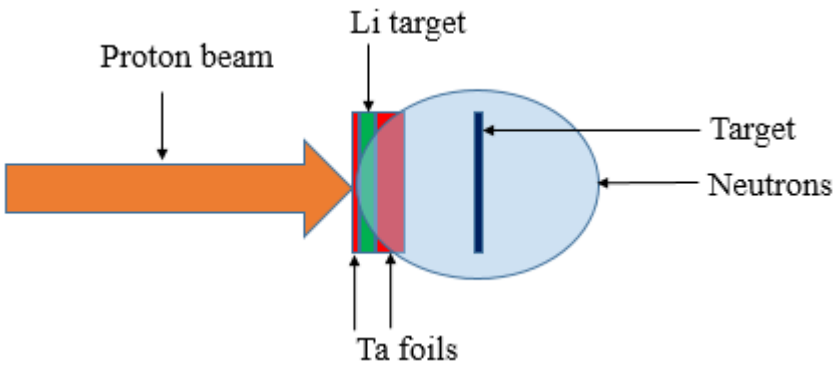

FIG 4.1(b) Experimental arrangement showing neutron production using Li (p, n) reaction

FIG 4.1(c) Gamma spectroscopy system for activity measurement

Table 4.1 Details of the irradiation at TIFR

	Irradiation - 1	**Irradiation-2**	**Irradiation-3**	**Irradiation-4**
Proton Energy (MeV)	18.8	7.0	15.0	11.0
Total Irradiation Time (hr:mm)	5:00	11:15	7:00	16:05
Beam Current (nA)	150	110	150	120

Table 4.2 Selected nuclear reactions, isotopic abundance, threshold energy of reaction, product isotope with half-life and prominent gamma ray energies with branching intensities

Reaction	**Isotopic Abundance (%) [14]**	**Threshold Energy (MeV) [15]**	**Product Nucleus**	**Half-life [16]**	**Prominent γ-ray (in keV) (Branching intensity %) [16]**
^{186}W(n, γ)^{187}W	28.43	-	^{187}W	24.0 h	479.5(26.6); 685.7(33.2)
^{182}W(n, p)^{182}Ta	26.50	1.037	^{182}Ta	114.74 d	1121.3(35.24)
^{154}Gd(n, 2n)^{153}Gd	2.18	8.953	^{153}Gd	240.4 d	103.1 (21.1)
^{160}Gd(n, 2n)^{159}Gd	21.86	7.498	^{159}Gd	18.479 h	363.5 (11.78)

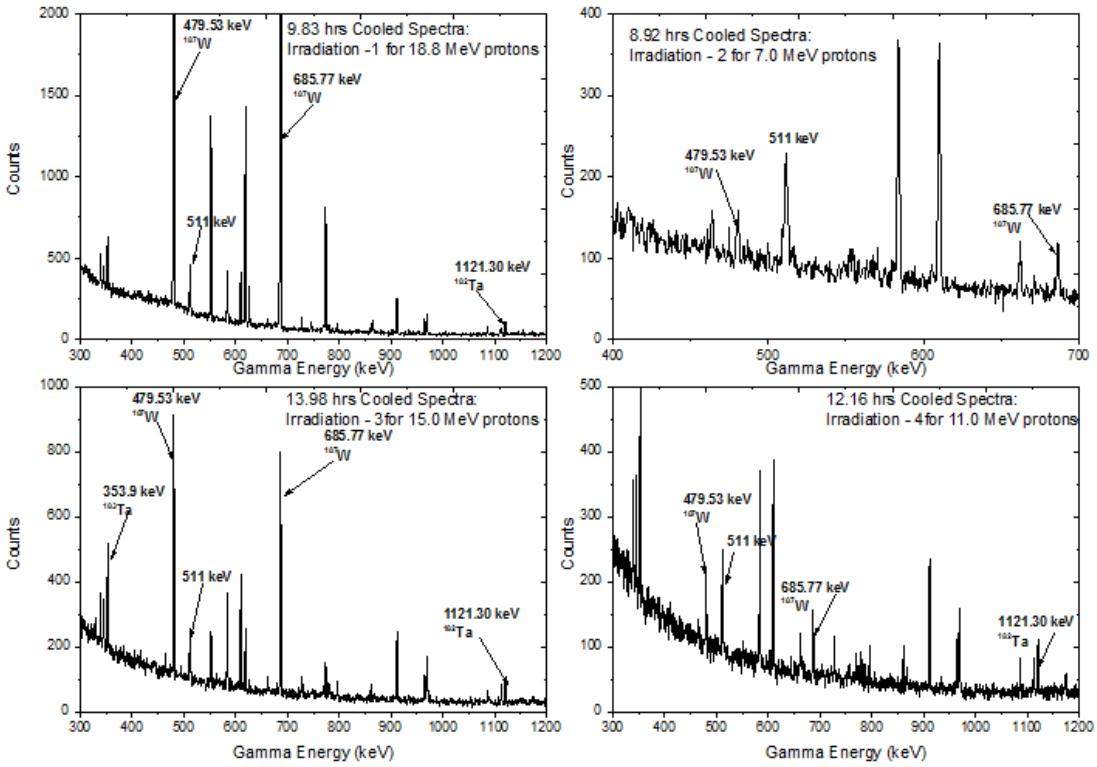

FIG 4.2(a) Typical γ-ray spectra for W targets obtained by using HPGe detector

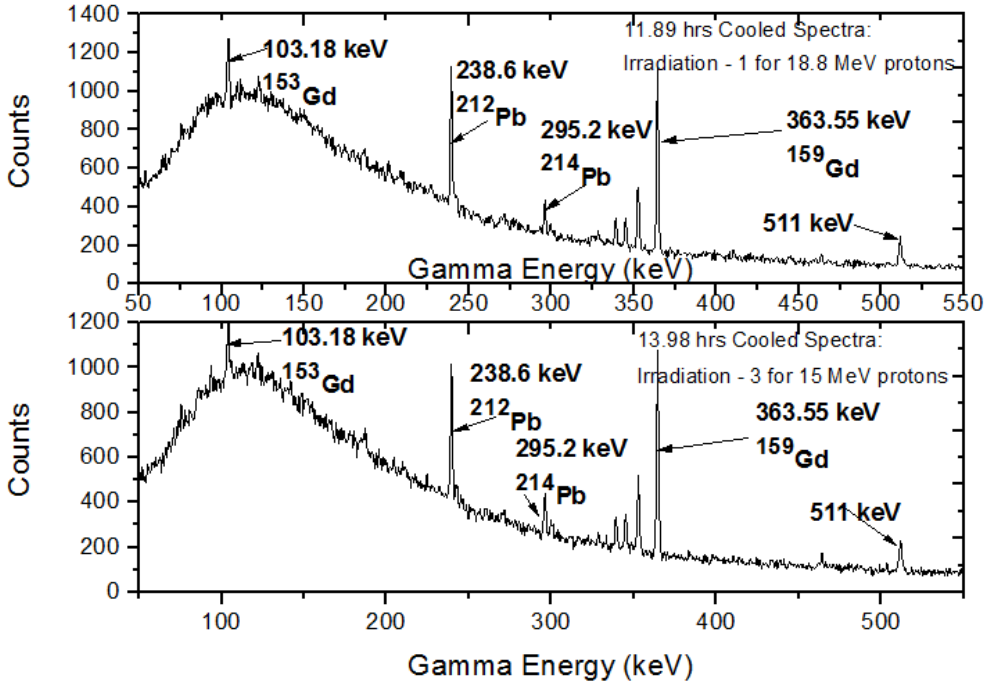

FIG 4.2(b) Typical γ-ray spectra for Gd targets obtained by using HPGe detector

4.3. Data analysis

4.3.1 Neutron Activation Analysis

The neutron activation analysis (NAA) method has already been discussed in Chapter – 1. The experimental data were analyzed by using this technique. A neutron interacts with the target nucleus and excites it by transferring the kinetic energy and it may follow the nuclear reaction. Through the nuclear reaction, the target nucleus transmutes into another product nucleus. This product nucleus may be radioactive and have certain half-life to decay. During the decay, it emits the radiation. This decay radiation carries the information of the production of the excited nucleus. The nuclear reaction rate or the rate of production of product isotopes depends on the number of target nuclei available and the neutron flux incident on it, as mentioned in eq. 1.13 of Chapter – 1. This method is usually used to measure reaction cross section by irradiating the target isotope with neutrons. The total production of the product nuclei can be measured by the characteristic gamma rays emitted from it. The cross section of the selected reactions can be determined using the following eq. 4.1 [17]. The derivation of eq. 4.1 is discussed in Chapter – 1.

$$\sigma = \frac{A_\gamma \cdot \lambda \cdot (t_c/t_r)}{N \cdot \emptyset \cdot I_\gamma \cdot \varepsilon \cdot (1-e^{-\lambda \cdot t_i}) \cdot (1-e^{-\lambda \cdot t_c}) \cdot e^{-\lambda \cdot t_w}} \qquad 4.1$$

Where,

A_γ= Number of detected gamma ray counts;

λ = Decay constant of product nucleus (s^{-1})

t_i = Irradiation time (s);

t_w = Cooling time (s);

t_c = Counting time (s);

t_r = Real time (Clock time) (s);

$\emptyset$ = Incident neutron flux ($n/cm^2/s$);

I_γ= Branching intensity of γ -ray;

ε = Efficiency of the detector for the chosen gamma ray;

N = Number of target atoms

In the above equation, the activity A_γ is measured using the HPGe detector for selected gamma rays emitted from the radioactive product isotope. The detector efficiency for different gamma ray energies was measured using ^{152}Eu multi-gamma

ray source. Keeping in view the half-lives of the interested isotopes, several rounds of gamma ray countings were done. The dead time of the detector system was kept below 0.6 % during the entire counting process. The numbers of target nuclei were calculated from the weight of the sample and isotopic abundances. The calculation of the neutron flux was done using the gamma ray spectra of irradiated In and Th foils. Other standard parameters of the reactions were taken from literature [14-16]. The cross section measurements of selected reactions along with other parameters are given in Table 4.2.

4.3.2 Peak average neutron energy

The neutrons were generated via ^{7}Li(p, n)^{7}Be reactions. The reaction Q – value is -1.886 MeV. Below 2.4 MeV, this reaction produces mono-energetic neutrons [18]. Above 2.4 MeV, the first excited state of ^{7}Be at 0.43 MeV may populate and produce the second group of neutrons [18, 19]. Above 6 MeV, the three body interaction takes place, and other excited states also get populated which can contribute to neutron production along with the main neutron group [18, 19]. Hence the source is not a pure mono energetic source. Although there are lower energy sub-group of neutrons, the primary (main) group of neutrons have always larger flux and can be used to measure the reaction cross section. The spectrum averaged neutron energy can be calculated using eq. 4.2 [20]. In this equation, one has to calculate the convolution of neutron flux values and energies, which are forming the peak neutrons. This is given by the numerator term in eq. 4.2. The denominator term gives the total neutron flux under the peak. The ratio of these two terms gives the spectrum peak averaged neutron energy. The neutron spectra corresponding to all the four incident proton energies are shown in FIG 4.3(a). And the FWHM energy has been taken for this energy range. This can be visualized in FIG 4.3(b). To calculate the neutron peak average energy, one has to take the energies from the starting energy of peak forming (E_{ps}) to peak ending (maximum, E_{max}) neutron energy and respective neutron production cross section/flux ($\emptyset_i$) with possible energy bins. The integration of the multiplications of E_i and $\emptyset_i$ taken between this two mention energy limits. Then it is divided with the total $\emptyset_i$ in between this energies.

$$E_{mean} = \frac{\int_{Eps}^{Emax} E_i \emptyset_i dE}{\int_{Eps}^{Emax} \emptyset_i dE} \quad 4.2$$

where E_{ps} = peak neutron energy forming start energy of the reaction

E_{max} = maximum neutron energy

E_i = energy bin

$\emptyset_i$ = neutron flux of energy bin E_i

E_{mean} = effective mean energy

The neutron spectra for 7.0, 11.0, 15.0 and 18.8 MeV proton energies were derived by taking data from various available literature [18-22].

4.3.3 Neutron Flux Calculation

In order to analyze the data, it is necessary to accurately calculate the neutron flux incident on the target. In the present experiment, ^{115}In(n, n′)^{115m}In and ^{232}Th(n, f)^{97}Zr were taken as monitor reactions for neutron flux measurement. The product nuclei of the reaction products ^{115m}In and ^{97}Zr have half-lives of 4.486 h and 16.749 h respectively [16]. The emitted characteristic gamma lines are given in Table 4.4. Typical gamma ray spectra obtained from both the monitors are shown in FIG 4.4.

The calculations of neutron flux incident on the target were done by using the spectrum averaged neutron cross section for the above monitor reactions by using the data available EXFOR data library [1]. The spectrum average cross section was calculated using the following eq. 4.3.

$$\sigma_{av} = \frac{\int_{Eth}^{Emax} \sigma_i \emptyset_i dE}{\int_{Eth}^{Emax} \emptyset_i dE} \quad 4.3$$

where E_{th} = threshold energy of the monitor reaction

E_{max} = maximum neutron energy

σ_i = Cross section at energy E_i for monitor reaction from EXFOR [23-30]

$\emptyset_i$ = neutron flux of energy bin E_i from the FIG 4.3 (a – c)

σ_{av}= Spectrum averaged cross section

The neutron flux incident on targets for all the four irradiations was calculated using the following activation, which is derived from eq. 4.1.

$$\emptyset = \frac{A_\gamma \cdot \lambda \cdot (t_c/t_r)}{N \cdot \sigma_{av} \cdot I_\gamma \cdot \varepsilon \cdot (1-e^{-\lambda \cdot t_i}) \cdot (1-e^{-\lambda \cdot t_c}) \cdot e^{-\lambda \cdot t_w}} \quad 4.4$$

All the parameters are similar to eq. 4.1.

In the case of fission reaction monitor, the fission yield term (Y) will come in the denominator on the right side of the above eq. 4.4. In the cross section calculations, the measured values of the average neutron flux from both the monitors were taken, as both, these values are in agreement with each other within the limits of the experimental error.

4.4. Cross section correction for lower energy neutrons

In order to measure the cross section accurately, it is necessary to make corrections due to the contributions from lower energy neutrons. This correction is not required when the neutron source is purely mono-energetic, which is not in the present case. As mentioned earlier, in addition to a primary neutron group, there exist secondary neutron groups. The contributions from secondary neutrons are due to the excited state of ^{7}Be and three-body reactions above 2.4 and 6 MeV respectively [18]. These secondary groups produce neutrons at energy lower in addition to the primary group neutrons [18, 19]. As the primary neutrons peak is always at much higher energy, it can be considered as a quasi mono-energetic source. It is possible to remove the contributions of low energy neutrons from the primary neutron groups by the process of tailing correction. In the present measurement, the tailing correction has been done using the method given in the literature [20].

First, the cross sections have been calculated using the NAA eq. 4.1 and neutron flux from monitor reactions. For a capture reaction, one has to use total neutron flux, but for the reactions having threshold energy, the neutron flux must be corrected i.e. the neutrons from threshold to maximum energy neutrons. To do this, one has to remove the neutron flux from minimum to threshold energy neutrons, by taking the area under the neutron spectra. For instance, ^{154}Gd(n, 2n)^{153}Gd reaction has threshold energy of 8.953 MeV. Hence, the flux for this reaction must be the area under the curve shown

from '**A'** (threshold energy) to '**B'** (maximum neutron energy) as shown in FIG 4.3(c). This will correct the actual neutron flux, which has produced the desired product isotopes. Using the correct neutron flux, a set of cross sections for all reactions has been calculated. These cross sections are from all the neutron flux including the peak area neutrons. In order to remove the effective spectrum average cross section from threshold to the energy from which peak is starting forming (E_{ps}), it is necessary to take the help of theoretical calculations using modular code TALYS – 1.8 or data available in different evaluated data libraries, to obtain the reaction cross section. These calculated cross sections at different energies are convoluted with the neutron flux. The spectrum average cross section for each reaction was calculated from threshold to energy E_{ps}, and it is subtracted from the previous cross section dataset. The final value thus obtained gives the cross section for the reaction at the spectrum average neutron peak energy.

Using the above method, the cross section for the $^{182}W(n, p)^{182}Ta$, $^{186}W(n, \gamma)^{187}W$, $^{154}Gd(n, 2n)^{153}Gd$ and $^{160}Gd(n, 2n)^{159}Gd$ reactions were measured at the neutron energies of 5.08, 8.96, 12.47 and 16.63 MeV. In the ^{160}Gd (n, 2n) ^{159}Gd and ^{158}Gd (n,γ) ^{159}Gd reactions, a common γ-ray of 363.55 keV (I_γ=11%) is emitted. Therefore, it is necessary to remove the part of the cross section from this capture reaction. At higher energy, the (n, γ) reaction has very small contribution as compared to the lower energy neutrons. Since the lower energy neutron part has been already corrected using the above method, therefore the cross section obtained is purely due to the (n, 2n) reaction. In the same way, the tailing corrections have been applied for all the reactions studied in the present work. The major uncertainties in the measured cross sections are given in Table 4.5.

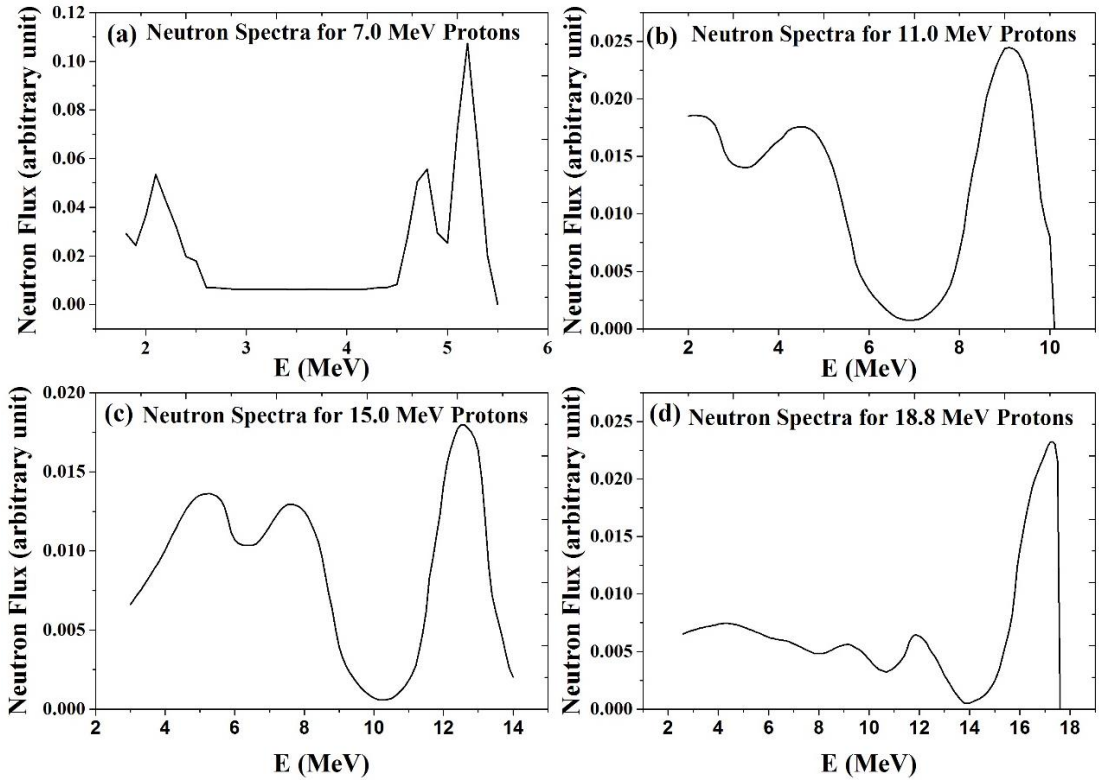

FIG 4.3(a) ^{7}Li (p, n) ^{7}Be neutron spectra for the 7.0, 11.0, 15.0 and 18.8 MeV proton energies

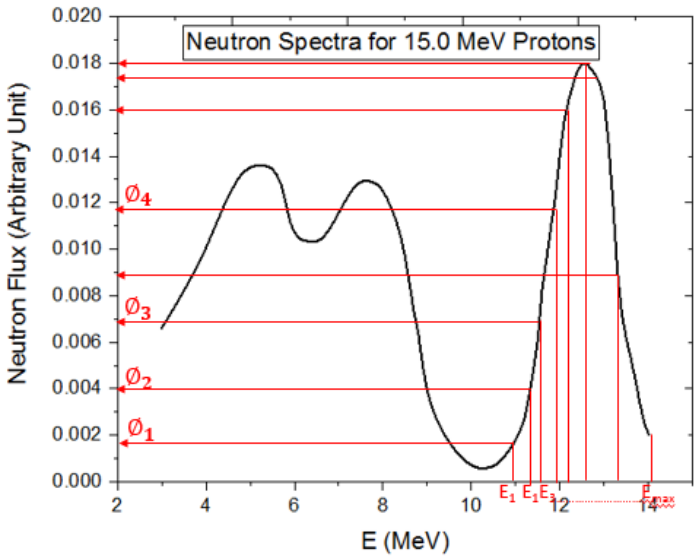

FIG 4.3(b) Visualization of peak averaged neutron energy for 15 MeV neutron peak

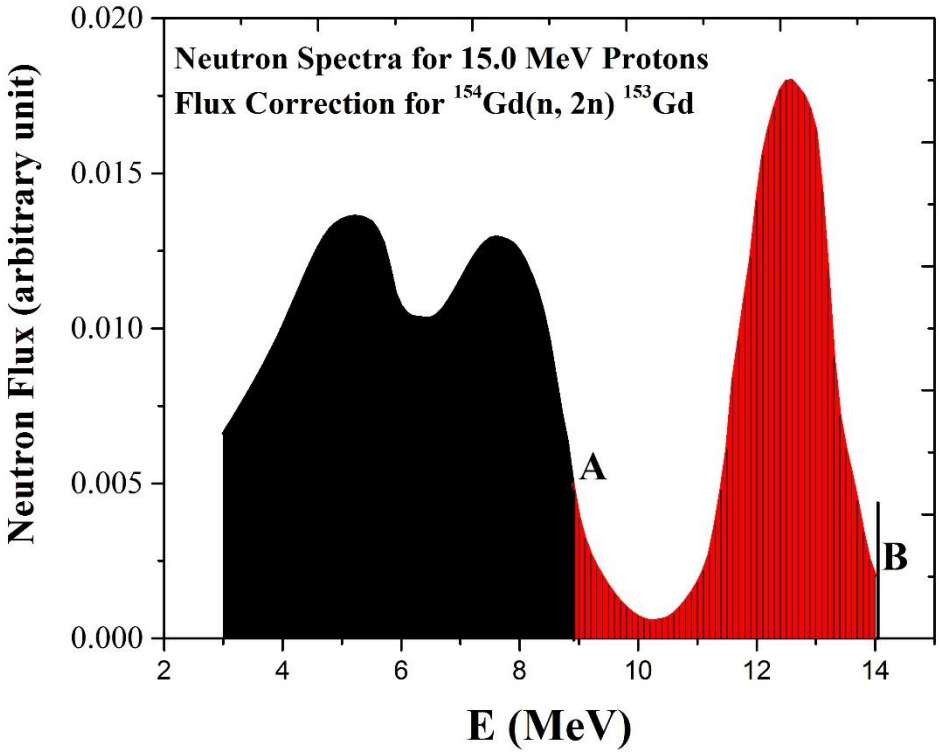

FIG 4.3(c) Neutron flux correction for the threshold energy reactions, shown for ^{154}Gd (n, 2n) ^{153}Gd reaction with threshold energy of 8.953 MeV labeled by **'A'** and maximum neutron energy labeled by **'B'**

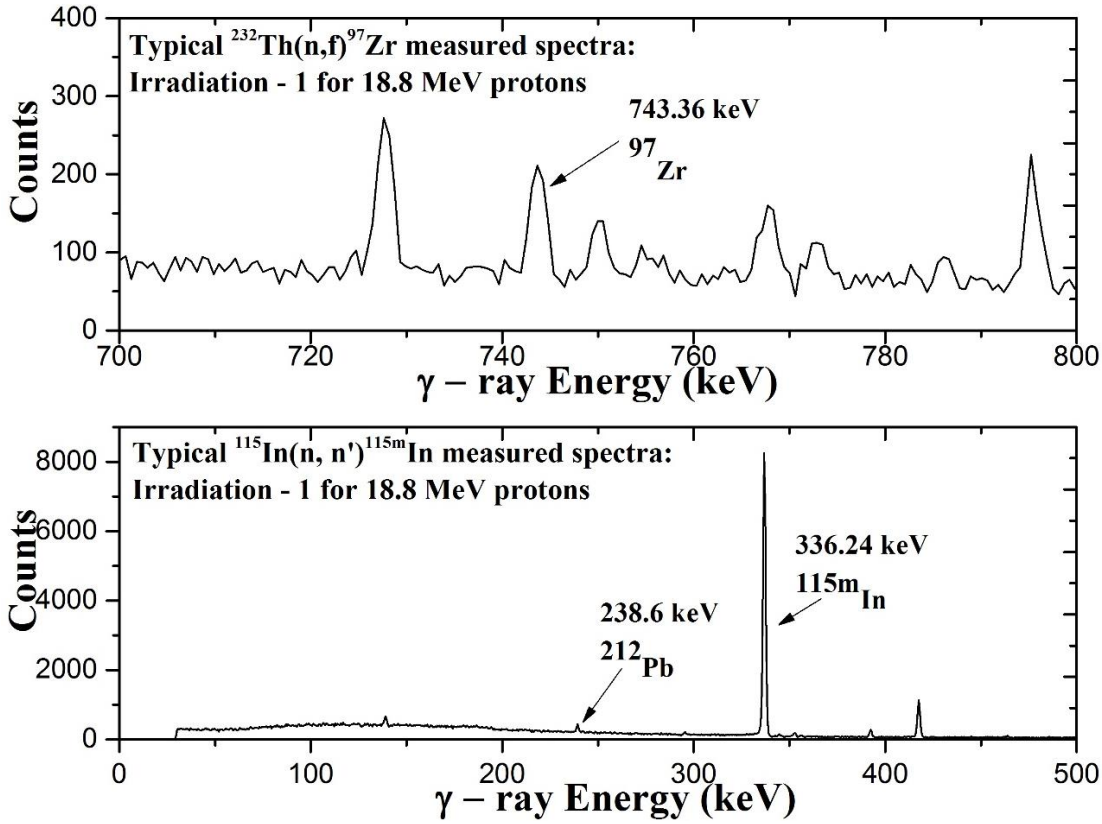

FIG 4.4 Typical monitor reaction gamma ray spectra using HPGe detector

Table 4.3 The spectrum averaged neutron energies and respective neutron flux from two different monitor reactions

	Irradiation - 1	**Irradiation-2**	**Irradiation-3**	**Irradiation-4**
Proton Energy (MeV)	18.8	7.0	15.0	11.0
Neutron Energy from eq. (2) (MeV)	16.63 ± 0.95	5.08 ± 0.165	12.47 ± 0.825	8.96 ± 0.77
Spectrum Averaged Cross section for In monitor (mb)	188.94	223.88	253.79	302.85
Calculated Neutron Flux from ^{115}In(n, n')^{115m}In (n cm^{-2} s^{-1})	6.2891×10^7	4.6304×10^6	1.8054×10^7	1.6009×10^6
Spectrum Averaged Cross section for Th monitor (mb)	341.67	99.04	269.58	220.01
Calculated Neutron Flux from ^{232}Th(n, f)^{97}Zr (n cm^{-2} s^{-1})	6.2885×10^7	4.5709×10^6	1.7090×10^7	1.5850×10^6

Table 4.4 The monitor reaction with the product isotope and prominent gamma lines

Monitor Reaction	**Product Nucleus (Half-life)** [16]	**Prominent gamma Line (in keV) (branching Intensity %)** [16]
^{115}In(n, n')^{115m}In	^{115m}In (4.486 h)	336.24 (45.8)
^{232}Th(n, f)^{97}Zr	^{97}Zr (16.749 h)	743.36 (93.0)

4.5. Theoretical calculations

In order to theoretically understand the measured cross section results, two well-known nuclear reactions modular codes TALYS – 1.8 and EMPIRE – 3.2.2 were used [13]. Both the codes are being used worldwide for nuclear data prediction for the emission of gamma, neutron, proton, deuteron, triton and other particles. Both codes used the reaction parameters from the RIPL database [31]. These codes consider the effect of level density parameters, compound, pre-equilibrium and direct reaction mechanism as a function of incident particle energy. The optical model parameters were obtained by using a global potential, proposed by Koning and Delaroche [32]. The compound reaction mechanism was incorporated using the Hauser-Feshbach model [33]. The pre-equilibrium contribution was accounted by an exciton model that was developed by Kalbach [34]. In the present work, the calculations have been done with all the default parameters except changing the ldmodel and level density parameters. The present results along with EXFOR data were compared with these predicted data as shown in FIG 4.5 (a-d).

4.6. Results and discussion

The main objective of the present study was to provide a set of reaction cross section data in the energy range where there are very few or no measurements available in the literature. These cross sections are important for the accurate reactor design and also to improve the existing nuclear database. Hence the present experimental data for W and Gd isotopes become more important. Further, in this energy region, the standard nuclear models play an important role to validate the present measured experimental data. The major uncertainties in the present reaction cross sections are given in Table 4.5.

The measured data were supported by the theoretical predictions using EMPIRE – 3.2.2 and TALYS – 1.8. There are different options of level density given in EMPIRE – 3.2.2. The level density parameter value levden = 0, 1, 2, 3, 4 uses various well known models described in various publications [31, 35-39]. By varying these parameters, the cross sections for the selected reactions from threshold to 20 MeV were calculated. The predicted and experimental results are shown in FIG 4.5 (a-d). In TALYS – 1.8, the different ldmodel options were varied from ldmodel1 to ldmodel6

for the selected nuclear reactions and the experimental cross sections were compared. The details of these parameters are given in the TALYS – 1.8 manual [39, 40].

As shown in FIG 4.5 (a) for $^{186}W(n, \gamma)^{187}W$ reaction, the levden = 2 of EMPIRE – 3.2.2 gives a relatively better agreement compared to other levden values. But at the lower energy, the levden = 2 does not give satisfactory predictions. Moreover, all other level density models of EMPIRE – 3.2.2 show discrepancies with each other and predicts lower cross section as compared to the present experimental results. In the case of TALYS – 1.8 analyses, results of all the ldmodels options are in good agreement with the data of present measurements. For the ^{182}W (n, p) ^{182}Ta reaction, all TALYS – 1.8 ldmodels are in good agreement. The EMPIRE levden models show a discrepancy with most of the EXFOR and the present data. For the ^{154}Gd (n, 2n) ^{153}Gd and ^{160}Gd (n, 2n) ^{159}Gd reactions, the experimental results are in good agreement with both the TALYS – 1.8 and EMPIRE – 3.2.2 predictions, except levden = 2, being listed as a future option in the EMPIRE input file. Only the measurement at 16.63 MeV neutron energy of $^{160}Gd(n, 2n)^{159}Gd$ is underestimated than the predicted values. Overall the theoretical predictions support the present results. The measured cross section values and the different model predicted values are compared at the same energies in Table 4.6. In general, TALYS – 1.8, for all the selected models, gives better agreement compared to EMPIRE – 3.2.2 in predicting the present experimental results.

Table 4.5 Major uncertainties incorporated in the present cross section results

Parameter	**Limit (%)**
Counting rate	≤ 4 - 5
Efficiency Calibration	≤ 3
Self - absorption	≤ 0.2
Mass	≤ 0.001
Neutron flux	≤ 6
I_γ	≤ 3

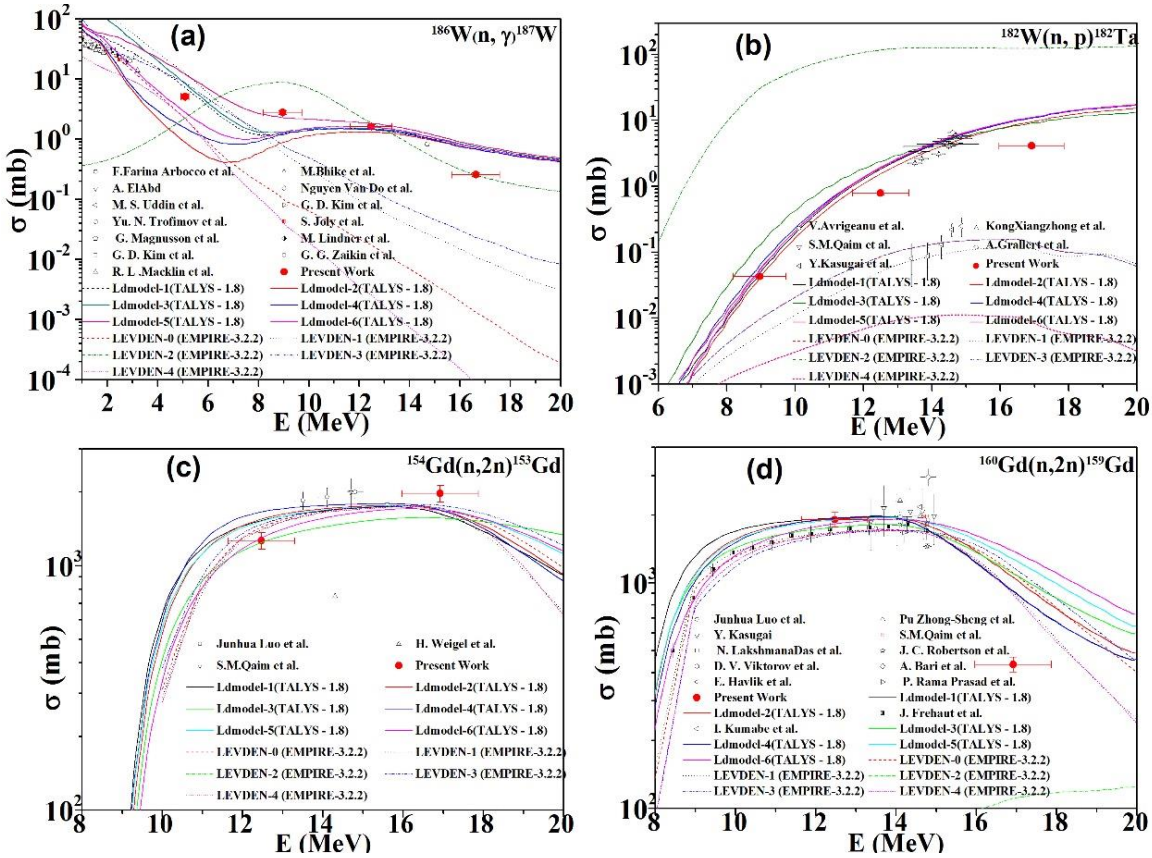

FIG 4.5 Present measured cross section for $^{186}W(n, \gamma)^{187}W$ and $^{182}W(n, p)^{182}Ta$, $^{154}Gd(n, 2n)^{153}Gd$ and $^{160}Gd(n, 2n)^{159}Gd$ reactions compared with EXFOR and predicted cross section data using different theoretical nuclear models of TALYS – 1.8 and EMPIRE – 3.2.2; The LEVDE-2 model of EMPIRE – 3.2.2 predicts very low values (below 100 mb) of cross sections comparing to other models hence it cannot be seen in plot of $^{154}Gd(n, 2n)^{153}Gd$

4.7. Summary and conclusions

Cross section for the $^{182}W(n, p)^{182}Ta$, $^{186}W(n, \gamma)^{187}W$, $^{154}Gd(n, 2n)^{153}Gd$ and $^{160}Gd(n, 2n)^{159}Gd$ reactions were measured at the neutron energies 5.08 ± 0.165, 8.96 ± 0.77, 12.47 ± 0.825 and 16.63 ± 0.95 MeV by using the neutron activation analysis technique and incorporating standard tailing corrections [18]. The cross sections have been measured in an energy range where very few or no measurements are available. The different correction terms are discussed in order to achieve accurate cross section results. The spectrum averaged neutron energy and accurate flux measurements have also been duly incorporated. The neutron flux at different energies have been calculated by using two monitor reactions and the values thus obtained were found to be in good agreement. The average flux values from the two monitor reactions were taken for cross sections calculation. The cross section for the $^{186}W(n, \gamma)^{187}W$ reaction have been measured at four different energies. In the case of $^{182}W(n, p)^{182}Ta$ the cross sections are reported at 8.96 ± 0.77, 12.47 ± 0.825 and 16.63 ± 0.95 MeV. For the $^{154}Gd(n, 2n)^{153}Gd$ and $^{160}Gd(n, 2n)^{59}Gd$ reactions, the cross sections are reported at 12.47 ± 0.825 and 16.63 ± 0.95 MeV neutron energies. All the measurements have been compared with the theoretical modular codes TALYS – 1.8 and EMPIRE – 3.2.2. It may be concluded that TALYS – 1.8 gives an overall satisfactory agreement with the present experimental and EXFOR results for most of the selected ldmodels as compared to EMPIRE – 3.2.2 predictions. However, in the case of (n, γ) reaction, levden = 2 of EMPIRE gives somewhat better predictions as compared to other levden models in the energy region above 12 MeV. The cross section data presented in this work are important for the future fission/fusion reactor technology.

References

[1] A. J. Koning, and J. Blomgren, Nuclear data for sustainable nuclear energy, JRC Scientific and Tech. Rep. EUR23977EN-2009, 15 (2009).

[2] Cross Section Information Storage and Retrieval System (EXFOR), IAEA, Vienna, Austria. http://www.nds.iaea.or.at/exfor/ (online).

[3] M. Lehnen, *et al*., J. Nucl. Mater. **463**, 39 (2013).

[4] J. Qing, Y. Wu, M. Regis, and J. W. Kwan, IEEE Trans. Nucl. Sci. **56**, 1312 (2009).

[5] J. Reijonen, F. Gicquel, S. K. Hahto, M. King, T. P. Lou, and K. N. Leung, Appl. Radiat. Isotopes **63**, 757 (2005).

[6] Y. Wu, J. P. Hurley, Q. Ji, J. Kwan, and K. N. Leung, IEEE Trans. Nucl. Sci. **56**, 1306 (2009).

[7] V. Voitsenya, *et al*., Rev. Sci. Instrum. **72**, 475 (2001).

[8] G. De Temmerman, R. A. Pitts, V. S. Voitsenya, L. Marot, G. Veres, M. Maurer, and P. Oelhafen, J. Nucl. Mater. **363**, 259 (2007).

[9] K. H. Behringer, J. Nucl. Mater.**145**, 145 (1987).

[10] Yousry Gohar, Igor Bolshinsky, and Ivan Karnaukhov, NEA/NSC/DOC (2015) 7, 254 (2015).

[11] R. Vijayalakshmi, D. K. Singh, M. K. Kotekar, and H. Singh, J Radioanal. Nucl. Chem. **300**, 129 (2014)

[12] S. Dutta, P. Suryanarayanan, A. R. Kandalgaonkar, R. S. Sharma, and H. Bose, BARC News Lett, **271**, 2 (2006).

[13] N. Dzysiuk, I. Kadenko, A. J. Koning, and R. Yermolenko, Phys. Rev. C **81**, 014610 (2010).

[14] K. J. R. Rosman, and P. D. P. Taylor, Pure Appl. Chem. **71**, 1593 (1999).

[15] http://www.nndc.bnl.gov/qcalc/index.jsp, retrieved on 11th November 2016.

[16] http://www.nndc.bnl.gov/nudat2/indx_dec.jsp, retrieved on 21st March 2017.

[17] Vibha Vansola, *et al*., Radiochim. Acta **103**, 817 (2015).

[18] C. H. Poppe, J. D. Anderson, J. C. Davis, S. M. Grimes, and C. Wong, Phys. Rev. C **14**, 438 (1976).

[19] J. D. Anderson, C. Wong, and V. A. Madsen, Phys. Rev. Letts. **24**, 1074 (1970).

[20] D. L. Smith, *et al*., " Corrections for Low Energy Neutrons by Spectral Indexing", Retrieved from: https://www.oecdnea.org/science/docs/2005/nsc-wpec-doc2005-357.pdf

[21] P. M. Prajapati, *et al*., Eur. Phys. J. A **48**, 1 (2012).

[22] M. W. Mcnaughton, N. S. P. King, F. P. Brady, J. L. Romero, and T. S. Subramanian, Nucl. Instrum. Methods 130, 555 (1975).

[23] A. A. Lapenas, Neutron Spect. Meas. by Activ., Riga 1975, (1975).

[24] G. Loevestam, M. Hult, A. Fessler,T. Gamboni, J. Gasparro, R. Jaime, P. Lindahl, S. Oberstedt, and H. Tagziria, Nucl. Instrum. Methods in Physics Res., Sect. A 580, 1400 (2007).

[25] Y. Agus, I. Celenk, and A.Ozmen Radiochimica Acta 92, 63 (2004).

[26] M. S. Uddin, Radiochimica Acta 101, 613 (2013).

[27] O. A. Shcherbakov, *et al*., Int. Sem. on Interactions of Neutrons with Nuclei 9, 257 (2001).

[28] R. K. Jain, Pramana 49, 515 (1997).

[29] I. Garlea, Chr.Miron-Garlea, and H. N. Rosu, Revue Roumaine de Physique 37, 19 (1992).

[30] F. Manabe, K. Kanda, T. Iwasaki, H. Terayama, Y. Karino, M. Baba, and N. Hirakawa, Fac. of Engineering, Tohoku Univ. Tech. Report 52, 97 (1988).

[31] R. Capote, et al., Nuclear Data Sheets 110, 3107 (2009).

[32] A. J. Koning, and J. P. Declaroche, Nucl. Phys. A 713, 231(2003).

[33] W. Hauser, and H. Feshbach, Phys. Rev. 87, 366 (1952).

[34] C. Kalbach, Phys. Rev. C **33**, 818 (1986).

[35] https://www-nds.iaea.org/RIPL-3/densities/, retrieved on 28th February 2017.

[36] A. V. Ignatyuk, K. K. Istekov, and G. N. Smirenkin, Sov. J. Nucl. Phys. **29**, 450 (1979).

[37] A.V. Ignatyuk, J. L. Weil, S. Raman, and S. Kahane, Phys. Rev. C **47**, 1504 (1993).

[38] A. Gilbert, and A. G. W. Cameron, Can. J. Phys. **43**, 1446 (1965).

[39] S. Hilaire, M. Girod, S. Goriely and A. J. Koning, Phys. Rev. C **86**, 1 (2012).

[40] A. Koning, S. Hilaire, and S. Goriely, TALYS-1.6 - A Nuclear Reaction Program, User Manual, 1stedition (NRG, The Netherlands, 2013).

Table 4.6 Comparison of present experimental data different model predictions using TALYS – 1.8 and EMPIRE – 3.2.2

Energy (MeV)	$^{186}W(n, \gamma)^{187}W$ reaction cross section (mb)											
	Measured	TALYS - 1.8						EMPIRE – 3.2.2				
		Ldmodel-1	Ldmodel-2	Ldmodel-3	Ldmodel-4	Ldmodel-5	Ldmodel-6	Levden-0	Levden-1	Levden-2	Levden-3	Levden-4
5.08±0.165	5.079±0.39	7.23	0.885	8.37	1.53	12.1	2.80	2.24	12.8	2.24	8.83	2.2903
8.96±0.77	2.767±0.19	1.22	0.871	1.31	1.17	2.26	1.26	0.108	0.618	9.01	0.827	0.0453
12.47±0.825	1.620±0.11	1.46	1.30	1.48	1.43	1.81	1.58	0.0181	0.0794	1.86	0.146	0.0027
16.63±0.95	0.257±0.02	0.726	0.676	0.753	0.683	0.799	0.716	0.00129	0.0107	0.249	0.0226	8.41E-5
Energy (MeV)	$^{182}W(n, p)^{182}Ta$ reaction cross section (mb)											
	Measured	TALYS - 1.8						EMPIRE – 3.2.2				
		Ldmodel-1	Ldmodel-2	Ldmodel-3	Ldmodel-4	Ldmodel-5	Ldmodel-6	Levden-0	Levden-1	Levden-2	Levden-3	Levden-4
8.96± 0.77	0.043±0.003	0.04813	0.04141	0.12659	0.06359	0.05509	0.05307	0.00964	0.00544	31.0747	0.00964	0.00194
12.47±0.825	0.793±0.06	1.789	1.52	2.33301	1.87	1.86	1.92	0.0842	0.0495	118	0.0842	0.00803
16.63±0.95	4.092±0.28	10.2	8.89	8.4404	10.2	10.4	10.5	0.163	0.147	124	0.163	0.0107
Energy (MeV)	$^{154}Gd(n, 2n)^{153}Gd$ Cross Section (mb)											
	Measured	TALYS - 1.8						EMPIRE – 3.2.2				
		Ldmodel-1	Ldmodel-2	Ldmodel-3	Ldmodel-4	Ldmodel-5	Ldmodel-6	Levden-0	Levden-1	Levden-2	Levden-3	Levden-4
12.47±0.825	1265 ±98	1534	1556	1248	1659	1520	1298	1444	1412	22.2	1479	1397
16.63±0.95	1973±153	1683	1725	1571	1737	1735	1703	1748	1744	65.3	1774	1744
Energy (MeV)	$^{160}Gd(n, 2n)^{159}Gd$ Cross Section (mb)											
	Measured	TALYS - 1.8						EMPIRE – 3.2.2				
		Ldmodel-1	Ldmodel-2	Ldmodel-3	Ldmodel-4	Ldmodel-5	Ldmodel-6	Levden-0	Levden-1	Levden-2	Levden-3	Levden-4
12.47±0.825	1913±143	1938	1919	1765	1935	1901	1828	1669	1679	52.9	1642	1660
16.63±0.95	435±33	1009	1155	1183	1005	1364	1465	1213	1027	106	1282	999

Chapter – 5

Measurement of $^{183}W(n, p)^{183}Ta$ and $^{184}W(n, p)^{184}Ta$ reaction cross section in ^{252}Cf neutron field

---

Publication related to this chapter:

Rajnikant Makwana, S. Mukherjee, L. Snoj, S. S. Barala, M. Mehta, P. Mishra, S. Tiwari, M. Abhangi, S. Khirwadkar, H. Naik, "Measurement of $^{183}W(n, p)^{183}Ta$ and $^{184}W(n, p)^{184}Ta$ reaction cross section"

Applied Radiation Isotopes,

http://dx.doi.org/10.1016/j.apradiso.2017.06.002

Impact Factor 1.136

5.1 Introduction

In the recent decades, there is an overwhelming demand of nuclear reaction cross section data compilation for the development of reactor science and technology. In the International Thermonuclear Experimental Reactor (ITER), fusion reaction process can be studied using the DT reaction. It produces neutrons with an energy of 14.1 MeV, and these neutrons are transmitted through the first wall of the reactor material [1 - 6]. First wall, divertor, blanket, and shielding are the main parts of the fusion reactor. The first wall, divertor and blanket are directly exposed to the DT plasma and bear the maximum amount of the neutron flux (~10^{15} n/cm^2/s). Divertor collects and exhausts heat and particles (neutral and charge), and the reactor walls scatter these neutrons from 14.1 MeV to the thermal neutron energy. Tungsten has been selected as divertor material for ITER [7]. It will face all the neutrons with energies from thermal to 14.1 MeV. These neutrons can open various reaction channels such as (n, γ), (n, p), (n, 2n), (n, d), (n, α) etc. in the reactor materials. It demands complete nuclear reaction cross section data for the different isotopes of tungsten i.e., ^{183,184}W, as they can produce different radioisotopes in the reactor [8]. It is very important as a part of reactor maintenance using remote handling. The reactions ^{183}W(n, p)^{183}Ta and ^{184}W(n, p)^{184}Ta are considered here for the cross section measurement using the ^{252}Cf spontaneous neutron source. There are plenty of experimental data available at 14 MeV for these reactions; however, very few measured data are available for energy range from thermal to 14 MeV. Cross sections at low MeV energy are relatively very important as there are very few measurements and considering the small value of (n, p) reaction cross section. The objective of the present work is to have accurate measurements of the cross section of the above mentioned reactions. Further, the measured data are important to validate evaluated data libraries for tungsten isotopes from different national projects (e.g., ENDF-B/VII.1[9], JENDL-4[10], FENDL[11], ROSFOND [12], CENDL-3.1 [13], JEEF-3.2 [14] etc. In the present chapter, measurement of the cross sections for such nuclear reactions have been discussed.

5.2 Experimental Details

5.2.1 Neutron Source and Target

The ^{252}Cf(sf) neutron field is a reference neutron spectra which is considered to be very well known. Mannhart evaluation [15-16] is currently accepted to be the best representation of this reference neutron spectra. Numerical data for this evaluated spectra are available from the IAEA IRDFF web page of IAEA [17]. The average neutron energy in the ^{252}Cf spectrum is 2.124 MeV. The ^{252}Cf isotope is an intense neutron emitter that decays by alpha emission (~ 96.31%) and spontaneous fission (~ 3.09%) with a half-life of 2.645 y. Its neutron emission rate is 2.314×10^6 n/s/μg [18].

A ^{252}Cf neutron source irradiation facility is available at the Defense Laboratory Jodhpur (India). This source is shielded with paraffin, borated wax and lead as shown in FIG 5.1(a). The irradiation of tungsten (W) sample was done by using this portable ^{252}Cf neutron source, having present neutron yield of 1.6064×10^8 n/s. Standard neutron activation analysis technique was used in the present measurements. In this method, a sample with proper weight is required to irradiate with neutrons. It is necessary to produce the desired isotope from this irradiation for the measurement of the selected nuclear reaction cross section. The tungsten sample with purity of 99.97 % was chosen for irradiation. The sample chosen for the irradiation was having dimensions of 8 mm × 8 mm × 5 mm and weighs 6.033 gm.

5.2.2 Neutron Irradiation

The sample was kept at a distance of 60 mm from the ^{252}Cf neutron source for 603 hours for continuous long irradiation. The average neutron spectrum inside the sample was calculated using the Monte Carlo N-Particle Code (MCNP), which is discussed in the next section. After irradiation, the sample was brought to the Neutronics Laboratory, Institute for Plasma Research (IPR), Gandhinagar, India, for counting purpose. The activated sample was kept near the window of the HPGe detector. An HPGe detector with 16K MCA manufactured by CANBERA was used for gamma counting. The counting setup is shown in FIG 5.1 (b). Counting has been done in two different phases; in the first phase a short counting time has been selected, immediately after the irradiation, then after two days of cooling another set of counting was done with larger time. The time of counting was sufficiently long, as the product isotopes have half-life from few hours to few days. The selected nuclear

reactions with their necessary details are given in Table 5.1. The gamma spectra obtained from the irradiated sample are shown in FIG 5.2. The cross sections for $^{183}W(n, p)^{183}Ta$ and $^{184}W(n, p)^{184}Ta$ reactions were estimated.

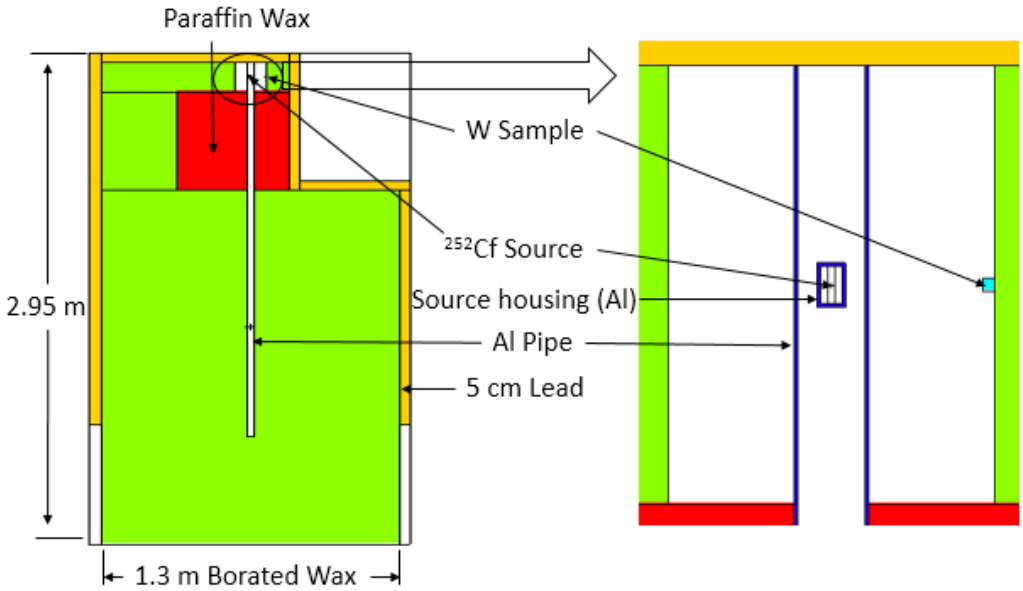

FIG 5.1 (a) MCNP modeling of the irradiation experimental setup

FIG 5.1 (b) Gamma counting setup at IPR, Gandhinagar

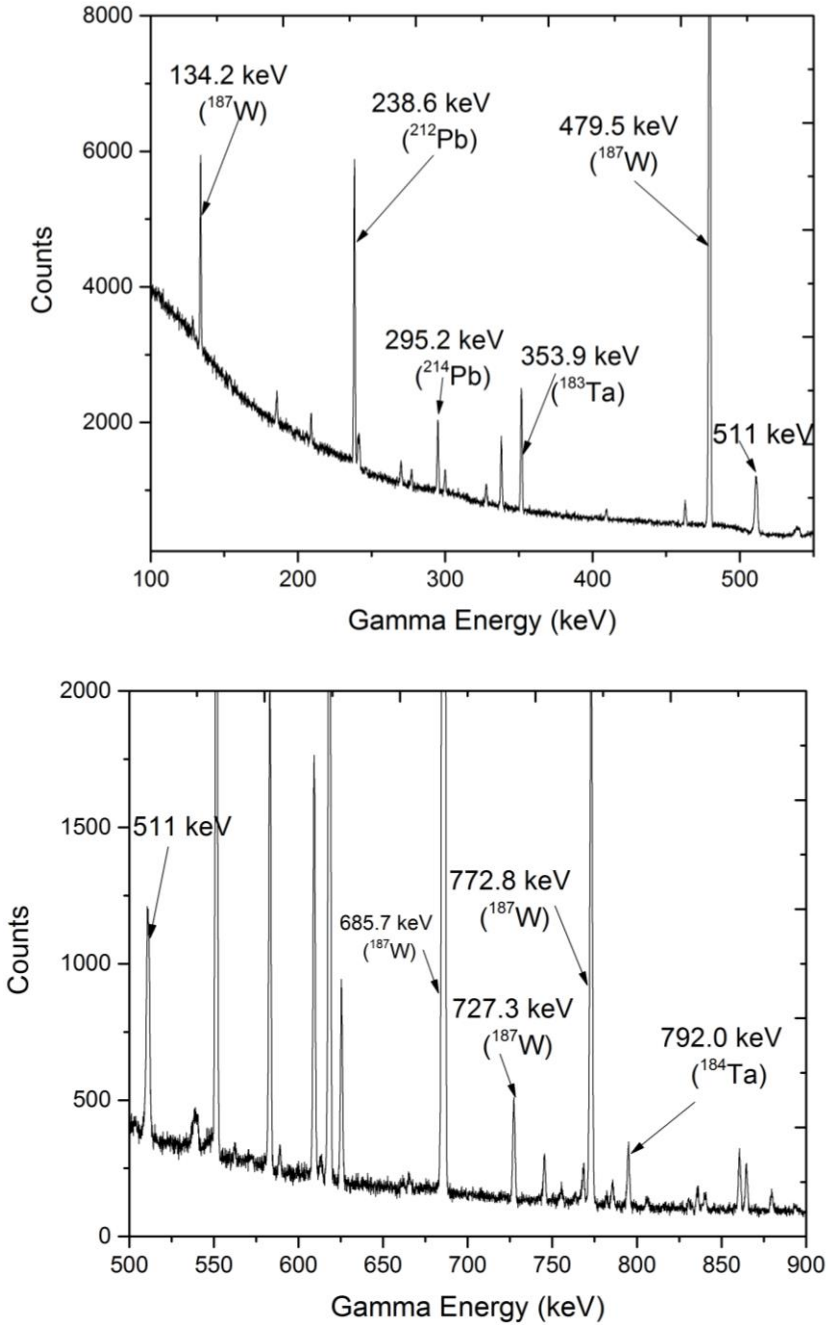

FIG 5.2 Gamma spectrum measured using HPGe detector

Table 5.1 Selected nuclear reactions with isotopic abundance, threshold energy, product half-life, and product gamma energy with its abundance

Reaction	Abundance of Target Isotope (%) [19]	Threshold Energy (MeV) [20]	Half life of product isotope [21]	γ - Energy (KeV)	Γ– Abundance
$^{186}W(n, \gamma)^{187}W$	28.43	-	23.72 h	479.5	21.8
				685.7	27.3
$^{183}W(n, p)^{183}Ta$	14.31	0.29	5.1 d	353.9	11.2
$^{184}W(n, p)^{184}Ta$	30.64	2.095	8.7 h	792.0	14.2

5.3 Theoretical Calculations Using MCNP

This section is divided into two parts; first part discusses the average neutron spectra calculation in the irradiated sample, and on the other hand is related to detector efficiency calculation in the second part. The MCNP – 6.1 code was used to perform these calculations. We have taken help of our collaborator L. Snoj from the Jožef Stefan Institute, Ljubljana, Slovenia for the MCNP calculations. This code has been widely used for the transport of neutron, photon, electron and many other particles. All calculations were performed with ENDF/B-VI cross section data library which comes along with MCNP package. Further, calculations were checked with ENDF/B-VII, in order to find the difference in results, but no significant change was observed in results. The detail of this code has been discussed in earlier Chapter – 2.

5.3.1 Neutron Spectra Calculation

The code MCNP is worldwide used for neutron transport calculation. It is possible to model the actual experimental geometry, with neutron source and material specifications etc. using the code. Once the experimental geometry is modeled, as described in Chapter – 2, the tally card can be used to calculate the neutron spectra at the desired location. It is necessary to model the neutron source accurately for the simulations. The ^{252}Cf source is having continuous neutron spectrum, therefore it was necessary to calculate the averaged neutron spectrum inside the sample. The ^{252}Cf

was modeled using the MCNP code, as explained by L. Snoj *et al*., [22]. The most rigorous approach as explained by L. Snoj *et al*., is to use evaluated neutron spectrum of Mannhart (IRDF-2002 [15-17, 22-23]). In the present work, the average neutron spectra over sample volume have been calculated by using the IRDF – 2002 ^{252}Cf spontaneous fission neutron spectra. Monte Carlo based MCNP code (MCNP – 6.1) with ENDF/B-VII data library was used to model the irradiation assembly as shown in FIG 5.1 (a). The tally F4, which gives volume averaged flux tally was used for the calculation. The definition of the F4 tally is represented by the following relation.

$$F4 = \frac{1}{V}\int_V dV \int_E dE \int_{4\pi} d\Omega\phi(r, E, \Omega) \qquad 5.1$$

where, V = volume of the sample,

E = energy of the neutron

Ω = solid angle

r = radial distance from source

ϕ = flux at distance

The calculated spectrum is shown in FIG 5.3. There has been a significant increment in lower energy neutrons due to scattering from the source shielding. However, the higher energy tail shape remained same as in the pure source spectra.

As the chosen reactions have different threshold energies, entire neutron spectrum was not used to produce the product isotopes. Only those neutrons that were above the threshold energy for both reactions are able to produce the product isotopes. Hence the low energy neutrons below the threshold can be removed from the neutron spectra for both the reactions. This gives the effective neutron spectrum for the respective reaction. This is shown in FIG 5.3(a-c). It can be seen from FIG 5.3(a), that the whole neutron spectrum contains a very large contribution from low energy (thermalized) neutrons, which are backscattered from the surrounding shielding materials. As our chosen reactions have a threshold above these neutron energies, they do not interfere. The effective neutrons spectra are shown for both reactions in FIG 5.3(b-c). Again there is a very small number of neutrons available above 4.5 MeV neutrons. The ratio of these neutrons to total neutrons is < 6 %. So the major contribution in the reaction product is due to the neutrons from threshold to 4.5 MeV neutrons. Therefore, the measure cross section can be reported at the spectrum averaged energy for these neutrons. Following formula has been used to calculate the spectrum averaged energy

from the calculated neutron spectra in the irradiated sample, which is known as the effective mean energy/spectrum [24],

$$E_{mean} = \frac{\int_{E_{th}}^{E_{max}} E_i \emptyset_i dE}{\int_{E_{th}}^{E_{max}} \emptyset_i dE} \quad 5.2$$

where,

E_{th} = threshold energy of the reaction

E_{max} = maximum neutron energy

E_i = energy bin

ϕ_i = neutron flux in energy bin E_i

E_{mean} = effective mean energy

This mean energy is used to quote for the measured cross section values.

5.3.2 Detector Efficiency Calibration

The HPGe detector, which was used for the activation measurement having crystal size of 64.80 mm diameter and 64.60 mm length. The window thickness is 0.60 mm and made of carbon composite. The efficiency of the detector was measured for the different gamma ray energies using mix-energy gamma source available at IPR, Gandhinagar, India. A mix-energy gamma source is contains different radioactive isotopes, such as ^{241}Am (59.54 keV, 919.19 Bq), ^{109}Cd (88.03 keV, 4.132 kBq), ^{57}Co (122.06, 136.47 keV, 144.85 Bq), ^{139}Ce (165.85 keV, 5.050 kBq), ^{51}Cr (320.08 keV, 0.09 Bq), ^{113}Sn(391.69 keV, 91.06 Bq), ^{85}Sr (514.00 keV, 11.85 Bq), ^{137}Cs (661.65 keV, 1.712 kBq), ^{88}Y (898.03 keV, 152.45 Bq), ^{60}Co (1173.22, 1332.49 keV, 2.183 kBq) and ^{88}Y (1836.05 keV, 152.45 Bq), that covers gamma energy from 59 keV to 1.8 MeV. Full efficiency curve was plotted using measured photopeak efficiency. In the present measurements, a point source was used to measure detector efficiency. However, in the actual experiment, the volume sample was used. Therefore, it was necessary to obtain efficiency for the volume source of the sample dimension. Further, the volume source attenuates photons from the subsequent layers towards the detector, and, a large number of photons are scattered from the backside layers of the sample. To study the self-shielding and back scattering effect from the W sample, another measurement has been carried out. The method used has been described in reference [25]. The W samples with the thickness of 1, 2, 3 and 5 mm were kept in between source and detector. In this arrangement, the gammas emitted from the

source were attenuated by the sample. The results are shown in FIG 5.4. It is clear from this figure, that the efficiency will be different for the volume source, due to attenuation. Also, the backscattering has a significant contribution.

The efficiency of the volume sample by considering backscattering and self-shielding effect can be calculated using the MCNP code. In this context, the detector was modeled by using this code as shown in FIG 5.5. The experimentally measured efficiency at various distances using the point gamma source, at different energies were calculated and compared with simulated efficiency in FIG 5.6(a). The model was optimized by getting the ratio of calculated efficiency to experimental efficiency (C/E ratio) ~ 1, which is shown in FIG 5.6(b). This model was used for the actual sample – detector geometry to estimate the efficiency of the detector. This method considers both the self-shielding and back scattering effect due to the volume of the sample. This efficiency values for different selected gamma energies were used to calculate the cross section using neutron activation technique.

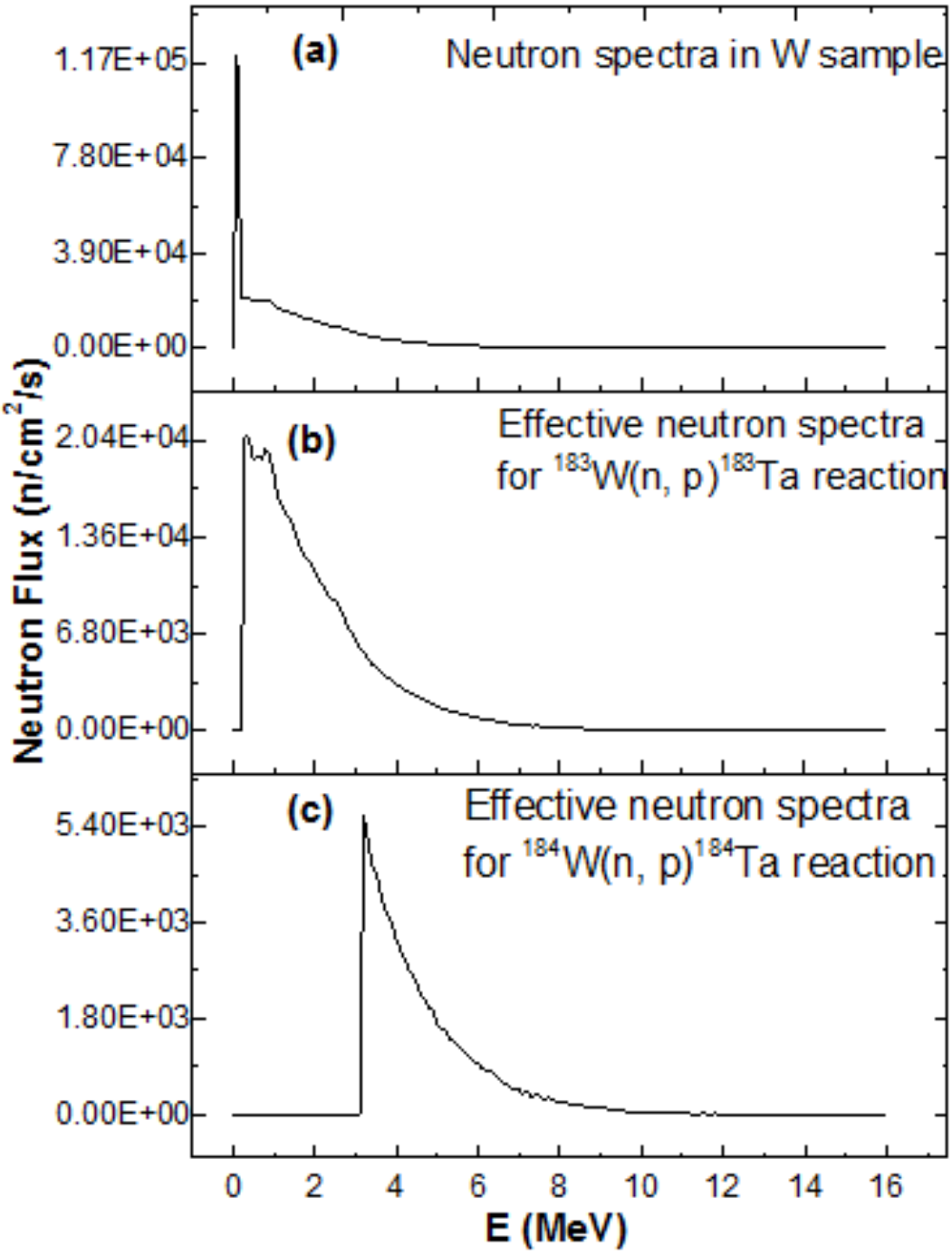

FIG 5.3 ^{252}Cf Source neutron spectra – average neutron spectra in W sample, and the effective neutrons for the selected reactions, which are above the threshold energy of the reactions

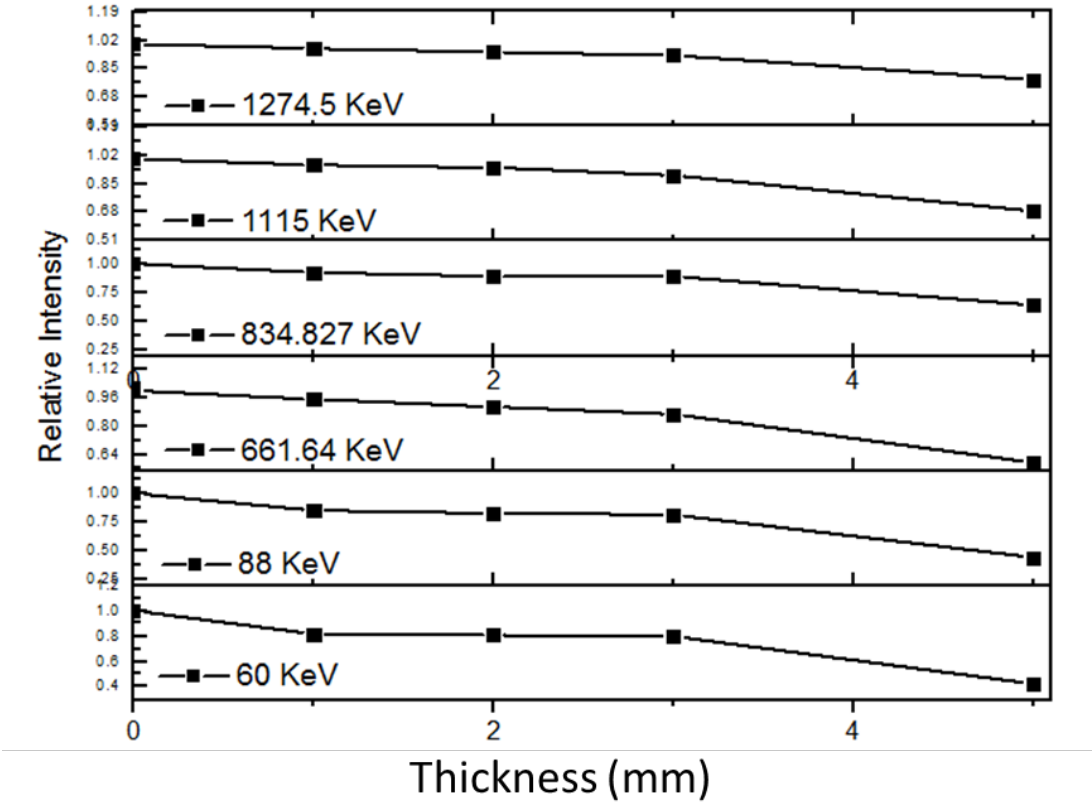

FIG 5.4 Relative intensity showing the self-shielding effect increases as the thickness of the sample increases

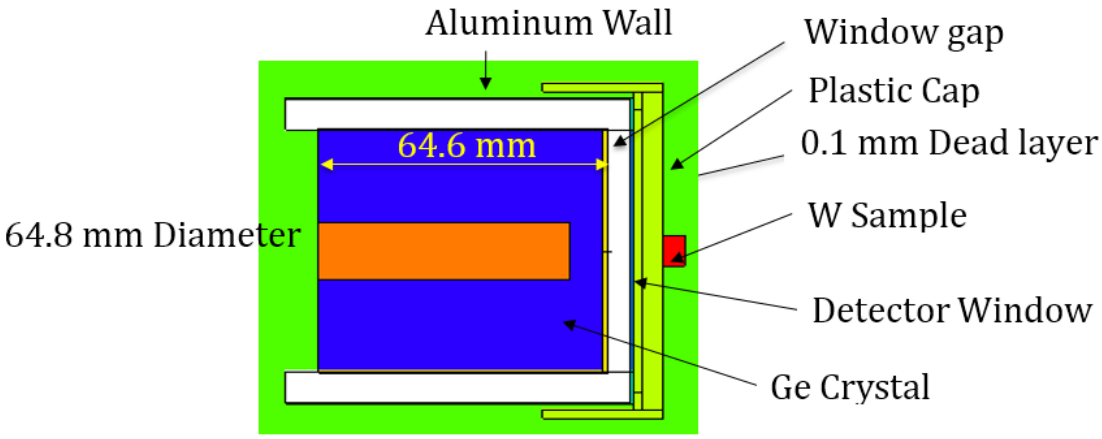

FIG 5.5 MCNP Model of the detector to calculate efficiency for irradiated volume sample placed on end cap of the detector

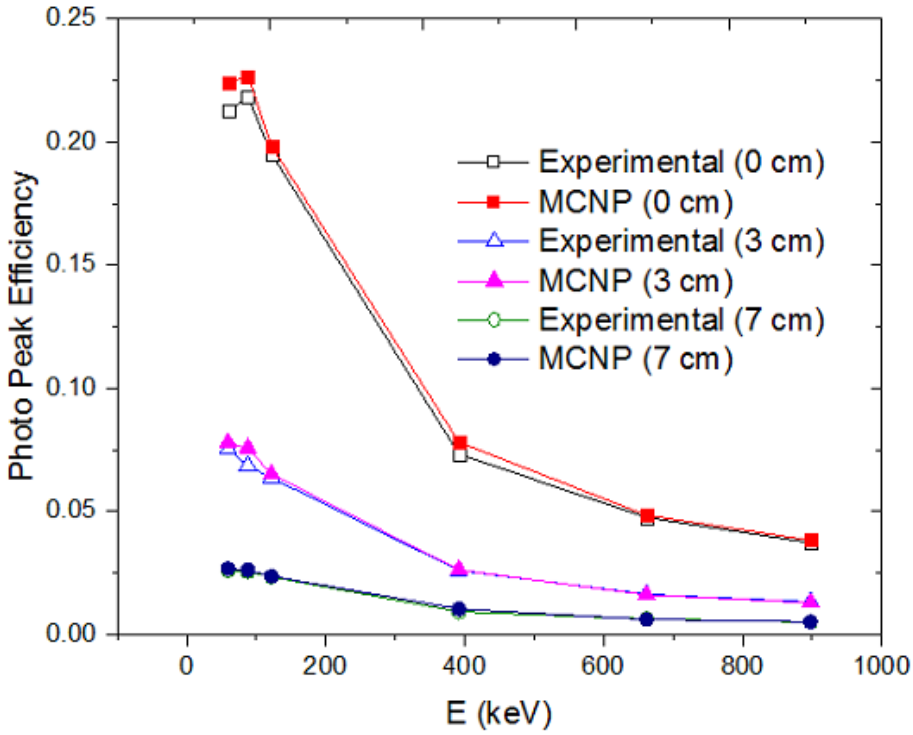

FIG 5.6(a) Comparison of measured and MCNP calculated detector efficiency at various gamma energies

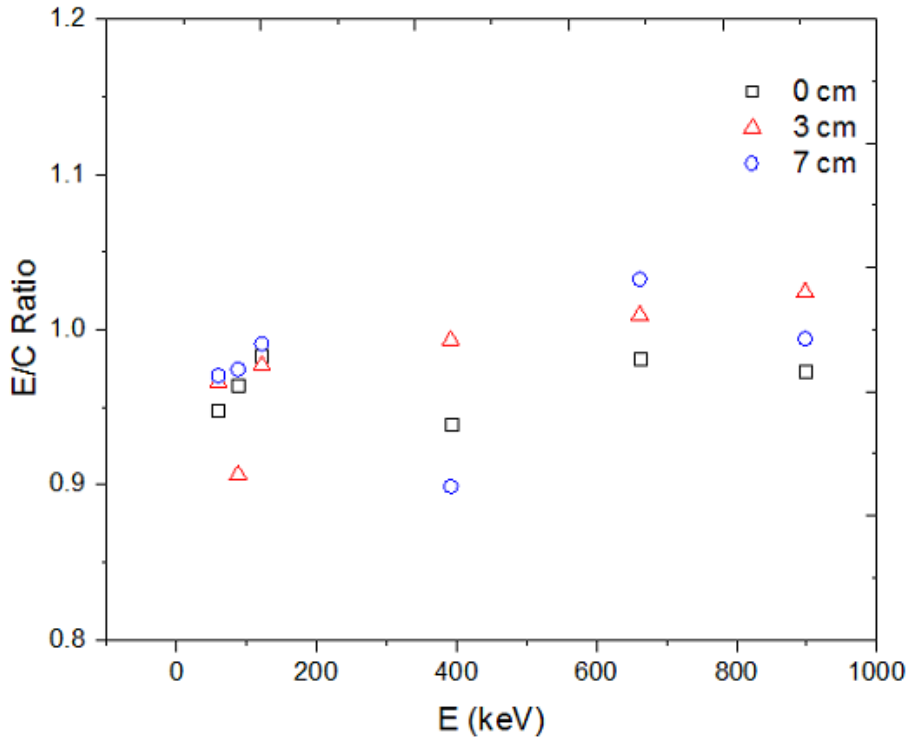

FIG 5.6(b) Comparison of Experimental to MCNP calculated detector efficiency ratio at various gamma energies

5.4 Data Analysis – Neutron Activation Analysis

The neutron activation analysis has been already discussed in Chapter – 4. The measured data along with the calculated efficiency and neutron flux using MCNP were used to calculate the reaction cross sections. The production cross section (σ) of the interested isotope from the desired reaction was obtained by using the following standard activation equation,

$$\sigma = \frac{A_I \cdot A_\gamma \cdot \lambda}{(\emptyset \theta_\gamma \epsilon_\gamma w_i P_i N_{av}) \cdot (1 - e^{-\lambda t_i}) \cdot (1 - e^{-\lambda t_c}) \cdot e^{-\lambda t_w}} \quad 5.5$$

Where, A_I = Gram Atomic Weight of the target

A_γ= Peak Counts of gamma energy

λ = Decay constant of product nucleus (s^{-1})

t_i = irradiation time

t_w = Cooling time

t_c = Counting time

$\emptyset$ = Incident neutron flux

θ_γ = γ intensity

ϵ_γ = Efficiency of detector at gamma chosen

w_i = weight of sample (gm)

P_i = Abundance of target isotope

N_{av} = Avogadro's number

The photopeak counts of the gamma rays emitted from the desired isotope were carefully measured from the gamma spectrum. The selected gamma energies along with their abundances for the desired radioisotopes are given in Table 5.1. The measured cross sections for the selected reactions are given in Table 5.2.

5.5 Nuclear Modular Code Prediction

In order to support the present measured nuclear cross section data, nuclear modular calculations were performed by using EMPIRE – 3.2.2 code. This code uses different nuclear models to predict nuclear reaction cross section. It can predict nuclear reaction data for neutron, gamma, proton, deuteron, triton, ^{3}He and alpha with an energy range from few keV to several hundreds of MeV. The EMPIRE – 3.2.2 uses

reaction parameters from Reference Input Parameter Library (RIPL) – 3. It considers the effect of level density, and all three nuclear reaction mechanisms: compound, pre-equilibrium, and direct reaction. The optical model parameters were obtained by using a global potential proposed by Koning and Delaroche [26]. The compound reaction mechanism was incorporated by Hauser-Feshbach model [27]. The pre-equilibrium contribution was included by exciton model, developed by Kalbach [28]. The details of these codes have been discussed in Chapter – 2.

In the present case, different parameters such as level density parameters were used to evaluate the cross section of the interested nuclear reactions. The calculated reaction cross sections for the production of selected radioisotopes were used to compare the measured reaction cross sections shown FIGS 5.7 – 5.8.

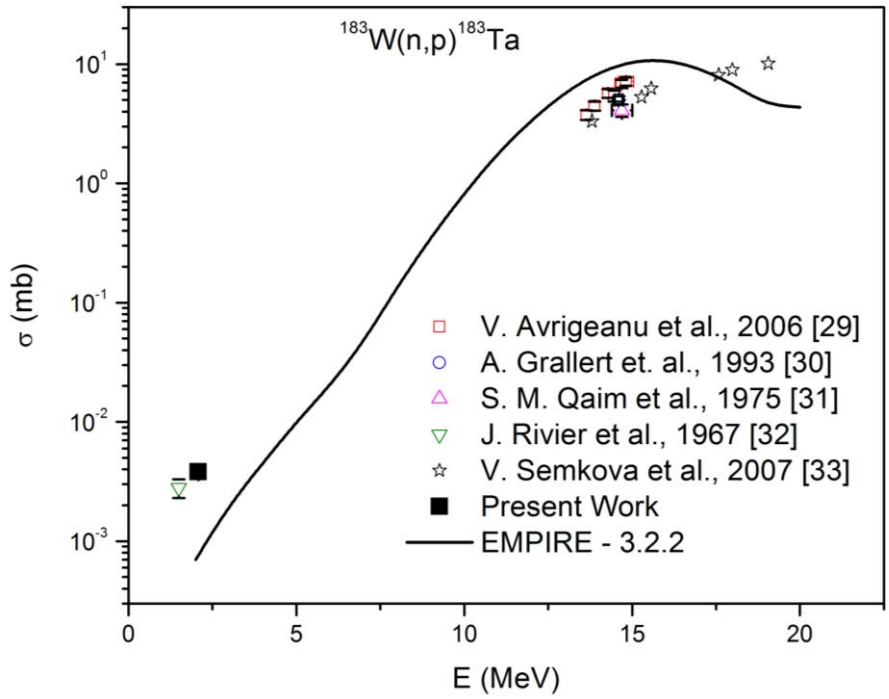

FIG 5.7 Comparison of present measured spectrum averaged cross section with experimental and EMPIRE-3.2.2 evaluated cross section for $^{183}W(n, p)^{183}Ta$; the present data and data point of J. Rivier et al., [32] are spectrum averaged cross sections, other experimental data are for mono energy neutrons

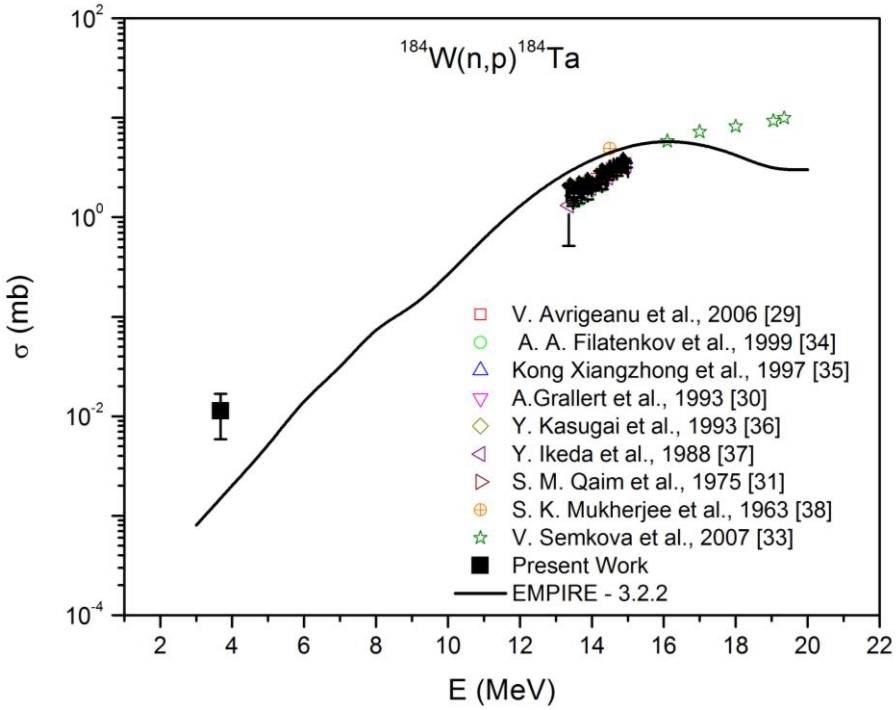

FIG 5.8 Comparison of measured cross section with experimental and EMPIRE-3.2.2 evaluated cross section for ^{184}W(n, p)^{184}W

5.6 Results and discussion

The cross sections were measured with improved accuracy, with the application of simulation technique, which incorporates, self-shielding, backscattering, volume source effect in efficiency etc. Geometrical effect and shielding effect on average neutron spectra inside the sample were calculated using MCNP simulation. To the best of our knowledge, the present measurements have been done for the first time in the above mentioned neutron energies. The effect of self-attenuation and backscattering, and the sample-volume geometry effect on the efficiency of the detector was corrected by optimizing MCNP model of the HPGe detector at different distances and for different energies of a gamma photon. The parameters for the error propagation in the final cross section estimations were considered. Major error contributions in the present data are due to relative efficiency (2 – 3 %), scattered neutron (1 – 3 %), statistical error (3 – 4 %), detector dead time (< 2 %). The overall error in the present measurement was < 6 %.

The EMPIRE – 3.2.2 nuclear modular code was used for evaluating the cross section of the selected nuclear reactions. The measured data were compared with the

evaluated data and available data in EXFOR data library in the FIGS. 5.7 – 5.8 [29 – 38]. In the case of $^{183}W(n, p)^{183}Ta$, there is a previous measurement for this reaction near to the present listed energy, by J. Rivier *et al*., [32], which is in agreement with the present data. In both the (n, p) reactions the measured cross sections are higher by a small factor in comparison with the evaluated data.

Table 5.2 Measured Cross section for the selected nuclear reactions

Reaction	**Spectrum Average Energy (MeV)**	**Measured Cross section ($\times 10^{-3}$mb)**
$^{183}W(n, p)^{183}Ta$	1.70 ± 1.35	3.8 ± 0.3
$^{184}W(n, p)^{184}Ta$	3.75 ± 1.26	11.3± 0.9

5.7 Summary and Conclusion

In the present measurements, cross sections of $^{183}W(n, p)^{183}Ta$, and $^{184}W(n, p)^{184}Ta$ reactions were measured using a ^{252}Cf neutron source at spectrum averaged energies above the threshold of the reaction to the maximum neutron energy. This is a material of interest for a fusion reactor. The averaged neutron spectra inside the sample volume were calculated using MCNP code. The data that have been presented for (n, p) reactions for the available energies has very few or no previous measurements. The theoretical estimation of the cross section was done by EMPIRE – 3.2.2 code. It may be observed that present experimental results are in agreement within the limits of the experimental error. The study shows that the cross section of (n, p) reaction for tungsten isotopes are having small values. But for the case of the fusion reactor, where the first wall is facing ~10^{15} neutrons/sec/cm^2, it can produce a considerable amount of radioactive waste.

References

[1] J. Qing, Y. Wu, M. Regis, and J. W. Kwan, IEEE Trans. Nucl. Sci., 56 (2009) 1312–1315.

[2] J. Reijonen, et al., Appl. Radiat. Isotopes, 63 (2005) 757–763.

[3] Y. Wu, et al., IEEE Trans. Nucl. Sci., 56 (2009) 1306–1311.

[4] V. Voitsenya et al., Rev. Sci. Instrum., 72 (2001) 475–482.

[5] G. De Temmerman, et al., J. Nucl. Mater., 363 (2007) 259–263.

[6] K. H. Behringer, J. Nucl. Mater., 145 (1987) 145–153.

[7] M. Lehnen, et al., Journal of Nuclear Materials 463 (2013) 39-48.

[8] R. A. Forrest, Energy Procedia 7 (2011) 540–552.

[9] M.B. Chadwick, et al., "ENDF/B-VII.1: Nuclear Data for Science and Technology: Cross Sections, Covariances, Fission Product Yields and Decay Data", Nucl. Data Sheets 112(2011)2887.

[10] Keiichi Shibata, et al., J. Nucl. Sci. Technol.. 48(1), 1-30 (2011).

[11] FENDL-3.1 data library, https://www-nds.iaea.org/fendl31/

[12] ROSFOND data library, http://www.ippe.ru/podr/abbn/english/libr/rosfond.php

[13] Z. G. Ge, et al., Journal of the Korean Physical Society, Vol. 59, No. 2, August 2011, pp. 1052

[14] JEFF-3.2 data library, https://www.oecd-nea.org/dbforms/data/eva/evatapes/jeff_32/

[15] W. Mannhart, IAEA-TECDOC-410 (1987) 158

[16] W. Mannhart, INDC(NDC)-220/L (1989) 305

[17] IRDF-2002, https://www-nds.iaea.org/IRDFF/IRDFF-v1-05_sp.endf

[18] Manojlovič S, et al., Applied Radiation and Isotopes, 101 (2015) 101–106.

[19] K. J. R. Rosman, P. D. P. Taylor, Pure Appl. Chem., 71 (1999) 1593-1607.

[20] Q value calculator, retrieved from: http://www.nndc.bnl.gov/qcalc/index.jsp.

[21] Table of Isotopes decay data, retrieved from: http://nucleardata.nuclear.lu.se/toi/listnuc.asp?Z=74.

[22] Narayan, Pradeep et al., Indian Journal of Pure & Applied Physics, 48 (2010) 798-801.

[23] IAEA, International reactor dosimetry file 2002 (IRDF-2002) Technical Report Series, International Atomic Energy Agency, Vienna (2006) 162.

[24] D. L. Smith, et al., " Corrections for Low Energy Neutrons by Spectral Indexing", Retrieved from: https://www.oecd-nea.org/science/docs/2005/nsc-wpec-doc2005-357.pdf

[25] J. Rama Rao, et al., Nucl. Instrum. Methods Phys. Res., Sect. B, 17 (1986) 368 - 371.

[26] A. J. Koning, and J. P. Declaroche, Nucl. Phys. A713 (2003) 231.

[27] W. Hauser, and H. Feshbach, Phys. Rev. C 87 (1952) 366.

[28] C. Kalbach, Phys. Rev. C 33 (1986) 818.

[29] V. Avrigeanu, et al., Nucl. Phys. A 765 (2006) 1.

[30] A. Grallert, et al., Rept.: IAEA Nucl. Data Section report to I.N.D.C. No. 286 (1993) 131.

[31] S. M. Qaim, and C. Graca, Nucl. Phys. A 242-2 (1975) 317.

[32] J. Rivier, et al., Jour. Radio Chemica Acta. 8 (1967) 1967.

[33] V. Semkova, R. Capote, R. Jaime Tornin, A. J. Koning, A. Moens, and A. J. M. Plompen, DOI: 10.1051/ndata:07320.

[34] P. Reimer, V. Avrigeanu, S. V. Chuvaev, A. A. Filatenkov, T. Glodariu, A. Koning, A. J. M. Plompen, S. M. Qaim, D. L. Smith, and H. Weigmann, Phys. Rev. C, 71 (2005) 044617.

[35] Kong Xlangzhong, et al., Rept.: Chinese report to I.N.D.C. No. 042 (1997) 9.

[36] Y. Kasugai, et al., Conf.: JAERI-M Report No. 92, 27 (1992) 268.

[37] Y. Ikeda, et al., Conference: JAERI-M Report No. 92, 27 (1992) 268.

[38] S. C. Gujarathi and S. K. Mukherjee, Indian J. Phys. 41 (1967) 667.

Chapter – 6

Measurement of (n, p) cross section for some structural materials at 14.2 MeV

Publication related to this chapter:

Nand Lal Singh, **Rajnikant Makwana**, S. Mukherjee, A. Chatterjee "Measurement of (n, p) Cross Section for Some Structural Materials at 14.2 MeV"

Published in: IEEE Conference Proceedings; 2016 17th International Scientific Conference on Electric Power Engineering (EPE)

DOI: https://doi.org/10.1109/EPE.2016.7521819

Impact Factor: 5.629

6.1 Introduction

Accurate knowledge of neutron induced reaction cross section is of interest to many areas of applied science and fundamental nuclear physics. These cross sections are important to estimate radiation levels, radiation shielding, and decay heat of materials that have been exposed to radiation fields. Other applications are designing of future fusion reactors, advanced fission reactors, in neutron dosimetry and development of nuclear theory. Structural materials are the base materials of any reactor either fusion or fission. The structural materials should have properties such as high strength, long durability, thermal stability, radiation shielding, less radiation transmutation and minimum activation [1]. As these materials are used for the reactor structure, and the neutrons produced from the fission or fusion mechanisms in a reactor are irradiating these materials. The D-T fusion reaction will produce high energy neutrons of 14 MeV. It is necessary to have all the known cross section for this neutron energy to calculate nuclear activation and transmutation, nuclear heating, nuclear damage. The (n, p) reaction channel easily opens for most of the materials above few MeV because of low threshold. The following reaction cross sections were measured by activation technique; ^{75}As(n, p)^{75}Ge, ^{66}Zn(n, p)^{66}Cu, ^{64}Zn(n, p)^{64}Cu, ^{55}Mn(n, p)^{55}Cr, ^{51}V(n, p)^{51}Ti, and ^{58}Ni(n, p)^{58}Co. The uncertainties arising due to self-absorption and self-scattering effects in the bulk samples and pile up effect in detector have been taken care by simulation method as described in the literature [2]. The literature survey reveals that the neutron induced reaction cross sections for these materials are widely studied using standard activation method and are available in EXFOR database [3]. There are large discrepancies among the previous experimental data by a factor of 1.4 to 4.0, hence further measurements are required. The measured cross sections are important for the fusion reactor as well as for the advanced accelerator based sub-critical system. Theoretical evaluation of (n, p) and (n, α) reaction cross sections are done using standard nuclear modular codes, TALYS – 1.6 and EMPIRE – 3.2.2. The predictive power of nuclear reaction models can be validated and improved in comparison with good quality experimental data and in turn, the model calculation provides estimates where no experimental data are available.

6.2 Structural materials for nuclear reactor

The structural materials play a crucial role in designing of a nuclear reactor [4]. It must have properties of long durability and radiation hardness in the radiation environment. The first wall, divertors, breeding blanket, limiters are the component which will face high energy neutrons from the DT fusion [4]. Their properties of mechanical and thermal strength are based on their ability to resist the neutron radiation transmutation. The prime importance of the development of new shielding materials is to develop a material with low activation production in high neutron exposure. In a fission reactor, it is also very necessary to develop new reactor structural materials in order to build new generation upgraded reactors with long durability. The structural materials used in the ITER fusion reactor design are given in FIG 6.1 [5]. The transition metals such as V, Mn, Ni, Zn are always used as a part of the composition of structural materials [6,7]. These materials provide the basic properties such as mechanical strength to the structural composites. The rareearth elements are always present as impurities as well as used with structural materials to enhance its properties [8]. These materials are continuously getting irradiated by neutrons in fusion and fission reactor. The reaction channels such as (n, p), (n, 2n), (n, α) become very important as they can transmute the natural isotopes of these materials into radioactive isotopes. As discussed in earlier chapters, the transmuted isotopes contain different structural properties. Further, the production of long lived radioactive isotopes is a serious problem to the radiation safety and nuclear reactor life. In order to select proper materials for reactor design, it is necessary to have nuclear data for all the structural materials at all the energies in the range of thermal to 20 MeV [8]. It is necessary to have data at 14 MeV for the fusion reactor structural materials. Such effort has been made in the present work for the isotopes of transition metals V, Mn, Zn, Ni and rare earth element As. Arsenic (As) becomes important material as it is used in the production of N – type semiconductors employed in digital electronics, which is part of different electronic components of the reactor. Hence, nuclear transmutation may change its composition and it can offer a change in the electronic response. With these considerations, present measurements become very important.

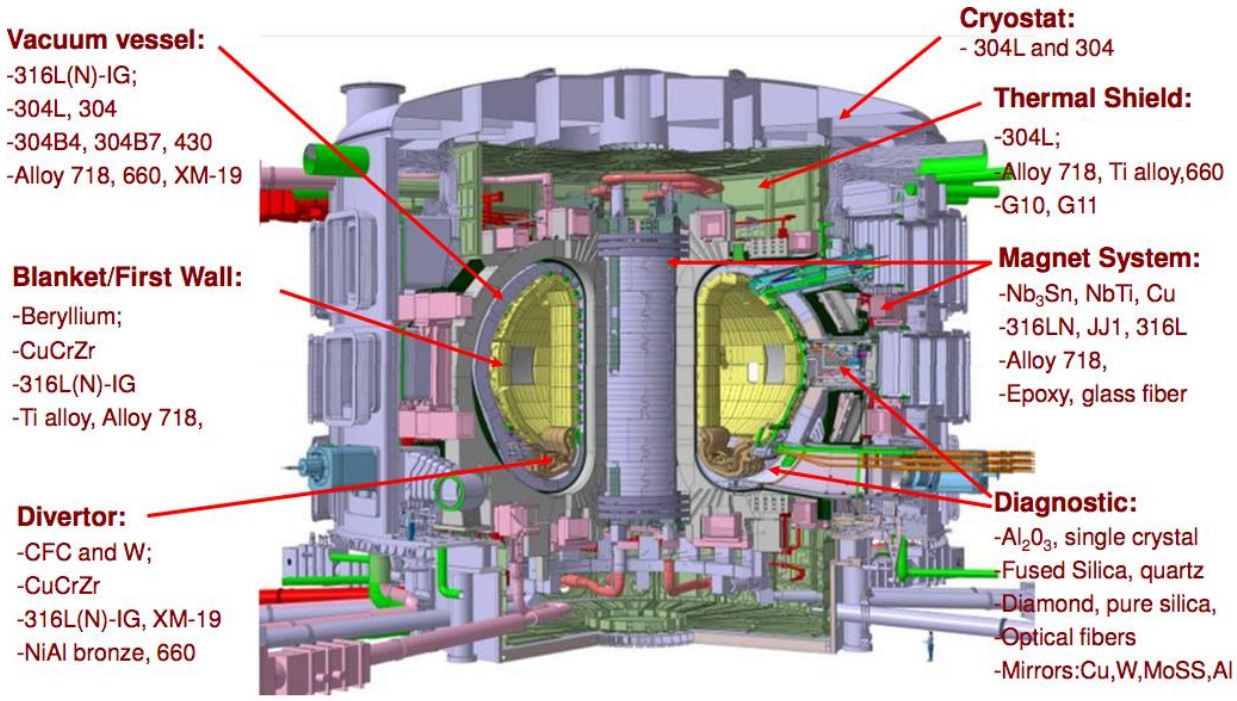

FIG 6.1 The structural materials used in ITER

6.3 Experimental

6.3.1 Target preparation and Irradiation

The target materials in powder form (^{75}As, $^{64,66}Zn$, ^{55}Mn), were uniformly mixed with aluminum powder and pressed into the form of a pellet of diameter 2.0 cm and thickness of about 2.0 mm each. Four to five pellets were prepared and used as a cylindrical experimental target. The mass of the aluminum and target was measured before addition. The aluminum was used as a monitor to measure the fast neutron flux, incident on the target.

The AN-400 Van de Graff Accelerator of Banaras Hindu University, Varanasi, India was used to produce 14 MeV neutron via $^{3}H(d, n)^{4}He$ reaction (DT reaction) using tritium target of 8 Ci activity and deuteron beam of energy ~280 keV. In this source, deuterium ions are extracted as a beam using the beam extracting system. Once the beam of the deuterium ions is formed, it is accelerated using the 400 keV Van de Graff accelerator. The energy of the ions must be reached such that they can overcome the Coulomb barrier of the tritium nuclei located on target. The beam exposed on the front side of the tritium target which can generate heat. The tritium target is such that the tritium on a titanium metal is continuously cooled through the

passing of cooled water from the back side. The DT source is a mono energetic neutron source, hence it is easy to measure the cross section at DT fusion neutrons energy. Further, the DT neutrons are having energy 14.2 MeV, which is much above the threshold of the presently selected reactions. Hence the considerable amount of activation was expected from the irradiation. In the case of nickel and vanadium instead of pellets, a stack of alternative Ni/V and Al foils were used as a target. These isotopes were irradiated with a beam current of 30 μA for 15 minutes to 4 hours as per the half-life of product isotope produced in the reaction.

6.3.2 Data acquisition and Analysis

A high purity germanium (HPGe) detector was used for the measurements of activation produced in the irradiated samples. A ^{152}Eu disc source of the same diameter of samples was placed between the sample pallets at different positions. Gamma spectrum at each position was measured with high resolution HPGe detector (1.8 keV FWHM at 1332 keV gamma energy) and 4096 channel multi-channel analyzer. The efficiency of the detector was calculated at different energies of ^{152}Eu with and without a sample to remove self-absorption and self-scattering effects in the samples and pile up effect in the detector as discussed in the literature [2] and is shown in FIG 6.2 for nickel and zinc oxide. It reveals that the percentage attenuation varies nearly 22% to 2.3% for ZnO and 16% to 1.9% for Ni sample for low energy (122 keV) to high energy (1408 keV) gamma rays respectively. The reaction products were identified by means of their characteristics gamma rays and half-life as listed in Table 6.1 [9]. The gamma spectra were measured for each sample using the above mentioned detector setup. As the half-lives of the various product isotopes are different, hence the irradiations were done from minutes to hours accordingly. Those reaction products whose half-lives are in minutes were measured just after the irradiation, with minimum cooling time. The counting were done for several half-lives. A typical gamma spectra from irradiated As the sample is given in FIG 6.2. The analysis was done using neutron activation analysis method as described in the Chapter – 4. The neutron fluxes incidents on the targets were measured by using the Al powder, which was used in the preparation of the target pallets. Al is suitable to measure the flux of high energy neutrons, as the reactions ^{27}Al(n, α)^{24}Na and ^{27}Al(n,

p)^{27}Mg have high threshold energy. Also, ^{27}Al is the only stable and 100% abundant isotope of aluminum [9]. The spectroscopic data for these monitor reactions are given in Table 6.2 [9-15]. Also, the accelerator based DT sources are providing a very small broadening of the neutron energy peak in the front direction [16,17]. The targets and the monitor foils were kept in the front directions with this consideration. The energy of the neutrons was taken as 14.2 ± 0.2 MeV. The cross section was calculated from the measured photopeak counts using the following activation eq. 6.1. The measured cross sections are given in Table 6.3.

$$\sigma = \frac{A_i A_\gamma \lambda e^{\lambda t_w}}{\phi \theta_\gamma P_\gamma w_i P_i N_{av} (1-e^{-\lambda t_i})(1-e^{-\lambda t_c})} \qquad 6.1$$

where,

A_i = Gram Atomic Weight of the target

$A\gamma$ = Peak Counts of gamma energy

λ = Decay constant of the product isotope

t_i = irradiation time

t_w = Cooling time

t_c = Counting time

ϕ = Incident neutron flux

$\theta\gamma$ = Efficiency of detector at gamma chosen

$P\gamma$ = Gamma intensity

w_i = Weight of the sample

P_i = Abundance of the target isotope

N_{av} = Avogadro's number

Table 6.1 Selected nuclear reactions with their product isotope, half-life and prominent gamma ray energies with intensities

Target isotope with abundance	**Nuclear reaction**	**Product Isotope (Half-life)** [9-15]	**Prominent Gamma ray energy (keV) with gamma intensity** [9-15]
^{75}As (100%)	^{75}As(n, p)^{75}Ge	^{75}Ge (82.78 m)	264.65 (11%)
^{66}Zn (27.73%)	^{66}Zn(n, p)^{66}Cu	^{66}Cu (5.120 m)	1039.23 (9.23%)
^{64}Zn (49.17%)	^{64}Zn(n, p)^{64}Cu	^{64}Cu (12.7 h)	1345.84 (0.475%)
^{55}Mn (100%)	^{55}Mn(n, p)^{55}Cr	^{55}Cr (3.497 m)	1528.3 (0.037%)
^{51}V (99.75%)	^{51}V (n, p)^{51}Ti	^{51}Ti (5.76 m)	320.07 (93.1%)
^{58}Ni (68.077%)	^{58}Ni(n, p)^{58}Co	^{58}Co (70.86 d)	511 (29.8%); 810.76 (99.45%)

Table 6.2 The Monitor reactions used for neutron flux measurements

Monitor Nuclear reaction	**Product Isotope (Half-life)** [9]	**Prominent Gamma ray energy (keV) with gamma intensity (%)** [9]
^{27}Al(n, α)^{24}Na	^{22}Na (14.96 h)	1368.6 (100)
^{27}Al(n, p)^{27}Mg	^{27}Mg (4.46 m)	843.8 (71.8)

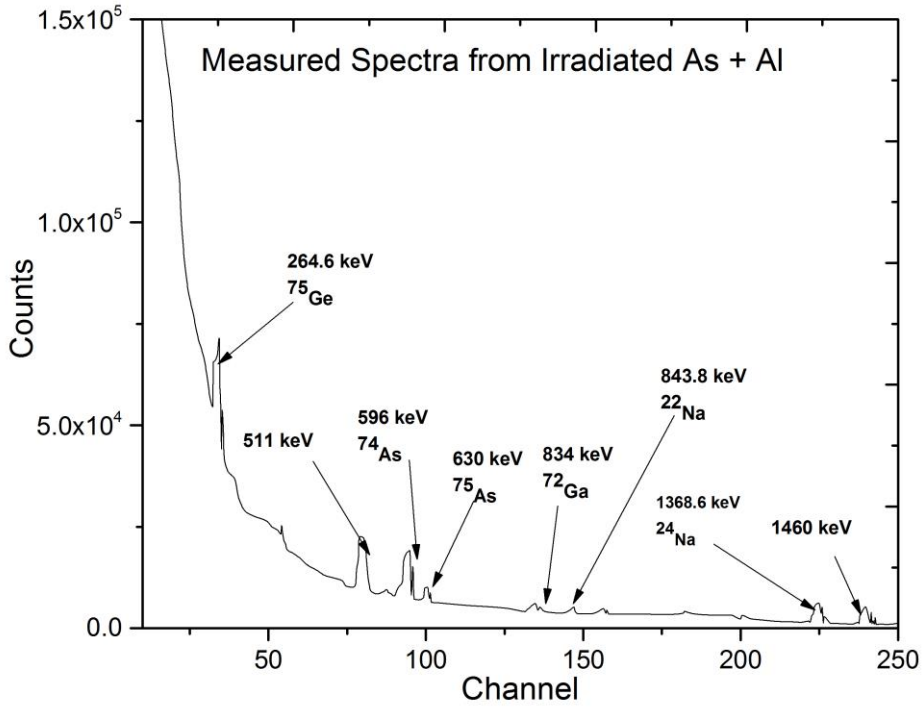

FIG 6.2 Typical measured gamma spectra from irradiated mixed powder of (As_2O_3, + Al) using HPGe detector

6.4 Theoretical Predictions

The nuclear modular codes are an important tool for the calculation and verification of the cross sections of various nuclear reactions at a different incident energy of the projectile. The latest version of nuclear modular codes TALYS-1.6/1.8 and EMPIRE-3.2.2 are used to evaluate (n, p) cross sections for the selected isotopes [18, 19]. The input parameters such as level density parameter have been precisely chosen for best estimation of the cross section. The details of these parameters have been already discussed in Chapter – 2.

6.4.1 TALYS-1.6 Calculations

TALYS is a computer code which is efficient to predict nuclear reaction cross section. It is a useful tool to do analysis of physics of nuclear reactions. TALYS – 1.6 nuclear code can calculate cross section for incident particles; gammas, neutrons, protons, deuterons, tritons, ^{3}He and alpha-particles in the incident energy range from 1 keV to 200 MeV for target nuclides of mass 12 and heavier nuclei. TALYS

considers all the possible channels for the above-mentioned particles. It has completely integrated optical model and Coupled-channels calculations by ECIS-06 code [20]. The optical model parameters are used for neutron and photon reaction calculations determined from global potential proposed by Koning and Delaroche [21]. The compound model contribution is developed from Hauser-Feshbach model [22]. The pre-equilibrium calculation is developed from the exciton model proposed by Kalbach [23]. In this calculation, pre-equilibrium effect is considered as default parameters.

6.4.2 EMPIRE – 3.2 Calculations

EMPIRE – 3.2 is another powerful nuclear modular system to predict nuclear reaction cross section. It considers reaction mechanism such as compound nucleus formation (Hauser-Feshbach model) with width fluctuation correction [22,24], pre-equilibrium using exciton model and direct reaction using the optical model parameters given in RIPL – 3 library. The present version of the EMPIRE code is the latest version. EMPIRE makes use of several codes, written by different authors, which were converted into subroutines and adapted for the present use [25]. For the present work, the level density parameter was changed to get the best agreement with the measured data (Level density parameter for EGSM, Gilbert-Cameron (EMPIRE) and GSM (RIPL) models [26,27].

Both the codes were used to calculate cross section for the selected reactions and are plotted in the FIGS. 6.4 – 6.9 along with the previous data. There is a fairly good agreement between present measured data with those of calculated data using TALYS-1.6 and EMPIRE-3.2.2. The present experimental result and theoretical predictions using above codes are also listed in Table 6.2.

6.5 Results and discussion

The cross sections were measured with improved accuracy using the simulation method, which takes care of self-absorption and self-scattering effects in the samples and pile up effect in the detector. The errors quoted on the cross section comprise the statistical error (1-3%), relative efficiency (2-3%) and the monitor crosses section (3%). The relative efficiency data with and without absorber for a particular

target-detector geometrical arrangement inclusive of all due to self-scattering, self absorption and geometrical solid angle for a cylindrical target was used to determine cross section, such curve for nickel and zinc oxide is presented in FIG 6.3. The present experimental results are compared with the available experimental data from EXFOR database [3] and evaluated with Talys – 1.6 and EMPIRE – 3.2.2 codes are shown in FIGS. 6.4 – 6.9. The cross section measured in the present work and by others with the same experimental method are in agreement within about 2-15%.

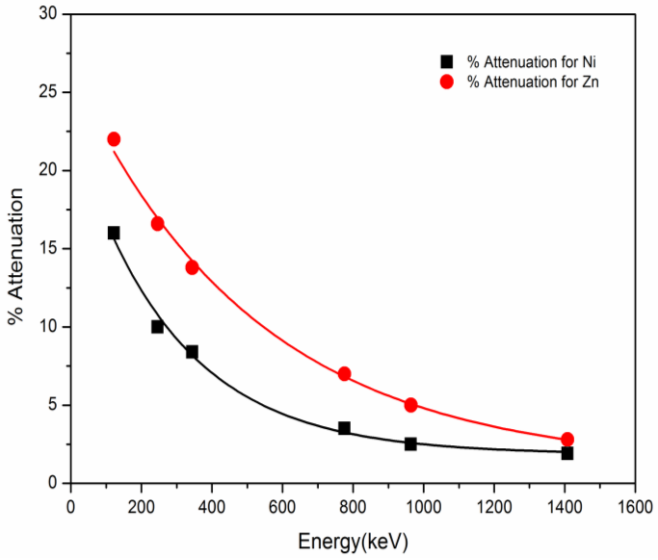

FIG 6.3 Self absorption and self scattering effect for Ni and Zn sample

Table 6.3 Comparison of measured and theoretically predicted cross section data for the present selected reactions

Nuclear Reaction	**Measured Cross section (mb) at 14.2 ± 0.2 MeV**	**Calculated Cross section (mb)**	
		TALYS – 1.6	**EMPIRE – 3.2.2**
$^{75}As(n, p)^{75}Ge$	27.2 ± 1.6	25.58	22.44
$^{66}Zn(n, p)^{66}Cu$	55.5 ± 3.3	50.72	49.32
$^{64}Zn(n, p)^{64}Cu$	170.0 ±10.2	137.12	176.33
$^{55}Mn(n, p)^{55}Cr$	45.8 ± 2.7	26.92	36.23
$^{51}V(n, p)^{51}Ti$	28.2 ± 1.7	35.90	30.52
$^{58}Ni(n, p)^{58}Co$	314.0 ± 18.8	278.96	263.83

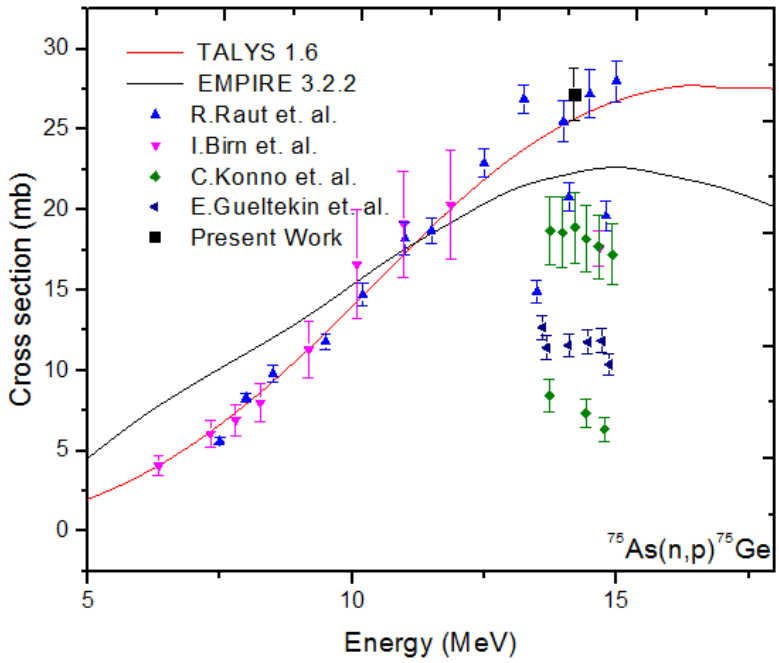

FIG 6.4 Comparison of measured ^{75}As(n, p)^{75}Ge Cross section with EMPIRE-3.2.2, TALYS-1.6, EXFOR data

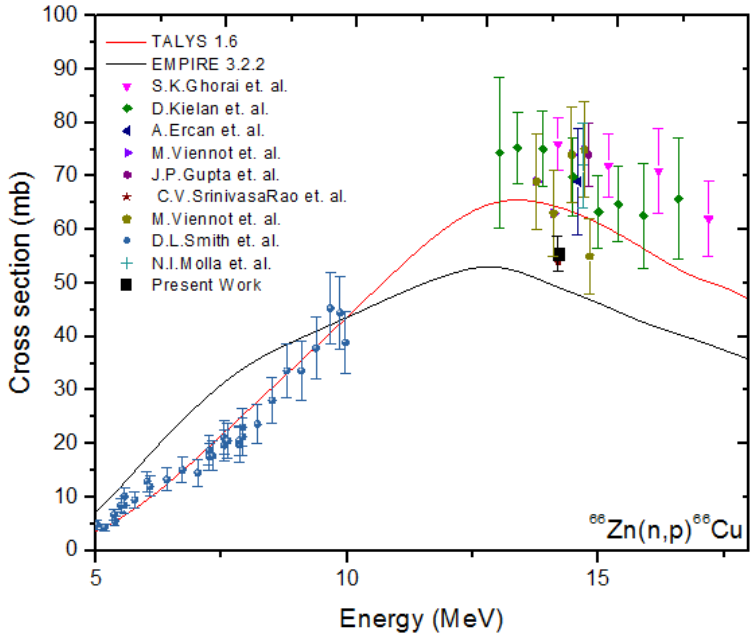

FIG 6.5 Comparison of measured ^{66}Zn(n, p)^{66}Cu Cross section with EMPIRE-3.2.2, TALYS-1.6, EXFOR data

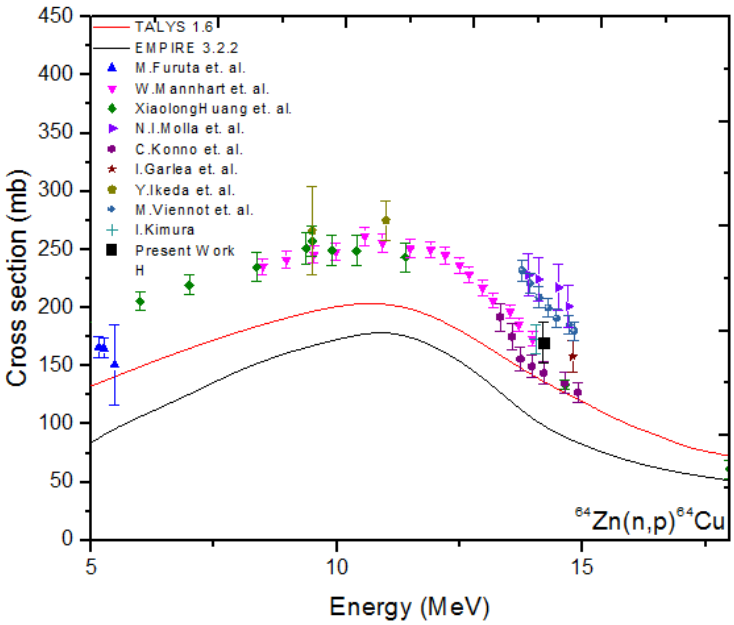

FIG 6.6 Comparison of measured $^{64}Zn(n, p)^{64}Cu$ Cross section with EMPIRE-3.2.2, TALYS-1.6, EXFOR data

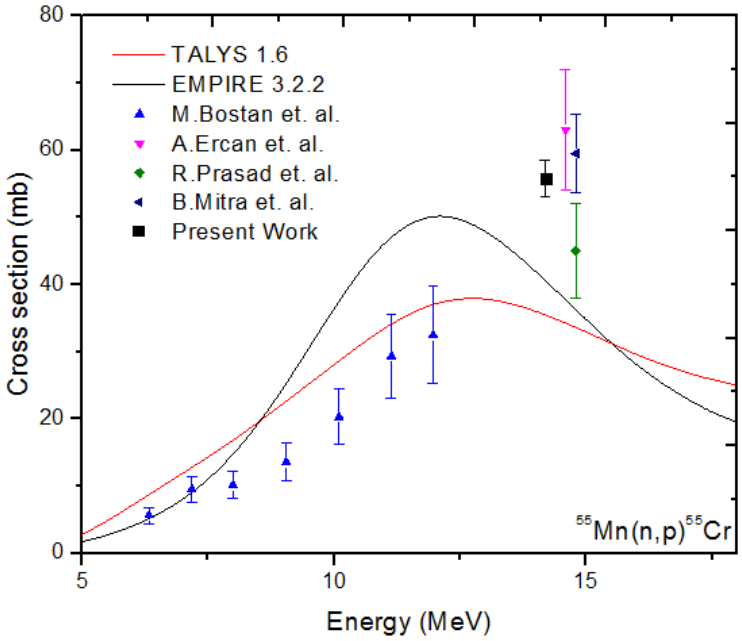

FIG 6.7 Comparison of measured $^{55}Mn(n, p)^{55}Cr$ Cross section with EMPIRE-3.2.2, TALYS-1.6, EXFOR data

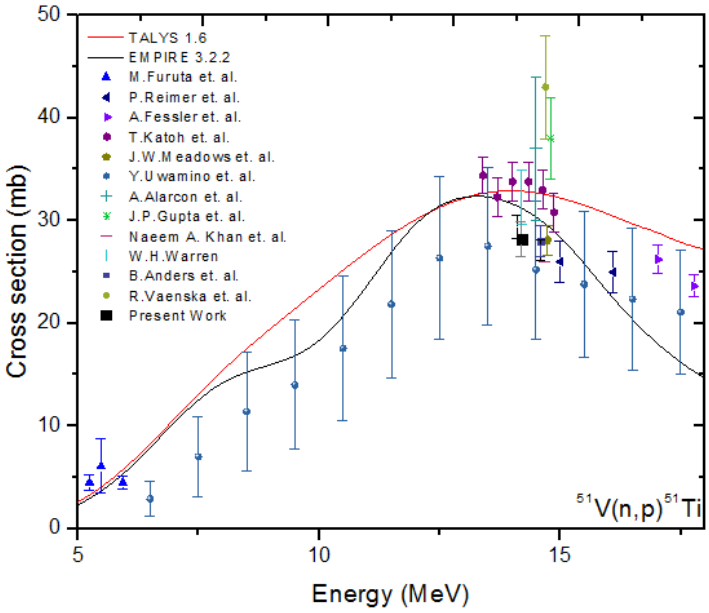

FIG 6.8 Comparison of measured ^{51}V(n, p)^{51}Ti Cross section with EMPIRE-3.2.2, TALYS-1.6, EXFOR data

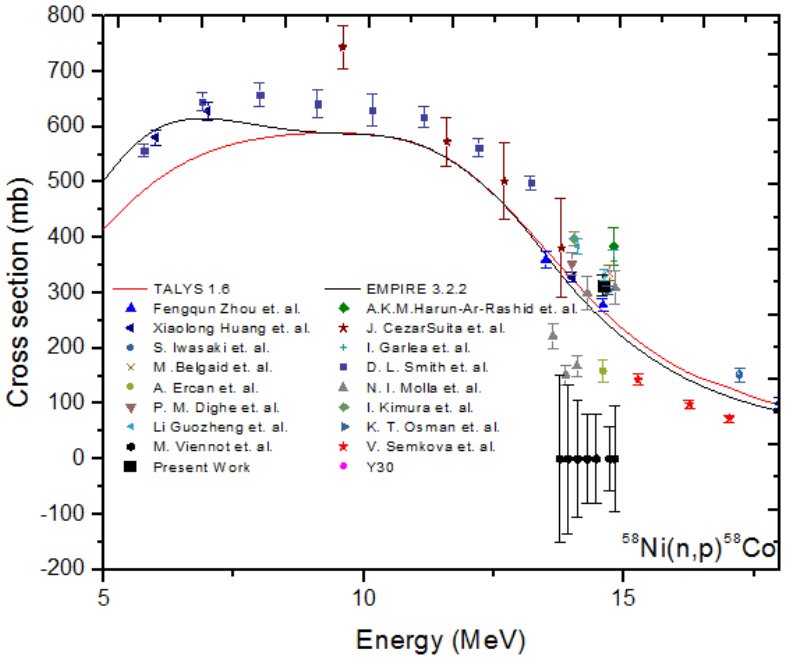

FIG 6.9 Comparison of measured ^{58}Ni(n, p)^{58}Co Cross section with EMPIRE-3.2.2, TALYS-1.6, EXFOR data

6.6 Summary and conclusions

In the present study, the (n, p) reaction cross sections for some of the structural materials such as ^{75}As, ^{66}Zn, ^{64}Zn, ^{55}Mn, ^{51}V and ^{58}Ni were measured at 14.2 ± 0.2 MeV. The offline gamma spectroscopy and neutron activation analysis method were used for the data analysis. The present results were compared with the previously measured data available in EXFOR database as well as theoretical predictions using code TALYS – 1.6 and EMPIRE – 3.2. Present results are in fairly good agreement with some previous measurements and also with theoretical predictions. The results are important for the DT fusion neutrons as well as for the enhancement of the nuclear data library.

References

[1] N. L. Singh, et al., Proc. of DAE Sympo. on Nucl. Phys. 59 (2014) 566. ; 60 (2015) 442.

[2] N. L. Singh, P. M. Prajapati, Electric Power Engineering, 739-742 (2014).

[3] Experimental Nuclear Reaction Data (EXFOR); https://www-nds.iaea.org/exfor

[4] M. Victoria, N. Baluc and P. Spätig, EPFL-CRPP Fusion Technology Materials, CH-5232 Villigen PSI, Switzerland.

[5] V. Barabash, First Joint ITER-IAEA Technical Meeting on "Analysis of ITER Materials and Technologies", 23 – 25 November 2010, Principality of Monaco.

[6] B. Raj and M. Vijayalakshmi, Joint ICTP/IAEA School on Physics and Technology of Fast Reactors Systems, "Radiation Damage of Structural Materials for Fast Reactor Fuel Assembly (3)", Strada Costiera, Italy.

[7] Y. Kasugai, et al., Fusion Engineering and Design 42 (1998) 299–305.

[8] D. Zhou, P. Peng, S. Xu, J. Liu, Research and application of rare earth in steel. Res. Stud. Foundry Equip. 2004, 3, 35–38.

[9] NNDC, ENSDF database, https://www.nndc.bnl.gov/chart/

[10] A. R. Farhan, S. Rab, Nuclear Datasheet for A=75, Nucl. Dat. Sheets 60, 735 (1990).

[11] M. R. Bhat, Nucl. Dat. Sheets 83, 789 (1998).

[12] Huo Junde, Nucl. Dat. Sheets 64, 723 (1991).

[13] B. Singh, Nucl. Dat. Sheets 78, 395 (1996).

[14] R. L. Auble, Nucl. Dat. Sheets 23, 163 (1978).

[15] C. D. Nesaraja, et al., Nucl. Dat. Sheets 111, 897 (2010).

[16] M. Pillon, et al., Fusion Engineering and Design 28 (1995) 683-688.

[17] Guan-bo Wang, et al., http://dx.doi.org/10.1016/j.nima.2014.04.079.

[18] A. J. Koning, et. al., Talys-1.6, A Nuclear reaction program, user manual, NRG-1755 Z. G. Petten, Netherlands(2011)

[19] M. Herman, et. al., EMPIRE-3.2.2 modular system for nuclear reaction calculations and nuclear data evaluation User's Manual

[20] J. Raynal, Notes on ECIS94, CEA Saclay Report No. CEA-N-2772, (1994).

[21] A. J. Koning, J. P. Declaroche, Nucl. Phys., A713: 231-310(2003).

[22] W. Hauser, H. Feshbach, Phys. Rev, 87:366(1952).

[23] C. Kalbach, Phy. Rev. C 33, 818–833 (1986).

[24] S. Hofmann, et al., Ann. Phys. 90, 403 (1975);
S. Hofmann, et al., Z. Physik A 297,153 (1980)

[25] A. V.Ignatyuk, J. Nucl Phys. 21, 255 (1975)

[26] A. Gilbert, et al., Can J. Phys. 43, 1446 (1965)

[27] S. Hilaire, et al., Nucl. Phys, A779: 63-81(2006).

Chapter – 7

Final Summary and Conclusions of the Thesis

In the present thesis a major contribution comes in the form of neutron and photon induced nuclear reactions on various structural and other materials. The energy range covered in this work is between 1 to 20 MeV of neutron energy, and in the GDR energy region for photons, that are important for the reactor applications. In the present thesis, the targets used for the measurement of neutron induced reaction cross sections are the isotopes of W, Gd, Ni, V, Mn, Zn and As, which are of prime importance as structural materials. This work is important from the point of view of enhancing the nuclear data, as well as for the validation of present nuclear reaction models. The neutron induced reactions are studied on $^{182\text{-}184,\ 186}$W, ^{154,160}Gd, ^{75}As, ^{64,66}Zn, ^{55}Mn, ^{51}V, and ^{58}Ni isotopes. In the present work, the nuclear reactions (n, γ), (n, p) and (n, 2n) were studied. The reactions on W isotopes were done using ^{252}Cf spontaneous neutron source and accelerator based ^{7}Li(p, n) neutron source. The reactions on ^{154,160}Gd were studied using accelerator based ^{7}Li(p, n) neutron source. The remaining reactions on isotopes ^{75}As, ^{66}Zn, ^{64}Zn, ^{55}Mn, ^{51}V, and ^{58}Ni were studied using DT neutron source. The selection of the neutrons energies was done by keeping in view the fact that either there are very few or no cross section data or available data points are with large errors.

In addition to this, the present thesis, the giant dipole resonance mechanism for the photoneutron production was studied. A pure empirical formula has been derived from the first principal and used to explain the photonuclear reactions in the GDR energy range. The work is limited to the only (γ, n) nuclear reactions. The behavior of the nuclear quadrupole moment in deformation of the GDR peak has been demonstrated with the present empirical formula. It has been shown that the formula is applicable to the isotopes with $Z \geq 60$. The isotopes, which have experimental data available in the EXFOR library has been used to validate the presently developed empirical formula. Further, the nuclear modular codes were used as a tool to compare the results from the derived empirical formula. These nuclear models were also used to predict the neutron induced reaction cross section results at various selected incident energies. The models are based on an agreement with the nuclear data available in experimental data library EXFOR. The nuclear reaction codes TALYS –

1.6/1.8 and EMPIRE – 3.2.2, which are based on various well known standard nuclear models predictions, were used in the present thesis. The data produced from TALYS – 1.6 has been compared with the TALYS – 1.8, which is the new version of the code that was released during the coarse of this work. The data predicted from the both versions in the present work are found almost similar and no major differences were found, and hence the data listed with both the version were used. The photonuclear reaction data were predicted using TALYS – 1.6 and EMPIRE – 3.2.2 codes. The agreement was found consistent with the generated data obtained from the presently derived empirical formula.

(I) The summarized outcomes of this thesis are listed below.

1. The photon induced (γ, n) reaction cross section predictions have been done for isotopes with $Z \geq 60$ using the presently derived empirical formula discussed in this thesis.
2. Following reactions on tungsten and gadolinium isotopes were experimentally measured by using the ^{7}Li(p, n) reaction obtained from the BARC-TIFR Pelletron facility in Mumbai.
   (a) The cross sections of ^{186}W(n, γ)^{187}W reaction are measured at 5.08 ± 0.165, 8.96 ± 0.77, 12.47 ± 0.825 and 16.63 ± 0.95 MeV.
   (b) The cross sections of ^{182}W(n, p)^{182}Ta reaction are measured at 8.96 ± 0.77, 12.47 ± 0.825 and 16.63 ± 0.95 MeV.
   (c) The cross sections of ^{154}Gd(n, 2n)^{153}Gd and ^{160}Gd(n, 2n)^{159}Gd reactions are measured at 12.47 ± 0.825 and 16.63 ± 0.95 MeV.
3. The cross sections of ^{183}W(n, p)^{183}Ta and ^{184}W(n, p)^{184}Ta reactions are measured at 1.70 ± 1.35 MeV and 3.75 ± 1.26 MeV respectively using the ^{252}Cf spontaneous neutron source.
4. The cross sections of ^{75}As(n, p)^{75}Ge, ^{66}Zn(n, p)^{66}Cu, ^{64}Zn(n, p)^{64}Cu, ^{55}Mn(n, p)^{55}Cr, ^{51}V (n, p)^{51}Ti and ^{58}Ni(n, p)^{58}Co reactions are measured at 14.2 ± 0.2 MeV using DT neutron source.
5. The role of nuclear modular codes, as well as the nuclear transport codes, have been discussed.

6. The reproduction of experimental reaction cross sections has been done by using the standard modular codes EMPIRE and TALYS.

(II) Following conclusions can be made from the entire work done here:

1. The prediction of GDR cross section from the new empirical formula is in general in agreement with the experimental data from several authors and the theoretical codes TALYS and EMPIRE.
2. The empirical formula derived in this thesis for (γ, n) reaction is limited to validity for $Z \geq 60$ and $N - Z \geq 22$, where Z and N are proton and neutron numbers of the isotope respectively.
3. The deformation and double peak are due to the nuclear quadrupole deformation.
4. In the case of the neutron induced reactions, the offline gamma ray spectroscopy and neutron activation analysis (NAA) techniques have been explored for the cross section evaluations.
5. The cross section measured for neutron induced reactions are in general agreement with the nuclear modular code predicted data for all the three experiments.
6. The different parameters, which can affect the results of the experiment were optimized and corrections have been demonstrated using the MCNP code.
7. The cross sections for $^{183}W(n, p)^{183}Ta$ and $^{184}W(n, p)^{184}Ta$ reactions using ^{252}Cf neutron source were relatively small.
8. The measured cross sections of $^{186}W(n, \gamma)^{187}W$ at 5.08 ± 0.165 MeV, 8.96 ± 0.77 MeV, 12.47 ± 0.825 MeV and 16.63 ± 0.95 MeV, $^{182}W(n, p)^{182}Ta$ at 8.96 ± 0.77 MeV, 12.47 ± 0.825 MeV and 16.63 ± 0.95 MeV,$^{154}Gd(n, 2n)^{153}Gd$ and $^{160}Gd(n, 2n)^{159}Gd$ at 12.47 ± 0.825 MeV and 16.63 ± 0.95 MeV are in agreement with the code evaluated data. In the case of the cross section of $^{160}Gd(n, 2n)^{159}Gd$ reaction at 16.63 ± 0.95 MeV, the value is under estimated.

9. The present results of (n, p) reaction cross section for ^{75}As, ^{66}Zn, ^{64}Zn, ^{55}Mn, ^{51}V and ^{58}Ni at 14.2 ± 0.2 MeV are in good agreement with the previous measurements and theoretical calculations.

Future Outlook

The present thesis discusses the cross section measurement of those isotopes having very few and scare data using the standard neutron activation analysis. In the future proposal, accelerator based neutron sources will be employed for the cross section measurement for those isotopes have wide prospects in reactors, but there is a complete lack of cross section data. There are several structural materials still have data shortage, which needs to be completed. The isotopes of tungsten will be taken for further measurements. The empirical formula, which is still applicable to the isotopes with $Z \geq 60$ will be extended to the whole periodic table. The present formula must be extended for the entire energy range and other photoneutron production channels too. Overall the present work has plenty of future scopes.

Reprints of Published Papers

New empirical formula for (γ, n) reaction cross section near GDR Peak for elements with $Z \geqslant 60$ *

Rajnikant Makwana[1;1)] S. Mukherjee[1] Jian-Song Wang(王建松)[2] Zhi-Qiang Chen(陈志强)[2]

[1] Physics Department, Faulty of Science, The Maharaja Sayajirao University of Baroda, Vadodara-390002. India
[2] Key Laboratory of High Precision Nuclear Spectroscopy and Center for Nuclear Matter Science, Institute of Modern Physics, Chinese Academy of Science, Lanzhou 730000, China

Abstract: A new empirical formula has been developed that describes the (γ, n) nuclear reaction cross sections for isotopes with $Z \geqslant 60$. The results were supported by calculations using TALYS – 1.6 and EMPIRE – 3.2.2 nuclear modular codes. The energy region for incident photon energy has been selected near the giant dipole resonance (GDR) peak energy. The evaluated empirical data were compared with available data in the experimental data library EXFOR. The data produced using TALYS – 1.6 and EMPIRE – 3.2.2 are in good agreement with experimental data. We have tested and presented the reproducibility of the present new empirical formula. We observe the reproducibility of the new empirical formula near the GDR peak energy is in good agreement with the experimental data and shows a remarkable dependency on key nuclei properties: the neutron, proton and atomic number of the nuclei. The behavior of nuclei near the GDR peak energy and the dependency of the GDR peak on the isotopic nature are predicted. An effort has been made to explain the deformation of the GDR peak in (γ, n) nuclear reaction cross sections for some isotopes, which could not be reproduced with TALYS – 1.6 and EMPIRE – 3.2.2. The evaluated data have been presented for the isotopes ^{180}W, ^{183}W, ^{202}Pb, ^{203}Pb, ^{204}Pb, ^{205}Pb, ^{231}Pa, ^{232}U, ^{237}U and ^{239}Pu, for which there are no previous measurements.

Keywords: photonuclear reactions, GDR, empirical formula, TALYS, EMPIRE, cross section

PACS: 25.20.-x **DOI:** 10.1088/1674-1137/41/4/044105

1 Introduction

Nuclear reactions are of prime importance in the application of nuclear reactor technology. Nuclear reactors (fusion-fission) require a complete dataset of neutron and photon induced reactions. Photonuclear reactions are becoming more important for fusion reactors and accelerator driven sub-critical system (ADS), where high-energy photons will be generated and subsequently interact with the materials. The study of (γ, n) reactions are important for a variety of current and emerging fields, such as radiation shielding design, radiation transport, absorbed dose calculations for medical, physics, technology of fusion-fission reactors, nuclear transmutation, and waste management applications [1,2]. In a fusion reactor, during the plasma shot, de-confined runaway electrons can interact with the first wall of the reactor and produce high energy photons [3]. These high energy photons can open reaction channels like (γ, n), (γ, p), (γ, 2n), (γ, 3n), etc. The most prominent reaction is (γ, n), as it has a lower threshold than multi-neutron emission, whereas for charged particle emission the Coulomb barrier needs to be considered. Exact information on the cross section for such nuclear reactions is needed to perform accurate nuclear transport calculations. Tungsten (W) and beryllium (Be) are selected as first wall materials for the International Thermonuclear Experimental Reactor (ITER) fusion reactor [4]. Among tungsten isotopes, only ^{182}W (26.5 %), ^{184}W (30.64%) and ^{186}W (28.43%) have experimental cross section data for the (γ, n) reaction. The cross sections of the (γ, n) reaction for ^{180}W (0.12%) and ^{183}W (14.31%) are needed, along with all the remaining long-lived unstable isotopes, as they will interact with high-energy photons during the confined runaways and disruption phase [5]. Gamma induced nuclear reactions are also important for nuclear transmutation (e.g. ^{234}U(γ, n)^{233}U), which is useful for nuclear safety and incineration. The importance of the gamma incineration technique has been studied in the case of many isotopes for nuclear waste management [6–8].

In ADSs, the high energy proton beam will inter-

Received 30 May 2016

* 1) E-mail: rajniipr@gmail.com

act with high Z elements such as W, Pb-Bi, Th and U, which will produce neutrons through spallation reactions [9]. This spallation process will produce high energy photons, which will subsequently interact with the materials. It is necessary to have a complete nuclear dataset of photonuclear reactions for all isotopes of these elements. This can be done by experimental measurements. The experimental measurements of the nuclear reaction cross-section are one of the important methods to complete the nuclear dataset. However, there are always limitations in the experimental measurements due to non-availability of all the energies of incident particles, and preparation of the target, which may itself be unstable. For complete nuclear data for several isotopes, nuclear modular codes such as TALYS – 1.6 and EMPIRE – 3.2.2 are available. Using these codes, one can predict the cross sections for different nuclear reaction channels. These codes basically use some nuclear models, and on the bases of the nuclear reaction theory, evaluation of the nuclear reaction data is done. The theory involved in photonuclear reaction cross section evaluation is discussed in the next section of the paper. Apart from this, nuclear systematics and empirical formulae provide alternative methods for such isotopes, and can efficiently predict the nuclear properties. Many authors have used this theoretical approach. Several systematics and empirical studies have already been made for photonuclear reactions [10]. These empirical formulae reduce experimental efforts, as they are basically dependent on well-known nuclear properties. A new empirical formula has been developed and tested with nuclear modular codes and experimental data for $Z \geqslant 60$ in the present paper. With the help of the present empirical formula, one can predict the cross section datasets for those isotopes where there is a complete lack of experimental data.

2 Theory of photo neutron production

The interaction of high energy photons with target material can cause ejection of the nucleon/s, depending upon the energy of the incident photon. This reaction is considered a photonuclear reaction. Photons should have sufficient energy above the binding energy of the nucleus for nucleon emission. As the nuclear binding energies are above 6 MeV for most isotopes, photons should have such a threshold energy [11]. There are three basic mechanisms for photonuclear reactions: (a) giant dipole resonance (GDR), (b) quasi-deuteron (QD) and (c) intranuclear cascade [12]. A photon with energy below 30 MeV follows the GDR mechanism. In this process, the photon energy is transferred to the nucleus by the oscillating electrical field of the photon, which induces oscillations among nucleons inside the nucleus. Photo neutron production is more probable since proton ejection needs to overcome a large Coulomb barrier. For different isotopes at a particular energy, there is a peak of photo neutron production for the (γ, n) reaction. This is called the GDR peak energy. For isotopes above $Z = 60$, the peak energies are between 10-18 MeV. Above 30 MeV, the photo neutron production is mainly due to the QD effect [12]. In this mechanism, a photon interacts with the dipole moment of a pair of proton-neutrons in place of the nucleus as a whole [12]. Above 140 MeV, photo neutron production results from photo-pion production [12]. Further study of thermal fluctuation on GDR parameters is also of interest and studies are ongoing [13–16].

3 Present empirical formula and theoretical calculations

According to the semi-classical theory of the interaction of photons with nuclei, the shape of the fundamental resonance of the photo absorption cross section follows a Lorentz curve [12, 17].

$$\sigma(E) = \frac{\sigma_i}{1 + \left[\dfrac{\left(E_\gamma^2 - E_{\rm m}^2\right)^2}{E_\gamma^2 \gamma^2}\right]}, \tag{1}$$

where, σ_i, E_γ and γ are the Lorentz parameters: peak cross section, resonance energy and full width at half maximum respectively [18].

In a more general way, by using nuclear modular codes, such as TALYS – 1.6 and EMPIRE – 3.2.2, the photo absorption cross section is calculated as the sum of two components [19],

$$\sigma_{\rm abs}\left(E_\gamma\right) = \sigma_{\rm GDR}\left(E_\gamma\right) + \sigma_{\rm QD}\left(E_\gamma\right). \tag{2}$$

The component $\sigma_{\rm GDR}\left(E_\gamma\right)$ represents the GDR and is given by a Lorentzian shape, which describes the giant dipole resonance. It is given from Eq. (1) by the following expression:

$$\sigma(E) = \sum_i \frac{\sigma_i \cdot \left(E_\gamma \cdot \Gamma_i\right)^2}{\left(E_\gamma^2 - E_i^2\right)^2 + \left(E_\gamma \cdot \Gamma_i\right)^2}, \tag{3}$$

where σ_i, E_i and Γ_i are: peak cross section, resonance energy and full width at half maximum respectively. The summation is limited to $i = 1$ for spherical nuclei, while for deformed nuclei the resonance is split and one uses i=1, 2. The component $\sigma_{\rm QD}\left(E_\gamma\right)$, is given by Levinger type theory given by Chadwick et al [19–21]. It is basically from the quasi-deuteron model. In the energy range from the photonuclear threshold to 30 MeV, the GDR mechanism is dominant, and from 30 – 140 MeV the QD mechanism is dominant. Above 140 MeV the threshold energy for pion production is achieved [20].

The above theory has been used in the TALYS – 1.6 and EMPIRE – 3.2.2 nuclear modular codes [22, 23].

Further details of these codes are given in Refs. [18, 24]. Using these codes, (γ, n) nuclear reaction cross sections for different isotopes ($Z \geqslant 60$) were calculated and are presented in the present work. Until now, the photonuclear reaction cross sections have been evaluated using the Lorentz parameters. These parameters for several isotopes are calculated by fitting the experimental data or by systematics [25].

3.1 Fundamental term

In the present paper, in contrast to the Lorentzian parameters, the basic properties of nuclei, A, N and Z, are used to estimate the photonuclear cross section. Levovskii has given empirical formulas for (n, p) and (n, 2n) reaction cross section at 14.0 MeV [26] as,

$$\sigma(\mathrm{n,p}) \propto \sigma_{\mathrm{p}} \cdot \mathrm{e}^{-\frac{33\cdot(N-Z)}{A}}, \tag{4}$$

$$\sigma(\mathrm{n,2n}) \propto \sigma_{\alpha} \cdot \mathrm{e}^{-\frac{33\cdot(N-Z)}{A}}, \tag{5}$$

where $\sigma_{\mathrm{p}} = \pi r_0^2 (A^{1/3}+1)^2$ and $\sigma_{\alpha} = 0.4 \cdot \pi r_0^2 (A^{1/3}+1)^2$, $r_0 = 1.2 \times 10^{-13}$ cm.

These empirical formulae are based on A, N and Z of a nucleus, and at an energy 14.0 MeV. Similarly it is possible to derive an empirical formula for photo induced (γ, n) nuclear reactions, which may be applied near GDR peak energy. For the (γ, n) reaction, the formula is modified in the following way,

$$\sigma(\gamma,\mathrm{n}) \propto \sigma_{\mathrm{m}} \cdot \mathrm{e}^{-\frac{33.5\cdot(N-Z)}{A}}, \tag{6}$$

$$\sigma_{\mathrm{m}} = \pi r_0^2 \cdot (A^{2/3}+1)^2 \cdot (N-Z) \cdot A^{\frac{-4}{3}}, \tag{7}$$

where r_0 is the average nuclear radius.

3.2 Isotopic dependent resonance term

The term $(N-Z)/A$ is the asymmetry parameter which considers the deformation of a nucleus. In this expression, there is no term containing energy dependency. Hence, an energy dependent term must be added, and the modified formula is as given below,

$$\sigma(\gamma,\mathrm{n}) \propto \sigma_{\mathrm{m}} \cdot \mathrm{e}^{-\frac{33.5\cdot(N-Z)}{A}} \cdot \mathrm{e}^{\left(-\left(\frac{(E_i - S_j \cdot R_{\mathrm{p}})}{2}\right)^2\right)} \tag{8}$$

where E_i is the incident photon energy, and R_{p} is the resonance parameter.

The parameter S_j is given by,

$$S_j = \frac{A^2}{2(N-Z)^2}. \tag{9}$$

The parameter R_{p} is estimated for an isotope by fitting the (γ, n) nuclear reaction cross section using the above formula for different isotopes of the same element. We observed that this parameter R_{p} follows a linear relationship against the atomic mass of different isotopes of the same element, which can be written in the form of the following equation,

$$R_{\mathrm{p}} = m \cdot A + C, \tag{10}$$

where A is the atomic mass of the isotope, and m and C are slope and intercept respectively, More details of this parameter (R_{p}) for different elements is given in Section 3.3.1.

This term $\mathrm{e}^{-\left\{\frac{(Ei - S_j \cdot R_p)}{2}\right\}^2}$ depends on the energy of the incident photon and the isotopic nature of the target nucleus. When a photon is incident on the nucleus the response of the nucleus depends on the photon energy. While the incident photon is below the threshold energy for photo fission the photon cannot eject a nucleon from the nucleus. If energy of the photon is above the threshold energy of the (γ, n) reaction, the reaction cross section increases until the resonance peak energy. After this energy the cross section decreases again. This is incorporated using this exponential term. The subtraction of $S_j \cdot R_{\mathrm{p}}$ from the incident photon energy shows the isotopic dependence of the resonance peak energy of the reaction. As the isotopic number increases it is observed in the experimental data that the GDR peak shifts towards the lower energy side. This back shift effect can be calculated with the exponential term considered here. The value of $S_j \cdot R_{\mathrm{p}}$ increases with addition of neutrons to the isotope nucleus. This means that when a photon is incident on the target isotope, it interacts with the last shell neutron in the nucleus. The binding energy of the last added neutron will be least. Hence the photon may require smaller energy to cause the resonance as the isotope number increases

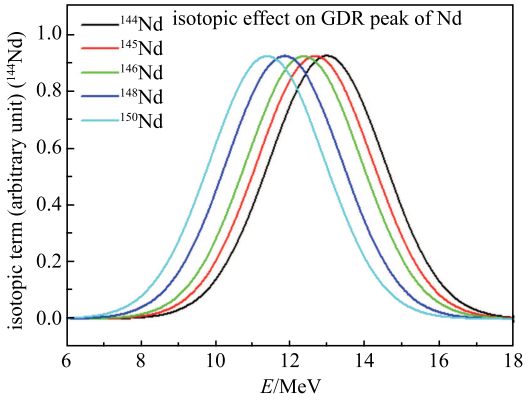

Fig. 1. (color online) Back shift of resonance peak energy in Nd isotopes, from the term $\mathrm{e}^{-\left\{\frac{(Ei - S_j \cdot R_p)}{2}\right\}^2}$.

This can be observed from Figs. 1 and 2, showing the isotopic effect for the resonance peak energy back shift in Nd and Pt isotopes from the above exponential term.

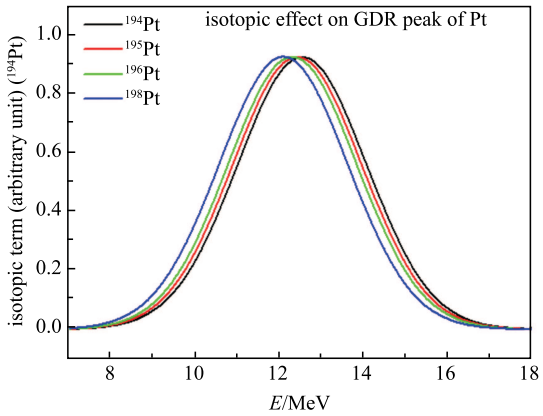

Fig. 2. (color online) Backshift of Resonance Peak Energy in Pt isotopes, from the term $e^{-\left\{\frac{(Ei-S_j\cdot R_p)}{2}\right\}^2}$.

3.3 Energy dependency term

It was found that another energy related term is required to make the formula more efficient to predict the cross section. If the photon energy increases, then the photon can transfer more energy to the nucleus. In the GDR mechanism, the oscillating electrical field transfers its energy to the nucleus by inducing an oscillation in the nucleus, which leads to relative displacement of tightly bound neutrons and protons inside the nucleus. [12]

When the energy of the photon is low (near threshold), the oscillating electric field of the photon interacts with the collective nucleus field produced by the sum effect of the nucleons. But as the energy of the photon increases, the oscillating electrical field interacts with a pair of neutron and proton rather than with the nucleus. This is followed by the term $e^{\sqrt{1+E^{\frac{2}{3}}}}$, where E is the energy of the incident photon. This term shows that the photon can have more energy to transfer to the nucleon as the incident photon energy increases. This indicates that as the energy of the photon increases, it can have less interaction time with nucleons, and hence the pre-equilibrium or direct reaction mechanism can be followed by the emission of the neutron.

Hence, by the addition of an energy dependent term, the modified formula is,

$$\sigma(\gamma,\mathrm{n}) \propto \sigma_{\mathrm{m}}\cdot e^{-\frac{33.5\cdot(N-Z)}{A}}\cdot e^{\left(-\left(\frac{(Ei-S_j\cdot R_{\mathrm{p}})}{2}\right)^2\right)}\cdot e^{\sqrt{1+E^{\frac{2}{3}}}}. \tag{11}$$

An additional factor S_{f}, which is an isospin dependent factor, has been introduced to complete the formula. This factor was plotted for different isotopes of the same element, and fitted. We observed this factor follows some exponential relation, which is described in Section 3.3.2. This empirical formula gives the cross section to the order of milli-barns.

The final modified formula is now,

$$\sigma(\gamma,\mathrm{n}) = \sigma_{\mathrm{m}}\cdot e^{-\frac{33.5\cdot(N-Z)}{A}}\cdot e^{\left(-\left(\frac{(Ei-S_j\cdot R_{\mathrm{p}})}{2}\right)^2\right)}\cdot e^{\sqrt{1+E^{\frac{2}{3}}}}\cdot S_{\mathrm{f}}. \tag{12}$$

3.3.1 R_{p} parameter

This parameter shows the dependency of the photo absorption cross section with respect to the atomic number (Z). In the empirical formula, the term $e^{-\left\{\frac{(Ei-S_j\cdot R_{\mathrm{p}})}{2}\right\}^2}$ has a subtraction factor containing S_j and R_{p}. R_{p} is responsible for the change in the cross section due to atomic number, and the multiplication of S_j and R_{p} is responsible for the isotopic back shift effect, as shown in Figs. 1 and 2. The parameter R_{p} for different isotopes can be calculated using a linear relation, viz Eq. (10), with the atomic mass number of isotopes for an element. Therefore, the plot of R_{p} vs A for different elements should show parallel lines with different intercepts on the R_{p} axis, as shown in Fig. 3. Parallel lines have the same slope but different intercepts. Hence, the mean slope of different elements has been taken as the standard slope for all elements ($Z \geqslant 60$). This value of the slope (m) mentioned in Eq. (10) is $\sim$ 0.03164 $\pm$ 0.00409. The intercept C for different elements are plotted against the atomic number of the element, and fitted with the mathematical software MATLAB using a 3$^{\mathrm{rd}}$ degree polynomial as shown in Fig. 4. The intercept C for different elements can be determined from the following equation:

$$C(Z) = p_1\cdot Z^3 + p_2\cdot Z^2 + p_3\cdot Z + p_4 \tag{13}$$

with $p_1 = -4.155\times10^{-5}$, $p_2 = 0.008971$, $p_3 = -0.7156$, and $p_4 = 15.78$, where Z is atomic number (SSE: 0.00147; R-square: 0.9998: Adjusted R-square: 0.9996; RMSE: 0.01917).

Hence, the intercept for any element can be evaluated using the above Eq. (13). Using this intercept and the slope 0.03164 $\pm$ 0.00409, one can calculate the parameter R_{p} from Eq. (10). The model values of the parameter R_{p} for different elements are compared with the previous manually selected values in Fig. 3.

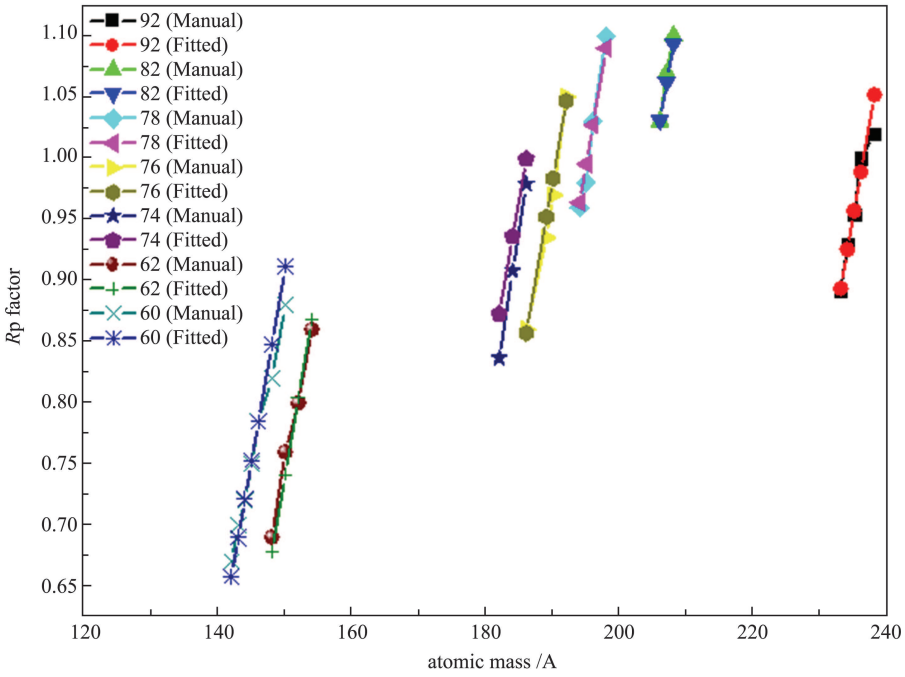

Fig. 3. (color online) $R_{\rm p}$ parameter fitting for different elements with Eq. (10).

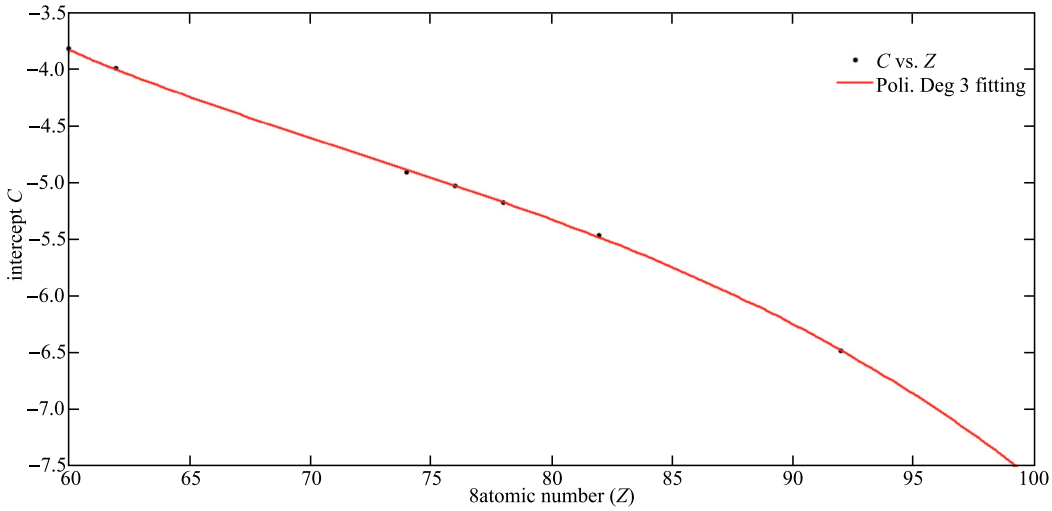

Fig. 4. Intercept C for Eq. (10) for different elements fitted with Eq. (11).

3.3.2 $S_{\rm f}$ Parameter

This parameter includes the isospin effect. This effect has been discussed by J. S. Wang et al. [27]. In order to include this effect in the empirical formula, an additional factor called $S_{\rm f}$ has been added. This factor was initially manually added and then, in order to generalize, it was fitted with different combinations of N, Z and A. It was found that it follows a complex exponential relation with $\exp((N-Z)/N)$ of an isotope. This parameter $S_{\rm f}$ is also considered a result of the asymmetry of the nucleus. As there is a difference in neutron and proton number, the fraction $(N-Z)/N$ is the available neutron fraction for a photon to eject. As this fraction value increases, the value of $S_{\rm f}$ increases correspondingly, which directly shows an increase in the photo absorption cross section of that isotope.

This isotopic factor $S_{\rm f}$ for different isotopes is plotted with respect to $e^{\frac{N-Z}{N}}$ and fitted with MATLAB software as shown in Fig. 4. The generalized expression to determine the $S_{\rm f}$ parameter for an isotope is as given below:

$$S_{\rm f} = a{\rm e}^{bx} + c{\rm e}^{dx}, \tag{14}$$

where, $x = (N-Z)/N, a = 1.21\times10^{-22}$, $b = 34.21, c = 7.71\times10^{-11}$, $d = 14.52$

(SSE: 0.006977; R-square: 0.9781; Adjusted R-square: 0.9759; RMSE: 0.01551).

Looking at Fig. 5 carefully, for some points when ${\rm e}^{\frac{(N-Z)}{N}}$ is near 1.40 to 1.42, they have almost the same $S_{\rm f}$ factor values. These $S_{\rm f}$ factor values are for $Z = 82$ and $N = 124$, 125, 126, which are either a magic number or near the magic number. $S_{\rm f}$ is purely dependent on $(N-Z)/N$, which is a shell dependent term. The anomalous behavior of the same $S_{\rm f}$ factor values for these isotopes is because of the magic shell effect.

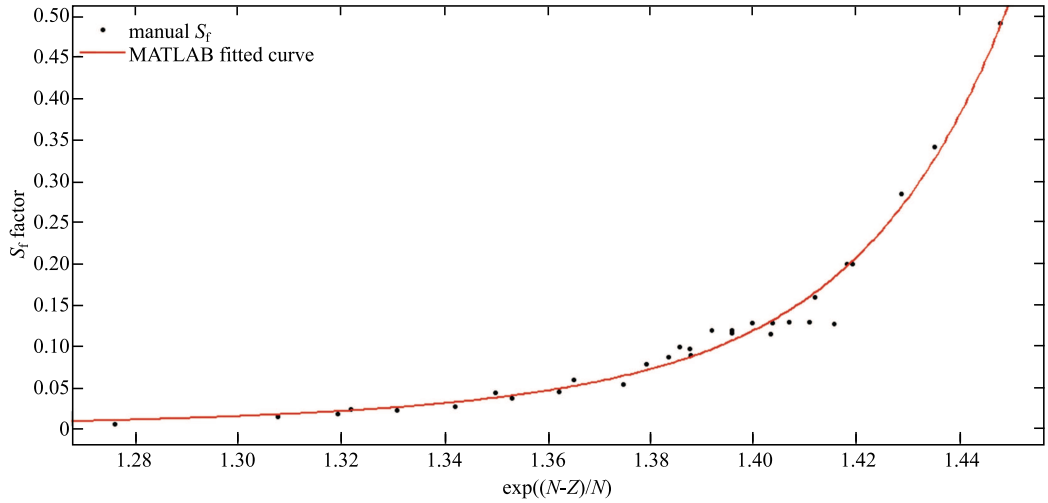

Fig. 5. $S_{\rm f}$ parameter for different $(N-Z)/N$ fitted with Eq. (14).

4 Results and discussion

The (γ, n) reaction cross sections are calculated using TALYS – 1.6, EMPIRE – 3.2.2 and the newly developed empirical formula for isotopes with $Z \geqslant 60$ and presented in Figs. 6–10. The cross sections are calculated for the energy range in which the GDR peak is observed. The theoretically calculated cross sections are compared with the experimentally available data in the EXFOR data library [28]. The data calculated using modular codes and empirical formula are in agreement with the experimental data, as shown in Figs.6–10. However, the cross section values and the nuclear behavior near the GDR peak predicted by the empirical formula are more appropriate. This empirical formula is good for those isotopes which have a single GDR peak. In most of the cases studied here that have a single GDR peak, the empirical formula gives good agreement near the GDR peak energy compared to the model based on Lorentz curve fitting.

In the case of isotopes with Z from 63 to 75, it is found that according to the collective model these isotopes have large nuclear quadrupole moments. The quadrupole exists because of the asymmetry of the nucleus. The nuclei are found in the middle of the 1d, 2 s shells in the range $145 < A < 185$. The energy difference between the ground state and the first excited state is of the order of hundreds of keV. In the deformed nucleus the incident photon can interact either with the ground state or with the excited state nucleon, and hence can produce a resonance at two different nearby energies. This is observed in the above isotopes. For such cases, the Lorentz curve based model, viz. TALYS – 1.6 and EMPIRE – 3.2.2, works reliably for these isotopes, as shown in Fig. 11. For some cases, however, the TALYS – 1.6 and EMPIRE – 3.2.2 model does not work well, e.g. Figs. 11(e – f). To apply the empirical formula for such isotopes, it is assumed that there may be two peaks due to unresolved resonances occurring near the energies of ground and excited nuclei, which are due to the quadrupole moment. This suggests parameters $R_{\rm p}$ and $S_{\rm f}$ can have two different values for these isotopes. It indicates that the energy dependence cross section curve is made of two curves with two different $R_{\rm p}$ ($R_{\rm p1}$ and $R_{\rm p2}$) and $S_{\rm f}$ values ($S_{\rm f1}$ and $S_{\rm f2}$) of parameters $R_{\rm p}$ and $S_{\rm f}$ respectively. These values can be estimated by multiplying the following factors to the $R_{\rm p}$ and $S_{\rm f}$ values calculated from Sections 3.3.1 and 3.3.2.

$$R_{\rm p1} = 0.95\times R_{\rm p}, \tag{15}$$

$$R_{\rm p2} = 1.20\times R_{\rm p1}, \tag{16}$$

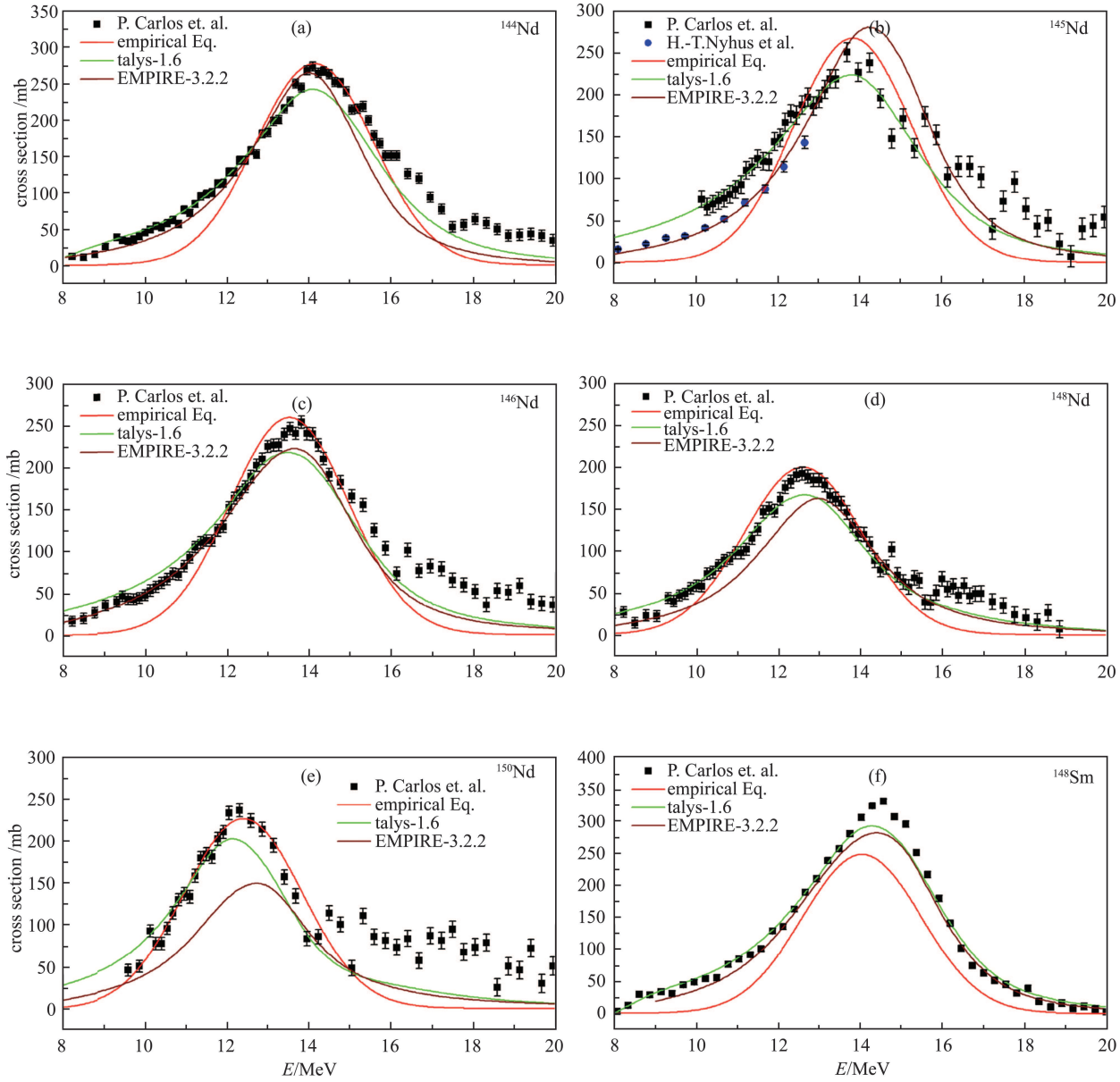

Fig. 6. (color online) Comparison of evaluated data using TALYS-1.6, EMPIRE-3.2.2, and empirical formula with experimental data from EXFOR, for ^{144}Nd, ^{145}Nd, ^{146}Nd, ^{148}Nd, ^{150}Nd, and ^{148}Sm.

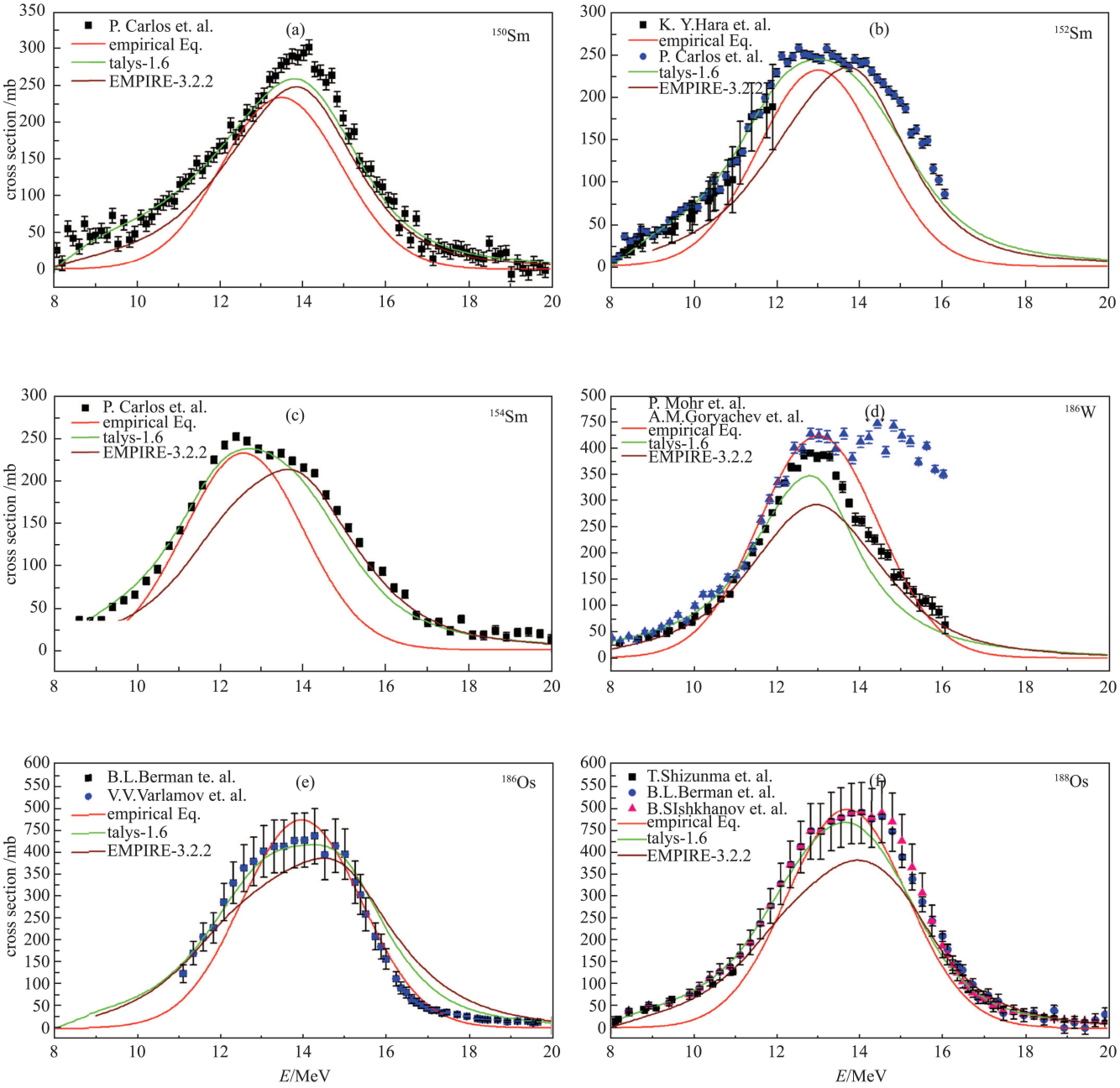

Fig. 7. (color online) Comparison of evaluated data using TALYS-1.6, EMPIRE-3.2.2, and empirical formula with experimental data from EXFOR, for ^{150}Sm, ^{152}Sm,^{154}Sm, ^{186}W, ^{186}Os, and ^{188}Os.

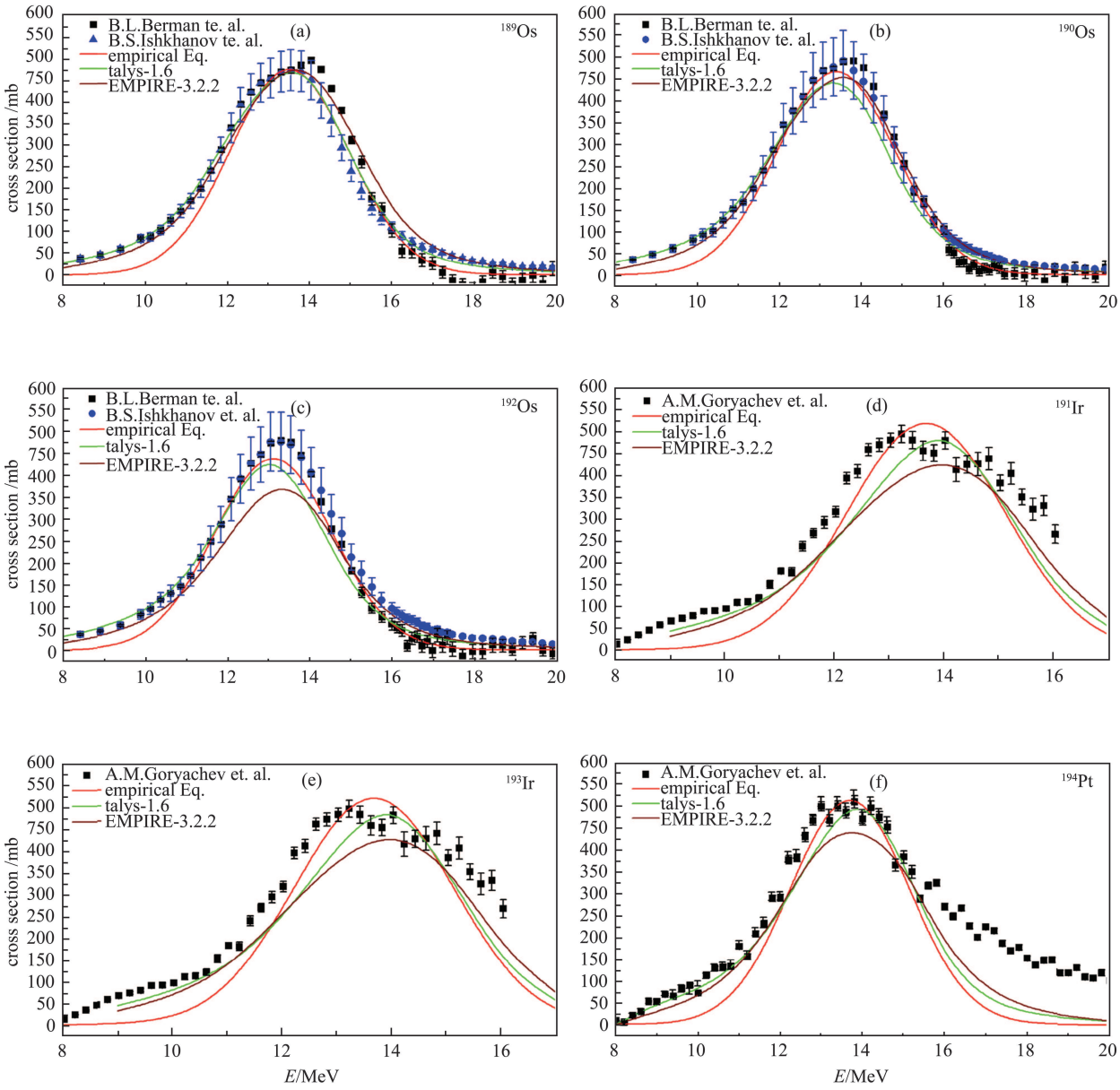

Fig. 8. (color online) Comparison of evaluated data using TALYS-1.6, EMPIRE-3.2.2, and empirical formula with experimental data from EXFOR, for ^{189}Os, ^{190}Os, ^{192}Os, ^{191}Ir, ^{193}Ir, and ^{194}Pt.

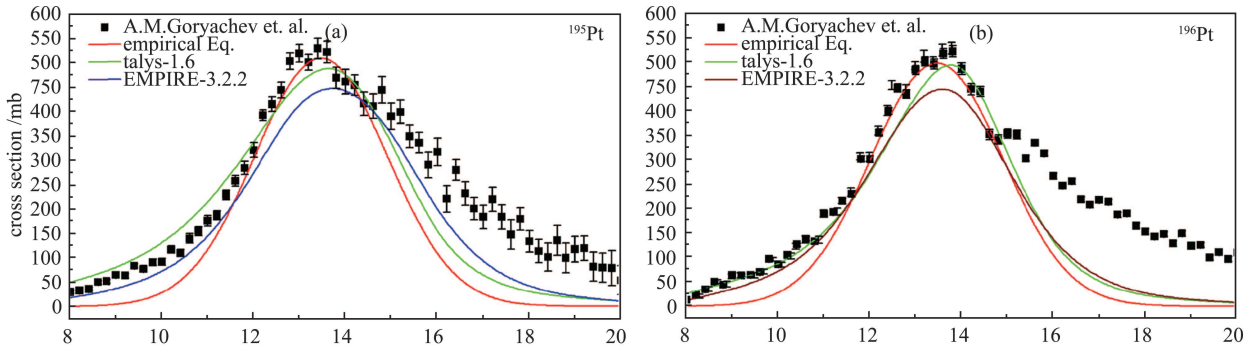

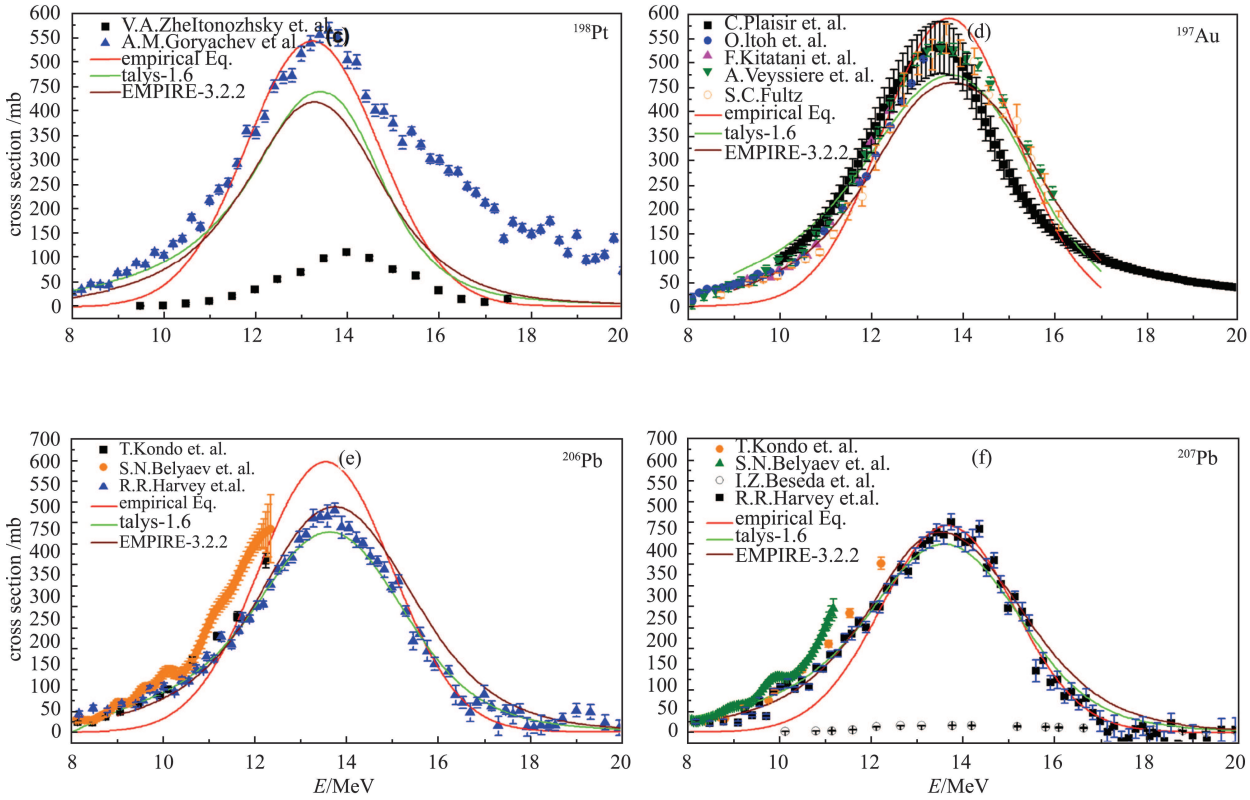

Fig. 9. (color online) Comparison of evaluated data using TALYS-1.6, EMPIRE-3.2.2, and empirical formula with experimental data from EXFOR, for ^{195}Pt, ^{196}Pt, ^{198}Pt, ^{197}Au, ^{206}Pb, and ^{207}Pb.

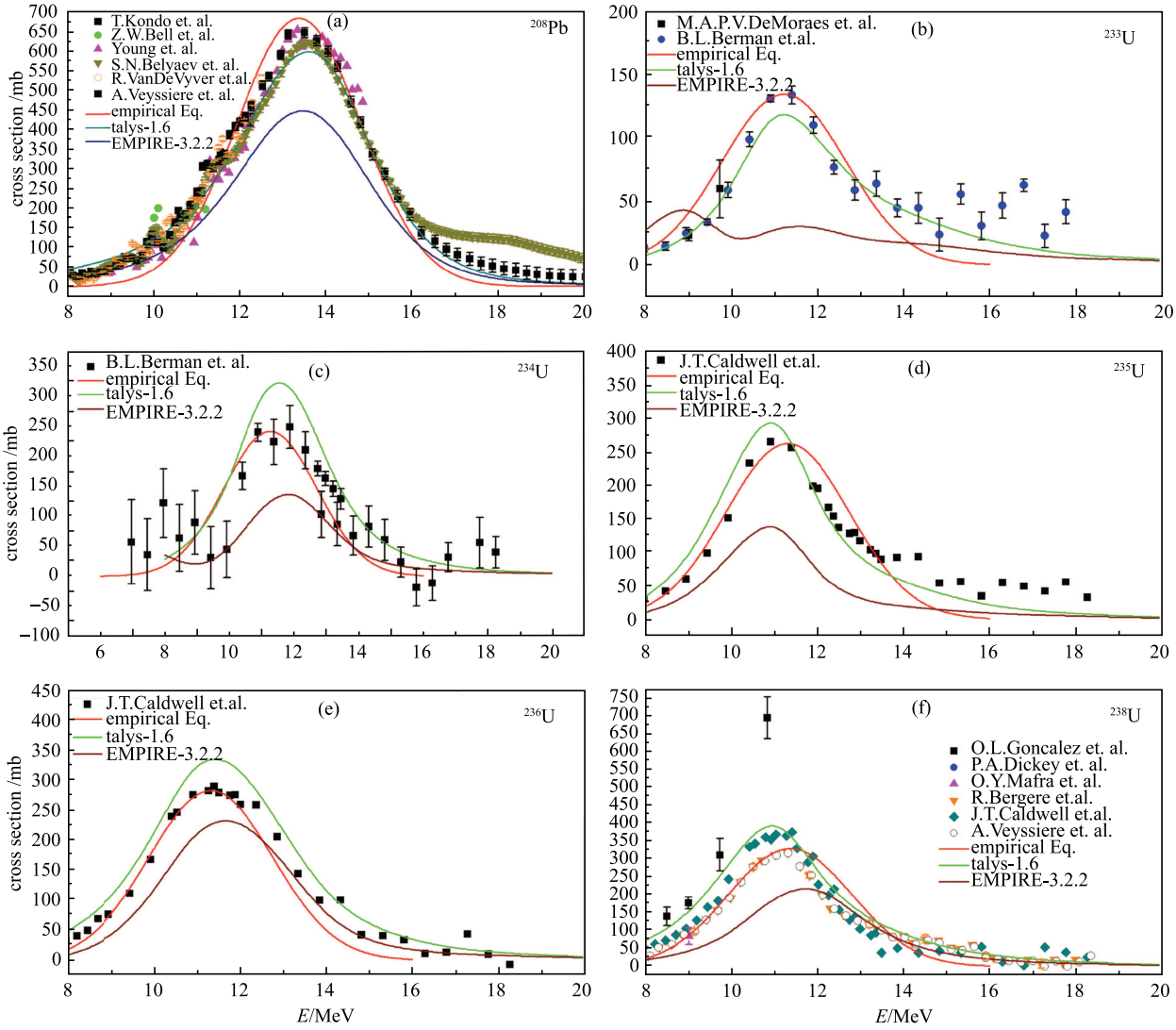

Fig. 10. (color online) Comparison of evaluated data using TALYS-1.6, EMPIRE-3.2.2, and empirical formula with experimental data from EXFOR, for ^{208}Pb, ^{233}U, ^{234}U, ^{235}U, ^{236}U, and ^{238}U.

$$S_{\rm f1} = 1.39 \times S_{\rm f}, \tag{17}$$

$$S_{\rm f2} = 0.28 \times S_{\rm f1}. \tag{18}$$

The two curves intersect at a deep point, where both curves should have the same value of cross section. This intersection point energy can be calculated by comparing the right-hand side of Eq. (12) for the above values.

$$\begin{aligned}&\sigma_{\rm m}\cdot {\rm e}^{-\frac{33.5(N-Z)}{A}}\cdot {\rm e}^{-\left(\frac{\left(Ei-S_j\cdot R_{\rm p1}\right)}{2}\right)^2}\cdot {\rm e}^{\sqrt{1+E^{\frac{2}{3}}}}\cdot S_{\rm f1}\\ &=\sigma_{\rm m}\cdot {\rm e}^{-\frac{33.5(N-Z)}{A}}\cdot {\rm e}^{-\left(\frac{\left(Ei-S_j\cdot R_{\rm p2}\right)}{2}\right)^2}\cdot {\rm e}^{\sqrt{1+E^{\frac{2}{3}}}}\cdot S_{\rm f2}.\end{aligned} \tag{19}$$

Solving this equation, we get

$$E_{\rm deep} = \frac{1}{2}S_j\cdot(R_{\rm p1}+R_{\rm p2}) + \frac{2\ln\left(\frac{S_{\rm f2}}{S_{\rm f1}}\right)}{Sj\,(R_{\rm p1}-R_{\rm p2})}. \tag{20}$$

This energy $E_{\rm deep}$ is near the threshold energy of the (γ, 2n) reaction. With this consideration the results are plotted in Fig. 11(a–f).

5 Applications

The (γ, n) cross section for several isotopes of W, Pb, Pa, U and Pu, which have no available experimental data, are calculated and presented using TALYS – 1.6, EMPIRE – 3.2.2 and the present empirical formula. Further, the predicted data of the isotopes were compared with different standard evaluated data libraries, wherever available.

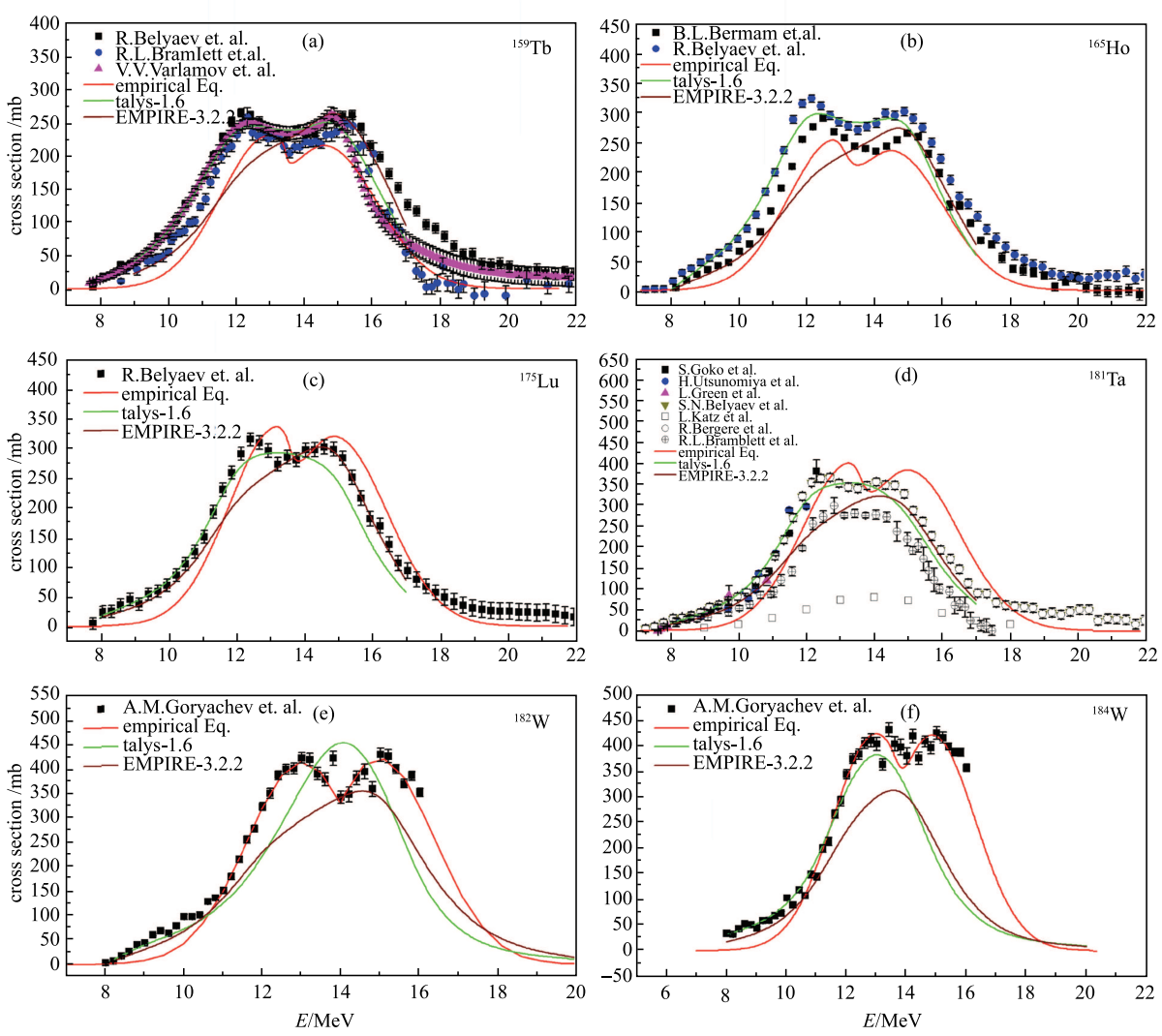

Fig. 11. (color online) Effect of deformed nuclei in (γ, n) nuclear reaction, data comparisons for TALYS – 1.6, EMPIRE – 3.2.2 and present empirical formula.

Tungsten is a prime candidate for the plasma facing component in a fusion reactor. It is selected for the diverter material in the ITER fusion reactor [4]. Tungsten isotopes ^{182}W, ^{184}W and ^{186}W have available experimental data for the (γ, n) reaction cross section [28]. The (γ, n) cross section for the remaining isotopes ^{180}W(0.12%) and ^{183}W(14.31%) are calculated and compared with the evaluated data available in ENDF/B-VII.1. No other standard data library has photonuclear data for these tungsten isotopes [18]. There is an agreement between the present evaluated data and ENDF/B-VII.1, as can be seen in Fig. 12 (a – b) data. Lead is a prime element of the Pb-Li blanket module of fusion reactors, as well as a candidate for the ADS target material [29]. Lead isotopes ^{206}Pb, ^{207}Pb and ^{208}Pb have available experimental data. The (γ, n) cross section for the remaining isotopes of lead ^{202}Pb (5.25×10^4 y, [30]), ^{203}Pb (51.92 h, [30]), ^{204}Pb (1.4×10^{17} y, [30]) and ^{205}Pb (1.73×10^7 y, [30]) are calculated and presented. These isotopes of lead have large half-lives and they face high energy photons during the runaway electron generation and the disruption phase in plasma [5]. Some isotopes of Pa and U, ^{231}Pa(3.27×10^4 y, [30]), ^{232}U(68.9 y, [30]) and ^{237}U(6.75 d, [30]), with no evaluated cross section data available in different standard data libraries such as ENDF/B-VII.1, JENDL-4.0, JEFF-3.1, ROSFOND and CENDL-3.1 [31, 32], are also calculated and presented here. The evaluated data for ^{239}Pu(2.41×10^4 y, [30]) and available data in ENDFB/VII.1 are presented in Fig. 13(d). Though in present context, the cross sections are evaluated for limited isotopes, it can be applied to calculate (γ, n) reaction cross sections for actinides using the nuclear

modular codes and present empirical formula. Further, the TALYS – 1.6 and EMPIRE – 3.2.2 codes can be used to calculate the (γ, n) reaction cross section for isotopes which have available GDR parameters, whereas the present empirical formula can be used to calculate cross section for any isotope with $Z \geqslant 60$.

Another important application is that, by using the nuclear modular codes and the present formula, it is possible to calculate the incident gamma energy for which the cross section will have its maximum value, i.e. the GDR peak energy. It can be used to calculate the incident charged particle (e.g. electron) beam energy for bremsstrahlung production, which is required to design a photo neutron source. There are some theoretical transport codes available to for electrons and photons, such as MCNP [12, 33, 34], FLUKA [35, 36], GEANT [37] etc. With these codes, one can estimate the bremsstrahlung spectra from the electron beam.

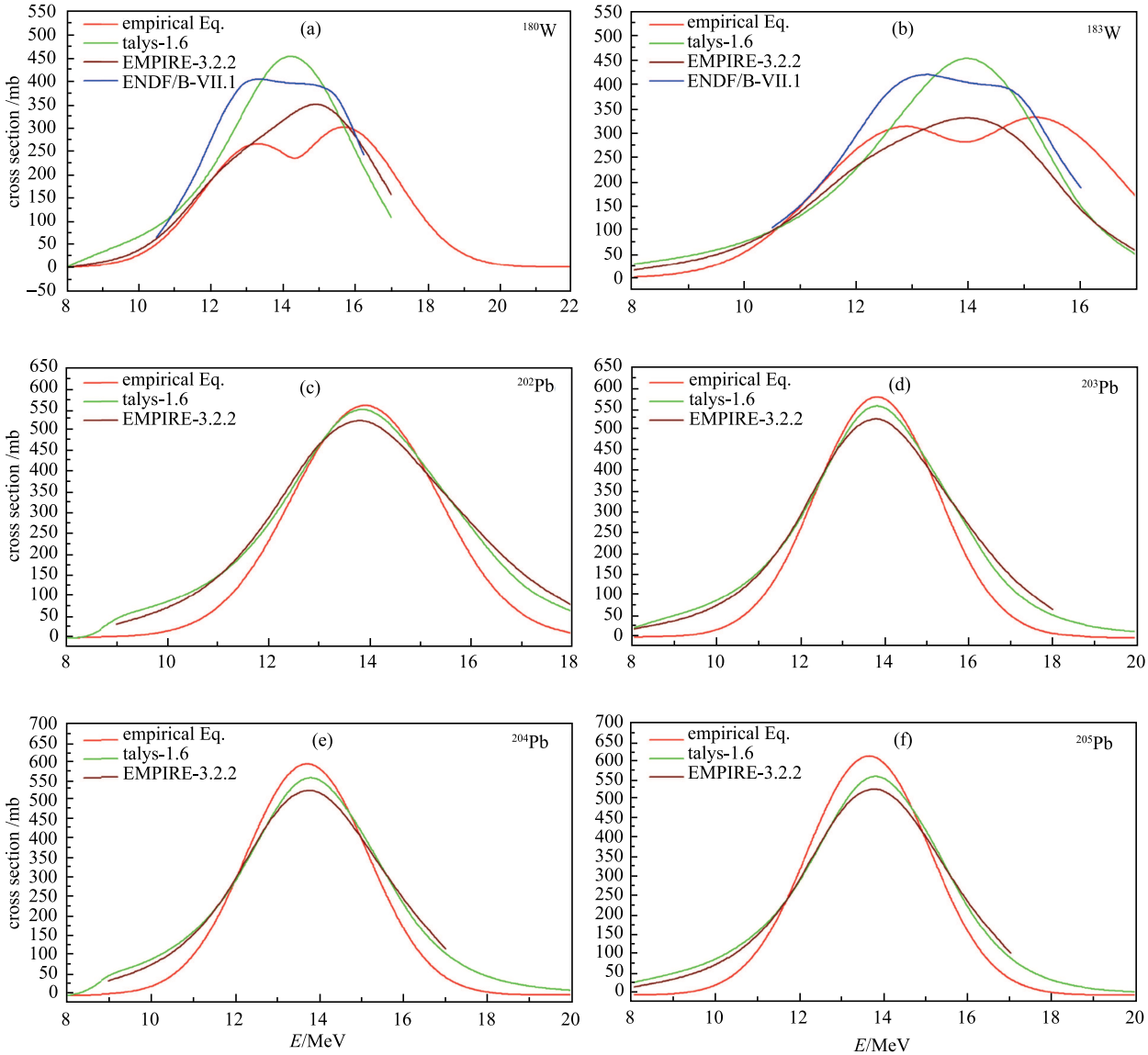

Fig. 12. (color online) Comparison of evaluated data for ^{180}W, ^{183}W, ^{202}Pb, ^{203}Pb, ^{204}Pb, ^{205}Pb using TALYS -1.6, EMPIRE- 3.2.2, and empirical formula.

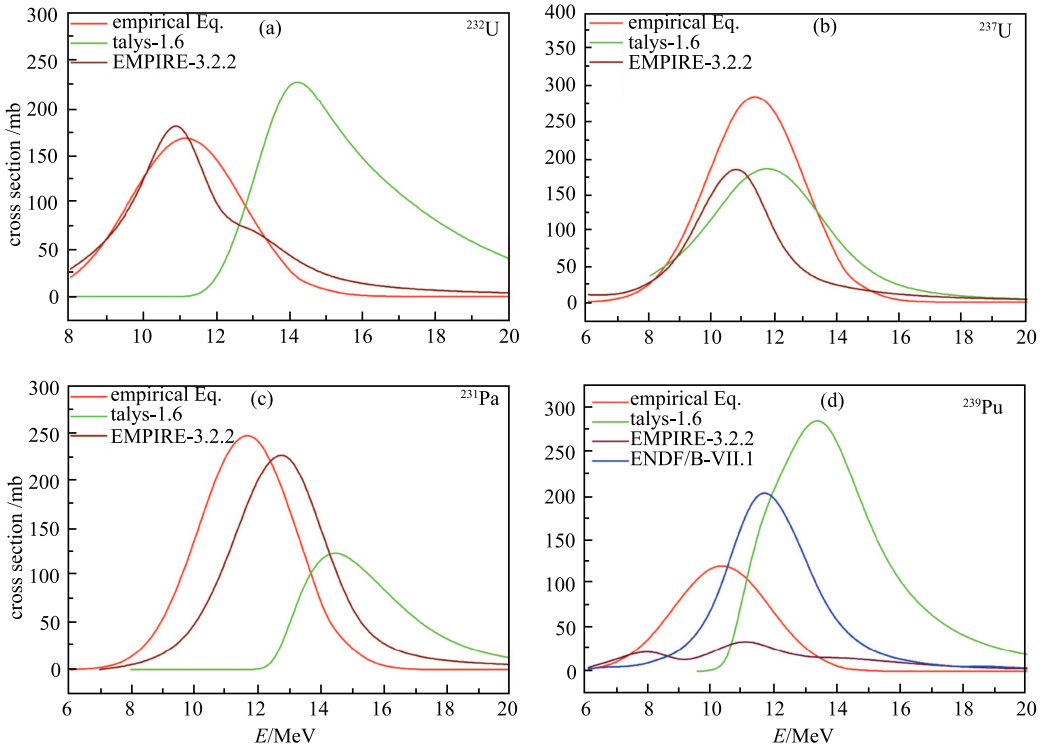

Fig. 13. (color online) Comparison of evaluated data for ^{231}Pa, ^{232}U, ^{237}U, ^{239}Pu using TALYS -1.6, EMPIRE-3.2.2, and empirical formula.

6 Conclusion

In the present work, a new empirical formula has been developed to investigate the (γ, n) reaction cross section for different isotopes with $Z \geqslant 60$ in the GDR energy region. The results for the (γ, n) reaction cross section obtained by using the above empirical formula have been reproduced by using the nuclear modular codes TALYS – 1.6 and EMPIRE – 3.2.2. It has been shown that TALYS – 1.6, EMPIRE – 3.2.2 and our empirical formula are in agreement with the experimental data. Further a conclusion may be drawn that there may be no deformation in the GDR peak of a pure (γ, n) reaction cross section for spherical nuclei. As a result of the quadrupole, which is due to the asymmetric shape of the nucleus, the present deformation has been observed.

In addition to this, the evaluated data for ^{180}W, ^{183}W, ^{202}Pb, ^{203}Pb, ^{204}Pb, ^{205}Pb, ^{231}Pa, ^{232}U, ^{237}U and ^{239}Pu using TALYS – 1.6, EMPIRE – 3.2.2 and our empirical formula have been presented. Among these only ^{180}W, ^{183}W and ^{239}Pu have evaluated data in ENDF/B-VII.1 [29], which are compared with the present evaluated data. For ^{180}W and ^{183}W, the present evaluated data are in good agreement, but in the case of ^{239}Pu, it is in disagreement. It is necessary to do experiments in the GDR energy range to validate the present evaluated data for ^{239}Pu. Further, though here only limited isotopes have been used for the (γ, n) reaction cross section evaluation, the empirical formula used in this paper may be useful for other isotopes provided $Z \geqslant 60$.

Intensive discussions with M. Herman (NNDC, Brookhaven National Laboratory, USA), R. Kapote (NAPC-Nucear Data Section, IAEA, Austria), P. K. Mehta (The M. S. University of Baroda, Vadodara), P. Mishra (The M. S. University of Baroda, Vadodara), and N. Agrawal (The M. S. University of Baroda, Vadodara) are gratefully to acknowledged.

References

1 http://www-pub.iaea.org/MTCD/publications/PDF/te_1178_prn.pdf, retrieved 16th May 2016
2 A.R. Junghans et al, Phys. Lett. B, **670**: 200 (2008)
3 S. J. Zweben, H. Knoepfel, Phys. Rev. Lett., **35**: 1340 (1975)
4 R. A. Pitts et al, Journal of Nuclear Materials, **463**: 39–48 (2013)
5 A. Shevelev et al, doi: 10.1063/1.4894038, retrieved 17th May 2016

6 B. L. Berman et al, Phys. Rev., **162**: 1098 (1967)
7 C. H. M. Broeders et al, Nucl. Eng. Des., **202**: 157 (2000)
8 F. R. Allum et al, Nucl. Phys. A, **53** 645 (1964)
9 H. Naik et al, Nucl. Phys. A, **916**: 168–182 (2013)
10 I. Raškinyteÿ et al, in Proc. Int. Conf. on Nuclear Reaction Mechanisms, (Varenna, Italy: Dapnia/SPhN, 2006), DAPNIA-06-147
11 G. Kim et al, Nucl. Instrum. Methods Phys. Res., Sect. A, **485**: 458–467 (2002)
12 V. C. Petwal et al, PRAMANA — journal of physics, **68**: 235 (2007)
13 M. Gallardo et al, Phys. Lett. B, **191**: 222–226 (1987)
14 M. Mattiuzzi et al, Phys. Lett. B, **364**: 13–18 (1995)
15 P. Heckman et al, Phys. Lett. B, **555**: 43 (2003)
16 Balaram Dey et al, Phys. Lett. B, **731**: 92–96 (2014)
17 H. Steinwedel et al, Z. Naturforsch., **5a**: 413 (1950)
18 B. L. Berman, At. Data Nucl. Data Tables, **15**: 319–390 (1975)
19 G. Reffo, Phys. Rev. C, **44**, 814 (1991)
20 S. Levinger, Phys. Rev., **84**: 43 (1951)
21 J. S. Levinger, in Nuclear Photo Disintegration (Oxford University Press, Oxford, 1960) p.54
22 A. Koning et al, TALYS – 1.6 A nuclear reaction program, (2013) p.62
23 M. Herman et al, EMPIRE – 3.2 Malta modular system for nuclear reaction calculations and nuclear data evaluation, (2013) p.18–20
24 M. Danos, Nucl. Phys., **5**: 23 (1958)
25 T. Belgya et al, Handbook For Calculations of Nuclear Reaction Data, (IAEA, Vienna, RIPL-2,IAEA-TECDOC-1506, 2006), http://www-nds.iaea.org/RIPL-2
26 V.N. Levkovski, J. Phys., **18**: 361 (1974)
27 J. S. Wang et al, Eur. Phys. J. A, **7**: 355–360 (2000)
28 https://www-nds.iaea.org/exfor/exfor.htm, retrieved 4^{th} December 2015
29 Akito Takahashi et al, Fusion Engineering and Design, **9**: 323 (1989)
30 http://www.nndc.bnl.gov/chart/chartNuc.jsp, retrieved 2^{nd} November 2015
31 https://www-nds.iaea.org/photonuclear/, retrieved 4^{th} December 2015
32 http://www.nndc.bnl.gov/sigma/index.jsp?dontshow=nn.6&as=9&lib=jendl3.3&nsub=20040, retrieved 4^{th} December 2015
33 Grady Hughes, Progress in Nuclear Science and Technology, **4**: 454–458 (2014)
34 X-5 Monte Carlo Team, MCNP-A General Monte Carlo N-Particle Transport Code, Version 5, (2000) 1
35 A. Fassò et al, Advanced Monte Carlo for Radiation Physics, Particle Transport Simulation and Applications, in Proceedings of the Monte Carlo 2000 Conference, edited by A. Kling, et. al., (Lisbon, 2000) 159–164
36 P. K. Sahani et al, Indian J. Pure Appl. Phys, **50**: 863–866 (2012)
37 Boubaker Askri, Nucl. Instrum. Methods Phys. Res., Sect. B, **360**: 1–8 (2015)

Applied Radiation and Isotopes 127 (2017) xxx–xxx

Contents lists available at ScienceDirect

Applied Radiation and Isotopes

journal homepage: www.elsevier.com/locate/apradiso

Spectrum average cross section measurement of ^{183}W (n, p)^{183}Ta and ^{184}W (n, p)^{184}Ta reaction cross section in ^{252}Cf(sf) neutron field

Rajnikant Makwana[a,*], S. Mukherjee[a], L. Snoj[b], S. S. Barala[c], M. Mehta[d], P. Mishra[a], S. Tivari[d], M. Abhangi[d], S. Khirwadkar[d], H. Naik[e]

[a] Department of Physics, The Maharaja Sayajrao University of Baroda, Vadodara 390002, India
[b] Jožef Stefan Institute, Jamova cesta 39, SI-1000 Ljubljana, Slovenia
[c] Defence Laboratory, Jodhpur, Rajasthan 342011, India
[d] Institute for Plasma Research, Gandhinagar, Gujarat 382428, India
[e] Radiochemistry Division, Bhabha Atomic Research Centre, Mumbai 400085, India

HIGHLIGHTS

- The present work describes the measurement of (n, p) reaction cross sections in Cf(sf) neutron field.
- It contains the different corrections using simulation techniques using Monte Carlo based MCNP codes.
- The measurements are on W isotopes which is a very important material for the case of Fusion reactor.
- The (n,p) reaction cross sections are important for the validation of nuclear models.

ABSTRACT

Neutron induced nuclear reactions are of prime importance for both fusion and fission nuclear reactor technology. Present work describes the first time measurement of spectrum average cross section of nuclear reactions ^{183}W(n,p)^{183}Ta and ^{184}W(n,p)^{184}Ta using ^{252}Cf spontaneous fission neutron source. Standard neutron activation analysis (NAA) technique was used. The neutron spectra were calculated using Monte Carlo N Particle Code (MCNP). The effects of self-shielding and back scattering were taken into account by optimizing the detector modeling. These effects along with efficiency of detector were corrected for volume sample in the actual source-detector geometry. The measured data were compared with the previously measured data available in Exchange Format (EXFOR) data base and evaluated data using EMPIRE – 3.2.2.

1. Introduction

In the recent decades, there is an overwhelming demand of nuclear reaction cross section data compilation for the development of reactor science and technology. In reactors like International Thermonuclear Experimental Reactor (ITER), fusion reaction process can be studied using the DT reaction. It produces neutrons with energy of 14.1 MeV, and these neutrons are transmitted through the first wall of the reactor material (Qing et al., 2009; Reijonen et al., 2005; Wu et al., 2009; Voitsenya, 2001; De Temmerman et al., 2007; Behringer, 1987). First wall, divertor, blanket and shielding are the main parts of the fusion reactor. First wall, divertor and blanket are directly exposed to the DT plasma and bear the maximum amount of the neutron flux (~10^{15} n/cm^2/s). Divertor collects and exhausts heat and particles, and the reactor walls scatter these neutrons from 14 MeV to the thermal neutron energy. Tungsten has been selected as divertor material for ITER (Lehnen et al., 2013). It will face all the neutron energies from thermal to 14 MeV. These neutrons can open reaction channels such as (n, γ), (n, p), (n, 2n), (n, d), (n, α) etc. It is necessary to have complete nuclear reaction cross section data for the different isotopes of tungsten i.e., ^{183,184,186}W, as they can produce different radio isotopes in the reactor (Forrest, 2011). It is very important as a part of reactor maintenance using remote handling.

The reactions ^{183}W(n, p)^{183}Ta and ^{184}W(n, p)^{184}Ta are considered here for the cross section measurement using the ^{252}Cf spontaneous neutron source. This is the first time measurement of spectrum average cross section in ^{252}Cf(sf) neutron field. There are plenty of experimental data available at 14 MeV for these reactions; however, very few

* Corresponding author.
E-mail addresses: rajniipr@gmail.com (R. Makwana), sk.mukherjee-phy@msubaroda.ac.in (S. Mukherjee).

http://dx.doi.org/10.1016/j.apradiso.2017.06.002
Received 12 August 2016; Received in revised form 25 April 2017; Accepted 1 June 2017
Available online 02 June 2017
0969-8043/

measured data are available for energy range from thermal to 14 MeV. Cross sections at low energy are relatively very important as the material tungsten is used in ITER (Forrest, 2011), where the neutron flux will be very high (almost facing ~10^{15} neutrons/sec-cm^2 first wall), the production of the daughter isotope will be expected high amount. Further, there are very few measurements are available and the cross sections are small for these (n, p) reactions, it is necessary to measure cross sections for these reaction with accuracy in order to predict the accurate production of the radioactive waste. Present work describes measurement of cross section for such nuclear reactions. Therefore, the objective of the present work is to have accurate measurements of the cross section of the above mentioned reactions. Further the measured data are important to validate evaluated data libraries for tungsten isotopes from different national projects e.g., ENDF-B/VII.1 (Chadwick et al., 2011), JENDL-4 (Shibata et al., 2011), FENDL (FENDL-3.1 data library, ⟨https://www-nds.iaea.org/fendl31/⟩.), ROSFOND (ROSFOND data library, ⟨http://www.ippe.ru/podr/abbn/english/libr/rosfond.php⟩.), CENDL-3.1 (Ge et al., AugustA 2011), JEEF-3.2 (JEFF-3.2 data library, ⟨https://www.oecd-nea.org/dbforms/data/eva/evatapes/jeff_32/⟩.) etc.

2. Experimental measurement

The ^{252}Cf(sf) neutron field is a reference neutron spectra which is considered to be very well known. Mannhart evaluation (Mannhart, 1987; Mannhart, 1989) is currently accepted to be best representation of this reference neutron spectra. Numerical data for this evaluated spectra are available from the IAEA IRDFF web page of IAEA (IRDF-, 2002). The average neutron energy in the ^{252}Cf spectrum is 2.124 MeV. The ^{252}Cf isotope is an intense neutron emitter that decays by alpha emission (~ 96.31%) and spontaneous fission (~ 3.09%) with half-life of 2.645 y. Its neutron emission rate is 2.314 × 10^6 n/s/μg (Manojlovič et al., 2015). This source is shielded with paraffin, borated wax and lead as shown in Fig. 1.

Standard neutron activation analysis technique was used in the present measurements. In this method a sample with proper weight is required for the irradiation, which is necessary to produce the desired isotope for the measurement of nuclear reaction cross section. The irradiation of W sample was done by using the portable ^{252}Cf neutron source available at the Defence Laboratory, Jodhpur, India, having present neutron yield of 1.6064 × 10^8 n/s. The tungsten sample with purity of 99.97% was kept at distance of 60 mm from the ^{252}Cf neutron source. The sample chosen for irradiation was having a dimension of 8 mm × 8 mm × 5 mm and weighing 6.033 gm. The sample was kept for 603.25 h for continuous long irradiation. The averaged neutron spectrum inside the sample was calculated using the Monte Carlo N Particle Code (MCNP), which is discussed in the next section. The

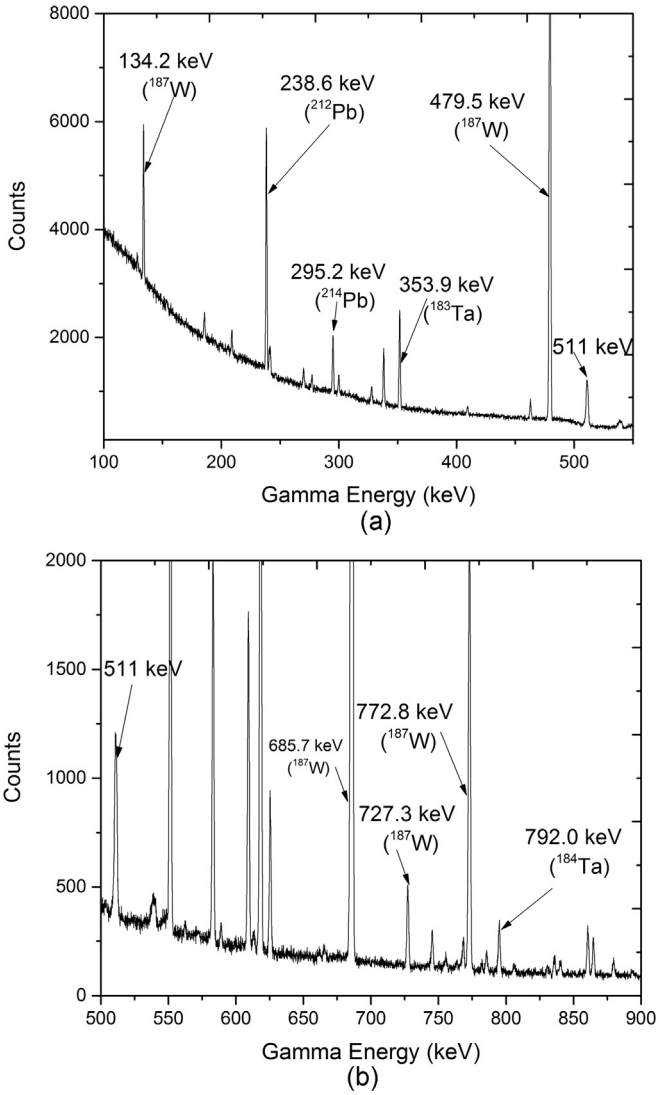

Fig. 2. (a). Gamma spectrum measured using HPGe detector (b). Gamma spectrum measured using HPGe detector.

sample was brought to the Neutronics Laboratory, Institute for Plasma Research (IPR), Gandhinagar, India, for counting purpose. The activated sample was kept near the window of the HPGe detector. Counting was done in two different phases; one was just after irradiation and next

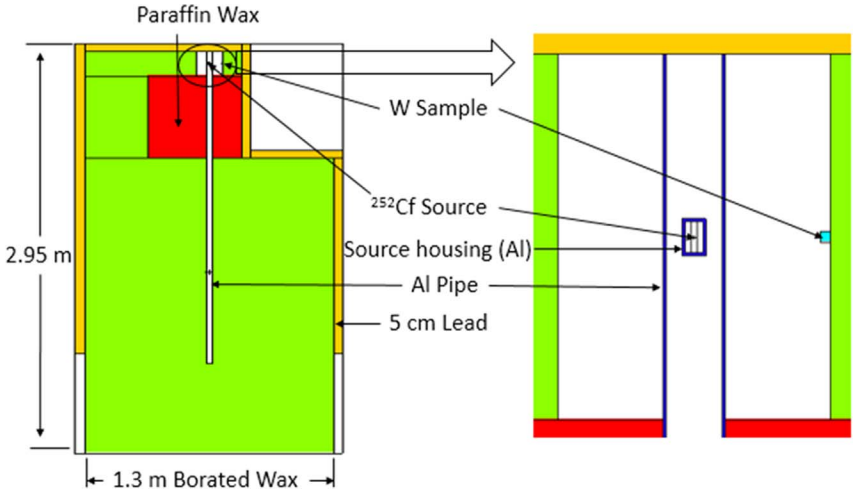

Fig. 1. MCNP modeling of the irradiation experimental setup.

after 2 days cooling. The time of counting was sufficiently long, as the daughter isotopes have half-life from few hours to few days. The gamma spectra measured from the irradiated sample are shown in Fig. 2(a–b). Analysis of the data was done by Neutron Activation Analysis (NAA) technique and cross sections for ^{183}W(n, p)^{183}Ta and ^{184}W(n, p)^{184}Ta reactions were estimated.

3. Theoretical calculations using MCNP

This section is divided into two parts, one is regarding the averaged neutron spectra calculation in the irradiated sample, and other is related to detector efficiency. The MCNP-6.1 code was used to perform these calculations. This code has been widely used for transport of neutron, photon, electron and many other particles. All calculations were performed with ENDF/B-VI cross section data library which comes along with MCNP package. Further calculations were checked with ENDF/B-VII, in order to find the difference in results, but no significant change was observed in results.

3.1. Neutron spectra calculation

The ^{252}Cf source is having continuous neutron spectrum, therefore it was necessary to calculate the averaged neutron spectrum inside the sample. The ^{252}Cf was modeled using the MCNP code, as explained by Snoj et al. (Narayan et al., 2010). The most rigorous approach as explained by Snoj et al. is to use evaluated neutron spectrum of Mannhart ((IRDF-, 2002) (Mannhart, 1987, 1989; IRDF-, 2002; [20]NT: IAEA, International reactor dosimetry file 2002 (IRDF-2002) Technical Report Series, International Atomic Energy Agency, Vienna (2006) 162.IAEA, International reactor dosimetry file 2002 (IRDF-2002) Technical Report Series, International Atomic Energy Agency, Vienna (2006) 162.)). In the present work, the average neutron spectra over sample volume have been calculated by using the IRDF – 2002 ^{252}Cf spontaneous fission neutron spectra. Monte Carlo based MCNP code (MCNP – 6.1) with ENDF/B-VII data library was used to model the irradiation assembly as shown in Fig. 1. The tally F4, which gives volume averaged flux tally was used for the calculation. The definition of the F4 tally is represented by following relation.

$$F4 = \frac{1}{V}\int_V dV \int_E dE \int_{4\Pi} d\Omega\phi(r, E, \Omega)$$

where, V = volume of the sample, E = energy of the neutron, Ω = solid angle, r = radial distance from source, ϕ = flux at distance.

The calculated spectra is shown in Fig. 3(a). There has been a significant increment in lower energy neutrons due to scattering from the source shielding. However, the higher energy tail shape remained same as in the pure source spectra.

As the chosen reactions have different threshold energies, not whole neutron spectrum was used to produce the daughter isotopes. Only those neutrons above the threshold energy for both reactions are able to produce the daughter isotopes. Hence the low energy neutrons below the threshold can be removed from the neutron spectra for both the reactions. This gives the effective neutron spectrum for the respective reaction. This is shown in Fig. 3(a-c). It can be seen from Fig. 3(a)., that the whole neutron spectrum contains very large contribution of low energy (thermalized) neutrons, which are back scattered neutrons from the surrounding shielding materials. As our chosen reactions have threshold above this neutron energies, they do not interfere. The effective neutrons spectra are shown for both reactions in Fig. 3(b,c). Again there is very small number of neutrons is available above 4.5 MeV neutrons. The ratio of these neutrons to total neutrons is < 6%. So the major contribution in the reaction product is due to the neutrons from threshold to 4.5 MeV neutrons. Therefor the measure cross section can be reported at the spectrum averaged energy for these neutrons. Following formula has been used to calculate the spectrum averaged energy from the calculated neutron spectra in the irradiated

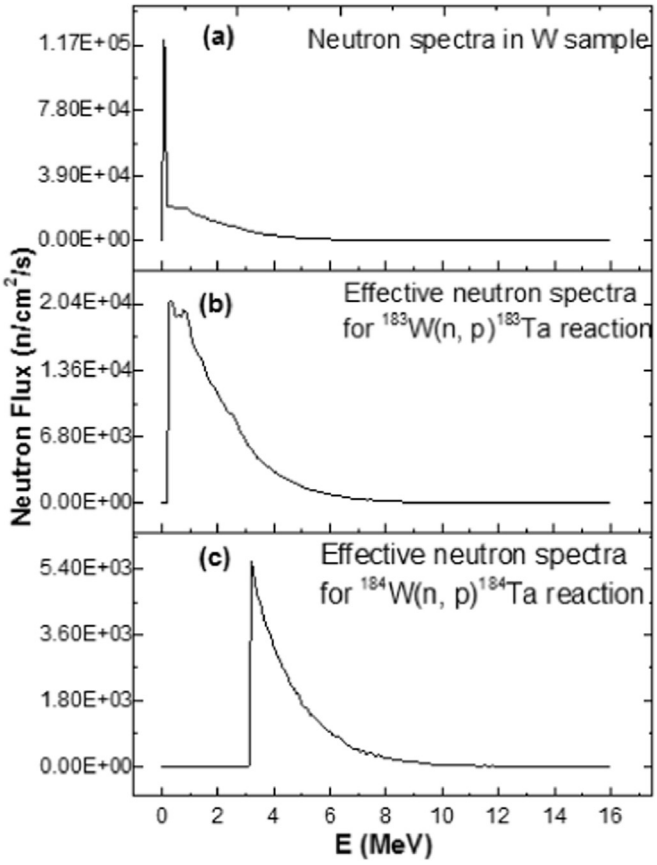

Fig. 3. (a,b,c). Average neutron spectra in W sample, and the effective neutrons above the threshold energy of the selected reactions, calculated using evaluated ^{252}Cf spectra (Koning and Declaroche, 2003; Hauser and Feshbach, 1952) as input source spectra in MCNP.

sample, which is known as the **effective mean energy/spectrum averaged energy** as given below (Smith).

$$E_{mean} = \frac{\int_{E_{th}}^{E_{max}} E_i \varnothing_i dE}{\int_{E_{th}}^{E_{max}} \varnothing_i dE}$$

In the above expression, E_{th} = threshold energy of the reaction, E_{max} = maximum neutron energy, E_i = energy bin, ϕ_i = neutron flux of energy bin E_i, E_{mean} = effective mean energy.

3.2. Detector efficiency calibration

The HPGe detector was used for the activation measurement having crystal size of 64.80 mm diameter and 64.60 mm length. The window thickness is 0.60 mm made of carbon composite. Efficiency of the detector was measured for different gamma ray energies using mix-energy gamma source available at IPR, Gandhinagar, India. A mix-energy gamma source is a mixture of different radioactive isotopes, such as ^{241}Am (59.54 keV, 919.19 Bq), ^{109}Cd (88.03 keV, 4.132 kBq), ^{57}Co (122.06, 136.47 keV, 144.85 Bq), ^{139}Ce (165.85 keV, 5.050 kBq), ^{51}Cr (320.08 keV, 0.09 Bq), ^{113}Sn(391.69 keV, 91.06 Bq), ^{85}Sr (514.00 keV, 11.85 Bq), ^{137}Cs (661.65 keV, 1.712 kBq), ^{88}Y (898.03 keV, 152.45 Bq), ^{60}Co (1173.22, 1332.49 keV, 2.183 kBq) and ^{88}Y (1836.05 keV, 152.45 Bq), which covers gamma energy form 59 keV to 1.8 MeV. Full efficiency curve was plotted using measured photo peak efficiency. In the present measurements, a point source was used to measure detector efficiency. However, in the actual experiment the volume sample was used. Therefore, it was necessary to obtain efficiency for the volume source of the sample dimension. Further the volume source attenuates photons from the subsequent layers towards the detector, and, large

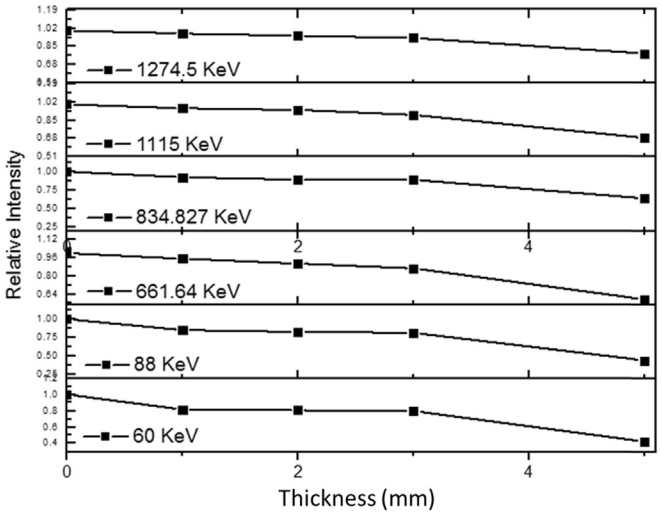

Fig. 4. Relative intensity showing the self-shielding effect increases as the thickness of the sample increases.

number of photons are scattered from the backside layers of the sample. To study the self-shielding and back scattering effect from the W sample, another measurement has been carried out. The method used have been described in reference (Rama Rao et al., 1986). The W samples with the thickness of 1, 2, 3 and 5 mm were kept in between source and detector. In this arrangement the gammas emitted from the source were attenuated by the sample. The results are shown in Fig. 4. It is clear from this figure, that the efficiency will be different for the volume source, due to attenuation. Also the back scattering have significant contribution.

The efficiency of the volume sample by considering back scattering and self-shielding effect can be calculated using the MCNP code. In this context detector was modeled by using this code as shown in Fig. 5. The experimentally measured efficiency at various distances using the point gamma source, at different energies were calculated and compared with simulated efficiency. The model was optimized by getting the ratio Calculated efficiency to Experimental efficiency (C/E ratio) ~ 1, which is shown in Fig. 6(a). The compared results are shown in Fig. 6(b). This model was used for the actual sample – detector geometry to estimate the efficiency of the detector. This method considers both the self-shielding and back scattering effect due to volume of the sample. This efficiency value for different selected gamma energies were used to calculate the cross section using neutron activation technique.

4. Data acquisition and reduction

After the irradiation the target samples were used to measure the gamma activities obtained from the desired isotopes. A typical gamma spectrum obtained from the activated target samples are shown in Fig. 2(a-b). The time of counting were chosen carefully to get the selected gamma energy peaks.

The time elapsed between end of irradiation and start of counting is

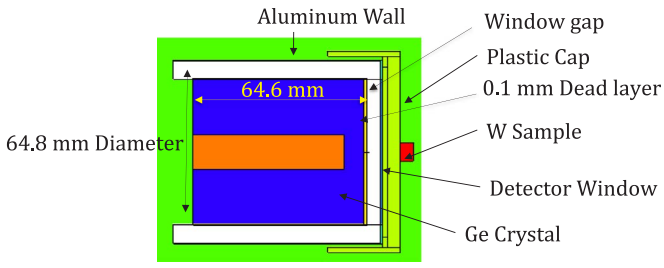

Fig. 5. MCNP Model of the detector to calculate efficiency for irradiated volume sample placed on end cap of the detector.

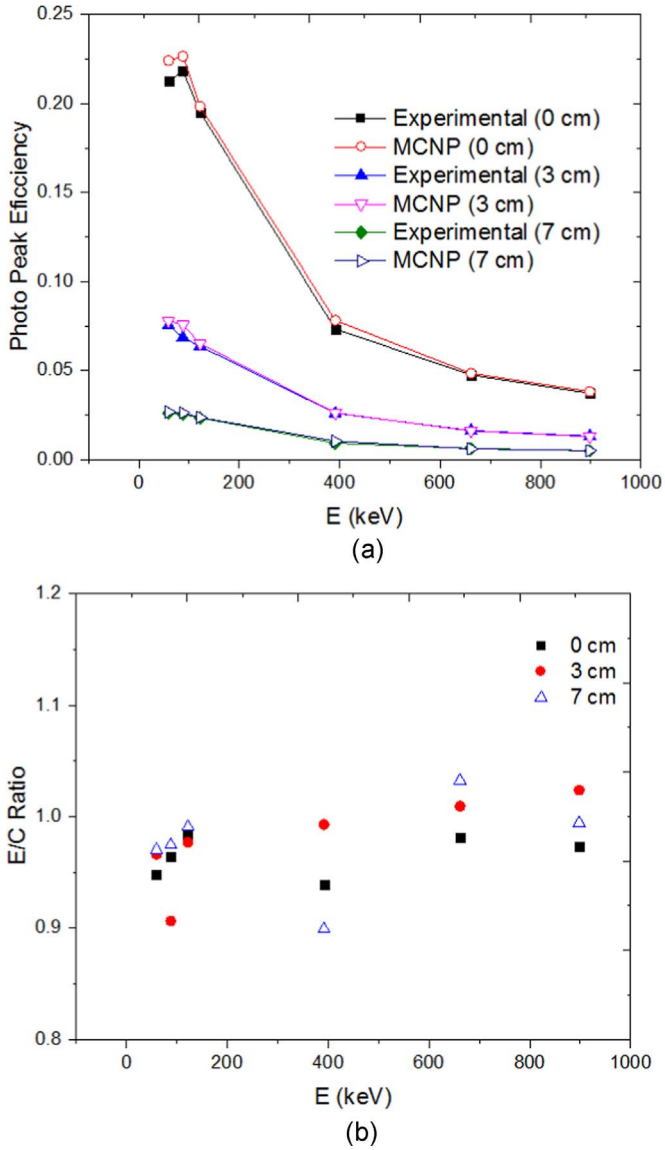

Fig. 6. (a). Comparison of measured and MCNP calculated detector efficiency at various gamma energies (b). Comparison of Experimental to MCNP calculated detector efficiency ratio at various gamma.

known as the cooling time (t_c). The production cross section (σ) of the interested isotope was obtained by using the following standard activation equation,

$$\sigma = \frac{\mathbf{A_I \cdot A_\gamma \cdot \lambda}}{(\varnothing \theta_\gamma \in_\gamma \mathbf{w_i P_i N_{av}}) \cdot (\mathbf{1} - \mathbf{e}^{-\lambda t_i}) \cdot (\mathbf{1} - \mathbf{e}^{-\lambda t_c}) \cdot \mathbf{e}^{-\lambda t_w}}$$

where, A_I = Gram Atomic Weight of the target; A_γ = Peak Counts of gamma energy; λ = Decay constant of product nucleus (s^{-1}), t_i = irradiation time; t_w = Cooling time; t_c = Counting time; ∅ = Incident neutron flux; θ_γ = γ intensity; $\in_\gamma$ = Efficiency of detector at gamma chosen; w_i = weight of sample (gm), P_i = Abundance of target isotope; N_{av} = Avogadro number.

The photo peak counts of the gamma rays emitted from the desired isotope was carefully measured from the gamma spectrum. The selected gamma energies along with their abundances for the desired radioisotopes are given in Table 1.

5. Nuclear modular code prediction

In order to support the present measured nuclear cross section data,

Table 1
Selected nuclear reactions with isotopic abundance, threshold energy, daughter half-life and daughter gamma energy with its abundance.

Reaction	Abundance of Target Isotope (%) (Rosman and Taylor, 1999)	Threshold Energy (MeV) (Q value calculator, retrieved from: <http://www.nndc.bnl.gov/qcalc/index.jsp>.)	Half life of daughter isotope (Table of Isotopes decay data, retrieved from: <http://nucleardata.nuclear.lu.se/toi/listnuc.asp?Z=74>.)	γ - Energy (KeV)	Γ– Intensity (%) (Table of Isotopes decay data, retrieved from: <http://nucleardata.nuclear.lu.se/toi/listnuc.asp?Z=74>.)
^{183}W(n, p)^{183}Ta	14.31	0.29	5.1 d	353.9	11.2
^{184}W(n, p)^{184}Ta	30.64	2.095	8.7 h	792.0	14.2

nuclear modular calculations were performed by using EMPIRE – 3.2.2 code. This code uses different nuclear models to predict nuclear reaction cross section. It can predict nuclear reaction data for neutron, gamma, proton, deuteron, triton, ^{3}He and alpha with energy range from few keV to several hundreds of MeV. It uses different reaction parameters from RIPL library. It considers effect of level density, and all three nuclear reaction mechanisms: compound, pre-equilibrium and direct reaction. The optical model parameters were obtained by using a global potential proposed by Koning and Delaroche (Koning and Declaroche, 2003). The compound reaction mechanism was incorporated by Hauser-Feshbach model (Hauser and Feshbach, 1952). The pre-equilibrium contribution was included by exciton model, developed by Kalbach (Kalbach, 1986).

In the present case different parameters such as level density parameters were used to evaluate the cross section of the interested nuclear reactions. The EMPIRE – 3.2.2 uses reaction parameters from Reference Input Parameter Library (RIPL) – 3. The calculated reaction cross sections for the production of selected radioisotopes were used to compare the measured reaction cross sections shown Figs. 7 and 8.

6. Results and discussion

The cross sections were measured with improved accuracy, with the application of simulation technique, which incorporates, self-shielding, back scattering, volume source effect in efficiency etc. Geometrical effect and shielding effect on averaged neutron spectra inside the sample was calculated using MCNP simulation. The measured nuclear reaction cross section data are given in Table 2. To the best of our knowledge,

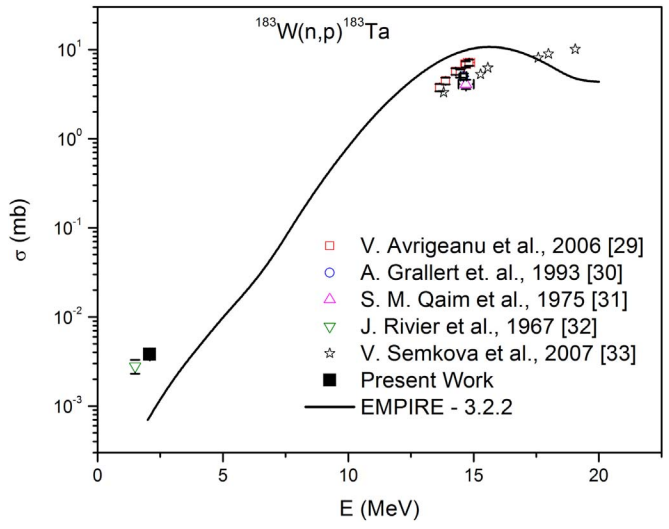

Fig. 7. Comparison of present measured spectrum averaged cross section with experimental data taken from references - Avrigeanu et al. (2006), Grallert et al. (1993), Qaim and Graca (1975), Rivier et al. (1967) and Semkova et al. (2007) and EMPIRE-3.2.2 evaluated cross section for ^{183}W(n, p)^{183}Ta; the present data and data point of Rivier et al. (1967) are spectrum averaged cross sections, other experimental data are for mono energy neutrons.

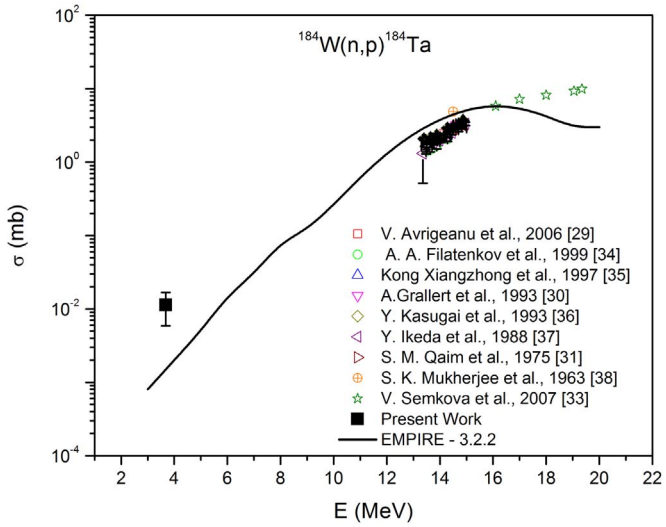

Fig. 8. Comparison of present measured spectrum averaged cross section with experimental data taken from references - Avrigeanu et al. (2006), Reimer et al. (2005), Kong Xlangzhong et al. (1997), Grallert et al. (1993), Kasugai et al. (1992), Ikeda et al. (1988), Qaim and Graca (1975), Gujarathi and Mukherjee (1967) and Semkova et al. (2007) and EMPIRE-3.2.2 evaluated cross section for ^{184}W(n, p)^{184}Ta; the present data and data point of Rivier et al. (1967) are spectrum averaged cross sections, other experimental data are for mono energy neutrons.

Table 2
Measured Cross section for the selected nuclear reactions.

Reaction	Neutron Energy (MeV)	Measured Cross section (mb)
^{183}W(n, p)^{183}Ta	1.70 ± 1.35	(3.8 ± 0.3)×10^{-3}
^{184}W(n, p)^{184}Ta	3.75 ± 1.26	(11.3 ± 0.9)×10^{-3}

the present measurements have been done for the first time in the above mentioned neutron energies. The neutron energy was taken as a spectrum averaged from calculated neutron spectra using MCNP code. The effect of self-attenuation and back scattering, and the sample-volume geometry effect on the efficiency of the detector, was corrected by optimizing MCNP model of the HPGe detector at different distances and for different energies of gamma photon. The parameters for the error propagation in the final cross section estimations were considered. Major error contributions in the present data are due to relative efficiency (2–3%), scattered neutron (1–3%), statistical error (3–4%), detector dead time (< 2%). The overall error in the present measurement were < 6%.

The EMPIRE-3.2.2 nuclear modular code was used for evaluating the cross section of the selected nuclear reactions. The measured data were compared with the evaluated data in the Figs. 7 and 8. In the case of ^{183}W(n, p)^{183}Ta, there is a previous measurement for this reaction near to the present listed energy, by Rivier et al. (Reimer et al., 2005). Although the measurement reported by Rivier et al. (Rosman and Taylor, 1999) was in reactor neutron field it presents cross section value

at spectrum average energy, which are in agreement with the present data. It should be noted that the average energy of a reactor spectrum is very difficult to define, we accept the energy, which Rivier at al. has listed for present reference. In both the (n, p) reactions the measured cross sections are higher by a small factor in comparison with the evaluated data.

7. Conclusions

In the present measurements, cross sections of ^{184}W(n, p)^{184}Ta, and ^{183}W(n, p)^{183}Ta reactions were measured using a ^{252}Cf neutron source at spectrum averaged energies from threshold of the reaction to the maximum available neutron energy. This is a material of interest for fusion reactor. The averaged neutron spectra inside the sample volume were calculated using MCNP code. The data that have been presented for (n, p) reactions for the available energies, have very few or no previous measurements. The theoretical estimation of the cross section was done by EMPIRE-3.2.2 code. It may be observed that present experimental results are in agreement within the limits of the experimental error. The study shows that the cross section of (n, p) reaction for tungsten isotopes are having small values. But for the case of the fusion reactor, where the first wall is facing $\sim 10^{15}$ neutrons/sec-cm^2, it can produce considerable amount of radioactive waste.

Acknowledgements

Authors are grateful to Mr. Mahavir from Defence Laboratory, Jodhpur, India, Mr. Naveen Agrawal, The M. S. University of Baroda, Vadodara, and Dr. B. Pandey from Pantanagar University, India for useful suggestions. One of the authors (SM) thanks DAE-BRNS, Government of India, for the sanction of a major research project.

References

Qing, J., Wu, Y., Regis, M., Kwan, J.W., 2009. IEEE Trans. Nucl. Sci. 56, 1312–1315.
Reijonen, J., Gicquel, F., Hahto, S.K., King, M., Lou, T.P., Leung, K.N., 2005. Appl. Radiat. Isot. 63, 757–763.
Wu, Y., Hurley, J.P., Ji, Q., Kwan, J., Leung, K.N., 2009. IEEE Trans. Nucl. Sci. 56, 1306–1311.
Voitsenya, V., et al., 2001. Rev. Sci. Instrum. 72, 475–482.
De Temmerman, G., Pitts, R.A., Voitsenya, V.S., Marot, L., Veres, G., Maurer, M., Oelhafen, P., 2007. J. Nucl. Mater. 363, 259–263.
Behringer, K.H., 1987. J. Nucl. Mater. 145, 145–153.
Lehnen, M., Aleynikova, K., Aleynikov, P.B., Campbell, D.J., Drewelow, P., Eidietis, N.W., Gasparyan, Yu, Granetz, R.S., Gribov, Y., Hartmann, N., Hollmann, E.M., Izzo, V.A., Jachmich, S., Kim, S.-H., Kocˇan, M., Koslowski, H.R., Kovalenko, D., Kruezi, U., Loarte, A., Maruyama, S., Matthews, G.F., Parks, P.B., Pautasso, G., Pitts, R.A., Reux, C., Riccardo, V., Roccella, R., Snipes, J.A., Thornton, A.J., de Vries, P.C., 2013. EFDA JET contributors. J. Nucl. Mater. 463, 39–48.
Forrest, R.A., 2011. Energy Procedia 7, 540–552.
Chadwick, M.B., Herman, M., Obložinský, P., Dunn, M.E., Danon, Y., Kahler, A.C., Smith, D.L., Pritychenko, B., Arbanas, G., Arcilla, R., Brewer, R., Brown, D.A., Capote, R., Carlson, A.D., Cho, Y.S., Derrien, H., Guber, K., Hale, G.M., Hoblit, S., Holloway, S., Johnson, T.D., Kawano, T., Kiedrowski, B.C., Kim, H., Kunieda, S., Larson, N.M., Leal, L., Lestone, J.P., Little, R.C., McCutchan, E.A., MacFarlane, R.E., MacInnes, M., Mattoon, C.M., McKnight, R.D., Mughabghab, S.F., Nobre, G.P.A., Palmiotti, G., Palumbo, A., Pigni, M.T., Pronyaev, V.G., Sayer, R.O., Sonzogni, A.A., Summers, N.C., Talou, P., Thompson, I.J., Trkov, A., Vogt, R.L., van der Marck, S.C., Wallner, A., White, M.C., Wiarda, D., Young, P.G., 2011. ENDF/B-VII.1: nuclear data for science and technology: cross Sections, covariances, fission product yields and decay Data. Nucl. Data Sheets 112, 2887.
Shibata, Keiichi, Iwamoto, Osamu, Nakagawa, Tsuneo, Iwamoto, Nobuyuki, Ichihara, Akira, Kunieda, Satoshi, Chiba, Satoshi, Furutaka, Kazuyoshi, Otuka, Naohiko, Ohasawa, Takaaki, Murata, Toru, Matsunobu, Hiroyuki, Zukeran, Atsushi, So, Kamada Jun-ichi Katakura K., Shibata, e., 2011. J. Nucl. Sci. Technol. 48 (1), 1–30.
FENDL-3.1 data library, ⟨https://www-nds.iaea.org/fendl31/⟩.
ROSFOND data library, ⟨http://www.ippe.ru/podr/abbn/english/libr/rosfond.php⟩.
Ge, Z.G., Zhao, Z.X., Xia, H.H., Zhuang, Y.X., Liu, T.J., Jhang, J.S., Wu, H.C., 2011. J. Korean Phys. Soc. 59 (2), 1052.
JEFF-3.2 data library, ⟨https://www.oecd-nea.org/dbforms/data/eva/evatapes/jeff_32/⟩.
Mannhart, W., 1987. IAEA-TECDOC-410 158.
Mannhart, W., 1989. INDC(NDC)-220/L 305.
IRDF-, 2002. ⟨https://www-nds.iaea.org/IRDFF/IRDFF-v1-05_sp.endf⟩.
Manojlovič S., Trkov A., Žerovnik G., Snoj L., 2015. Applied Radiation and Isotopes, 101, pp. 101–106.
Narayan, Pradeep, Meghwal, L.R., Songara, K.C., Vaijapurkar, S.G., Bhatnagar, P.K., 2010. Indian J. Pure Appl. Phys. 48, 798–801.
. IAEA, International reactor dosimetry file 2002 (IRDF-2002) Technical Report Series, International Atomic Energy Agency, Vienna (2006) 162.
Smith, D.L. et al., Corrections for Low Energy Neutrons by Spectral Indexing, Retrieved from: ⟨https://www.oecd-nea.org/science/docs/2005/nsc-wpec-doc2005-357.pdf⟩.
Rama Rao, J., Singh, N.L., Singhal, S., Mohan Rao, A.V., Mukherjee, S., Chaturvedi, L., 1986. Nucl. Instrum. Methods Phys. Res., Sect. B 17, 368–371.
Koning, A.J., Declaroche, J.P., 2003. Nucl. Phys. A 713, 231–310.
Hauser, W., Feshbach, H., 1952. Phys. Rev. C 87, 366.
Kalbach, C., 1986. Phys. Rev. C 33, 818–833.
Rosman, K.J.R., Taylor, P.D.P., 1999. Pure Appl. Chem. 71, 1593–1607.
Q value calculator, retrieved from: ⟨http://www.nndc.bnl.gov/qcalc/index.jsp⟩.
Table of Isotopes decay data, retrieved from: ⟨http://nucleardata.nuclear.lu.se/toi/listnuc.asp?Z=74⟩.
Avrigeanu, V., Chuvaev, S.V., Eichin, R., Filatenkov, A.A., Forrest, R.A., Freieslebe, H., Herman, M., Koning, A.J., Seidel, K., 2006. Nucl. Phys. A 765, 1–28.
Grallert, A., Csikai, J., Buczk, Cs.M., 1993. Rept.: IAEA Nucl. Data Sect. Report. I. N. D. C. No. 286, 131.
Qaim, S.M., Graca, C., 1975. Nucl. Phys. A 242, 317–322.
Rivier, J., Blachot, J., Hocquenghem, J.C., 1967. J. Radio Chem. Acta 8, 196.
Semkova, V., Capote, R., Jaime Tornin, R., Koning, A.J., Moens, A., Plompen, A.J.M., 2007. doi: http://dx.doi.org/10.1051/ndata:07320.
Reimer, P., Avrigeanu, V., Chuvaev, S.V., Filatenkov, A.A., Glodariu, T., Koning, A., Plompen, A.J.M., Qaim, S.M., Smith, D.L., Weigmann, H., 2005. Phys. Rev. C 71, 044617.
Kong Xlangzhong et al., 1997. Rept.: Chinese report to I.N.D.C. No. 042 9.
Kasugai, Y., Tokushima, T., Kawade, K., Yamamoto, H., Katoh, T., Takahashi, A., Iida, T., 1992. Conference: JAERI-M Report No. 92, 27, 268.
Ikeda, Y., Konno, C., Oishi, K., Nakamura, T., Miyade, H., Kawade, K., Yamamoto, H., Katoh, T., 1988. JAERI Reports No.1312, 1.
Gujarathi, S.C., Mukherjee, S.K., 1967. Indian J. Phys. 41, 667.

Measurement of (n,p) Cross Section for Some Structural Materials at 14.2 MeV

Nand Lal Singh, Rajnikant Makwana,
S. Mukherjee, and A. Chatterjee
Department of Physics,
The Maharaja Sayajirao University of Baroda,
Vadodara – 390 002, India
nl.singh-phy@msubaroda.ac.in

***Abstract*—The (n,p) reaction cross section for some structural materials such as ^{75}As, ^{66}Zn, ^{64}Zn, ^{55}Mn, ^{51}V and ^{58}Ni was measured at 14.2±0.2 MeV using activation and off line gamma ray spectroscopic technique. For the purpose of safe and economical design of reactors, the neutron cross section data for structural materials are required with high precession and accuracy. The neutron cross section data for important structural materials are collected and evaluated systematically and data files are prepared for the reactor design. However, considerably large discrepancies exist among different evaluated nuclear data files. Hence there is a need to study these reactions with better accuracy. The results were compared with existing data available in EXFOR data base. The measured cross sections were also estimated theoretically using nuclear modular codes: TALYS-1.6 and EMPIRE-3.2.2.**

Keywords—Activation technique; Structural materials; Neutrons 14 MeV; TALYS-1.6; EMPIRE

I. INTRODUCTION

Accurate knowledge of neutron induced reaction cross sections is of interest to many areas of applied science and fundamental physics. These cross sections are important to estimate radiation levels and decay heat of materials that have been exposed to radiation fields. Other applications are designing of future fusion and advanced fission reactors, in neutron dosimetry and development of nuclear theory. Structural materials are very important part of any reactor. They must have capability of radiation hardness and long durability [1]. As these materials are used for a reactor structure, the neutrons produced from the fission or fusion mechanism of reactor are irradiating them. The D-T fusion reaction will produce high energetic neutrons of 14 MeV. It is necessary to have all the known cross section for this neutron energy to calculate nuclear activation and transmutation, nuclear heating, nuclear damage. The (n, p) reaction channel easily opens for most of the materials above a few MeV of neutron energy. The uncertainties arising due to self-absorption and self-scattering effects in the bulk samples and pile up effect in detector have been taken care by simulation method as discussed in our earlier papers [2].The following reaction cross section was measured by activation technique;^{75}As(n,p)^{75}Ge;^{66}Zn(n,p)^{66}Cu;^{64}Zn(n,p)^{64}Cu; ^{55}Mn (n,p)^{55}Cr;^{51}V(n,p)^{51}Ti and ^{58}Ni(n,p)^{58}Co. The literature survey reveals that the neutron induced reaction cross sections for these materials are widely studied using standard activation method and are available in EXFOR data base [2]. There is often large discrepancy among the previous experimental data by a factor of 1.4 to 4.0, hence further measurements are required. The measured cross section is important for the fusion reactor as well as for the advance accelerator based sub-critical system. Theoretical evaluation of (n,p) reaction cross sections are done using standard nuclear modular codes, TALYS-1.6 and EMPIRE-3.2.2. The predictive power of nuclear model codes can be validated and improved in comparison with good quality experimental data and in turn the model calculation provide estimates where no experimental data are available.

II. EXPERIMENTAL

A. Sample preparation and efficiency of the detector

The isotope of ^{75}As, ^{66}Zn, ^{64}Zn, ^{55}Mn is in spectrally pure oxide form and pallets of 2.0 cm diameter and thickness of about 2.0 mm each were prepared by mixing uniformly aluminium powder with each isotope. Few pellets were used as a cylindrical experimental target. In the case of nickel and vanadium instead of pellets, the stack of alternative Ni/V and Al foils was used as a target. A ^{152}Eu disc source of same diameter was placed between the pellets at different positions. Gamma spectrum at each position was measured with high resolution HPGe detector (1.8 keV FWHM at 1332 keV gamma energy) and 4096 channel multi-channel analyser. Efficiency of detector was calculated at different energies of ^{152}Eu with and without sample to remove self-absorption and self-scattering effects in the samples and pile up effect in detector as discussed in our earlier papers [2] and is shown in Fig.1 for nickel and zinc oxide. It reveals that the percentage attenuation varies nearly 22% to 2.3% for ZnO and 16% to 1.9% for Ni sample for low energy (122 keV) to high energy (1408 keV) gamma rays respectively.

B. Description of irradiation

The AN-400 Van de Graff Accelerator of Banaras Hindu University, Varanasi, India was used to produce 14 MeV neutron via ^{3}H(d,n)^{4}He reaction using tritium target of 8 Ci activity and deuteron beam of energy 180 keV having a beam current ~ 30 μA.The samples were placed at 0^{o} angle relative

978-1-5090-0908-4/16/$31.00 ©2016 IEEE

to the beam direction at a distance of about 3.0 cm

These isotopes were irradiated with a flux of the order of 10^7n/s for15 min to 4 hours as per the half-life of product produced in the reaction. The reaction products were identified by means of their characteristics gamma rays and half-life as listed in Table-1.

C. Measurement of cross section by gamma spectroscopy

The gamma spectra were measured for each sample using the above mentioned detector setup. The cross section was calculated from the measured photo peak counts using the following activation equation [2].

$$\sigma = \frac{A_i A_\gamma \lambda (\, e^{\lambda t_w})}{\phi\, \theta_\gamma P_\gamma w_i P_i N_{av} (1 - e^{-\lambda t_i})\,(1 - e^{-\lambda t_c})} \qquad (1)$$

where, σ is the cross section for the reaction (mb), A_i is the gram atomic weight of the target element, A_γ is the area under the photo peak of the characteristic gamma ray of the residual nucleus, λ is the disintegration constant of the product nucleus (s^{-1}), $\phi$is the flux of the incident particle (particle s^{-1}), θ_γ is the absolute γ- ray intensity per decay of the residual nucleus, P_γ is the photopeak efficiency of the gamma ray, w_i is the weight per unit area of the target (g cm^{-2}), P_i is the fractional abundance by weight of the target isotope of interest, N_{av} is the Avogadro number (6.023×10^{23} atoms $mole^{-1}$), t_i is the time duration for irradiation, t_w is the time elapsed between the end of irradiation and start of counting, t_c is the data collection time (or counting time).

TABLE I. SELECTED NUCLEAR REACTIONS

Nuclear Reaction	Q – Value (MeV)	Half-life	Emitted Gamma (keV)	Γ– Abundance
$^{75}As(n,p)^{75}Ge$	– 0.3954	82.78m [4]	264.65	11
			198.60	1.19
$^{66}Zn(n,p)^{66}Cu$	– 1.8592	5.120 m [5]	1039.23	9
$^{64}Zn(n,p)^{64}Cu$	0.2040	12.7 h [7]	1345.84	0.473
$^{55}Mn(n,p)^{55}Cr$	– 1.8213	3.497 m [6]	1528.3	0.037
$^{51}V\ (n,p)^{51}Ti$	– 1.6837	5.76 m [8]	320.07	93.1
$^{58}Ni\ (n,p)^{58}Co$	0.4021	70.86 d [9]	511	29.8
			810.76	99.45
Monitor Reactions				
$^{27}Al\ (n,\alpha)^{54}Na$	– 3.1302	14.96 h	1368.6	100
$^{27}Al\ (n,p)^{57}Mg$	-1.8269	4.46 m	843.8	71.8

The activities produced in the reaction products of monitor and samples were measured via gamma rays spectrometry. The counting geometry was kept in such a way so that the dead time of detector was about 4%.The average neutron flux was determined from Al-monitor via $^{27}Al(n,p)^{27}Mg$ and $^{27}Al(n,\alpha)^{24}Na$ reactions.

TABLE II. MEASURED CROSS-SECTION DATA

Nuclear Reaction (Half life)	Measured Cross section (mb) 14.2±0.2MeV	Evaluated Data Cross section (mb)	
		TALYS 1.6	EMPIRE 3.2.2
$^{75}As(n,p)^{75}Ge$	27.2 ± 2.1	25.58	22.44
$^{66}Zn(n,p)^{66}Cu$	55.5 ± 4.4	50.72	49.32
$^{64}Zn(n,p)^{64}Cu$	170.0±13.6	137.12	176.33
$^{55}Mn(n,p)^{55}Cr$	45.8± 3.7	26.92	36.23
$^{51}V\ (n,p)^{51}Ti$	28.2 ± 2.3	35.90	30.52
$^{58}Ni\ (n,p)^{58}Co$	314.0 ± 25.1	278.96	263.83

D. Results and Discussion

The cross section was measured with improved accuracy using the simulation method, which takes care of self-absorption and self-scattering effects in the samples and pile up effect in detector. The area under the peak of characteristics gamma rays was corrected for self-attenuation effect in the samples and used for cross section calculation. The relative efficiency data with and without absorber for a particular target-detector geometrical arrangement inclusive of all due to self-scattering, self-absorption and geometry solid angle for a simulated cylindrical target was used to determine cross section, such curve for nickel and zinc oxide is presented in Fig.1. The cross section was calculated relative to the standard reactions of monitor as mentioned in the Table 1.For this reason, each sample was thoroughly mixed with aluminum powder and then pellets were made or Al foils were placed alternatively in the case of foil samples. The (n,p) cross section will be affected by the low energy neutrons since reactions have low threshold energies. In addition, the effect of low energy neutrons scattered from the walls of the laboratory and other heavy masses around the target will give rise to inelastically scattered neutrons. In our case the distance of walls from the centre of the target is 521 cm and there is a pit in the floor of diameter 310 cm and depth of 272 cm. Therefore, the contribution from low energy back ground is expected to be small and may be of the order of 3-5% depending on the reaction threshold of the investigated reactions.

The uncertainties quoted on the cross section comprise the statistical error (1-3%), relative efficiency (2-3%), monitor crosses section (3%) and neutron scattering (3-5%).The present experimental results are compared with the available experimental data from EXFOR database [4-8] and are shown in Figs.2-7. The cross section measured in the present work

and by others with same experimental method is in agreement within about 2-15%.

III. THEORETICAL PREDICTIONS

The nuclear modular codes are important tool for the calculation and verification of the cross sections of various nuclear reactions at different incident energy of projectile. The latest version of nuclear modular codes TALYS-1.6 and EMPIRE-3.2.2 were used to evaluate (n, p) cross sections for the selected isotopes [10,11]. The input parameters such as level density parameter have been precisely chosen for best estimation of cross section.

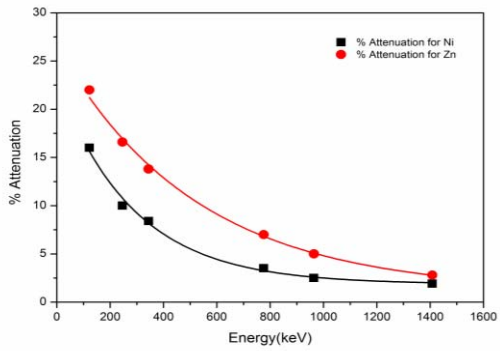

Fig. 1. Self-absorption and self-scattering effect for Ni and Zn sample

A. *TALYS-1.6 calculations*

TALYS is a computer code which is efficient to predict nuclear reaction cross section. It is useful tool to do analysis of physics of nuclear reactions. TALYS-1.6 nuclear code can calculate cross section for incident particles; gammas, neutrons, protons, deuterons, tritons, ^{3}He and alpha-particles in the incident energy range from 1 keV to 200 MeV for target nuclides of mass 12 and heavier nuclei. TALYS considers all the possible channels for the above-mentioned particles. It has completely integrated optical model and coupled-channels calculations by ECIS-06 code [12]. Talys-1.6 is the most advance version of all the version of the TALYS code. The optical model parameters are used for neutron and photon reaction calculations determined from global potential proposed by Koning and Delaroche [13]. The compound model contribution is developed from Hauser-Feshbach model [14]. The pre-equilibrium calculation is developed from the exciton model proposed by Kalbach [15]. In this calculation, pre-equilibrium effect was also considered.

B. *EMPIRE-3.2 calculations*

EMPIRE-3.2 is another powerful nuclear modular system to predict nuclear reaction cross section. It considers reaction mechanism such as compound nucleus formation (Hauser-Feshbach model with width fluctuation correction [14, 16], pre-equilibrium using exciton model and direct reaction using the optical model parameters given in RIPL-3 library. The present version of the EMPIRE code is the latest version. EMPIRE makes use of several codes, written by different authors, which were converted into subroutines and adapted for the present use [17]. For the present work, the level density parameter was changed to get the best agreement with the measured data (Level density parameter for EGSM, Gilbert-Cameron (EMPIRE) and GSM (RIPL) models [18,19].

Both the codes were used to calculate cross section for the selected reactions and are plotted in the Figs.2-7 along with the previous data. There is a fairly good agreement between present measurements with those of calculated results using TALYS-1.6 and EMPIRE-3.2.2. The present experimental result and theoretical predictions using above codes are also listed in Table-2.

IV. CONCLUSIONS

In the present study the (n,p) reaction cross section for some of the structural materials such as ^{75}As, ^{66}Zn, ^{64}Zn, ^{55}Mn, ^{51}V and ^{58}Ni were studied at 14.2 ± 0.2 MeV. The present results were compared with the previously measured data available in EXFOR database as well as theoretical predictions using code TALYS-1.6 and EMPIRE-3.2. Present results are in fairly good agreement with some previous measurements and also with theoretical predictions.

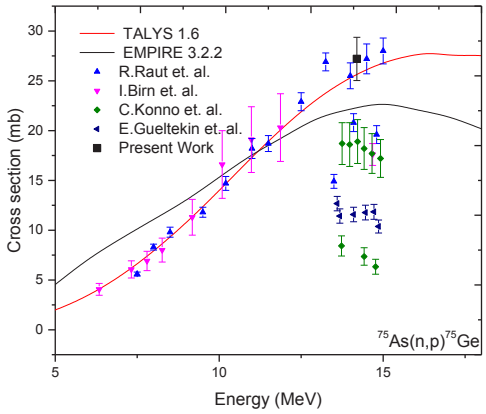

Fig. 2. Comparison of measured ^{75}As(n,p)^{75}Ge cross section with EMPIRE-3.2.2, TALYS-1.6, EXFOR

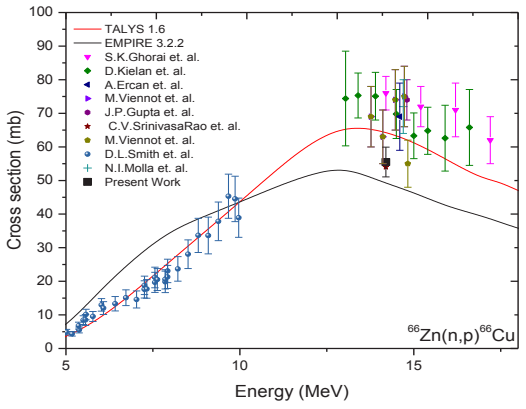

Fig. 3. Comparison of measured ^{66}Zn(n,p)^{66}Cu cross section with EMPIRE-3.2.2, TALYS-1.6, EXFOR

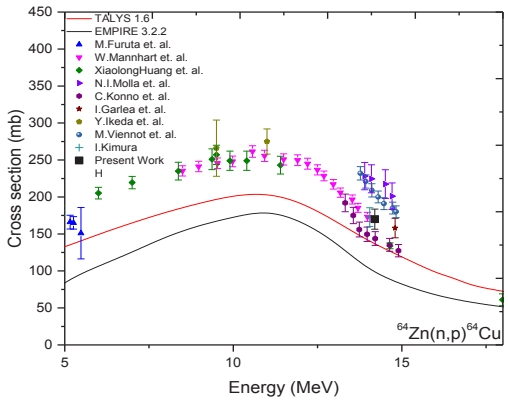

Fig. 4. Comparison of measured ^{64}Zn(n,p)^{64}Cu cross section with EMPIRE-3.2.2, TALYS-1.6, EXFOR

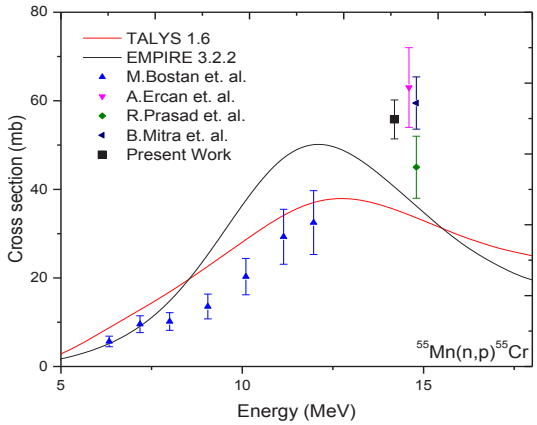

Fig. 5. Comparison of measured ^{55}Mn(n,p)^{55}Cr cross section with EMPIRE-3.2.2, TALYS-1.6, EXFOR

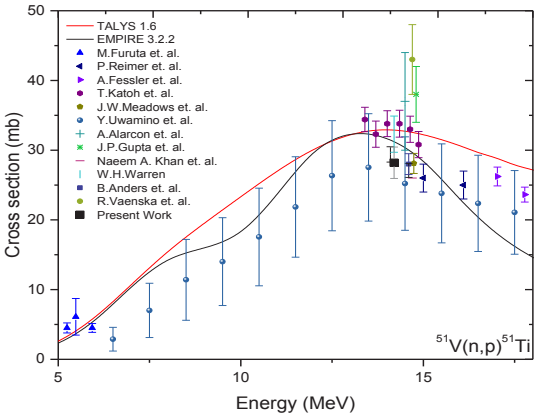

Fig. 6. Comparison of measured ^{51}V(n,p)^{51}Ti cross section with EMPIRE-3.2.2, TALYS-1.6, EXFOR

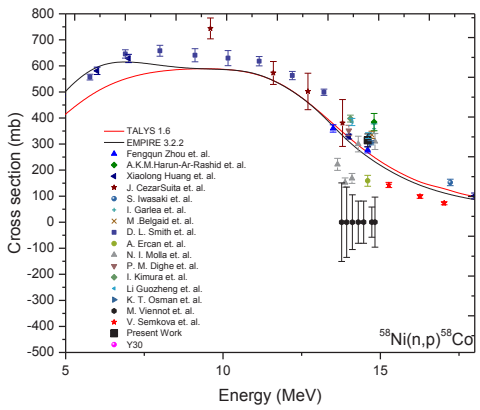

Fig. 7. Comparison of measured ^{58}Ni(n,p)^{58}Co cross section with EMPIRE-3.2.2, TALYS-1.6, EXFOR

ACKNOWLEDGMENT

The authors thank to (Late) Prof. J. Rama Rao and (Late) Prof. L. Chaturvedi for their support to carry out neutron activation measurements at BHU, Varanasi, India.

REFERENCES

[1] N.L. Singh, et al., Proc. of DAE Sympo. on Nucl. Phys. 59 (2014) 566. ; 60 (2015) 442.

[2] N.L. Singh, P.M. Prajapati, Proc. of Electric Power Engineering, EPE-2014, 739-742 (2014).

[3] International Atomic Energy Agency – Nuclear Data Section (team of authors), "Experimental Nuclear Reaction Data Library (EXFOR)"; https://www-nds.iaea.org/exfor, cited March 10, 2016.

[4] A.R. Farhan, S. Rab, "Nuclear Datasheet for A=75", Nucl. Dat. Sheets 60, 735 (1990).

[5] M.R. Bhat, "Nuclear Datasheet for A=75", Nucl. Dat. Sheets 83, 789 (1998).

[6] Huo Junde, "Nuclear Datasheet for A=75", Nucl. Dat. Sheets 64, 723 (1991).

[7] B. Singh, "Nuclear Datasheet for A=75", Nucl. Dat. Sheets 78, 395 (1996).

[8] R.L. Auble, "Nuclear data sheets for A = 51", Nucl. Dat. Sheets 23, 163 (1978).

[9] C.D. Nesaraja, S.D. Geraedts, B. Singh, "Nuclear Datasheet for A=58", Nucl. Dat. Sheets 111, 897 (2010).

[10] A.J.Koning, et. al., "TALYS-1.6, A Nuclear reaction program", user's manual, NRG-1755 ZG Petten, The Netherlands (2011).

[11] M. Herman, et. al., "EMPIRE-3.2.2 modular system for nuclear reaction calculations and nuclear data evaluation", user's manual, 2013.

[12] J. Raynal, "Notes on ECIS94", CEA Saclay Report No. CEA-N-2772, (1994).

[13] A.J.Koning and J.P. Declaroche, Nucl.Phys., A713, 231-310(2003).

[14] W. Hauser and H. Feshbach, Phys. Rev, 87, 366(1952).

[15] C. Kalbach, Phy.Rev.C 33, 818–833 (1986).

[16] S. Hofmann, et al., Ann. Phys. 90, 403 (1975); S. Hofmann, et al.,Z.Physik A 297,153 (1980).

[17] A.V. Ignatyuk, J. Nucl Phys. 21, 255 (1975).

[18] A. Gilbert, et al., Can J. Phys. 43, 1446 (1965).

[19] S. Hilaire, et al., Nucl. Phys, A779: 63-81(2006).

Accepted in Physical Review C

Measurements of the cross sections of $^{186}W(n, \gamma)^{187}W$, $^{182}W(n, p)^{182}Ta$, $^{154}Gd(n, 2n)^{153}Gd$, $^{160}Gd(n, 2n)^{159}Gd$ reactions at neutron energies between 5 to 17 MeV

Rajnikant Makwana[1], S. Mukherjee[1,*], P. Mishra[1], H. Naik[2], N. L. Singh[1], M. Mehta[3], K. Katovsky[4], S. V. Suryanarayana[5], V. Vansola[1], Y. Santhi Sheela[6], M. Karkera[6], R. Acharya[2], S. Khirwadkar[3]

[1]Physics Department, Faulty of Science, The Maharaja Sayajirao University of Baroda, Vadodara-390002, India

[2]Radiochemistry Division, Bhabha Atomic Research Centre, Mumbai – 400 085, India

[3]Divertor Division, Institute for Plasma Research, Gandhinagar – 382 428, India

[4]Brno University of Technology, Department of Electrical Power Engineering, Brno, Česká Republika

[5]Nuclear Physics Division, Bhabha Atomic Research Centre, Mumbai - 400 085, India

[6]Manipal University, Department of Statistics, Manipal-576 104, India

The cross sections of the $^{186}W(n, \gamma)^{187}W$, $^{183}W(n, p)^{183}Ta$ and $^{154}Gd(n, 2n)^{153}Gd$, $^{160}Gd(n, 2n)^{159}Gd$ reactions were measured at the neutron energies 5.08±0.165, 8.96±0.77, 12.47±0.825 and 16.63±0.95 MeV. Standard neutron activation analysis technique and off-line gamma ray spectrometry were used for the measurement and analysis of the data. Measurements are done in the energy range, where few or no measured data are available. The results from the present work are compared with the literature data based on the EXFOR compilation. The experimental results are supported by theoretical predictions using nuclear modular codes TALYS – 1.8 and EMPIRE – 3.2.2. The predictability of different ldmodels available in TALYS – 1.8 and levden models in EMPIRE – 3.2.2 were tested. A detailed comparison of experimental results with theoretical model calculations is made.

(*) Corresponding Author: sk.mukherjee-phy@msubaroda.ac.in

I. INTRODUCTION

Nuclear reaction cross section data is of prime importance for reactor technology. When the reactor is in operation, it produces neutrons that penetrate through several materials, such as fuel, structural, controlling and shielding materials, etc. It is important to have nuclear reaction cross section data for all these materials, at all possible neutron energies [1] for the development of the reactor technology. There are numerous measured nuclear data available in the EXchange FORmat (EXFOR) library [2]. However, it is important to have more experimental nuclear data, measured with high accuracy in the energy range between thermal to 20 MeV for a number of reactor materials [2]. Tungsten (W) and gadolinium (Gd) are two such materials. W is selected as a diverter material for the upcoming fusion device – International Thermonuclear Experimental Reactor (ITER) [3]. In ITER the DT reaction generates 14.6 MeV neutrons, which are scattered from the surrounding materials, thus neutrons will have energies from thermal to 14.6 MeV [4-9]. These neutrons interact with the diverter material of the reactor and can open different nuclear reaction channels. In Accelerator Driven Subcritical system (ADSs), W is used in different parts, hence it can face neutrons with higher energies [10]. Further, Gd is an important rare earth element, which is used in control rods. Its nitrate form is useful for reactor control through moderator as liquid poison, as well as a secondary shutdown device in PHWR reactors [11]. Gadolinium nitrate is more advantageous due to its properties, such as; high thermal neutron capture cross section, quick burnout, greater solubility and a more efficient removal by ion exchange systems compared with boron [12]. Hence it is important to have accurate cross section data for all the tungsten and gadolinium isotopes in the energy range from thermal to 20 MeV. Accurate experimental data is also needed to validate the various theoretical nuclear models [13]. In view of this, in the present work, cross sections for the ^{186}W(n, γ)^{187}W, ^{183}W(n, p)^{183}Ta, ^{154}Gd(n, 2n)^{153}Gd and ^{160}Gd(n, 2n)^{159}Gd reactions at the neutron energies of 5.08 ± 0.165, 8.96 ± 0.77, 12.47 ± 0.825 and 16.63 ± 0.95 MeV were measured by neutron activation analysis (NAA) and the off-line gamma ray spectrometry technique. The above mentioned reaction cross-sections were also calculated by using the computer codes TALYS – 1.8 and EMPIRE – 3.2.2. Different ldmodels available in TALYS – 1.8 and

levden models in EMPIRE – 3.2.2 were used to validate the present experimental results.

In this paper, the experimental details are discussed in section II. Section III describes the data analysis. The neutron flux and average neutron energy calculations used to obtain reaction cross sections, with suitable corrections incorporated to obtain accurate cross section results, are also discussed in this section. Section IV presents the theoretical calculations, followed by results and discussions in section V. A summary and conclusions are given in section VI.

II. EXPERIMENTAL DETAILS

The experiment was carried out by using the BARC-TIFR Pelletron facility in Mumbai, India. The neutrons were produced using the ^{7}Li(p, n)^{7}Be reaction. A proton beam was targeted on natural lithium foil of thickness 8.0 mg/cm^2. The Li foil was wrapped with 3.7 mg/cm^2 tantalum in front and 4.12 mg/cm^2 on the back. The energies of the proton beam were selected to be 7.0, 11.0, 15.0 and 18.8 MeV. The samples were kept at a distance of 2.1 cm from the Li – target in the forward direction. The targets were irradiated for different irradiation times. The irradiation details are given in Table I. A schematic view of the irradiation setup is shown in Fig. 1. In the present measurements, the natural samples of W (99.97 %) in the form of 1.0 mm thick and about a quarter of a circle with radius of 1 to 3 cm were used. Gd samples were made in the form of a pellet with radius of 0.65 cm and of thickness from 0.5 to 1.0 mm using Gd_2O_3 (99.9 %) powder. The weight of the samples was measured using digital micro balance weighing machine. The mass of W samples in different sets of irradiations were 3.6689 g (Irradiation – 1), 0.7826 g (Irradiation – 2), 0.8344 g (Irradiation – 3) and 0.504 g (Irradiation – 4). The samples of Gd were with mass of 0.4071 g (Irradiation – 1) and 0.9102 g (Irradiation – 3). In each irradiation, indium (In) and thorium (Th) foils were used as flux monitors. After a suitable cooling time, the irradiated samples were mounted on different Perspex plates and kept in front of the pre-calibrated High Purity Germanium (HPGe) detector. A Baltic company HPGe detector with 4k channels MCA and MAESTRO spectroscopic software was used to measure the gamma ray spectra from the irradiated sample. The HPGe detector system was calibrated using a standard ^{152}Eu multi-gamma ray source. The efficiency of the detector was also determined at different gamma energies using the same source. The gamma ray activities of the irradiated samples were measured for different counting times. The prominent gamma ray energies emitted from the irradiated samples and other spectroscopic data are given

in Table II. Isotopic abundances are taken from the literature [14]. The threshold energies of the reactions are calculated using the Q – value calculator provided online by NNDC [15]. The daughter nuclide half-life and details of the emitted prominent gamma rays are taken from literature [16]. Typical gamma ray spectra obtained from the irradiated W and Gd samples are shown in Figs. 2 (a-b).

Table I. Details of the irradiation in the present experiment

	Irradiation - 1	**Irradiation - 2**	**Irradiation - 3**	**Irradiation - 4**
Proton Energy (MeV)	18.8	7.0	15.0	11.0
Total Irradiation Time (hr:min)	5:00	11:15	7:00	16:05
Beam Current (nA)	150	110	150	120

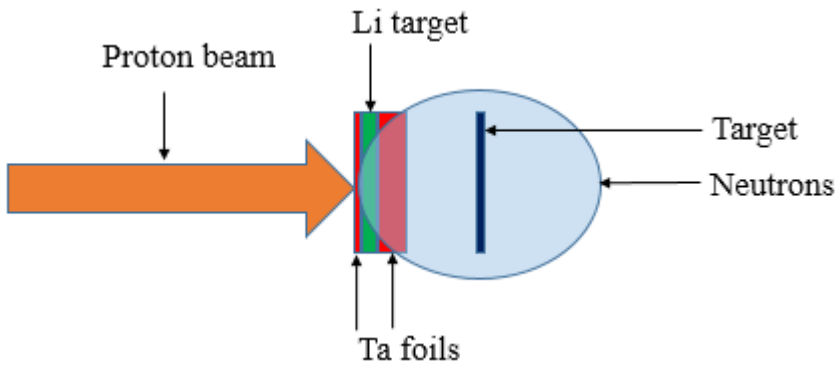

FIG. 1. (Color online) Experimental arrangement showing neutron production using Li(p, n) reaction

Table II. Selected nuclear reactions, target isotopic abundance, threshold energy of reaction, product nucleus with half-life and energies of prominent gamma rays with branching intensities.

Reaction	Isotopic Abundance (%) [14]	Threshold Energy (MeV) [15]	Product Nucleus	Half-life [16]	Prominent γ-ray Energy (keV); (Branching intensity %)
^{186}W(n, γ)^{187}W	28.43	-	^{187}W	24.0 h	479.5(26.6); 685.7(33.2)
^{182}W(n, p)^{182}Ta	26.50	1.037	^{182}Ta	114.74 d	1121.3(35.24)
^{154}Gd(n, 2n)^{153}Gd	2.18	8.953	^{153}Gd	240.4 d	103.1 (21.1)
^{160}Gd(n, 2n)^{159}Gd	21.86	7.498	^{159}Gd	18.479 h	363.5 (11.78)

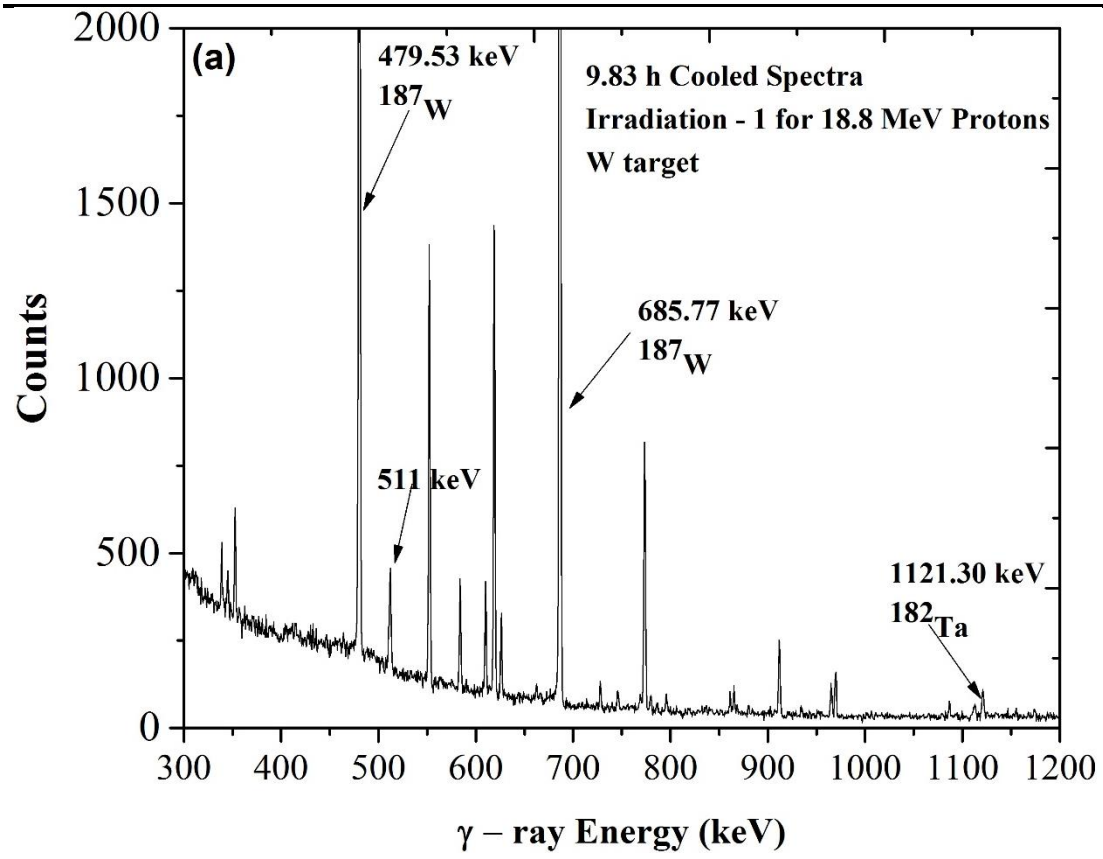

FIG. 2 (a). Typical γ-ray spectra for W target obtained by using HPGe detector

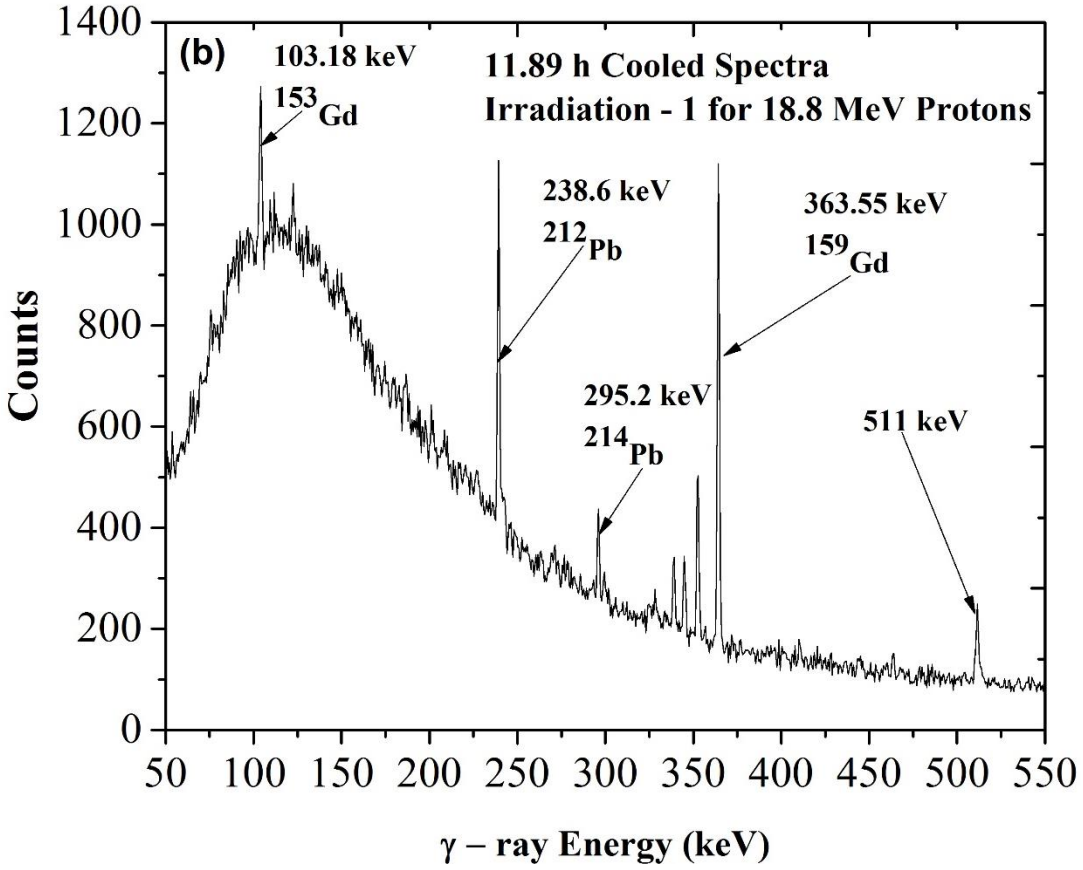

FIG. 2 (b). Typical γ-ray spectra for Gd target obtained by using HPGe detector

III. DATA ANALYSIS

A. Neutron Activation Analysis

The experimental data were analyzed by using the standard neutron activation analysis (NAA) technique. In this technique, the nuclear reaction rate or the rate of production of daughter isotopes depends on the number of target nuclei available and the neutron flux incident on it. This activation method is generally followed to measure reaction cross section by irradiating the target isotope with neutrons, when the products emit characteristic gamma rays having sufficiently long half-life and gamma branching abundances. The cross section of the selected reactions can be determined using the following equation [17].

$$\sigma = \frac{A_\gamma \cdot \lambda \cdot (t_c / t_r)}{N \cdot \phi \cdot I_\gamma \cdot \varepsilon \cdot \left(1 - e^{-\lambda \cdot t_i}\right) \cdot \left(1 - e^{-\lambda \cdot t_c}\right) \cdot e^{-\lambda \cdot t_w}} \quad (1)$$

Where,

A_γ = Number of detected gamma ray counts;

λ = Decay constant of product nucleus (s^{-1})

t_i = Irradiation time (s);

t_w = Cooling time (s);

t_c = Counting time (s);

t_r = Real time (Clock time) (s);

ϕ = Incident neutron flux (n $cm^{-2}s^{-1}$);

I_γ = Branching intensity of γ-ray;

ε = Efficiency of detector for the chosen gamma ray;

N = Number of target atoms

In the above equation, the activity (A_γ) is measured using an HPGe detector for different gamma rays emitted from the daughter isotopes. Because of the half-lives of the isotopes of interest, several rounds of gamma ray counting were done. The dead time of the detector system was kept below 0.6 % during the entire counting process. The numbers of target nuclei were calculated from the weight of the sample and isotopic abundances. The calculation of the neutron flux was done using the gamma ray spectra of irradiated In and Th foils. Other standard parameters of the reactions were taken from the literature [14-16].

B. Neutron flux and Average neutron energy

The neutrons were generated by ^{7}Li(p, n)^{7}Be reactions. Below 2.4 MeV, this reaction produces mono-energetic neutrons [18]. Above 2.4 MeV, the first excited state of ^{7}Be at 0.43 MeV is populated and produces a second group of neutrons [18, 19]. Above 6 MeV, the three body interaction, and other excited states also contribute in the neutron production along with the main neutron group [18, 19]. Although there are lower energy sub-group of neutrons, the primary (main) group of neutrons can be used to measure the reaction cross section as it has higher neutron flux and higher neutron energy (forming a peak). The reaction cross section measured at this averaged peak energy. The spectrum averaged neutron energy can be given as [20],

$$E_{mean} = \frac{\int_{E_{ps}}^{E_{\max}} E_i \phi_i dE}{\int_{E_{ps}}^{E_{\max}} \phi_i dE} \tag{2}$$

Where,

E_{ps} = peak forming start neutron energy

E_{max} = maximum neutron energy

E_i = energy bin

ϕ_i = neutron flux of energy bin E_i

E_{mean} = effective mean energy

The neutron spectra for 7.0, 11.0, 15.0 and 18.8 MeV were derived by taking data from various available publications [18-22]. The neutron spectra corresponding to all the four incident proton energies are shown in Fig. 3 (a – d). The average peak energies obtained by using equation (2) are given in Table III.

In order to analyze the data, it is necessary to accurately calculate the neutron flux incident on the target. In the present experiment, ^{115}In(n, n′)^{115m}In and ^{232}Th(n, f)^{97}Zr monitor reactions were used for the neutron flux measurement. The reaction products ^{115m}In and ^{97}Zr have a half-life of 4.486 h and 16.749 h respectively [16]. The emitted characteristic gamma lines are given in Table IV. Typical gamma ray spectra obtained from both the monitors are shown in Fig. 5.

The calculations of the neutron flux incident on the target were done by using the spectrum averaged neutron cross section for the monitor reactions by using the relatively recent data available from the EXFOR data library for ^{115In}(n, n') [23- 26] and for ^{232}Th(n, f) [27-30]. The spectrum averaged cross section was calculated using the following equation,

$$\sigma_{av} = \frac{\int_{E_{th}}^{E_{max}} \sigma_i \phi_i dE}{\int_{E_{th}}^{E_{max}} \phi_i dE} \tag{3}$$

Where,

E_{th} = threshold energy of the monitor reaction

E_{max} = maximum neutron energy

σ_i = Cross section at energy E_i for monitor reaction from EXFOR [23-30]

ϕ_i = neutron flux of energy bin E_i from the Fig. 4 (a – d)

σ_{av} = Spectrum averaged cross section

The calculated spectrum averaged cross sections for both the monitor reactions are given in Table III. The neutron flux incident on targets for all the four irradiations were calculated using the following activation equation (1).

$$\phi = \frac{A_\gamma \cdot \lambda \cdot (t_c / t_r)}{N \cdot \sigma_{av} \cdot I_\gamma \cdot \varepsilon \cdot \left(1 - e^{-\lambda \cdot t_i}\right) \cdot \left(1 - e^{-\lambda \cdot t_c}\right) \cdot e^{-\lambda \cdot t_w}} \tag{4}$$

All the parameters are same as in equation (1).

In the case of fission reaction monitor, the fission yield term (Y) will come in the denominator on the right side of the above equation (4). In the cross section calculations, the measured values of the average neutron flux from both the monitors were taken, as both these values are in agreement with each other within the limits of the experimental errors as discussed later in section V.

C. Cross section correction for lower energy neutrons

In order to measure the cross section for neutrons of main peak, it is necessary to make corrections due to the contributions from lower energy neutrons. This correction is not required when the neutron source is purely mono-energetic, which is not the present case. As mentioned earlier, in addition to a primary neutron group, there exist secondary neutron groups arising due to an excited state of ^{7}Be and three-body reactions above 2.4 and 6 MeV respectively [18]. These secondary groups produce neutrons, at lower energies and in addition to the primary group neutrons [18, 19]. As the primary neutron exhibit a distinct broad peak always at much higher energy with a high neutron flux, it can be considered as quasi mono-energetic source. It is possible to remove the contributions to the reaction cross sections due to low energy neutrons from the primary neutron group by the process of making a tailing correction. In the present work, the tailing correction has been done using the method given in the literature [20].

The cross sections have been calculated using the NAA equation (1) and the neutron flux from monitor reactions. For a capture reaction, one has to use total neutron flux, but for the reactions having threshold energy, the neutron flux must be corrected. To do this, one has to remove the neutron flux from minimum to threshold energy neutrons, by taking the area under the neutron spectra. For instance, the ^{154}Gd(n, 2n)^{153}Gd reaction has a threshold energy of 8.953 MeV. Hence, the flux for this reaction must be the area under the curve shown from '**A**' (threshold energy) to '**B**' (maximum neutron energy) [Fig 4]. This will correct the actual neutron flux used to produce the desired daughter isotopes. Using this neutron flux, a set of cross sections of all reactions has been calculated. In order to remove the effective spectrum average cross section from the threshold to the minimum energy of the peak of interest (E_{ps}), theoretical calculations using modular code TALYS – 1.8 have been carried out to obtain the reaction cross sections versus neutron energy. These calculated cross sections at different energies are convoluted with the neutron flux as shown in Fig. 3 (a). The

spectrum average cross section for each reaction was calculated from threshold to minimum energy (E_{ps}), and it is subtracted from the previous cross section dataset. Thus the final value obtained gives the cross section for the reaction at the spectrum average neutron peak energy.

Using the above method, the cross sections for the $^{182}W(n, p)^{182}Ta$, $^{186}W(n, \gamma)^{187}W$, $^{154}Gd(n, 2n)^{153}Gd$ and $^{160}Gd(n, 2n)^{159}Gd$ reactions were measured at the neutron energies of 5.08, 8.96, 12.47 and 16.63 MeV. In the $^{160}Gd(n, 2n)^{159}Gd$ and $^{158}Gd(n, \gamma)^{159}Gd$ reactions, a common γ-ray of 363.54 keV (Iγ = 11.78%) is emitted. Therefore, it is necessary to remove this part of the cross section from this capture reaction. At higher energies, the (n, γ) reaction has a very small contribution compared to the lower energy neutrons. Since the lower energy neutron part has been already corrected using above method, therefore the cross section obtained is purely due to the (n, 2n) reaction. In the same way, the tailing corrections have been applied for all the reactions studied in the present work.

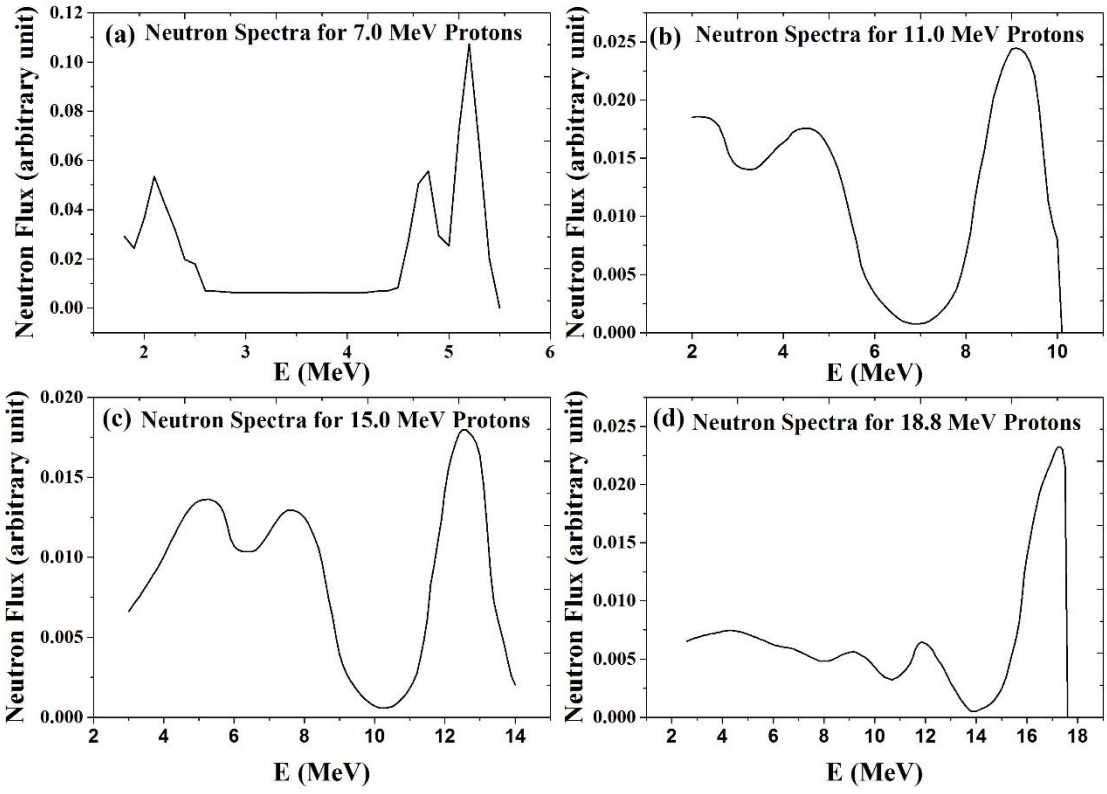

FIG. 3 (a – d). ^{7}Li (p, n) ^{7}Be neutron spectra for the 7.0 (a), 11.0 (b), 15.0 (c) and 18.8 (d) MeV proton energies

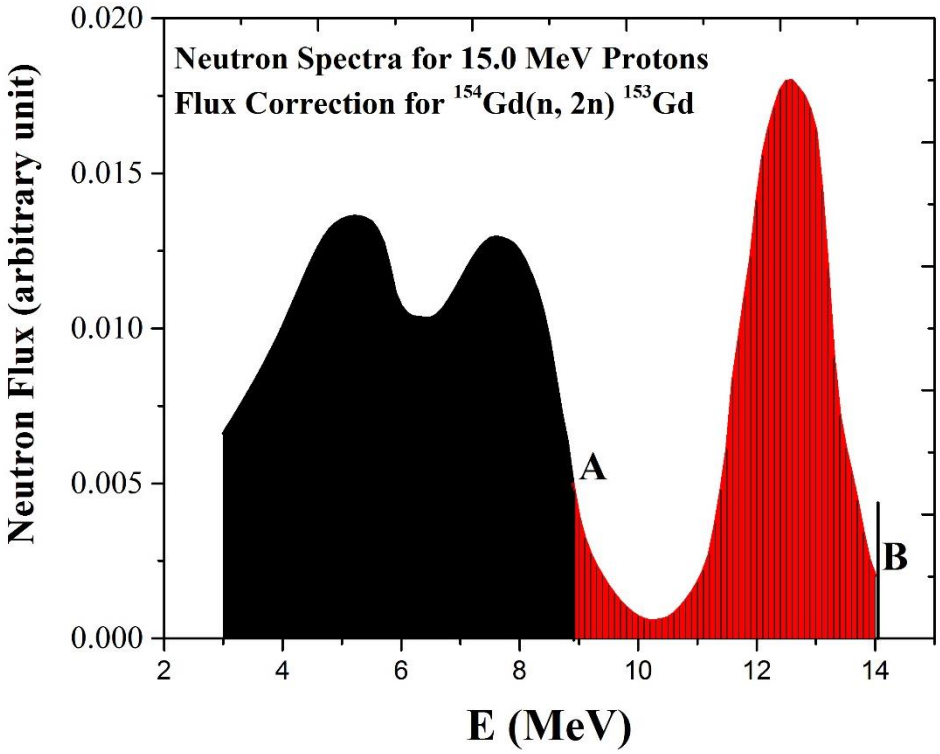

FIG. 4. (Color online) Neutron flux correction for the threshold energy reactions, shown for ^{154}Gd (n, 2n) ^{153}Gd reaction with threshold energy of 8.953 MeV labeled by **'A'** and maximum neutron energy labeled by **'B'**

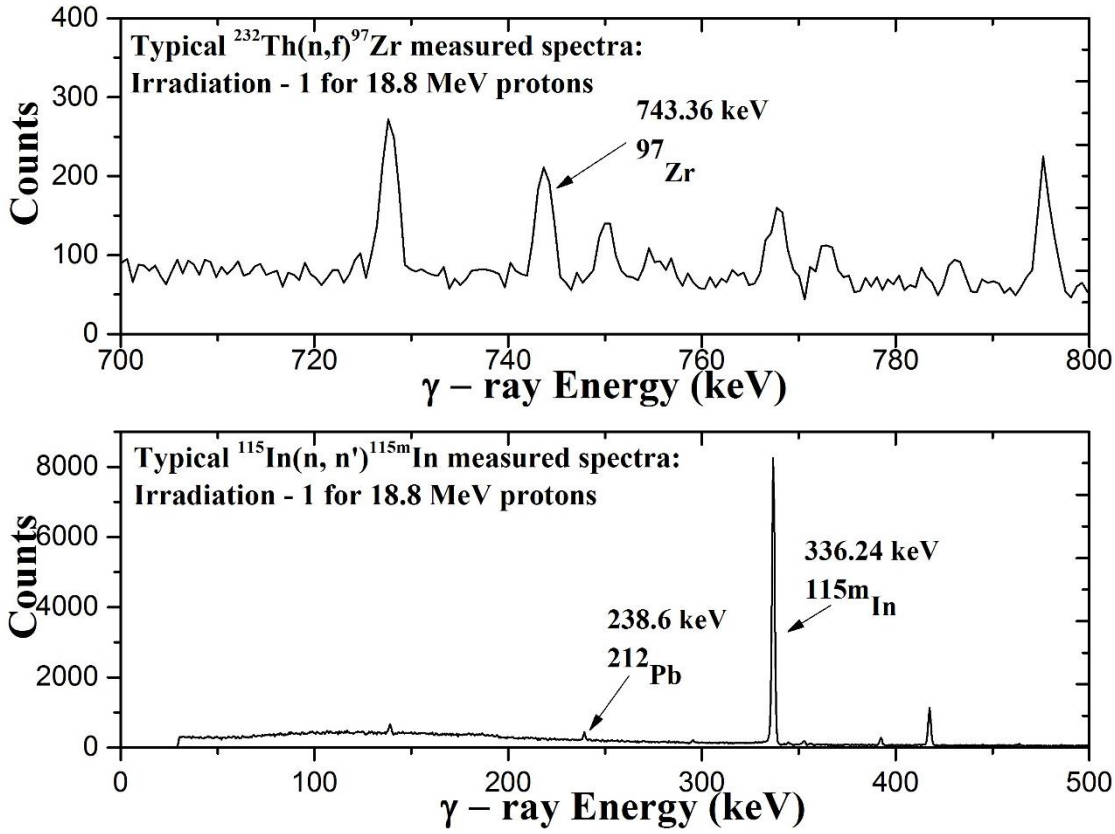

FIG. 5. Typical monitor reaction gamma ray spectra using HPGe detector

Table III. The spectrum averaged neutron energies and respective neutron flux from two different monitor reactions

	Irradiation - 1	**Irradiation-2**	**Irradiation-3**	**Irradiation-4**
Proton Energy (MeV)	18.8	7.0	15.0	11.0
Neutron Energy from eq. (2) (MeV)	16.63 ± 0.95	5.08 ± 0.165	12.47 ± 0.825	8.96 ± 0.77
Spectrum Averaged Cross section for In monitor (mb)	188.94	223.88	253.79	302.85
Calculated Neutron Flux from ^{115}In(n, n')^{115m}In (n cm^{-2} s^{-1})	6.2891×10^7	4.6304×10^6	1.8054×10^7	1.6009×10^6
Spectrum Averaged Cross section for Th monitor (mb)	341.67	99.04	269.58	220.01
Calculated Neutron Flux from ^{232}Th(n, f)^{97}Zr (n cm^{-2} s^{-1})	6.2885×10^7	4.5709×10^6	1.7090×10^7	1.5850×10^6

Table IV. The monitor reaction with the product nucleus and prominent gamma lines

Monitor Reaction	Product Nucleus (Half-life) [16]	Prominent gamma Line (branching Intensity %) [16]
^{115}In(n, n')^{115m}In	^{115m}In (4.486 h)	336.24 (45.8)
^{232}Th(n, f)^{97}Zr	^{97}Zr (16.749 h)	743.36 (93.0)

IV. THEORETICAL CALCULATIONS

In order to theoretically understand the measured cross section results, two well-known nuclear reactions modular codes TALYS – 1.8 and EMPIRE – 3.2.2 were used [13]. Both the codes are being used worldwide for nuclear data prediction for the emission of gamma, neutron, proton, deuteron, triton and other particles. Both codes used the reaction parameters from the RIPL database [31]. These codes consider the effect of level density parameters, compound, pre-equilibrium and direct reaction mechanism as a function of incident particle energy. The optical model parameters were obtained by using a global potential, proposed by Koning and Delaroche [32]. The compound reaction mechanism was incorporated using the Hauser-Feshbach model [33]. The pre-equilibrium contribution was accounted for by an exciton model that was developed by Kalbach [34]. In the present work, the calculations have been done with all the default parameters except changing the ldmodel and level density parameters. The present results along with EXFOR data were compared with these predicted data as shown in Figs. 6 (a-b).

V. RESULTS & DISCUSSION

The main objective of the present study was to provide a set of reaction cross section data in the energy range where there are very few or no measurements available in the literature. These cross sections are important for the accurate reactor design and also to improve the existing nuclear database. Hence the present experimental data for W and Gd isotopes become more important. Further, in this energy region, the standard nuclear models play an important role to validate the present measured experimental data. The major uncertainties in the present reaction cross sections are given in Table V.

The measured data were supported by the theoretical predictions using EMPIRE – 3.2.2 and TALYS – 1.8. There are different options of level density given in EMPIRE – 3.2.2. The level density parameter values levden = 0, 1, 2, 3, 4 uses various well known models described in various publications [31, 35-39]. By varying these parameters, the cross section for the selected reactions from threshold to 20 MeV were calculated. The predicted and experimental results are shown in Figs. 6 (a-d). In TALYS – 1.8, the different ldmodel options were varied from ldmodel1 to ldmodel6 for the selected nuclear reactions and the experimental cross sections were compared. The details of these parameters are given in the TALYS – 1.8 manual [39, 40].

As shown in Fig. 6 (a) for $^{186}W(n, \gamma)^{187}W$ reaction, the levden = 2 of EMPIRE – 3.2.2 gives a relatively better agreement compared to other levden values. But at lower

energy the levden = 2 does not give satisfactory predictions. Moreover, all other level density models of EMPIRE – 3.2.2 show discrepancies with each other and predicts lower cross section as compared to the present experimental results. In the case of TALYS – 1.8 analyses, results of all the ldmodels options are in good agreement with the data of present measurements. For the ^{182}W (n, p) ^{182}Ta reaction, all TALYS – 1.8 ldmodels are in good agreement. The EMPIRE levden models show a discrepancy with most of EXFOR and the present data. For the ^{154}Gd (n, 2n) ^{153}Gd and ^{160}Gd (n, 2n) ^{159}Gd reactions, the experimental results are in good agreement with both the TALYS – 1.8 and EMPIRE – 3.2.2 predictions, except levden = 2, being listed as a future option in the EMPIRE input file. Only the measurement at 16.63 MeV neutron energy of ^{160}Gd(n ,2n)^{159}Gd is under estimated then the predicted values. Overall the theoretical predictions support the present results. The measured cross section values and the different model predicted values are compared at the same energies in Table VI. In general, TALYS – 1.8, for all the selected models, gives better agreement compared to EMPIRE – 3.2.2 in predicting the present experimental results.

Table V. Major uncertainties incorporated in the present cross section results

Parameter	Limit (%)
Counting rate	≤ 4 - 5
Efficiency Calibration	≤ 3
Self - absorption	≤ 0.2
Mass	≤ 0.001
Neutron flux	≤ 6
I_γ	≤ 3

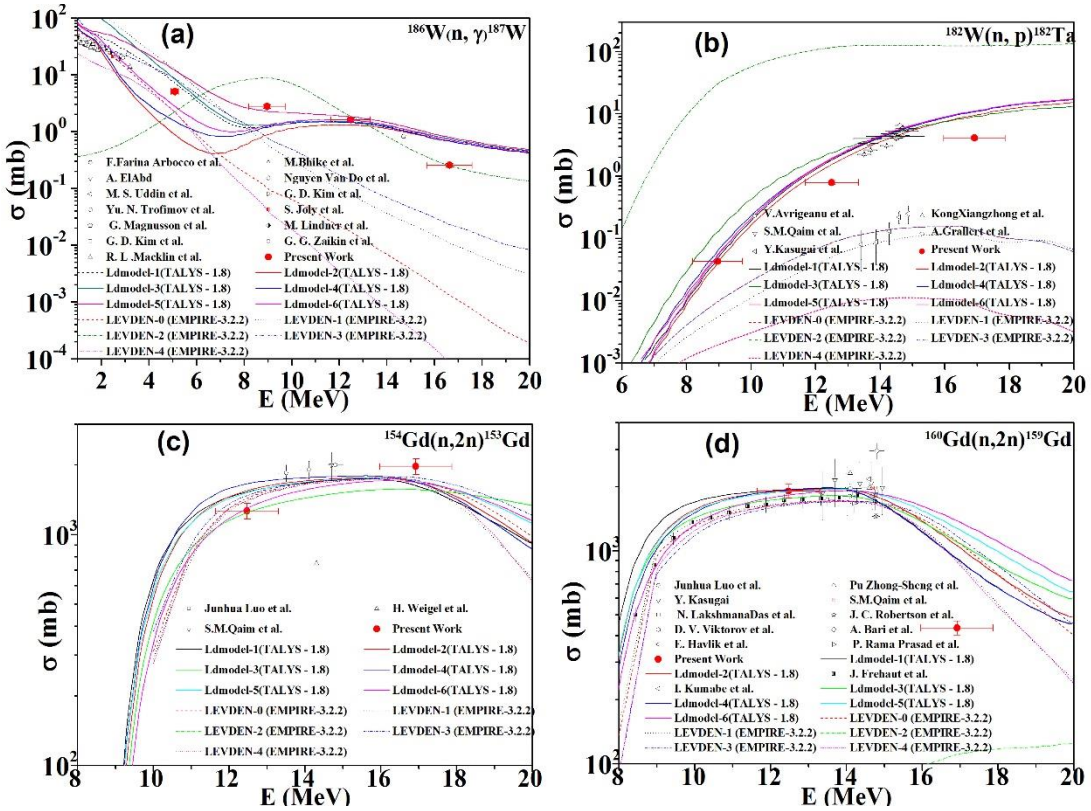

FIG. 6 (a – d). (Color online) Present measured cross section for ^{186}W(n, γ)^{187}W and ^{182}W(n, p)^{182}Ta, ^{154}Gd(n, 2n)^{153}Gd and ^{160}Gd(n, 2n)^{159}Gd reactions compared with EXFOR and predicted cross section data using different theoretical nuclear models of TALYS – 1.8 and EMPIRE – 3.2.2; The LEVDE-2 model of EMPIRE – 3.2.2 predicts very low values (below 100 mb) of cross sections comparing to other models hence it cannot be seen in plot of ^{154}Gd(n, 2n)^{153}Gd

VI. SUMMARY & CONCLUSIONS

Cross section for the ^{182}W(n, p)^{182}Ta, ^{186}W(n, γ)^{187}W, ^{154}Gd(n, 2n)^{153}Gd and ^{160}Gd(n, 2n)^{159}Gd reactions were measured at the neutron energies 5.08 ± 0.165, 8.96 ± 0.77, 12.47 ± 0.825 and 16.63 ± 0.95 MeV by using the neutron activation analysis technique and incorporating standard tailing corrections [18]. The cross sections have been measured in an energy range where very few or no measurements are available. The different correction terms are discussed in order to achieve accurate cross section results. The spectrum averaged neutron energy and accurate flux measurements have also been duly incorporated. The neutron flux at different energies have been calculated by using two monitor reactions and the values thus obtained were found to be in good agreement. The average flux values from the two monitor reactions were taken for cross sections calculation. The cross section for the ^{186}W(n, γ)^{187}W reaction have been measured at four different energies. In the case of ^{182}W(n, p)^{182}Ta the cross sections are

reported at 8.96 ± 0.77, 12.47 ± 0.825 and 16.63 ± 0.95 MeV. For the ^{154}Gd(n, 2n)^{153}Gd and ^{160}Gd(n, 2n)^{59}Gd reactions, the cross sections are reported at 12.47 ± 0.825 and 16.63 ± 0.95 MeV neutron energies. All the measurements have been compared with the theoretical modular codes TALYS – 1.8 and EMPIRE – 3.2.2. It may be concluded that TALYS – 1.8 gives an overall satisfactory agreement with the present experimental and EXFOR results for most of the selected ldmodels as compared to EMPIRE – 3.2.2 predictions. However, in the case of (n,γ) reaction, levden = 2 of EMPIRE gives somewhat better predictions as compared to other levden models in the energy region above 12 MeV. The cross section data presented in this work are important for the future fission/fusion reactor technology.

Acknowledgements

One of the authors (SM) thanks the DAE-BRNS for the sanction of a major research project (Sanction Number: 36(6)/14/22/2016-BRNS). The authors are grateful to Dr. S. C. Sharma (Scientific Officer, BARC – TIFR Pelletron Accelerator Facility) for preparing Li-target and for his help in the experimental setup. The authors acknowledge gratefully the help of Prof. John F. Sharpey Schafer, Retired Professor, Liverpool University and former Director, iThemba LABS, South Africa, for his valuable suggestions and corrections in the manuscript. Thanks are also due to Nishant Barot, Naveen Agrawal, P. K. Mehta, and Ketan Chaudhari from the department for their help in the target preparation.

References

[1] A. J. Koning, and J. Blomgren, Nuclear data for sustainable nuclear energy, JRC Scientific and Tech. Rep. EUR23977EN-2009, 15 (2009).

[2] Cross Section Information Storage and Retrieval System (EXFOR), IAEA, Vienna, Austria. http://www.nds.iaea.or.at/exfor/ (online).

[3] M. Lehnen, *et al*., J. Nucl. Mater. **463**, 39 (2013).

[4] J. Qing, Y. Wu, M. Regis, and J. W. Kwan, IEEE Trans. Nucl. Sci. **56**, 1312 (2009).

[5] J. Reijonen, F. Gicquel, S. K. Hahto, M. King, T. P. Lou, and K. N. Leung, Appl. Radiat. Isotopes **63**, 757 (2005).

[6] Y. Wu, J. P. Hurley, Q. Ji, J. Kwan, and K. N. Leung, IEEE Trans. Nucl. Sci. **56**, 1306 (2009).

[7] V. Voitsenya, *et al*., Rev. Sci. Instrum. **72**, 475 (2001).

[8] G. De Temmerman, R. A. Pitts, V. S. Voitsenya, L. Marot, G. Veres, M. Maurer, and P. Oelhafen, J. Nucl. Mater. **363**, 259 (2007).

[9] K. H. Behringer, J. Nucl. Mater.**145**, 145 (1987).

[10] Yousry Gohar, Igor Bolshinsky, and Ivan Karnaukhov, NEA/NSC/DOC (2015) 7, 254 (2015).

[11] R. Vijayalakshmi, D. K. Singh, M. K. Kotekar, and H. Singh, J Radioanal. Nucl. Chem. **300**, 129 (2014)

[12] S. Dutta, P. Suryanarayanan, A. R. Kandalgaonkar, R. S. Sharma, and H. Bose, BARC News Lett, **271**, 2 (2006).

[13] N. Dzysiuk, I. Kadenko, A. J. Koning, and R. Yermolenko, Phys. Rev. C **81**, 014610 (2010).

[14] K. J. R. Rosman, and P. D. P. Taylor, Pure Appl. Chem. **71**, 1593 (1999).

[15] http://www.nndc.bnl.gov/qcalc/index.jsp, retrieved on 11th November 2016.

[16] http://www.nndc.bnl.gov/nudat2/indx_dec.jsp, retrieved on 21st March 2017.

[17] Vibha Vansola, *et al*., Radiochim. Acta **103**, 817 (2015).

[18] C. H. Poppe, J. D. Anderson, J. C. Davis, S. M. Grimes, and C. Wong, Phys. Rev. C **14**, 438 (1976).

[19] J. D. Anderson, C. Wong, and V. A. Madsen, Phys. Rev. Letts. **24**, 1074 (1970).

[20] D. L. Smith, *et al*., " Corrections for Low Energy Neutrons by Spectral Indexing", Retrieved from: https://www.oecdnea.org/science/docs/2005/nsc-wpec-doc2005-357.pdf

[21] P. M. Prajapati, *et al*., Eur. Phys. J. A **48**, 1 (2012).

[22] M. W. Mcnaughton, N. S. P. King, F. P. Brady, J. L. Romero, and T. S. Subramanian, Nucl. Instrum. Methods 130, 555 (1975).

[23] A. A. Lapenas, Neutron Spect. Meas. by Activ., Riga 1975, (1975).

[24] G. Loevestam, M. Hult, A. Fessler,T. Gamboni, J. Gasparro, R. Jaime, P. Lindahl, S. Oberstedt, and H. Tagziria, Nucl. Instrum. Methods in Physics Res., Sect. A 580, 1400 (2007).

[25] Y. Agus, I. Celenk, and A.Ozmen Radiochimica Acta 92, 63 (2004).

[26] M. S. Uddin, Radiochimica Acta 101, 613 (2013).

[27] O. A. Shcherbakov, *et al*., Int. Sem. on Interactions of Neutrons with Nuclei 9, 257 (2001).

[28] R. K. Jain, Pramana 49, 515 (1997).

[29] I. Garlea, Chr.Miron-Garlea, and H. N. Rosu, Revue Roumaine de Physique 37, 19 (1992).

[30] F. Manabe, K. Kanda, T. Iwasaki, H. Terayama, Y. Karino, M. Baba, and N. Hirakawa, Fac. of Engineering, Tohoku Univ. Tech. Report 52, 97 (1988).

[31] R. Capote, et al., Nuclear Data Sheets 110, 3107 (2009).

[32] A. J. Koning, and J. P. Declaroche, Nucl. Phys. A 713, 231(2003).

[33] W. Hauser, and H. Feshbach, Phys. Rev. 87, 366 (1952).

[34] C. Kalbach, Phys. Rev. C **33**, 818 (1986).

[35] https://www-nds.iaea.org/RIPL-3/densities/, retrieved on 28th February 2017.

[36] A. V. Ignatyuk, K. K. Istekov, and G. N. Smirenkin, Sov. J. Nucl. Phys. **29**, 450 (1979).

[37] A.V. Ignatyuk, J. L. Weil, S. Raman, and S. Kahane, Phys. Rev. C **47**, 1504 (1993).

[38] A. Gilbert, and A. G. W. Cameron, Can. J. Phys. **43**, 1446 (1965).

[39] S. Hilaire, M. Girod, S. Goriely and A. J. Koning, Phys. Rev. C **86**, 1 (2012).

[40] A. Koning, S. Hilaire, and S. Goriely, TALYS-1.6 - A Nuclear Reaction Program, User Manual, 1st edition (NRG, The Netherlands, 2013).

Table VI. Comparison of present experimental data different model predictions using TALYS – 1.8 and EMPIRE – 3.2.2

Energy (MeV)	$^{186}W(n,\gamma)^{187}W$ reaction cross section (mb)											
	Measured	TALYS - 1.8						EMPIRE – 3.2.2				
		Ldmodel-1	Ldmodel-2	Ldmodel-3	Ldmodel-4	Ldmodel-5	Ldmodel-6	Levden-0	Levden-1	Levden-2	Levden-3	Levden-4
5.08±0.165	5.079±0.39	7.23	0.885	8.37	1.53	12.1	2.80	2.24	12.8	2.24	8.83	2.2903
8.96±0.77	2.767±0.19	1.22	0.871	1.31	1.17	2.26	1.26	0.108	0.618	9.01	0.827	0.0453
12.47±0.825	1.620±0.11	1.46	1.30	1.48	1.43	1.81	1.58	0.0181	0.0794	1.86	0.146	0.0027
16.63±0.95	0.257±0.02	0.726	0.676	0.753	0.683	0.799	0.716	0.00129	0.0107	0.249	0.0226	8.41E-5
Energy (MeV)	$^{182}W(n,p)^{182}Ta$ reaction cross section (mb)											
	Measured	TALYS - 1.8						EMPIRE – 3.2.2				
		Ldmodel-1	Ldmodel-2	Ldmodel-3	Ldmodel-4	Ldmodel-5	Ldmodel-6	Levden-0	Levden-1	Levden-2	Levden-3	Levden-4
8.96± 0.77	0.043±0.003	0.04813	0.04141	0.12659	0.06359	0.05509	0.05307	0.00964	0.00544	31.0747	0.00964	0.00194
12.47±0.825	0.793±0.06	1.789	1.52	2.33301	1.87	1.86	1.92	0.0842	0.0495	118	0.0842	0.00803
16.63±0.95	4.092±0.28	10.2	8.89	8.4404	10.2	10.4	10.5	0.163	0.147	124	0.163	0.0107
Energy (MeV)	$^{154}Gd(n,2n)^{153}Gd$ Cross Section (mb)											
	Measured	TALYS - 1.8						EMPIRE – 3.2.2				
		Ldmodel-1	Ldmodel-2	Ldmodel-3	Ldmodel-4	Ldmodel-5	Ldmodel-6	Levden-0	Levden-1	Levden-2	Levden-3	Levden-4
12.47±0.825	1265 ±98	1534	1556	1248	1659	1520	1298	1444	1412	22.2	1479	1397
16.63±0.95	1973±153	1683	1725	1571	1737	1735	1703	1748	1744	65.3	1774	1744
Energy (MeV)	$^{160}Gd(n,2n)^{159}Gd$ Cross Section (mb)											
	Measured	TALYS - 1.8						EMPIRE – 3.2.2				
		Ldmodel-1	Ldmodel-2	Ldmodel-3	Ldmodel-4	Ldmodel-5	Ldmodel-6	Levden-0	Levden-1	Levden-2	Levden-3	Levden-4
12.47±0.825	1913±143	1938	1919	1765	1935	1901	1828	1669	1679	52.9	1642	1660
16.63±0.95	435±33	1009	1155	1183	1005	1364	1465	1213	1027	106	1282	999